AD NUMBER: AD0343274
CLASSIFICATION CHANGES
TO: Confidential
FROM: Secret
AUTHORITY
31 July 1975, DoDD 5200.10, gp-3

AD _____

DEFENSE DOCUMENTATION CENTER

FOR

SCIENTIFIC AND TECHNICAL INFORMATION

CAMERON STATION ALEXANDRIA, VIRGINIA

Operation

NOUGAT

SHOT HARD HAT

POR-1801
(WT-1801)

This document consists of 439 pages
No. 132 of 206 copies, Series A

PROJECT OFFICERS REPORT—PROJECT 3.1

LOADING, RESPONSE, AND EVALUATION OF TUNNELS AND TUNNEL LINERS IN GRANITE (U)

R. S. Holmes, Project Officer

L. T. Kwan
E. H. Skinner
E. Y. Wong

Holmes and Narver, Inc.
Los Angeles, California

Issuance Date: July 19, 1963

Inquiries relative to this report may be made to

Chief, Defense Atomic Support Agency
Washington 25, D. C.

When no longer required, this document may be destroyed in accordance with applicable security regulations.

DO NOT RETURN THIS DOCUMENT

USAEC Division of Technical Information Extension, Oak Ridge, Tennessee

(5) 412 900

SECRET

(18) DASA

(19) POR-1801; (WT-1801)

(21) Report on

OPERATION NOUGAT,

SHOT HARD HAT,

PROJECT OFFICERS REPORT—PROJECT 3.1

(6) LOADING, RESPONSE, AND EVALUATION OF TUNNELS AND TUNNEL LINERS IN GRANITE (U)

(8)

(10) by R.S. Holmes,
~~Project Officer~~

L.T. Kwan,
E.H. Skinner and
E.Y. Wong.

Holmes and Narver, Inc.
Los Angeles, California

SECRET

ABSTRACT

This project, sponsored by the Defense Atomic Support ~~Agency, was an evaluation of~~ the response of tunnels and tunnel liners in granite subjected to a 5.9-kiloton, contained, underground nuclear explosion, was evaluated as ~~It was~~ a part of the Hard Hat Shot of Operation Nougat, ~~at the Nevada Test Site.~~

The objectives were to obtain information on the mechanics of tunnel damage and on the loading and response of various tunnel liners. The ultimate use of such information will be the development of improved design procedures for underground protective construction in rock.

~~This~~ The experiment included 43 test sections, of which ~~thirty~~ 30 had liners and backpacking materials. The remaining ~~thirteen~~ 13 were either unlined or were lined without shock isolation material. ~~The liner~~ types ranged from rigid (reinforced concrete), through rigid-flexible (wide flange rings with lagging), to flexible (corrugated tunnel liner plate). Volcanic cinders and rigid polyurethane foam were used as shock isolation materials. The foam was utilized in twenty test sections and had a nominal density of 6 pcf.

The test sections were in test drifts located 244, 334, and 457 feet from the shot point. In general, identical test sections were located in each of the three drifts.

Electronic instrumentation was used to obtain measurements of velocities, accelerations, strains, pressures on liners, diameter changes, and compression of the backpacking material. Most of these measurements were made within the test liners, but measurements in the rock were also taken. Mechanical gages were used to supplement the electronic instruments. These consisted of reed gages for obtaining displacement shock spectra, scratch gages for measuring diameter change or compression of backpacking material, and deForest gages for recording strains. Static measurements included extensive pre- and postshot survey measurements and Whittemore gage readings of permanent strain.

Generally, the results indicated that the measured values of the various shock parameters were within the preshot estimates. The damage at the closest and farthest test drifts was about as expected; however, the damage at the intermediate-range drift was somewhat greater than expected. Data recovery and the results of the electronic and mechanical measurements

were insufficient for complete quantitative evaluation of response of the test sections. However, the data, together with damage observations, permitted reasonable inferences of response to be made.

There was no apparent influence of size, shape, or orientation (parallel or perpendicular to shock wave) on damage to unlined tunnels. However, it was evident that there was a significant increase in damage in local zones of incompetent granite.

Shock isolation materials were effective in reducing damage and shock spectra. There was little advantage of foam over cinders of comparable thicknesses. At the intermediate range, only the reinforced concrete liner with 24-inch foam survived undamaged. At the closest range, all test sections were destroyed with the exception of the reinforced concrete liner with 24-inch foam, which was very heavily damaged.

In view of the meaningful qualitative and quantitative information obtained, it is considered that the test was successful and that the general test objectives have been achieved.

PREFACE

This project was planned, designed, and conducted by Holmes & Narver, Inc., with technical guidance and assistance by the Department of Civil Engineering, University of Illinois. The advice and assistance of Dr. N. M. Newmark and Dr. J. L. Merritt, University of Illinois, during all phases of the project were particularly valuable.

The direction provided by Mr. Sherwood B. Smith, formerly Chief Research Engineer, Holmes & Narver, Inc., during the initial planning and development of the project, contributed substantially to the project.

Mr. B. H. Anderson, Sandia Corporation, assisted in the solution of problems relating to polyurethane foam and in the preparation of Appendix A. Valuable assistance was also provided by Mr. L. M. Swift, Stanford Research Institute; Mr. W. R. Perret, Sandia Corporation; Mr. F. A. Pieper, Space Technology Laboratories, Inc.; and Dr. Leonard Obert, Applied Physics Research Laboratory, U. S. Bureau of Mines.

CONTENTS

FIGURES

CHAPTER 1

INTRODUCTION

1.1 OBJECTIVES

The general objectives of this project were to obtain basic information from the effects of an underground nuclear detonation on the mechanics of tunnel damage in granite, and to relate this information to the loading and structural response of various tunnel liners subjected to such a detonation. This information was needed to establish damage-distance relationships, and to improve design criteria for tunnel liners at close-in ranges.

Among the criteria for design to be determined were specification of ranges at which liners are required, and selection of the type of liner structure suitable for a particular design requirement. In addition, transient free-field phenomena were to be determined and related to the tunnel response, in order to develop methods of predicting damage and to formulate procedures for design, based on estimated free-field phenomena.

Fulfillment of the project objectives would provide a basis for the development of criteria and procedures for the design of underground facilities in rock to provide protection against

nuclear attack. A collateral benefit would be improved design procedures for the protection of scientific equipment, and for re-entry facilities for Department of Defense (DOD) and Atomic Energy Commission (AEC) projects involving underground detonations.

1.2 BACKGROUND

1.2.1 Previous Underground Tests. Significant tests of damage to tunnels in rock from nearby explosions were conducted by the Corps of Engineers during the Underground Explosion Test (UET) series from 1948 to 1952. These tests are described in Reference 1. TNT charges ranging from 320 to 320,000 pounds were detonated in sandstone, granite, and limestone. The effects of these charges on unlined tunnels of various scaled diameters and at various scaled distances were studied. The full scale test involved 320,000 pounds of TNT and a tunnel diameter of 30 feet. This full-scale high-explosive test represented a 1/5 scale model of an explosion producing 20-kt of blast energy. The tunnel size was chosen somewhat arbitrarily, however.

Transient strains and accelerations were recorded. Pre- and postshot surveys determined the permanent displacements

and rock breakage. High-speed stereographic photography was used in an attempt to record fly-rock.

From the UET tests, tunnel damage was classified into four degrees or zones. These were designated as Zones 1, 2, 3, and 4. The characteristics of each of these zones are fully described in Section 1.4.3 of this report.

The first underground nuclear explosion in rock was the Rainier event in 1957 at the Nevada Test Site (NTS). This was a 1.7-kt device, placed at the end of a long, unlined tunnel in the Oak Spring Tuff of the Rainier Mesa. The shot room was at the end of a spiral configuration designed to induce self-sealing. The vertical depth of burial was 900 feet, and the distance to the nearest surface point on the slope of the mesa was 790 feet. The detonation was completely contained.

Some transient measurements of strain and acceleration were obtained in the tunnel and in vertical bore holes drilled from the top of the mesa, but most of the information on permanent damage to the unlined tunnel was obtained upon re-entry.

Damage-distance relationships for a nuclear detonation in tuff were established from this shot. The distances from the shot point to the point of tunnel closure and to the limiting range of damage were determined to be approximately 200 feet and 500 feet, respectively. These distances, when scaled by cube root scaling to a 1-kt yield, are 168 feet and 420 feet, respectively.

In 1958, four more essentially-contained underground nuclear explosion tests were conducted in the same general location as the Rainier event. These events, Tamalpais, Evans, Logan, and Blanca, were part of the Hardtack Phase II series. In each case, the tunnels were lined with steel horse-shoe-shaped sets and wood lagging. No significant transient measurements of structural response were obtained, but useful information on permanent damage to tunnels and tunnel linings was documented. For detailed information on the Hardtack Phase II test, see Reference 2.

The Tamalpais and Evans detonations took place at the end of tunnels with hooked configurations, similar to the tunnel used for the Rainier event. Due to the unexpected low yield from the Evans event, little information was obtained from this shot. On the other hand, the scaled damage-distance relationships from

Tamalpais compared favorably with those observed from Rainier, as indicated in Table 1.1.

The Logan and Blanca events took place in straight-end tunnels with sandbag plugs installed to provide containment. The damage to the tunnels from these shots was considerably greater than would have been predicted, based upon results of the Rainier and Tamalpais events. Table 1.1 shows that the scaled distances to points of closure for either Logan or Blanca are not consistent with Rainier and Tamalpais.

Re-entry to the Logan drift revealed that considerable energy had been transmitted through the drift before closure took place. This was evidenced by the existence of several conditions such as the translation of large lead block barricades, the extreme damage to objects installed in the tunnel, and the presence, at considerable distance from zero point, of fused rock material which had been melted from exposure to the fireball.

It was concluded, therefore, that the extreme ranges of tunnel damage for the Logan and Blanca events resulted from insufficient containment. As a consequence, the damage-distance relationships established for Rainier and Tamalpais were considered the most reliable data for contained nuclear detonations in tuff.

1.2.2 Project Lollipop. In view of the absence of a comprehensive program to study nuclear explosion effects on tunnels and tunnel liners in previous test operations, and the need for better design criteria and procedures for tunnel liners, a test program was developed by Holmes & Narver, Inc. (H&N). This program, originally planned for Project Gnome of the Plowshare Program, was submitted in April, 1959, to the Office of Test Operations, AEC, and an information copy was furnished to Headquarters, Defense Atomic Support Agency (Hq/DASA).

When the program was reviewed by Hq/DASA, it was determined that the H&N proposal was closely related to one submitted to Hq/DASA by the University of Illinois (U of I). Consequently, in July, 1959, a meeting was held with representatives of DASA, AEC, and H&N, where it was decided to combine the two proposals and include them in Project Lollipop as Program 29, Structural Response Program. Lollipop, a planned nuclear detonation in granite, was part of the Seismic Improvement Program (SIP). H&N was chosen as the project agency and was to design the experiment with technical guidance from the U of I. The Stanford Research Institute (SRI) and Sandia Corporation (SC) were named as supporting agencies to make electronic measurements of structural response and free-field effects, respectively.

Following the completion of design for the Lollipop experiment, construction started in Area 15 (Station 1500) of the Nevada Test Site in early November, 1959, and continued until October, 1960, when Lollipop was suspended. At the time, construction of 27 test sections was completed, installation of sixteen tunnel liners in the remaining test sections was in progress, and drilling for instrumentation holes had been started.

1.2.3 Project Hard Hat. During June, 1961, representatives of the cognizant agencies met at Hq/ DASA, and plans were made to resume necessary construction for completion of the Lollipop experiment as a structural effects test. This test was sponsored and executed by DOD, and was subsequently renamed Project Hard Hat.

The primary purpose of Hard Hat was to obtain data on the response of tunnels and tunnel liners in granite. All of the previous Lollipop projects, with objectives directly related to the measurement of input to, and response of, the tunnel liner structures, were included in Program 3 of Hard Hat. Accordingly, Program 3 ultimately included the following projects:

Project No.	Agency	Function
3.1	Holmes & Narver, Inc. (H&N)	Experimental Design and and Evaluation; Survey and Static Measurements
3.2	Stanford Research Institute (SRI)	Transient Response Measurements
3.3	Sandia Corporation (SC)	Free-Field Measurements
3.6	Applied Physics Research Laboratory (APRL), U.S. Bureau of Mines	Pre- and Postshot In-Situ Measurements
3.11	Edgerton, Germeshausen & Grier, Inc. (EG&G)	Fly-rock Photography
3.12	Space Technology Laboratories, Inc. (STL)	Shock Spectra Measurements

Information needed for analyses of loading and response of the tunnel liners was to be obtained by each of the above agencies.

1.3 SITE GEOLOGY

Project Hard Hat was located in an intrusive mass of granitic rock, called the Climax stock, in Area 15, NTS. Detailed descriptions of the geology of this area are given in References 3 and 4.

It is generally accepted that the stock was intruded from depth into a sequence of Paleozoic carbonate rocks. Subsequent erosion of the carbonate rocks exposed the granitic mass at the surface. Following the erosion cycle, an extended period of volcanic activity deposited a thick sequence of beds of volcanic tuff, commonly known as the Oak Spring formation. These tuff beds appear to have blanketed the entire area. After the deposition of the tuff, erosion again took place, and this resulted in the re-exposure of the Climax stock at the surface.

The surface exposures of the Climax stock and adjacent rocks are shown in Figure 1.1. It can be seen that the outcrop of the stock takes the general shape of the letter "L", each limb being about 2,500 feet wide and about 6,500 feet long. It is inferred from geologic mapping and limited subsurface exploration that the intrusive contact of the granitic rocks with the carbonate rocks dips about 45^{o} or more, away from the exposed granitic mass, as illustrated in Figure 1.2.

A relatively straight contact between the stock and the bounding sediments may be observed along the southeast portion of the stock. This is due to a vertical fault along which Yucca

Valley has dropped downward as a block. The magnitude of the movement is estimated conservatively as being several hundred feet.

The Climax stock consists of two large masses of very similar granitic rocks in distinct contact with one another. The northern limb of the exposed outcrop is a medium-grained granodiorite. It is in contact with a predominately medium-grained, partially porphyritic quartz-monzonite, which occupies the southern limb and the entire southeastern boundary. These two rock types have been differentiated on the basis of a subtle difference in the abundance and type of feldspar and free silica constituents. However, these differences are so slight as to be of little consequence to the engineering aspects of Project Hard Hat.

Microscopic analyses indicate that the rock composing the stock contains between 27 and 29 percent quartz, 60 and 65 percent feldspars, and four and seven percent biotite. It further contains about one percent accessory minerals and about two or three percent derived by alteration of the above minerals. Detailed chemical analyses given in Reference 5 show further similarities in the granodiorite and quartz-monzonite.

Weathering had reduced most of the surface rock to small, blocky outcrops, partially covered and surrounded by coarse quartzose sand, commonly known as decomposed granite. The thickness of the weathered layer is generally only a few feet, although iron oxide staining along fracture planes and other oxidation effects are abundant to depths of thirty feet or more. Although these features decrease with depth, iron oxide staining of fracture surfaces has been noted at all explored depths. Observations extended to a depth of 1,000 feet.

Physical discontinuities in the form of faults, fractures, and joints are relatively abundant throughout the Climax stock, without observable variance in distribution between the two mapped lithologies. Most of the faults, joints, and fractures observed on the surface in the construction area cannot be traced or accurately projected for more than a few tens of feet, due to covering by the weathered layer. Most of the faults and shear zones observed underground are nearly vertical, and strike west of north, as can be seen in Figures 1.3 through 1.5 (from Reference 6). From the available evidence, these faults and shear zones appear to be present in many places in the Climax stock.

Joints are present in most places, as is commonly the case in most masses of intrusive rock. Their development is attributed to cooling stresses, relief of overburden pressures, and tectonic movements. Three principal joint sets are present in the Climax stock. The most prominent joint set is inclined about 20° from the horizontal in a northeasterly direction. The other two joint sets occupy two approximately vertical groups of planes, each normal to the other. One joint set strikes northeasterly and the other southeasterly. The spacing between the joint planes is very frequently less than one foot. This results in separating the stock into a sequence of close fitting, angular blocks, generally less than one cubic foot in volume. Figures 1.6 and 1.7 are photographs of jointed and fractured rock revealed in the underground excavation.

The joints and the faults are generally permeable to water at shallow depths. With increasing depth, the joints tend to be tight and/or healed with introduced materials; therefore, permeability is reduced. During shaft excavation, a total water flow of approximately one gallon per minute was encountered. This was observed to have originated along the approximately horizontal system of joints mentioned previously. Seasonal and

cyclical fluctuations of seepage have been observed, which indicate that the water is of meteoric origin.

Hydrothermal alteration has apparently pervaded the entire Climax stock and has affected the physical properties of the original rock, to varying degrees, through chemical changes in the constituent minerals. Alteration has been most intense along shear zones or fault zones which afforded passage for the rising hydrothermal solutions. In these zones, the rocks have been substantially weakened through conversion of the fresh, hard feldspars and ferromagnesian minerals to clays and friable minerals. The intensely altered rock is weak and crumbling. Although the intensity of hydrothermal alteration decreases with distance from the larger fault and shear zones, most of the rock in the Climax stock is affected to some degree by the alteration. It has been estimated that the average rock in the Climax stock contains approximately three percent alteration products.

Physical tests were made on representative rock specimens taken from an exploratory core hole. Eight unconfined compressive strength tests indicate that the ultimate strength of the rock is between 6,720 psi and 23,800 psi. Although the

ultimate strength of the rock is not uniform, it tends to increase with depth.

Determinations by the Lawrence Radiation Laboratory (LRL) of the University of California (see Reference 6) show that the average bulk specific gravity of the rock mass is approximately 2.66. Tests of samples from the most highly altered zones indicate a minimum specific gravity of 1.80. The average water content of the rock was approximately one percent. Porosity of the rock as a whole, both altered and unaltered, is essentially zero.

The rock is permeable only along shear and fracture zones, as mentioned above. These tend to become closed with depth, or healed with introduced material or alteration products.

1.4 THEORY

1.4.1 General. The detonation of a contained underground nuclear device results in a sudden release of energy which creates a roughly spherical cavity around the point of detonation. This energy, emerging from the cavity, heats and crushes the surrounding medium to a distance consistent

with such variables as the size of the explosion, the strength of the medium, and the efficiency of coupling and confinement.

In a zone beyond the limit of crushing, known as the plastic zone, this energy, in the form of a stress wave, continues to produce permanent deformation by plastic flow until the peak stress of the stress wave has decreased to a value equal to the dynamic yield strength of the medium. Beyond the limit of the plastic zone, the stress wave propagates elastically at the seismic velocity characteristic of the medium. Properties of the wave, such as peak stress, rise-time, and pulse duration, are continuously altered as the wave moves away from the point of detonation.

Upon reaching a boundary surface, such as a tunnel wall, the wave is reflected. Interaction between the reflected pulse and the trailing portion of the incident pulse may produce tension which may cause detachment of portions of the surrounding medium.

As the wave passes, the tunnel opening is translated and is subjected to stresses which tend to close the opening. In any

case, damage to the opening occurs when the stresses around the opening exceed the ultimate strength of the material.

The mechanics of tunnel failure, due to an underground nuclear explosion, are complex and not too well understood. However, from previous underground tests, data were available on free-field effects, such as stress, strain, and particle motion, from which the shock parameters for this project could be estimated by extrapolation. With these estimates of the free-field effects and with an assumed stress field, the stresses around a tunnel opening could be computed. Therefore, the estimation of free-field effects was of importance in the planning of this project.

Two approaches, which formed the basis for the design of this experiment, were used to estimate the response of tunnel opening. The first was an analytical approach using the free-field particle motion (accelerations) and strain data, together with wave theory, to estimate the modes of response. The second was an empirical approach involving extrapolations of the damage-distance criteria obtained from previous high explosive tests in granite, as well as previous underground nuclear tests in tuff. The two methods used are presented below.

1.4.2 Method I, Analytical Approach. In making these analyses, it was assumed that the major effects in the range of interest would be caused by the compression wave (P-wave). However, the possible presence of a shear wave (S-wave) was also considered. Reference 7 gives expressions for stress, strain, and particle motion of the granite medium for this project. These expressions take into account the test data from the UET experiment and the Rainier event.

Particle velocity was related to the strain by means of plane wave theory. A nuclear equivalence factor relating nuclear blast energy to that of high explosives (TNT) was derived, based on equivalent strain value. With minor modifications, the expressions given in Reference 7 are plotted in Figure 1.8 and 1.9 for a 5-kt yield. The assumed physical properties for granite were as follows:

Modulus of elasticity	8,000,000 psi
Seismic velocity	16,000 fps
Compressive strength	25,000 psi
Tensile strength	1,000 psi

Compressive strain at failure	0.01 in/in
Tensile strain at failure	0.0005 in/in
Density	173 pcf

When a stress wave passes a circular tunnel opening, the resulting stress distribution depends on the general dynamic or transient character of the stress field. With little error and for reason of simplicity, it was assumed that the stress distribution follows that of a static stress field having a magnitude equal to the maximum transient value. It was reasoned that this approach was justified in view of the uncertainties in the estimation of the free-field effects. The stress distribution at the circular boundary due to various static stress fields is shown in Figure 1.10. The stress distribution in the medium near the boundary surface for various static stress fields is shown in Figures 1.11 through 1.13. Possible modes of failure for a circular opening are as follows:

Compressive Failure. This occurs when the maximum compressive stress around the opening exceeds the compressive strength of the rock.

The boundary stress concentration at critical points around a circular opening can be two, three, or four times the free-field stress, depending on the stress field, i.e., hydrostatic compression, uniaxial compression, or compression in one direction and tension in the perpendicular direction, respectively. The latter state of stress corresponds to a condition of pure shear from shear waves which, within the range of test drifts, was considered unlikely to occur. It was assumed, therefore, that the compression wave would produce the major effects and that the maximum stress concentration factor applicable to elastic conditions would be between two and three for a circular opening. On this basis, it was estimated, for this project, that the distance to which the granite would be crushed around openings causing closure would be between 240 feet and 290 feet from the point of detonation. If the effect of the shear wave had been considered

to predominate, this distance would have been approximately 330 feet because of the greater stress concentration factor of four for a shear wave.

Tensile Splitting. If the state of stress around an opening is uniaxial compression, the peak tensile stress in the rock at the boundary is equal in magnitude to the free-field compressive stress at some distance removed from the opening. Based on this assumed state of stress, it was estimated for this project that rock falls due to tensile splitting would occur as far as 740 feet from the point of detonation. Had the effect of shear wave been considered, the range of tensile splitting would have been estimated at approximately 1,500 feet.

Spalling. When a compression wave reaches an extensive free-face, two reflected waves may be generated. These are primarily a reflected tensile wave and, probably to a lesser degree in effects, a shear wave. The reflected tensile wave tends to

break the rock at a point where the magnitude of the reflected tensile wave exceeds that of the oncoming compression wave by an amount equal to the algebraic sum of the ultimate tensile strength and the lithostatic stress of the rock. In general, the rock tends to fail parallel to the free surface. In estimating the spall or scab thickness, a triangular-shaped wave with instantaneous rise-time was assumed. The spall thickness is proportional to the pulse length and tensile strength of the rock and inversely porportional to the magnitude of the compressive pulse. In the case of a circular opening, a spall thickness greater than the tunnel diameter cannot form completely. For this project, calculations indicated that beyond 300 feet from the point of detonation spalling would not occur.

1.4.3 Method II, Empirical Approach. The second method used to estimate the response of the tunnel openings was by extrapolation of test results obtained in the UET series, the Rainier event, and Hardtack Phase II events. Account was taken of the differences in media, energy source (chemical

vs. nuclear equivalent), degree of containment, and other factors. Four zones of damage, as defined in the UET series (Reference 1), are described in terms of the damage profile of the tunnel surface nearest the charge. Figure 1.14 shows a typical damage profile with the damage zones as labelled.

Zone 1. The outer limit of Zone 1 is that point where the damage profile begins. The rock is completely crushed out to a point defined by the compressive strength of the rock. Beyond the area of complete crushing, the rock is broken from all sides of the tunnel, completely closing the tunnel. A damage profile does not exist in this zone. Indications from limited test observations by motion picture photography show that fly-rock may have a maximum velocity of about 100 ft/sec, with lower velocities for the larger masses of rock. The rock is propelled radially from the charge. When scaled to the anticipated yield for this project, the outer limit of Zone 1 would be approximately 190 feet from the point of detonation.

Zone 2. The outer limit of Zone 2 is that point where the general shape of the damage profile changes from a line distinctly inclined to the original tunnel surface to a line nearly parallel to the original tunnel surface. The rock breakage is continuous and increases in thickness nearer to the explosion. The breakage extends far around the tunnel. Large volumes of rock are broken, and the pieces are coarse and block-like. The general shape of the damage profile is a line distinctly inclined to the original tunnel surface. The damaged area varies from 30 to 80 percent of the original cross-sectional area of the tunnel. The maximum fly-rock velocity ranges from 30 to 60 ft/sec. The rock is propelled radially from the charge. Calculations indicated that the outer limit of Zone 2 for this project would be approximately 340 feet from the zero point.

The point of closure of the tunnel occurs within Zone 2. Based on data in Reference 2, this distance was estimated to be about 300 feet from the point of detonation.

Zone 3. The outer limit of Zone 3 is that point at which rock breakage and the damage profile become discontinuous. The rock breakage is continuous and relatively uniform in thickness; it is principally on the side toward the explosion. The damaged area varies from 5 to 30 percent of the original tunnel cross-sectional area. The maximum fly-rock velocity is about 20 to 30 ft/sec, and the larger rocks are believed to fall almost vertically. Calculation indicated that outer limit of Zone 3 for this project would be approximately 520 feet from the zero point.

Zone 4. The outer limit of Zone 4 is that point beyond which no significant rock breakage occurs. The rock breakage is

irregular and intermittent; breakage may include the dislodging of material previously loosened by tunnel driving. The damage profile is discontinuous in this zone. The damaged area increases the cross-sectional area of the tunnel from zero to five percent. Maximum fly-rock velocity is about two ft/sec. Available evidence indicates that the rocks drop vertically. Unlike the three zones of damage mentioned above, the estimated outer limit of Zone 4 for this project was based on UET data on sandstone, rather than granite, because such data agree closely with those of the previous contained underground nuclear tests. The limit of Zone 4 from the zero point was thus calculated to be 750 feet.

1.4.4 Comparison of Methods I and II. Results of the estimated effects based on the foregoing two approaches generally gave comparable results. These results are shown schematically in Figure 1.15.

It can be seen that the analytical estimates of compressive failure and tensile splitting agree closely with empirical damage-distance observations. The limiting range for spalling, as shown, is somewhat less than that observed in previous high explosive tests. The spalling range of a nuclear explosion is generally thought to be less than that of a chemical explosion, because the pulse length may be longer for the nuclear case. This produces a potentially larger spall thickness at each zone of damage. The relatively small size of the tunnel openings in this project limits the formation of spalls to a lesser scaled range than those observed in the UET tests.

In summary, the estimates of tunnel response by the two methods are considered to be consistent. These estimates formed the basis for the experimental design in the selection of the number and location of the test drifts relative to the zero point and the design of the tunnel liners.

1.4.5 Requirements of Tunnel Liners. In determining the requirements for tunnel liners to resist the effects of the estimated free-field phenomena, an analysis was first made to find the proportions of a perfect liner.

The perfect liner is defined as one which has the same deformability as that of the medium (granite in this case) it replaces. If a circular steel liner is to have the same deformability as the excavated medium under a uniform radial loading, the required liner thickness is proportional to the ratio of the modulus of elasticity of the liner to that of the medium.

For uniform loading in granite, the steel liner thickness would be more than one-quarter of the tunnel radius. Furthermore, under an anti-symmetrical four-lobed sinusoidal loading, pushing inward at the sides and outward at the top and bottom (see Figure 1.16), the required liner thickness is proportional to the cube root of the ratio of the modulus of elasticity of the liner to that of the medium. In the latter case, the steel liner thickness would be almost two-thirds of the tunnel radius, in order to have the desired deformability. Consequently, it was impractical to consider liners of sufficient proportions to restore the effectiveness of the excavated granite.

Since the required thickness for a liner consistent with the full strength of the rock excavated is, for most cases,

unreasonably large, the design of tunnel liners of lesser proportions requires consideration of the motion of the opening and the response of the liner.

Because the motion of the rock can not be well defined for any given design condition, a composite type of tunnel liner, capable of functioning over a wide range of rock motion, offers advantages not available in a simple type of liner. For example, if a crushable filler or backpacking material of sufficient thickness were placed between the rock wall and the tunnel liner, the rock wall could distort and partly close up without coming into physical contact with the liner itself. The backpacking material could absorb much of the kinetic energy from potential fly-rock and distribute concentrated loads, so that the lining would be subjected to a reduced loading. Furthermore, the motion of the medium, as characterized by acceleration, velocity, and displacement, could be attenuated when transmitted through the backpacking to the liner. Hence, the composite liner type was chosen as the basic structural unit to be experimentally evaluated. A circular shape was chosen as the basic configuration.

The design criteria used in proportioning the backpacking thickness and liner design were based on the following considerations. The thickness and the strength of the backpacking material were based primarily on the requirement to absorb the fly-rock energy. This energy was determined from the estimated quantity and the velocity of the fly-rock. The energy absorption properties of the backpacking material are a function of its stress-strain characteristics.

It is shown in Reference 7 that a strong backpacking material would not be required to stop the fly-rock at distances beyond the point of closure; materials of low strength, of the order of a few hundred psi, could effectively resist the fly-rock. Also, the required thickness of the backpacking depends on the distortions of the rock wall. Sufficient thickness must be provided to allow deformation of the backpacking without transmitting undue loads to the liner or permitting the rock to come into contact with the liner.

For a given thickness and strength of the backpacking material, the liner design was based on consideration of the interaction of the liner with the backpacking. If the liner

were to deform into an oval shape under a given load, it would meet with resistance at the ends of the long axis. The ovalling tendencies of the liner could then be considered to be a result of two components of backpacking loading. One would correspond to a uniform radial compression, and the other may be taken as a four-lobed sinusoidal variation, with inward and outward radial loading alternating over the quadrants of the liner. Figure 1.16 illustrates such component or modal loadings.

The contribution of each of the two component loadings for a given backpacking material is a function of the flexibility or stiffness of the liner. For a highly flexible liner, the backpacking and liner interaction would result in the liner ovalling until the loading became essentially a uniform radial compression component. Conversely, for a rigid liner, the backpacking and liner interaction generally would produce an alternating component loading because of the greater flexural resistance to ovalling.

For a given liner, the contribution of each component loading may be computed by considering the static equilibrium and by satisfying the conditions of consistent deformations of the liner under the action of two component loadings. In any

case, the minimum strength requirement for a liner is governed by the uniform component loading acting alone, and the maximum strength requirement can be determined by the flexural component loading acting alone. The design of the composite liners used in this project was based on these theoretical considerations.

1.5 EXPERIMENTAL CONCEPT

1.5.1 Experimental Plan. The estimated magnitudes of free-field effects and tunnel response at various ranges, based on consideration of simple wave theory and extrapolation from previous test results, are approximate, at best. Because of these approximations, three drifts were placed within zones of anticipated heavy, intermediate, and light damage, respectively. Several types of experimental and conventional liners were designed and selected for testing. The same liner types were placed in all three drifts to obtain a distinct gradation of effects. This experimental concept was opposed to one that was considered less flexible, i.e., the test liners in each of the three test drifts would be designed for the estimated effects associated with their particular range. The concept used provided a broader coverage against possible extreme variations in the loading and response

from the estimated effects, thus assuring fulfillment of project objectives.

Placement of identical liners at the three different ranges provided a direct inter-drift comparison of the response. Also, placement of various types of test liners at the same range provided a direct intra-drift comparison between basic structural types. Moreover, indirect comparison of a given liner type and range, with another liner type and range, were possible by analytical means. Hence, sufficient test data to permit comprehensive parametric studies were assured under this experimental concept and plan.

In selecting the locations of the three test drifts, the concept was to place the closest group of test sections at such a range that the intensity of the effects would be likely to cause complete collapse of the test sections. The farthest drift was so placed that test sections contained therein would experience some plastic distortion. The location of the middle drift was determined by taking the geometric mean distance of the closest and farthest drifts. This was done because data from previous underground detonations indicated that the shock effects generally attenuated as a logarithmic function of range. The foregoing concept of drift locations is treated in greater detail in Reference 8.

The drifts were designated as A, B, and C, with Drift A being closest to the point of detonation. The distances from the zero point to the test drifts and access shaft were to be as follows:

Drift A	250 feet
Drift B	350 feet
Drift C	500 feet
Access Shaft (horizontal distance)	800 feet

During construction, a fault zone was encountered near Drift C, resulting in construction difficulties. For this reason, and to avoid locating Drift C in an incompetent rock, the nominal drift locations, based upon the assumed zero point location, were revised. Again, the geometric progression was used in determining the relative ranges of each drift. The planned locations were:

Drift A	250 feet
Drift B	340 feet
Drift C	460 feet

For a final layout of the shaft, access tunnel, drifts, and zero point, based on the actual Hard Hat point of detonation, see Figure 1.17. The elevation of the test drifts was higher than the point of detonation, so that Drifts B and C would not be shielded by Drift A or B.

Within the three test drifts, the following general types of test sections were planned for testing: (1) unlined square and circular sections without reinforcement; (2) square and circular sections reinforced with rock bolts and wire mesh; (3) circular liners with two kinds of backpacking material (three types of such composite liners were chosen: rigid liner—reinforced concrete, flexible liner—corrugated steel liner plate, and rigid-flexible liner—steel rings with lagging); (4) conventional steel horseshoe-shaped sets with wood lagging; and (5) circular reinforced concrete liners cast against rock.

These liner types are illustrated in Figures 1.18 through 1.25 and their locations and designations are summarized in Table 1.2. A three-character designation was assigned to each test section. The first character denotes the drift location, the second refers to the type of liner, and the third represents the type of backpacking associated with each type of liner. The arrangement of the test sections is shown in Figure 1.26. Each type of test section was placed in Drift B, with an identical test section duplicated in either Drift A or C. Some test sections were duplicated in both Drifts A and C. There were 43 test sections, of which 30 contained liners with backpacking.

All test sections were nominally 15 feet in length. The excavated diameters varied in accordance with the type of test sections; however, the nominal inside diameters of all liners were six feet. A nominal spacing of two feet between test sections was provided. A plane, containing the longitudinal axis of the test section and passing through the zero point, was used as a zero degree reference for each test section, as can be seen in Figures 1.18 through 1.25. The arrangement of the test liners within each test drift was generally based on ease of construction and drainage. Another consideration was the desirability of placing similar liners together, to facilitate comparison of response. In general, the test sections requiring the largest diameters of excavation were placed closest to the access tunnel. This arrangement minimized abrupt changes in diameter between adjacent test sections. Sections without liners were placed at the ends of test drifts to facilitate re-entry, since these sections were expected to be the most severely damaged.

1.5.2 Data Requirements. Two general methods were considered necessary to acquire the required data for this experiment. They were physical measurements and visual observations, as described below:

Measurements. An extensive measurement program was planned to obtain the necessary data on the free-field effects, the response of the tunnel opening, the interaction of the tunnel opening with the liner, and the response of the liner. The shock attenuation afforded by the backpacking material was also to be measured. The means for measuring the transient phenomena and permanent deformations are described in Section 2.2. They are broadly classified into four general categories: (1) Electronic—these instruments measure the transient effects during the event and record remotely at a surface station. The records give a time history of the phenomena measured; (2) Mechanical—these gages measure the transient peaks and residual deformations. A time history is normally not provided, and the gages must be recovered to obtain the data; (3) Photographic—motion picture camera equipment is used to record transient effects in the test drifts. The film must be recovered after the event for analysis, (4) Static—

these are pre- and postshot measurements using surveying methods and mechanical extensometers for precisely determining physical demensions.

The most useful records of the transient phenomena are those provided by the electronic gages. The instrumentation plan was designed to measure the essential transient effects by electronic gages, augmented by a comprehensive mechanical, photographic, and static measurement program. The number and types of planned measurements are summarized in Table 1.3.

The Instrumentation Plan (Figure 2.38) shows the locations of the planned measurements. A composite test section, depicting the types of electronic measurements, is also shown in this figure.

In selecting the instruments, an estimate of the magnitudes of the anticipated effects was necessary to properly evaluate the sensitivity required. The estimates developed by the U of I are given in Table 1.4.

They were also used as a basis for designing the mechanical scratch gages for this project.

Damage Observations. A comprehensive visual examination of the damage sustained by underground openings was considered essential to a complete understanding of the mechanics of tunnel and tunnel liner failure, and to establish damage-distance relationships for conventional openings in granite. It was anticipated that the following observations would be made during the postshot re-entry phase: (1) characteristics of rock breakage at various ranges; (2) effects of faults, joints, and other geologic discontinuities on damage; (3) effects of size and shape of opening on damage; and (4) mechanics of failure of the various types of tunnel liners.

1.6 EXPERIMENTAL DESIGN

1.6.1 Distribution of Test Liners. In the design of the tunnel liners for this project, the composite liner, which has been defined as a circular liner with a backpacking material, was selected as the basic liner type.

To obtain a comprehensive evaluation of the influence of the backpacking characteristics and the liner characteristics on the structural response, two backpacking materials and three types of liners were used. The two backpacking materials were polyurethane foam and volcanic cinders. The three liner types were:

(1) flexible type—corrugated steel tunnel liners,

(2) rigid type—circular reinforced concrete sections, and

(3) rigid-flexible type—rigid steel rings with flexible longitudinal lagging.

Four backpacking thicknesses and two liner strengths were used to obtain a further comparison of backpacking and liner variations. The composite liners are located in the test drifts, as summarized in Table 1.5.

To obtain a comparison of the thirty liners having backpacking with other types of construction, thirteen test sections without backpacking were located within the three drifts. These

included unlined circular and square openings, circular and square openings reinforced with rock bolts and metal mesh, reinforced concrete liners cast against the rock, and horse-shoe-shaped steel sets with wood lagging. The distribution of the liners without backpacking is shown in Table 1.6.

1.6.2 Design of Test Liners. In the design of the composite liners, three of the liners were proportioned based on the use of nine-inch-thick foam as backpacking. These three liners were: (1) steel wide-flange rings with three-inch-thick wood lagging, (2) steel wide-flange rings with steel lagging, and (3) twelve-inch-thick reinforced concrete. It was assumed that the foam would be an ideal elasto-plastic material with an extensive plastic strength of 150 psi. On this basis, the design of the tunnel liners could proceed without knowing the exact distortional and translational motion of the tunnel opening, provided that the liner was located in a region where the foam would not be compressed beyond the plastic range into the locking range, where the compressive stress increases rapidly.

The dynamic and inertial forces were not considered in the design, because the same liner was to be placed at three different

ranges to obtain a gradation of the dynamic effects. Furthermore, preliminary test results indicated that polyurethane foam exhibits little or no increase in yield stress under rapid rate of loading. Hence, for design purposes, the above three liners were proportioned based on static loading of 150 psi.

The increased strength of materials for steel, wood, and concrete, due to rapid rate of loading, was used in the design. Also, ultimate strength design procedures were followed to effect a more realistic estimate of the structural resistance of the tunnel liner. A nominal factor of safety of one was used.

The steel and wood laggings used with the steel wide-flange rings were designed as continuous longitudinal members over several supports under a uniform 150-psi loading. Possible arching action of the backpacking was neglected. The steel wide-flange ring was designed to develop the full strength of the lagging under dynamic loads, taking into consideration both the symmetrical and the anti-symmetrical modes of loading in the plane of the ring.

The design of the 12-inch-thick reinforced concrete liners was based on the interaction of the liner and the foam backpacking.

For example, if the distortion of the tunnel opening were assumed to be uniformly radial, and to cause the foam to yield, the foam would transmit a constant pressure to the concrete liner. In this case, the liner need be only of sufficient strength to resist a uniform radial loading equal to 150 psi.

Actually, the loading on the concrete liner would not be uniformly radial because of possible fly-rock, ovalling of the opening, or translation of the opening. The effects of these and other phenomena are neither well understood nor precisely defined; hence, for design purposes, it was assumed that any unsymmetrical loading on the foam backpacking would transmit a maximum of 150 psi to the liner. This unsymmetrical loading would tend to deform the liner into an oval shape and develop reaction stresses at the ends of the long axis of the deformed liner. This interaction of the liner and backpacking was discussed at some length in Section 1.4.5.

The remainder of the test sections were selected on the basis of the following considerations.

First, in selecting a thickness for the thicker foam, consideration was given to the practical mining tolerances imposed

on the excavation of the test drifts. With the specified construction tolerances, as shown in Figure 2.3, the nominal nine-inch foam which constitutes the basic liner design could be as thick as fourteen inches. If a nominal 24-inch foam was used, the permissible tolerances could limit the foam thickness to a minimum of 21 inches which, as compared with the 14-inch foam due to over excavation, would be greater by at least 50 percent. It was believed that this difference in backpacking thickness would be the threshold of noticeable effects in liner response. Consequently, the thickness was established at 24 inches.

As mentioned in the case of the nine-inch foam, it was assumed that a maximum pressure of 150 psi would be transmitted to the liner. This same assumption holds true for the 24-inch foam when strained beyond its elastic limit. The required reinforced concrete liners for the two different foam thicknesses are nearly the same, although the reaction stresses for the two cases, mentioned previously, are different. However, in order to augment the noticeable differences in liner response, the effective flexural depth of the liner associated with the 24-inch foam was arbitrarily reduced about 50 percent while keeping the

same percentage of steel reinforcement. This resulted in the selection of the eight-inch reinforced concrete liners.

For the corrugated steel liners, the heaviest catalogued tunnel liner plate from one manufacturer was chosen. A thinner plate was also selected, so that the ratio of its thickness to that of the thicker plate was approximately the same as the ratio of the eight-inch to 12-inch reinforced concrete liners. This was the basis for the selection of the three-gage and the eight-gage corrugated steel liners.

In order to compare the effectiveness between the foam and the volcanic cinders as backpacking materials, most of the test liners with foam were duplicated using cinders as backpacking. The nominal thickness of the cinders was nine inches.

The reinforced concrete test sections cast against rock were the same as the 12-inch concrete liners with nine-inch foam. It was believed that by keeping the same strength in the two liner types, a direct comparison of their response would be facilitated.

The test sections composed of steel horseshoe-shaped sets with wood lagging were identical to the ones used in the tunnels in the Rainier Mesa during the Hardtack Phase II test series (1958). They were included in this experiment for a comparison of damage in tuff and granite.

For the unlined test sections reinforced with rock bolts and mesh, the rock bolt pattern and the method of installing the mesh, followed conventional tunnel practice. These and the test sections without rock bolts were included to permit response comparisons between lined and unlined test sections. No design was involved in the unlined sections.

1.6.3 Physical Properties of Backpacking Materials.

Polyurethane Foam. An idealized stress-strain diagram of the polyurethane foam, with values of stress and strain that were used in design, is shown in Figure 1.27.

The extensive horizontal region of the stress-strain curve indicates that the material undergoes

considerable plastic deformation without a substantial change in stress. This characteristic is desirable in an energy-absorbing backpacking material. Foam having a suitable yield stress may be selected to meet a particular shock isolation requirement. Figure 1.28 shows a stress-strain curve from an unconfined compression test of a foam sample from test section B6b. Tables 1.7 and 1.8 list the properties of the foam sampled in the various test sections.

As described in Appendix A, polyurethane foam is generally not an isotropic material because of its cellular structure. The compressive yield stress parallel to the direction of foam rise is generally greater than that perpendicular to the rise. The foam yield strength used for design (150 psi) was assumed to be the average value in the the two directions because of the uncertainties involved in the actual orientation of foam cast-in-place in the field.

Cinders. The cinders used in this experiment were from volcanic ash. This material is readily available from volcanic cinder cones throughout the western United States. The material used for this project was obtained from a cinder cone located approximately 70 miles north of NTS. The cinders are reddish-brown in color and were screened for a maximum size of 3/4 inch and a minimum size of 1/4 inch. Bulk density when dry is about 32 pcf. The stress-strain curve for the cinders is generally concave upward. Figure 1.29 shows a typical stress-strain curve (Reference 9) for the cinders used. In the confined compression tests, the cinders were contained in a rigid metal cylinder, 25/32 inch thick, seven inches inside diameter, and seven inches high. The loading device consisted of a stiffened piston, 6-7/8 inches in diameter and 7-1/4 inches high. The cinders were placed in the cylinder, and the density was determined in accordance with the procedures outlined in the American Society for Testing Materials Standards C29-55T, except that each layer was rodded

20 times, using a 1/2-inch-diameter rod. This tamping accounts for the higher density than the bulk density mentioned above. For a detailed description of the compression tests, see Reference 9.

It was expected that cinders as a backpacking material would not be as effective as foam, due to the absence of an extensive horizontal region in the stress-strain curve. However, cinders were used in this experiment to obtain a comparison with foam.

Lightweight Concrete. Because of the difficulties encountered in the installation of polyurethane foam during the initial construction phase of the experiment (See Chapter 2), alternate backpacking materials with physical properties similar to the foam were sought. As a result of this investigation, two air-entrained lightweight concrete mixtures were developed. These were, first, an aerated concrete, using expanded perlite as an aggregate; and, second, a simple aerated cement mixture. Although both displayed desirable stress-strain characteristics under static loading, they were considered unsatisfactory for application

in underground protective construction because of their permeability. In a wet environment, these materials would become saturated, thereby subjecting the liners to hydrostatic loading with little attenuation in the event of a suddenly applied load. Attempts to waterproof the aerated cement by means of bituminous additives were unsuccessful within the limited scope of this work. Additional information on the design and characteristics of these lightweight concrete mixtures may be found in Appendix B.

1.6.4 Physical Properties of Liner Materials. In order to minimize the number of variables which would have to be considered in postshot analysis, all like liner materials were planned, insofar as possible, to have the same physical properties. To accomplish this, a specific concrete mix design was used rather than merely specifying a minimum 28-day compressive strength. Also, all steel liner materials of the same size and type were specified to be from a minimum number of mill heats. This included all reinforcing steel of a given size, all 3-gage corrugated liner plate, all 8-gage corrugated liner plate, all wide flange

rings, and all steel lagging. Specimens from each mill heat were tested by the U of I, except the reinforcing steel used in the initial phase of the construction, which was tested in the fabricator's plant. The concrete cylinders and foam specimens were tested by commercial laboratory under contract to H&N. Tables 1.9 through 1.12 contain the results of the tests of liner properties.

Flexible Liner. Corrugated steel tunnel liners were selected as representative of flexible liners. The average static strength properties of the material used are given in Table 1.9.

Rigid Liners. Circular reinforced concrete sections were representative of the rigid liners. The structural properties used for design were as follows:

Dynamic modulus of elasticity, concrete	=	3,200,000 psi
Dynamic compressive strength, concrete	=	4,000 psi
Dynamic tensile strength, steel	=	50,000 psi

The actual strength properties, as determined by static tests of concrete cylinders and reinforcing bars, are given in Table 1.10.

Rigid-Flexible Liners. Heavy steel rings with longitudinal timber or steel lagging were representative of the rigid-flexible liners. The structural properties used for design were as follows:

Dynamic yield strength, steel	=	42,000 psi
Dynamic flexural strength, wood	=	6,000 psi

The properties, as determined by laboratory tensile tests, are given in Table 1.11.

Horseshoe Sets. The properties of the steel horseshoe sets are given in Table 1.12.

TABLE 1.1 SCALED DISTANCES OF CLOSURE AND LIMIT OF DAMAGE

Event & Tunnel	Tunnel Configuration	Distance Zero Point to Closure (feet)	Yield (kt)	Distance to Point of Closure Scaled to 1-kt (feet)	Outer Limit Zone 4, Scaled to 1-kt (feet)
RAINIER U-12b	Hooked	200	1.7	168	420
TAMALPAIS U-12b.02	Hooked	80	0.09	179	420 (Approx.)
LOGAN U-12e.02	Straight	820	4.5	496	1190 (Approx.)
EVANS U-12b.04	Hooked	Unknown	0.045	Unknown	Unknown
BLANCA U-12e.05	Straight	870	23	306	690 (Approx.)

TABLE 1.2 TEST SECTION SCHEDULE

TEST SECTION DRIFT				SHAPE	LINER TYPE	BACKPACKING
	B	C	1a		Unlined	NONE
	B	C	1b		Lined with Rock Bolts & Wire Mesh	NONE
	B	C	2a		Unlined	NONE
	B	C	2b		Lined with Rock Bolts & Wire Mesh	NONE
A	B	C	3a		Reinforced Concrete	NONE
A	B	C	3b		Reinforced Concrete	FOAM
A	B	C	3c		Reinforced Concrete	FOAM
A	B	C	3d		Reinforced Concrete	CINDER
A	B	C	4a		Steel Set with Steel Lagging	CINDER
A	B	C	4b		Steel Set with Steel Lagging	FOAM
A	B	C	4c		Steel Set with Wood Lagging	FOAM
A	B		5a		3 Gage Steel	FOAM
A	B		5b		3 Gage Steel	FOAM
A	B		5c		3 Gage Steel	CINDER
	B	C	6a		8 Gage Steel	FOAM
	B	C	6b		8 Gage Steel	FOAM
	B	C	6c		8 Gage Steel	CINDER
	B	C	7a		Steel WF & Wood Lagging	NONE

TABLE 1.3 MEASUREMENT PLAN

		ELECTRONIC			MECHANICAL			PHOTOGRAPHIC			STATIC			
	TEST DRIFTS →	A	B	C	A	B	C	A	B	C	A	B	C	TOTALS
TUNNEL RESPONSE	Circumferential Strain in Rock	2	18	0										20
	Radial Strain in Rock	1	7	0										8
	Shock Spectra in Access Tunnel				1	2	*4							7
	Absolute Displacement										(SURVEYING)			
TUNNEL-LINER INTERACTION	Fly-rock Velocity							0	2	1				3
	Pressure on Lining	4	11	2										17
	Compression of Filler	0	2	0	27	36	27				45	60	45	242
LINER RESPONSE	Lining Velocity	7	13	1										21
	Circumferential Strain in Lining	3	13	0	50	70	55				20	36	30	277
	Longitudinal Strain in Lagging	0	2	0	0	0	0				15	15	15	47
	Diameter Change in Lining	9	12	1	20	38	32				20	38	32	202
	Shock Spectra in Lining				3	6	4							13
TOTALS		26	78	4	101	152	122	0	2	1	100	149	122	
		108			375			3			371			857

* (Including 2 @ 723')

TABLE 1.4 ESTIMATES FOR INSTRUMENT SETTINGS

			UNITS	DRIFT A			DRIFT B			DRIFT C		
				min.	ave.	max.	min.	ave.	max.	min.	ave.	max.
TUNNEL RESPONSE	Circumferential Strain in Rock		%	0.1	0.4	1.2	0.06	0.2	0.6	0.03	0.1	0.3
	Radial Strain in Rock		%	0.1	0.4	1.2	0.06	0.2	0.6	0.03	0.1	0.3
	Shock Spectra in Access Tunnel			NOT ESTIMATED								
	Absolute Displacement		inches	1	4	12	1	2	4	0.3	1	2
TUNNEL–LINER INTERACTION	Fly-rock Velocity		fps	26	60	150	13	26	60	4	13	26
	Pressure on Lining		psi	120	300	900	120	150	300	40	120	150
	Compression of Filler	Cinders	inches	1	3	6	0.5	1	3	0.1	0.5	1
		9" Foam	inches	2	5	8	1	2	5	0.5	1	2
		24" Foam	inches	3	9	20	1	3	9	0.5	1	3
LINER RESPONSE	Lining Velocity	Cinders	fps	20	45	110	10	20	45	3	10	20
		Foam	fps	13	30	75	6	13	30	2	6	13
	Circumferential Strain in Lining		%	0.2	0.5	2.0	0.05	0.2	0.6	0.02	0.06	0.2
	Longitudinal Strain in Lagging		%	0.3	1.0	3	0.15	0.3	1.0	0.05	0.15	0.3
	Diameter Change in Lining		inches	4	12	36	1	4	12	0.5	1	4
	Shock Spectra in Liner			NOT ESTIMATED								

TABLE 1.5 DISTRIBUTION OF COMPOSITE LINERS IN TEST DRIFTS

		LINERS WITH BACKPACKING						
		FLEXIBLE (Corrugated Steel)		RIGID (Reinforced Concrete)		RIGID-FLEXIBLE (Steel Rings with Wood or Steel Lagging)		Totals
		8 Ga.	3 Ga.	8"	12"	Wood	Steel	
FOAM	5"	B, C	A, B	–	*C	*A, B, C	*A, B, C	11
	9"	–	–	–	*A, B	–	–	2
	20"	B, C	A, B	C	–	–	–	5
	24"	–	–	A, B	–	–	–	2
CINDER	9"	B, C	A, B	–	A, B, C	–	A, B, C	10
Totals		6	6	3	6	3	6	30

* These liners are designed for 150 p s i loading

TABLE 1.6 DISTRIBUTION OF LINERS WITHOUT BACKPACKING IN TEST DRIFTS

	LINERS WITHOUT BACKPACKING				
	Unlined	Rock Bolts and Mesh	Reinforced Concrete Against Rock	Steel Set with Wood Lagging	Totals
CIRCULAR	B, C	B, C	A, B, C	–	7
SQUARE	B, C	B, C	–	–	4
HORSESHOE	–	–	–	B, C	2
Totals	4	4	3	2	13

TABLE 1.7 PHYSICAL PROPERTIES OF PRECAST FOAM

TEST SECTION	NOMINAL THICKNESS (Inches)	NUMBER OF SAMPLES	PARALLEL TO DIRECTION OF RISE						PERPENDICULAR TO DIRECTION OF RISE					
			DENSITY (lbs. per cubic ft.)			COMPRESSIVE YIELD STRESS (psi)			DENSITY (lbs. per cubic ft.)			COMPRESSIVE YIELD STRESS (psi)		
			MIN.	AVE.	MAX.	MIN.	AVE.	MAX.	MIN.	AVE.	MAX.	MIN.	AVE.	MAX.
A4b	5	20	5.08	5.89	6.39	103.4	146.0	171.2	5.20	5.88	6.38	99.0	143.0	175.3
A4c	5	12	5.24	5.73	5.95	123.3	142.6	155.3	5.31	5.76	6.00	117.0	134.2	144.7
A5a	20	20	5.38	6.18	7.09	124.7	149.3	202.5	5.48	6.16	7.10	109.7	141.0	178.3
A5b	5	24	5.20	5.94	6.40	111.2	137.9	162.5	5.24	5.94	6.37	120.5	147.5	164.5
B4b	5	22	4.98	5.58	6.92	100.0	130.9	192.9	5.13	5.58	6.49	98.3	127.6	175.0
B4c	5	12	5.46	5.87	6.41	117.3	146.0	165.0	5.46	5.86	6.50	127.0	141.1	167.5
B5a	20	24	5.26	6.05	6.88	106.5	153.9	196.1	5.12	5.96	6.59	106.5	141.9	171.2
B5b	5	20	5.30	5.81	6.37	105.0	135.5	166.2	5.34	5.82	6.35	124.7	142.8	161.1
B6a	20	24	5.14	5.82	6.55	106.5	139.6	174.5	5.26	5.83	6.59	109.3	134.1	168.7
B6b	5	20	5.38	5.82	6.48	114.0	136.6	158.8	5.34	5.82	6.37	119.6	139.8	166.1
C3b	5	16	5.36	5.74	6.20	124.5	145.9	163.3	5.39	5.73	6.20	114.6	142.6	169.2
C3c	20	52	5.34	5.97	7.43	105.9	142.5	191.1	5.34	5.98	8.35	100.0	144.2	206.2
C4b	5	17	5.25	6.07	6.74	115.3	150.4	200.7	5.20	6.08	6.86	92.9	144.1	190.0
C4c	5	12	5.40	5.71	6.31	126.0	143.9	169.2	5.41	5.72	6.29	120.0	142.8	169.8
C6a	20	20	5.73	6.10	6.54	142.0	155.3	179.2	5.47	6.03	6.41	119.0	145.7	174.8
C6b	5	24	5.05	5.63	6.14	109.3	133.8	155.0	5.06	5.63	6.14	100.3	122.6	140.5

TABLE 1.8 PHYSICAL PROPERTIES OF CAST-IN-PLACE FOAM

TEST SECTION	NOMINAL THICKNESS (inches)	NUMBER OF SAMPLES	DENSITY (lbs. per cubic ft.)			* COMPRESSIVE YIELD STRESS (psi)		
			MIN.	AVE.	MAX.	MIN.	AVE.	MAX.
A3b	9	4	5.41	5.75	6.04	62.5	80.4	108.0
A3c	24	8	5.95	6.29	6.90	78.5	107.7	157.5
B3b	9	12	5.88	6.24	7.09	107.0	128.7	156.0
B3c	24	16	5.75	6.35	7.86	86.0	132.4	179.0

* Average value of test samples orientated at 0°, 45°, 90° and 135° with respect to assumed direction of foam rise.

TABLE 1.9 AVERAGE STRENGTH PROPERTIES FOR FLEXIBLE TUNNEL LINERS

TEST SECTIONS	Yield Strength (ksi)	Ultimate Strength (ksi)	Reduction in Area (%)	Elongation in 2 inches (%)
B6c, C6c	38.8	59.9	60.9	31.3
B6a, B6b, C6a, C6b	51.7	70.9	61.0	29.1
A5c, B5c	32.9	59.0	51.0	34.7
A5a, A5b, B5a, B5b	39.6	68.7	58.7	31.1

TABLE 1.10 AVERAGE STRENGTH PROPERTIES OF RIGID TUNNEL LINERS

CONCRETE CYLINDER TEST					
TEST SECTION	28-DAY COMPRESSIVE STRENGTH (PSI)	TEST SECTION	28-DAY COMPRESSIVE STRENGTH (PSI)	TEST SECTION	28-DAY COMPRESSIVE STRENGTH (PSI)
A3a	3030	B3a	2820	C3a	2860
A3b	3260	B3b	3150	C3b	3330
A3c	2710	B3c	2990	C3c	2980
A3d	3160	B3d	3540	C3d	3260

REINFORCING STEEL TEST *				
TEST SECTION	REINFORCING STEEL SIZE	YIELD STRENGTH (KSI)	ULTIMATE STRENGTH (KSI)	ELONGATION IN 8 INCHES (%)
A3c, B3c	#3	52.7	74.4	21.9
	#5	49.2	79.4	23.0
A3a, A3b. A3d, B3a B3b, B3d, C3a, C3d	#4	53.5	76.9	21.2
	#6	49.8	73.1	19.4
C3c	#3	53.7	80.8	17.9
	#5	54.0	83.8	22.6
C3b	#4	52.3	82.9	19.5
	#6	47.4	76.2	22.5

* Modulus of Elasticity determined to be 29×10^6 to 31×10^6 psi

TABLE 1.11 AVERAGE STRENGTH PROPERTIES FOR RIGID-FLEXIBLE TUNNEL LINERS

TEST SECTION	COMPONENT		YIELD STRENGTH (KSI)	ULTIMATE STRENGTH (KSI)	REDUCTION IN AREA (%)	ELONGATION IN 2 INCHES (%)
A4a, B4a C4a, A4c B4c, C4c	Steel Decking		49.3	55.6	50.5	26.4
	WF Rings	Flange	42.7	69.6	47.1	33.6
		Web	36.7	61.7	49.9	34.9
A4b, B4b C4b	Steel Decking		42.8	54.8	51.0	23.6
	WF Rings	Flange	36.6	61.4	42.2	34.3
		Web	44.1	67.5	44.7	30.7

TABLE 1.12 AVERAGE STRENGTH PROPERTIES FOR HORSESHOE-SHAPED SETS

TEST SECTION	COMPONENT		YIELD STRENGTH (KSI)	ULTIMATE STRENGTH (KSI)	REDUCTION IN AREA (%)	ELONGATION IN 2 INCHES (%)
B7a, C7a	WF Sets	Flange	42.2	67.3	57.4	33.7
		Web	51.3	70.4	51.7	25.1

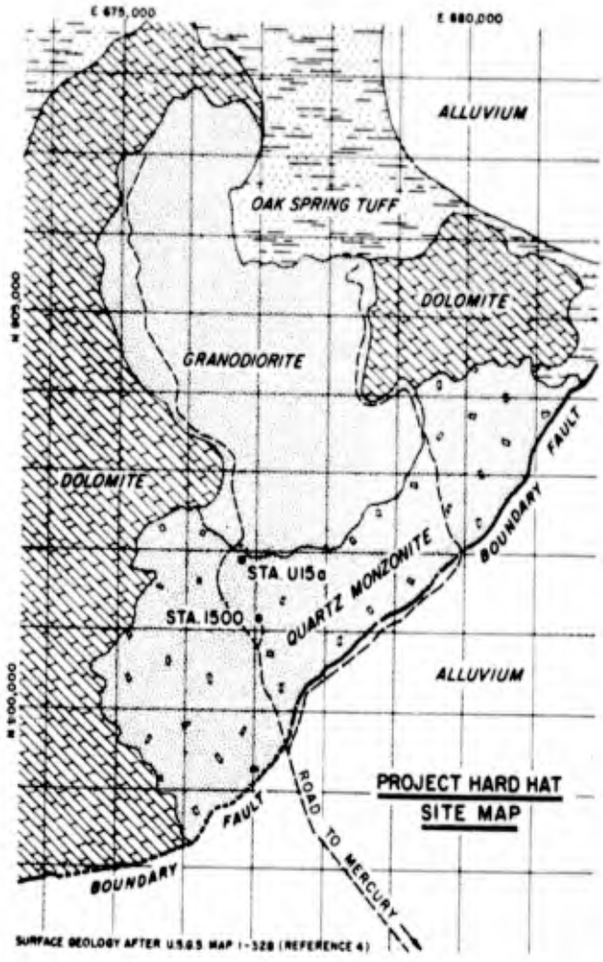

Figure 1.1 Surface geology.

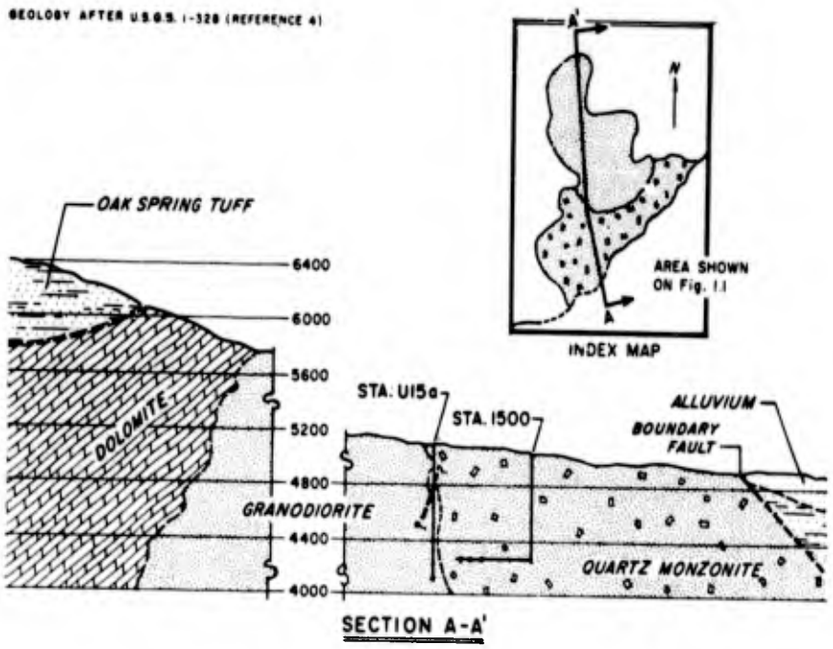

Figure 1.2 Geologic cross section, Project Hard Hat.

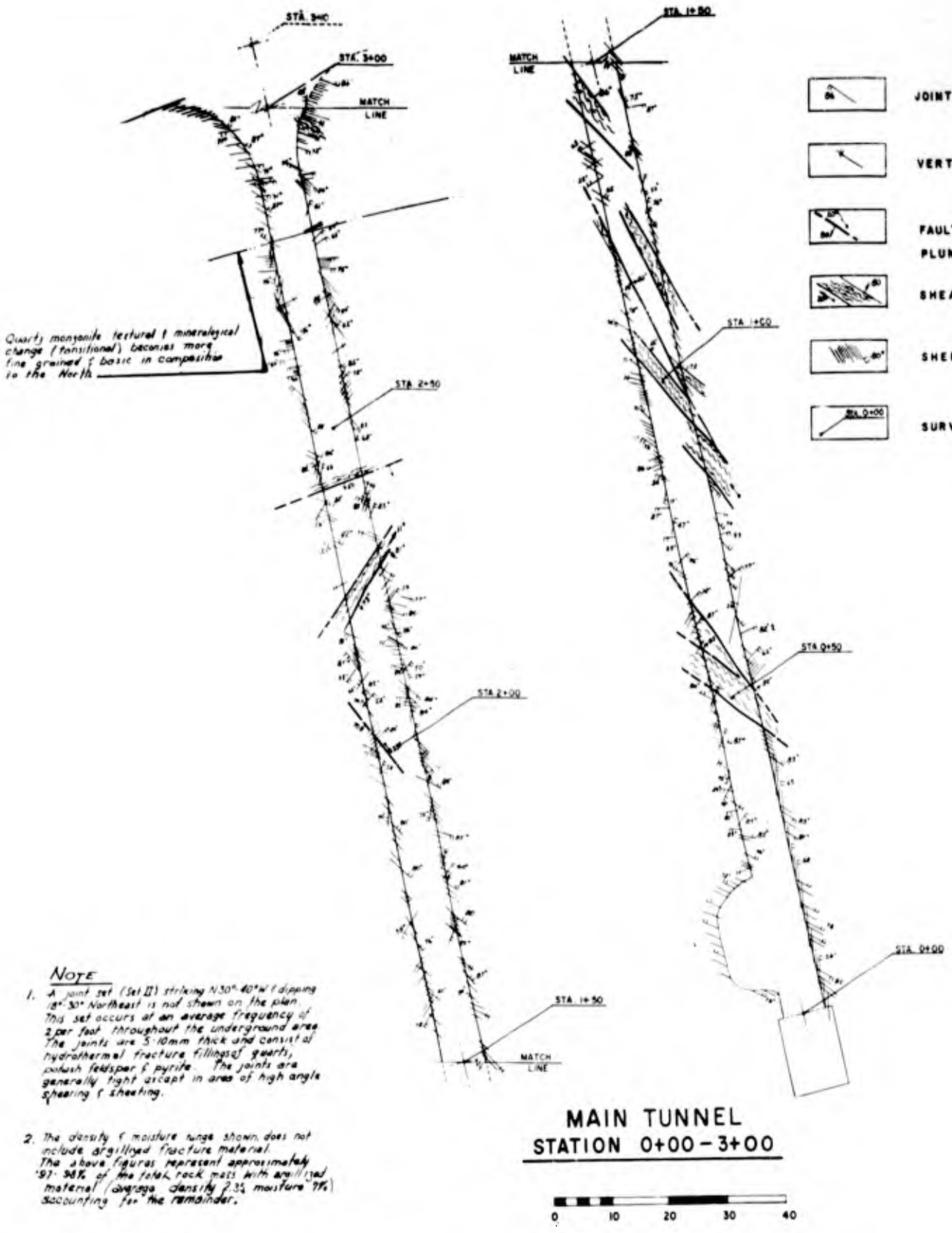

MAIN TUNNEL
STATION 0+00 – 3+00

Fig

NOTE

1. A joint set (Set II) striking N30°-40°W dipping 18°-30° Northeast is not shown on the plan. This set occurs at an average frequency of 2 per foot throughout the underground area. The joints are 5-10mm thick and consist of hydrothermal fracture fillings of quartz, potash feldspar & pyrite. The joints are generally tight except in areas of high angle shearing & sheeting.

2. The density & moisture range shown does not include argillized fracture material. The above figures represent approximately 92-98% of the total rock mass with argillized material (average density 2.3% moisture 9%) accounting for the remainder.

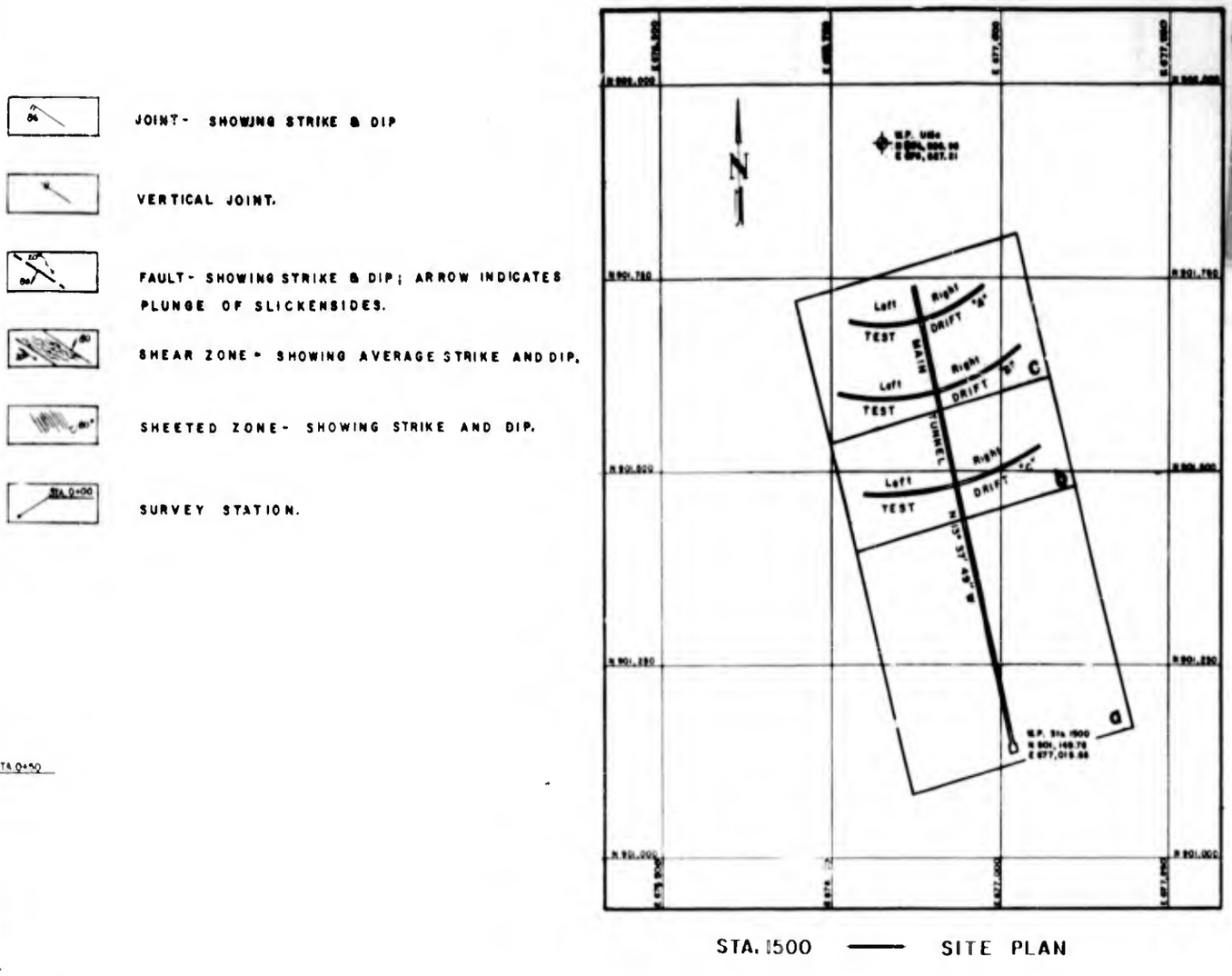

STA. 1500 —— SITE PLAN

Figure 1.3 Underground geology, main tunnel, Hard Hat.

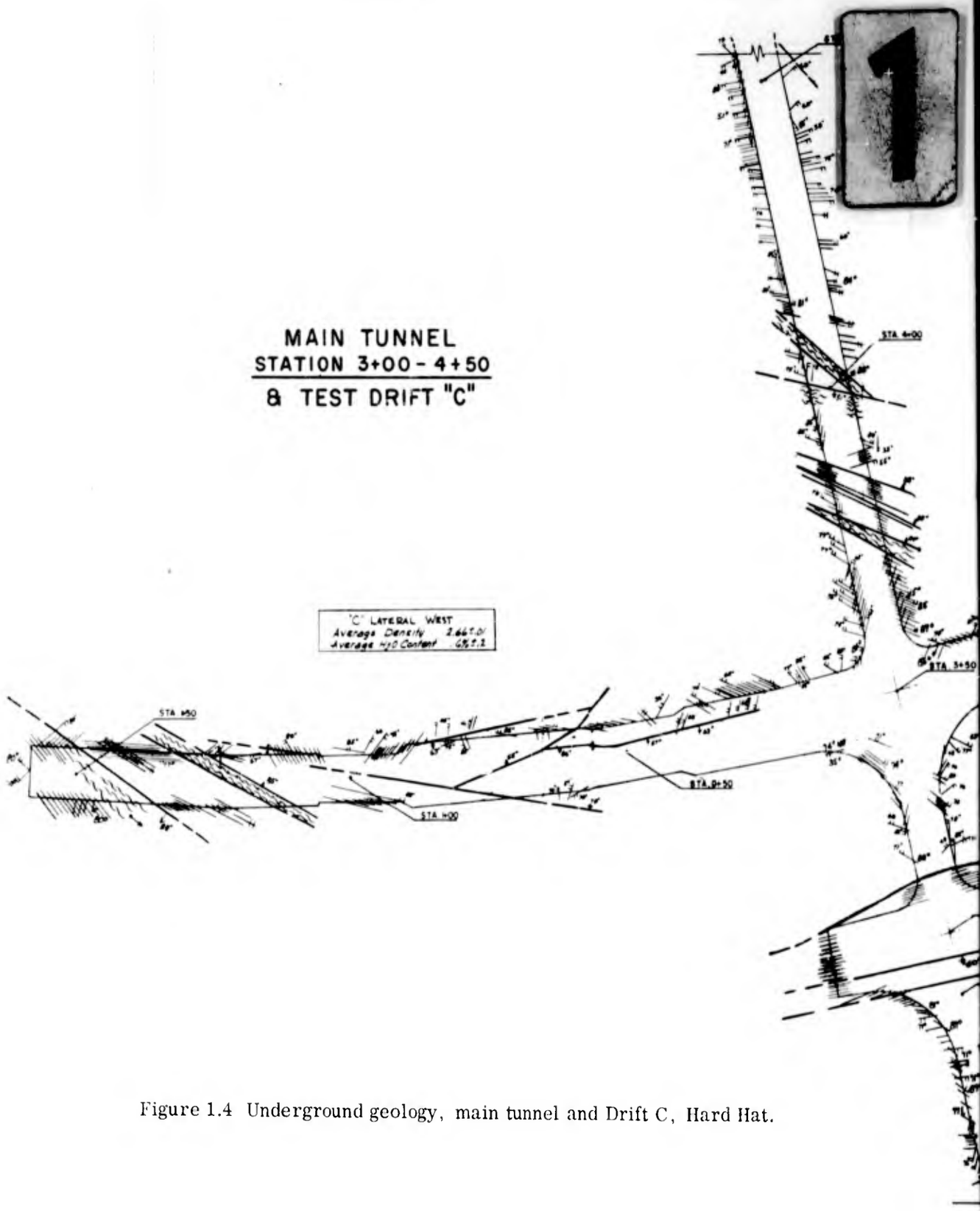

Figure 1.4 Underground geology, main tunnel and Drift C, Hard Hat.

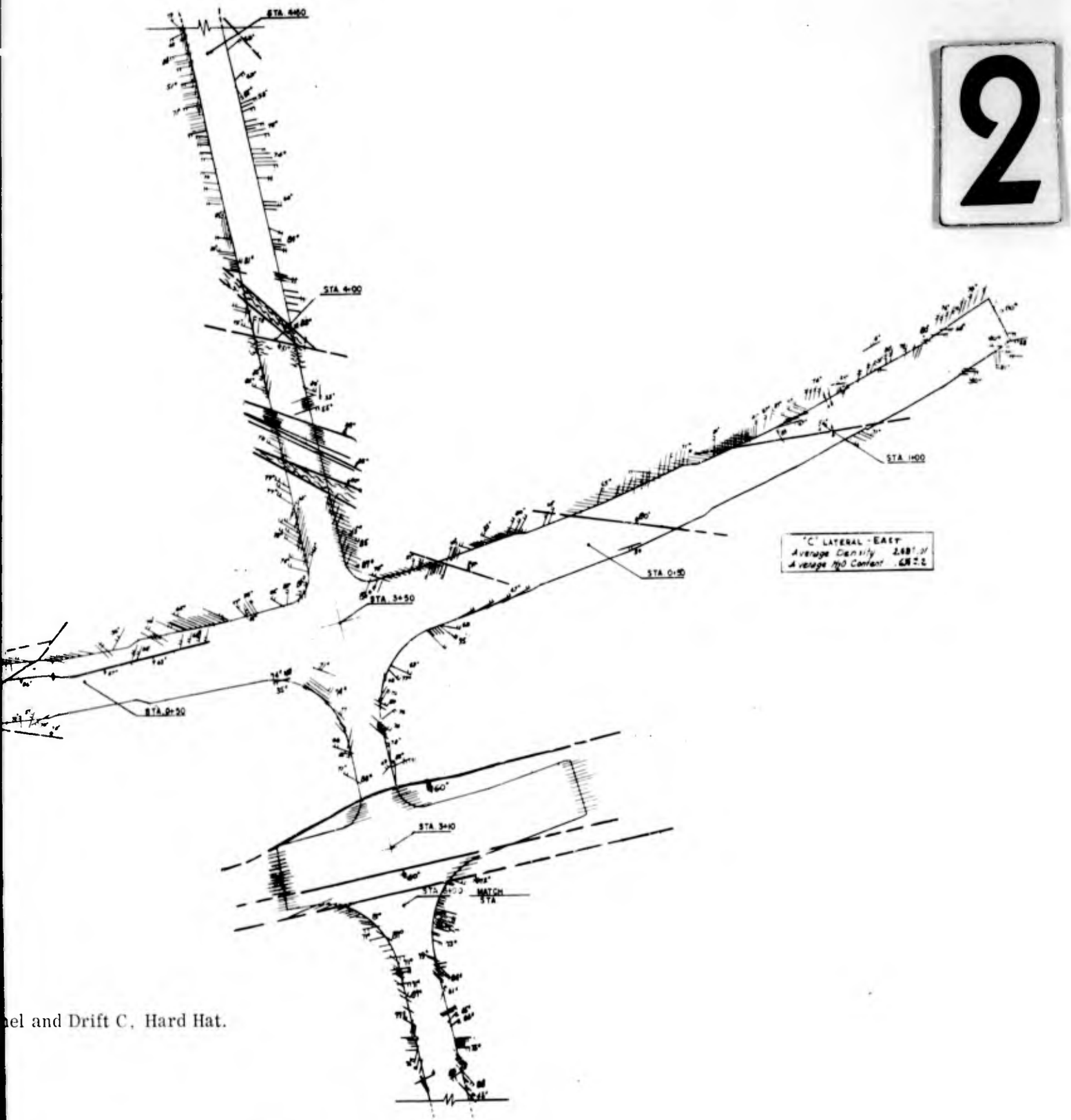

2

el and Drift C, Hard Hat.

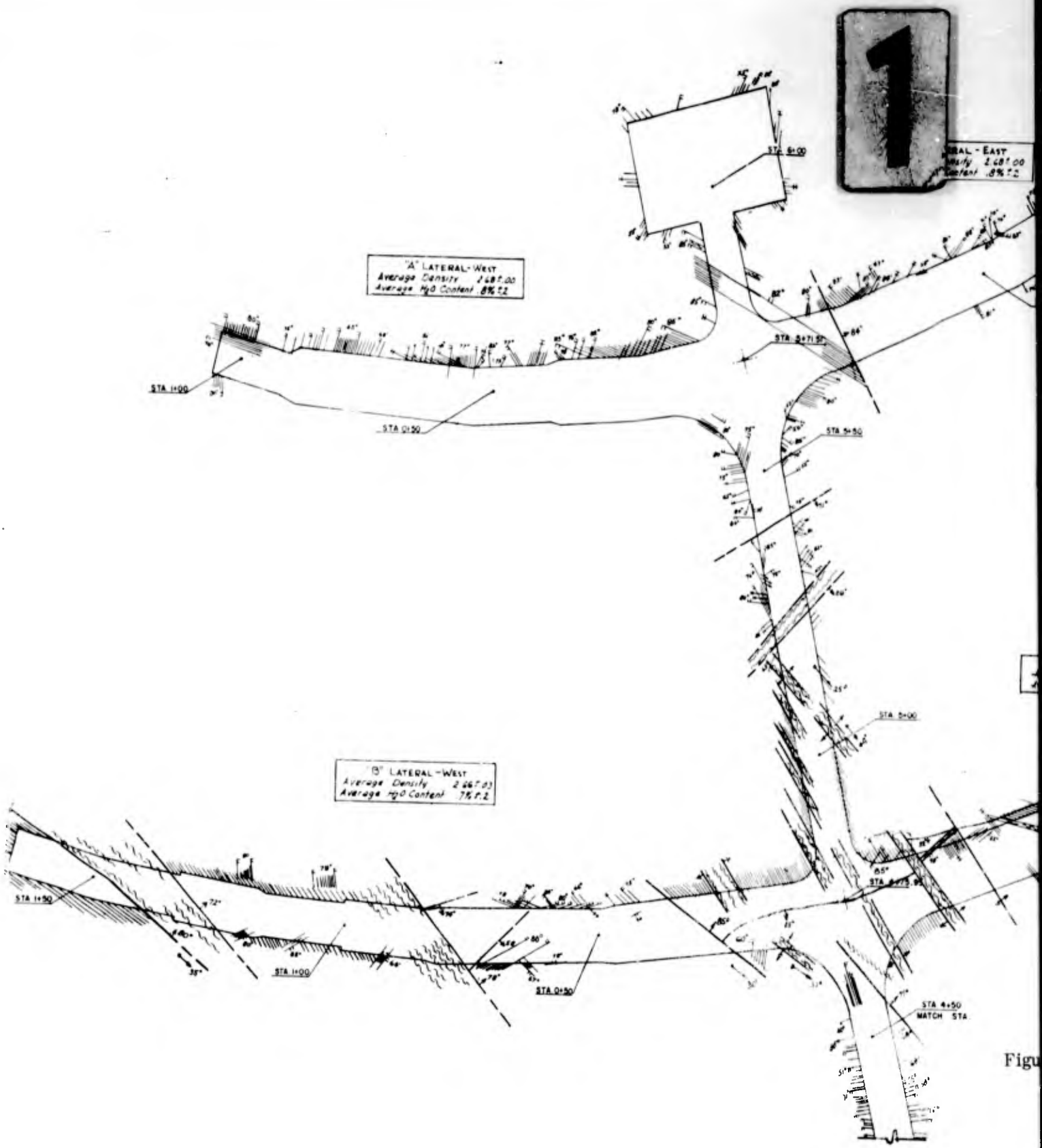
1
'A' LATERAL - WEST
Average Density 2.68 T.00
Average H2O Content .8% T.2
'B' LATERAL - WEST
Average Density 2.66 T.03
Average H2O Content 7% T.2
STA 0+00
STA 0+50
STA 1+00
STA 1+50
STA 2+71.50
STA 3+50
STA 5+00
STA 4+50
MATCH STA

Figu

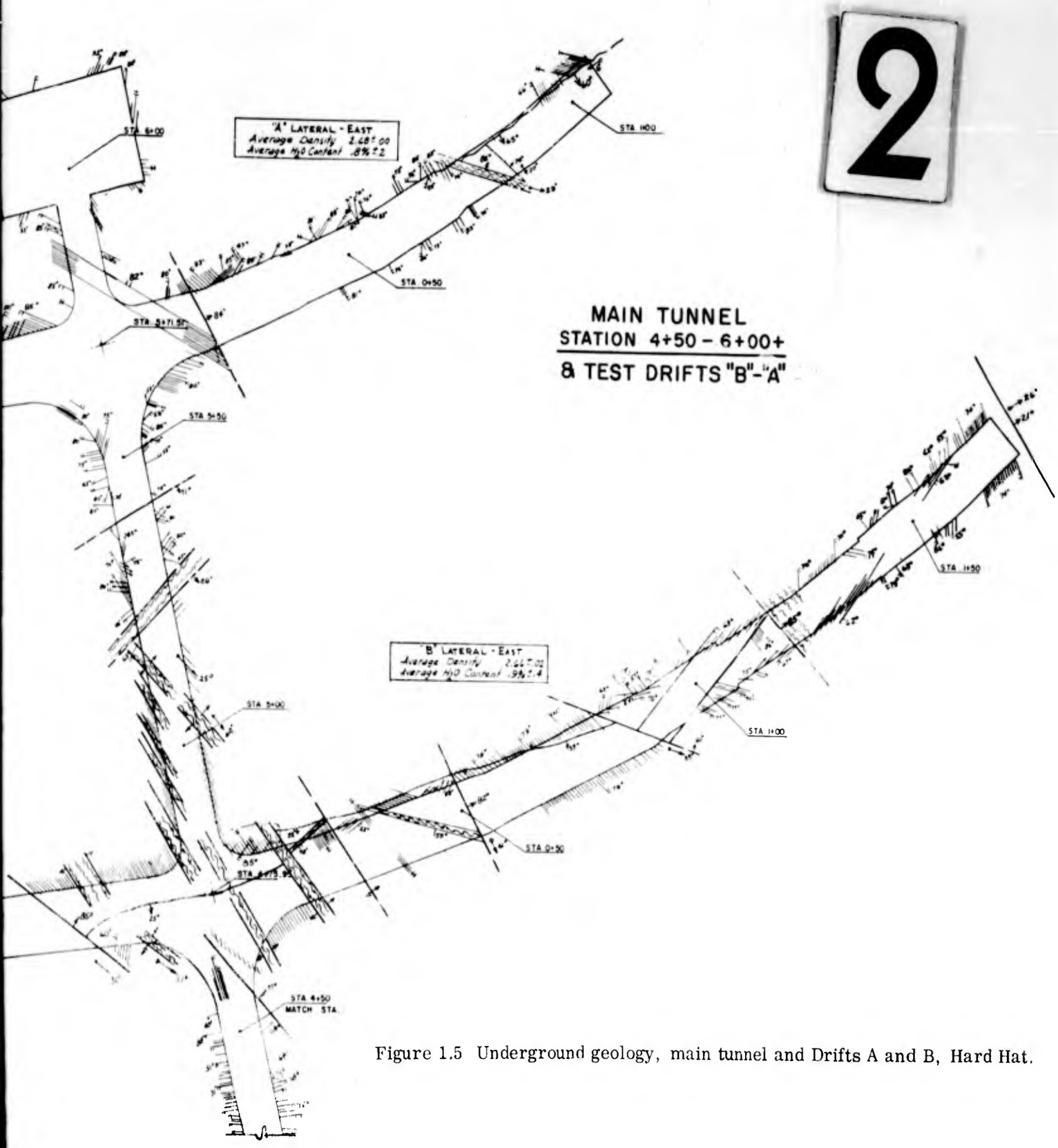

Figure 1.5 Underground geology, main tunnel and Drifts A and B, Hard Hat.

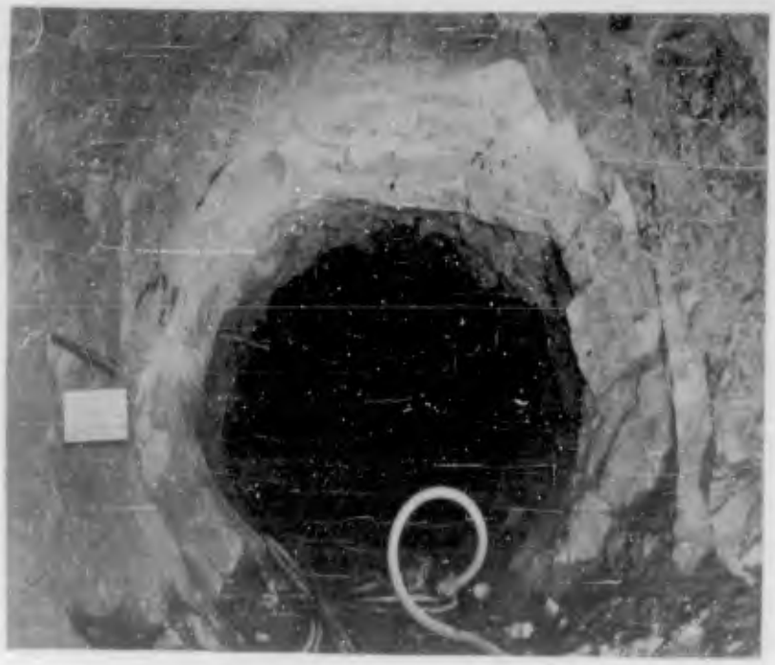

Figure 1.6 Typical jointing of exposed rock.
(H&N-AEC 60-762-10, 1960)

Figure 1.7 Closeup view of joints at top of tunnel.
(H&N-AEC 60-762-11, 1960)

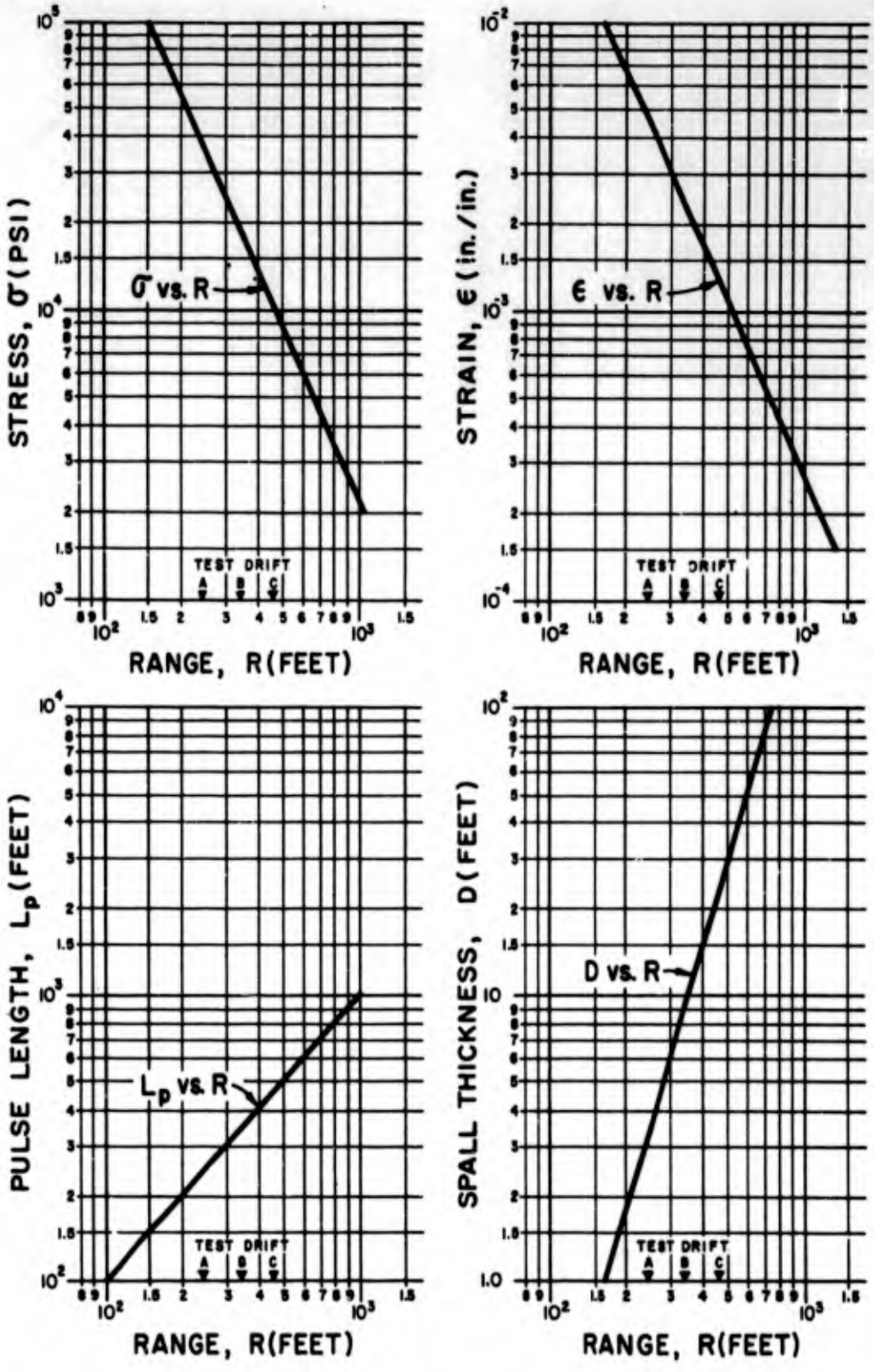

Figure 1.8 Estimates of shock parameters—stress, strain, pulse length, and spall thickness.

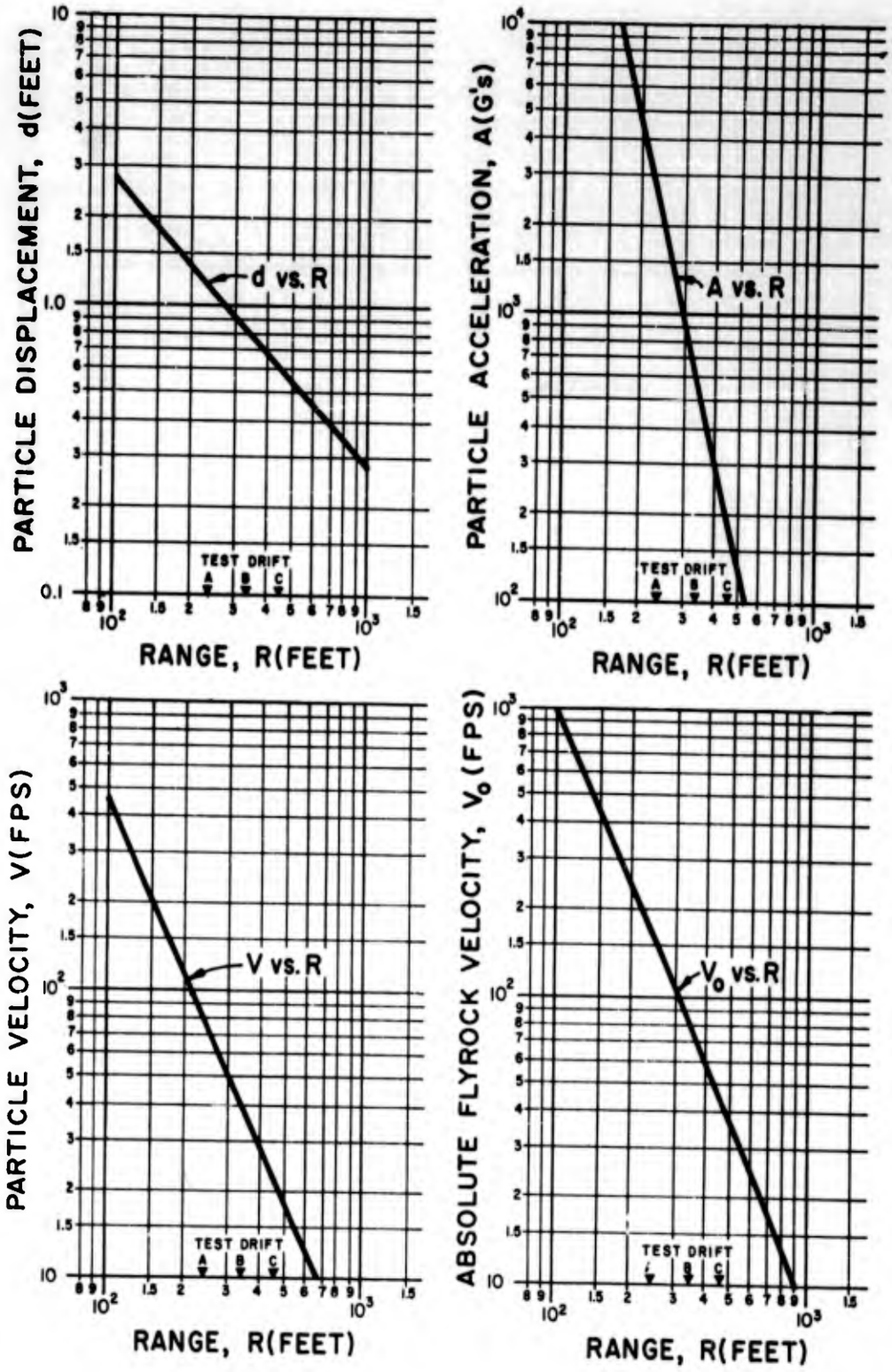

Figure 1.9 Estimates of shock parameters—particle displacement, particle acceleration, particle velocity, and absolute flyrock velocity.

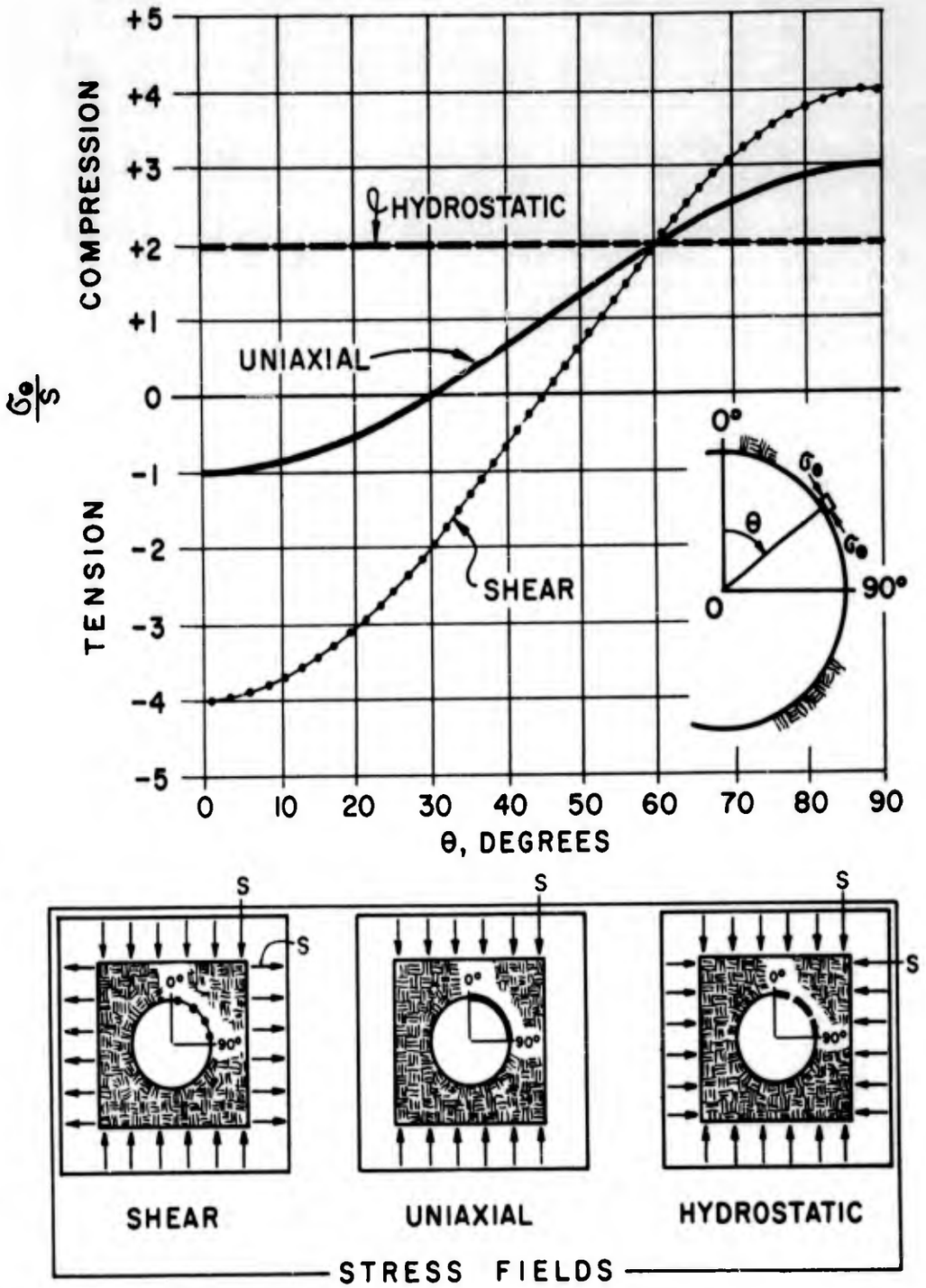

Figure 1.10 Boundary stress concentration for circular tunnels.

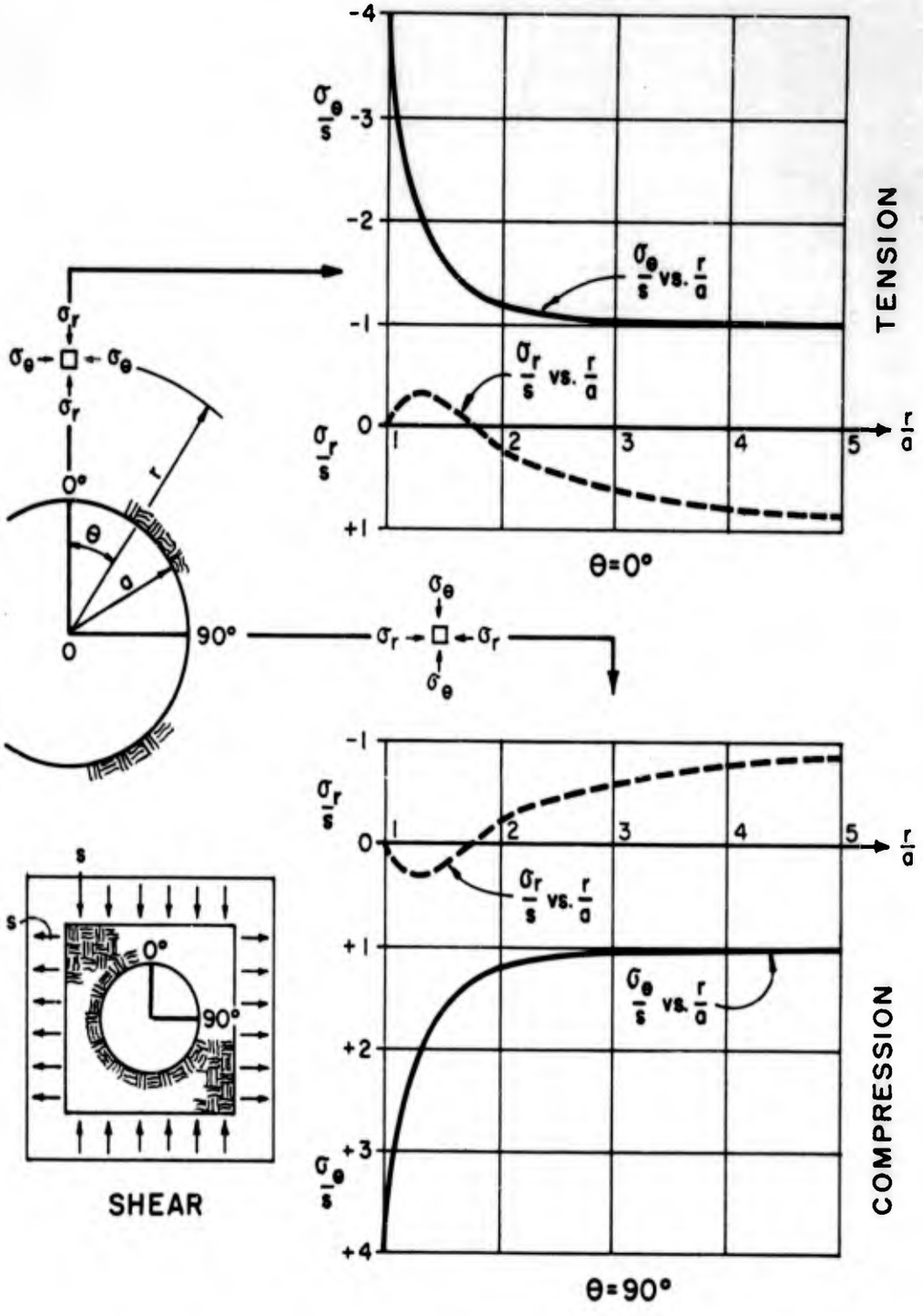

Figure 1.11 Stress concentration along radial axes of symmetry for circular tunnel, shear stress field.

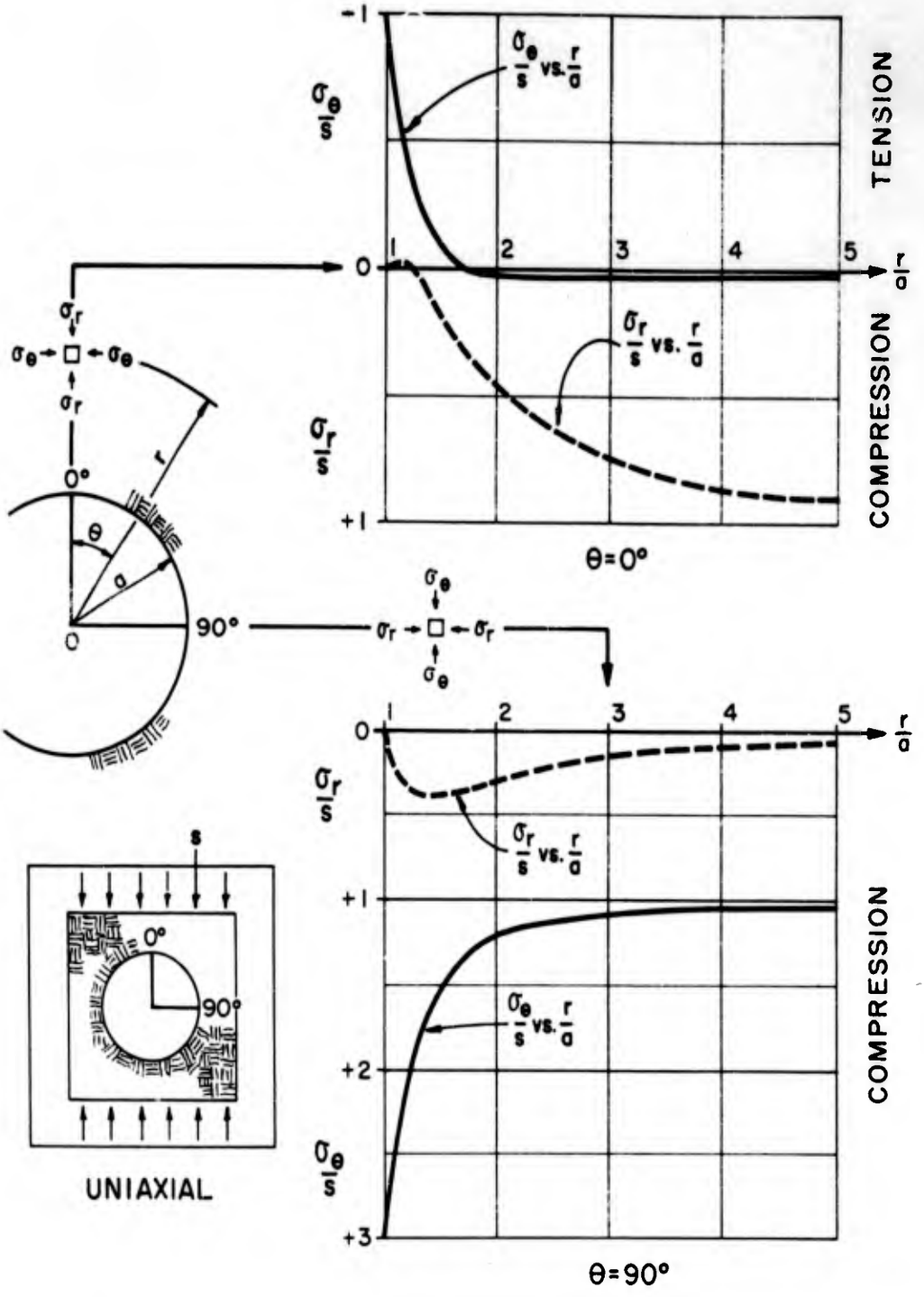

Figure 1.12 Stress concentration along radial axes of symmetry for circular tunnel, uniaxial stress field.

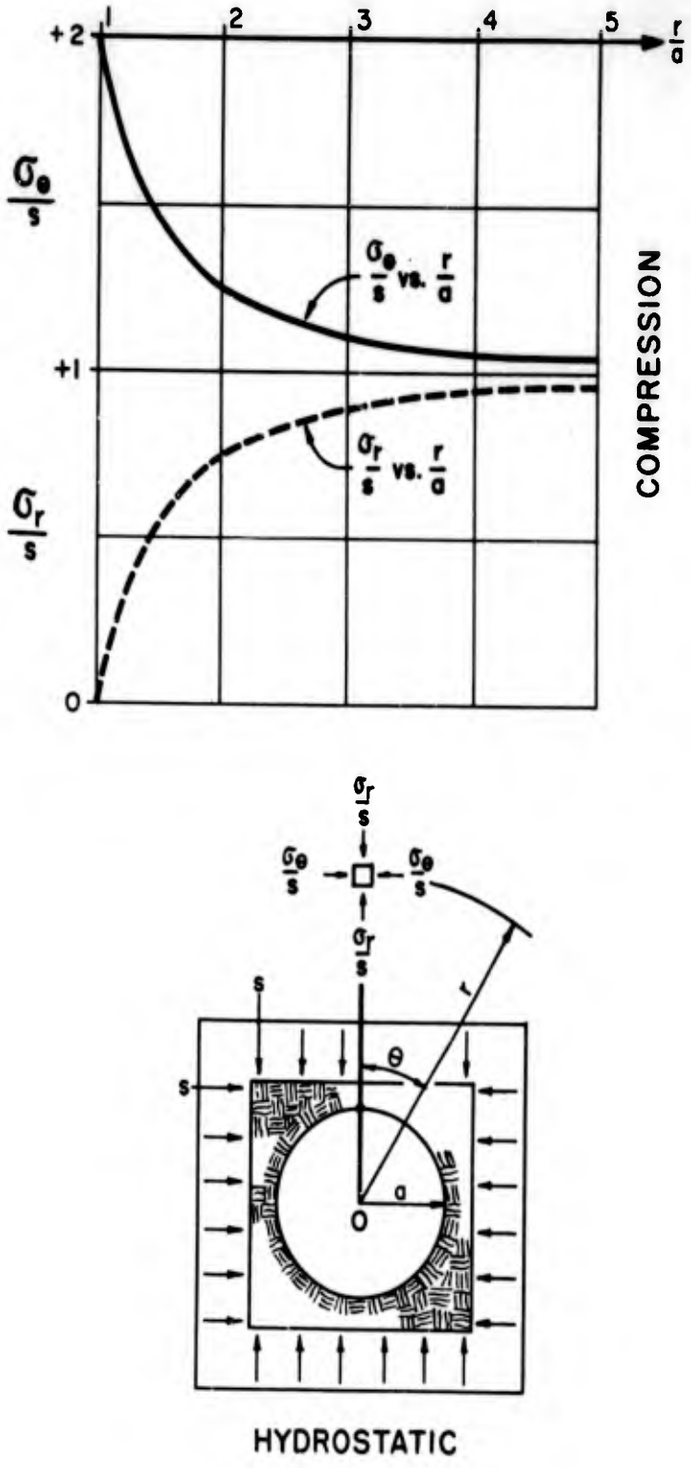

Figure 1.13 Stress concentration along radial axes of symmetry for circular tunnel, hydrostatic stress field.

SECRET

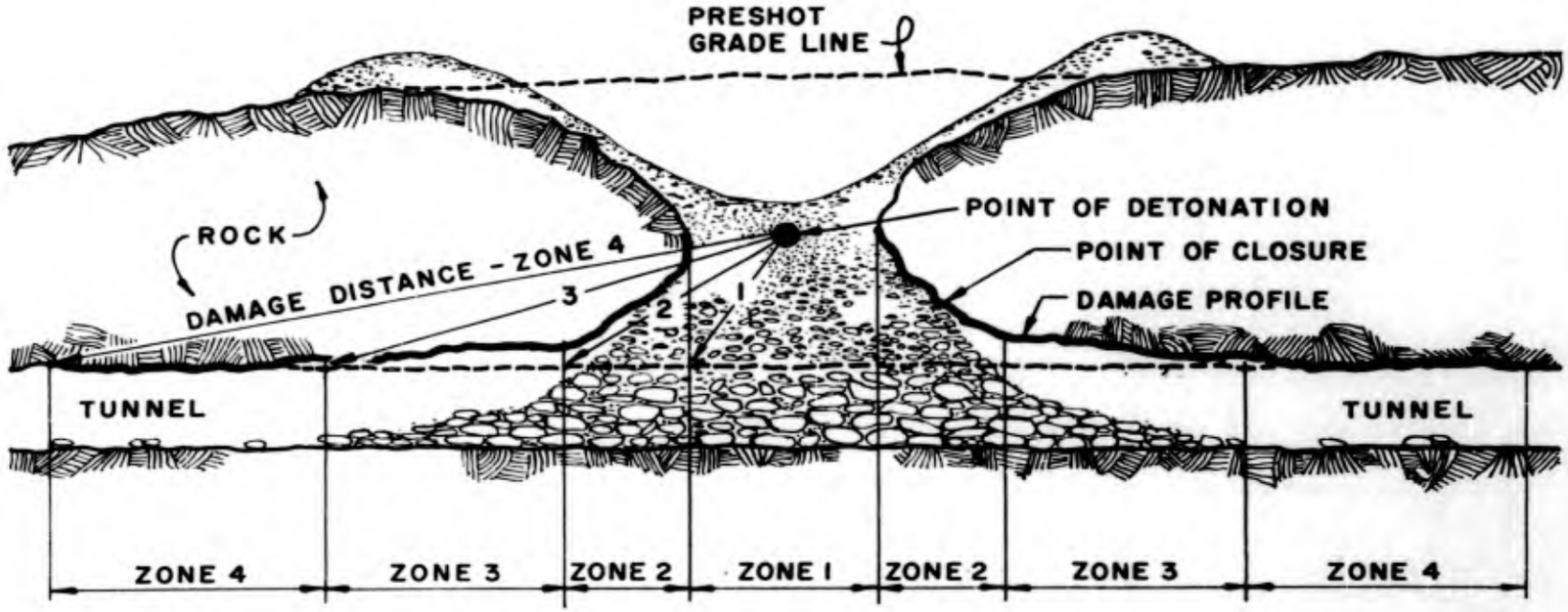

Figure 1.14 Tunnel profile showing zones of damage.

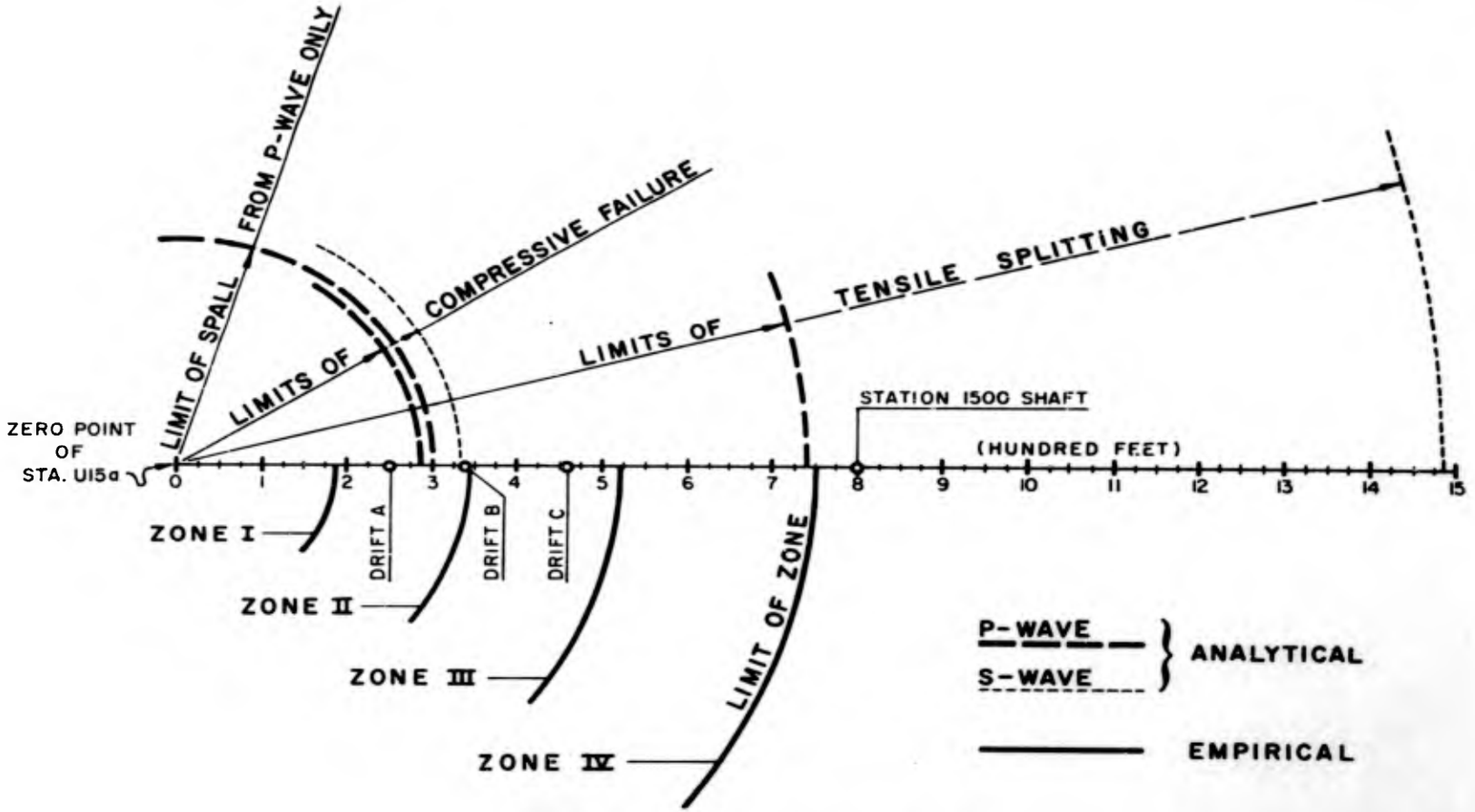

Figure 1.15 Comparison of analytical versus empirical method for estimating tunnel response.

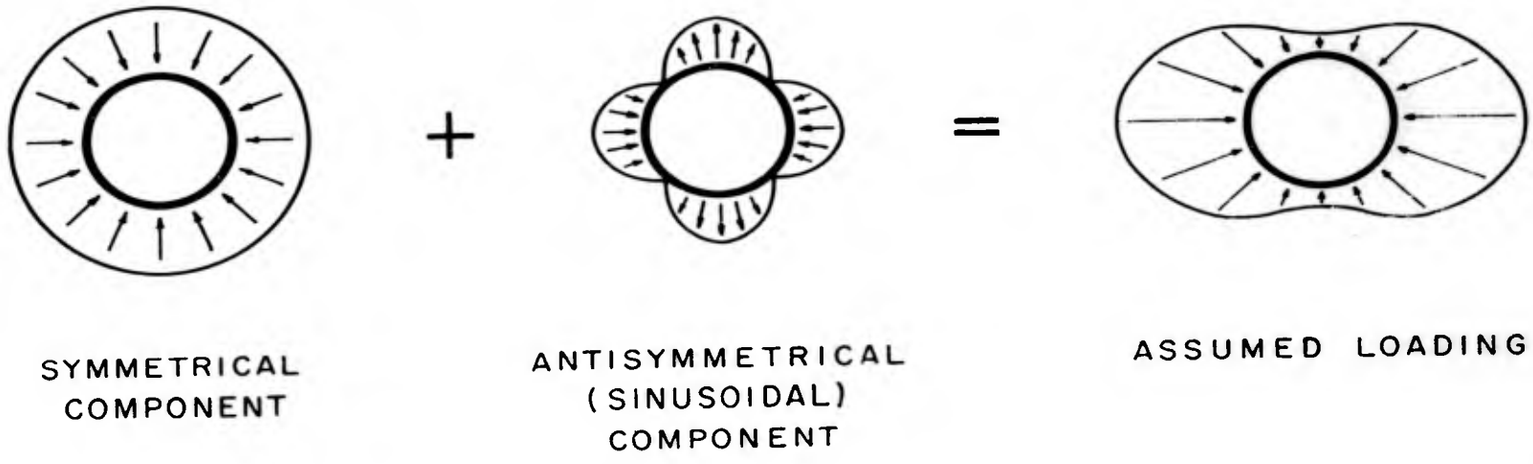

Figure 1.16 Component loadings assumed for liner design.

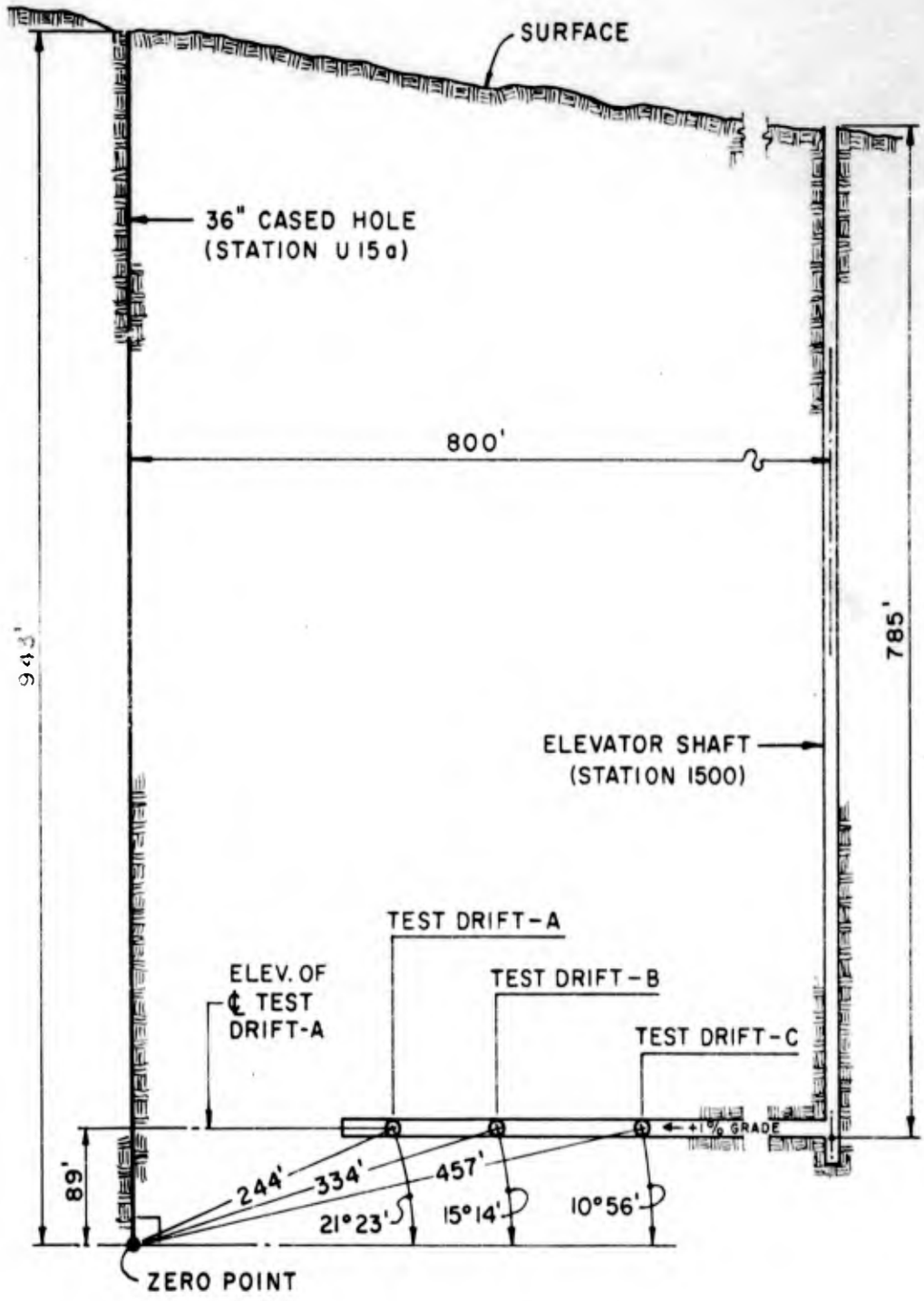

Figure 1.17 Vertical section, Hard Hat.

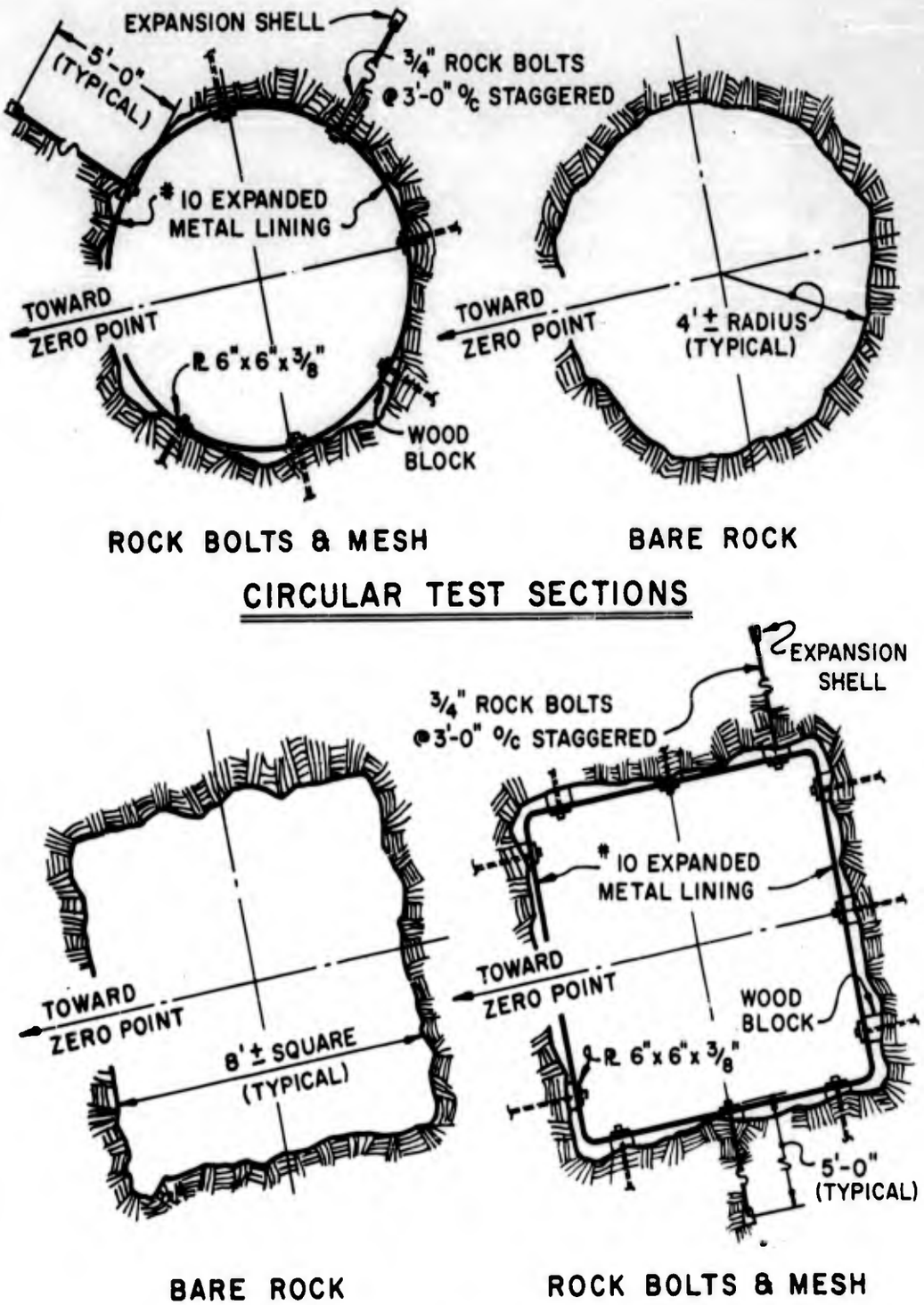

Figure 1.18 Details of four unlined test sections.

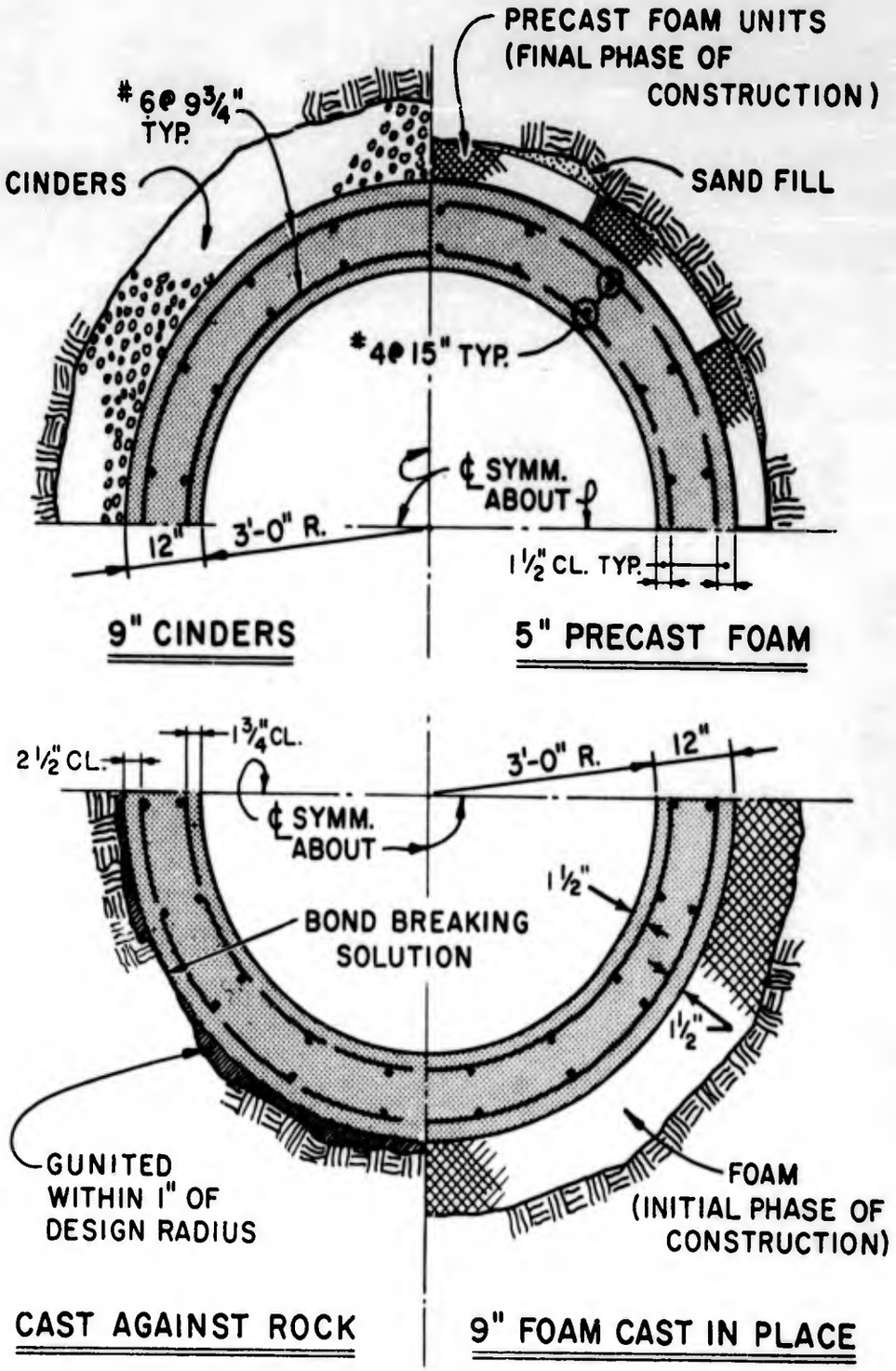

Figure 1.19 Quarter sections of four types of 12-inch reinforced concrete liners.

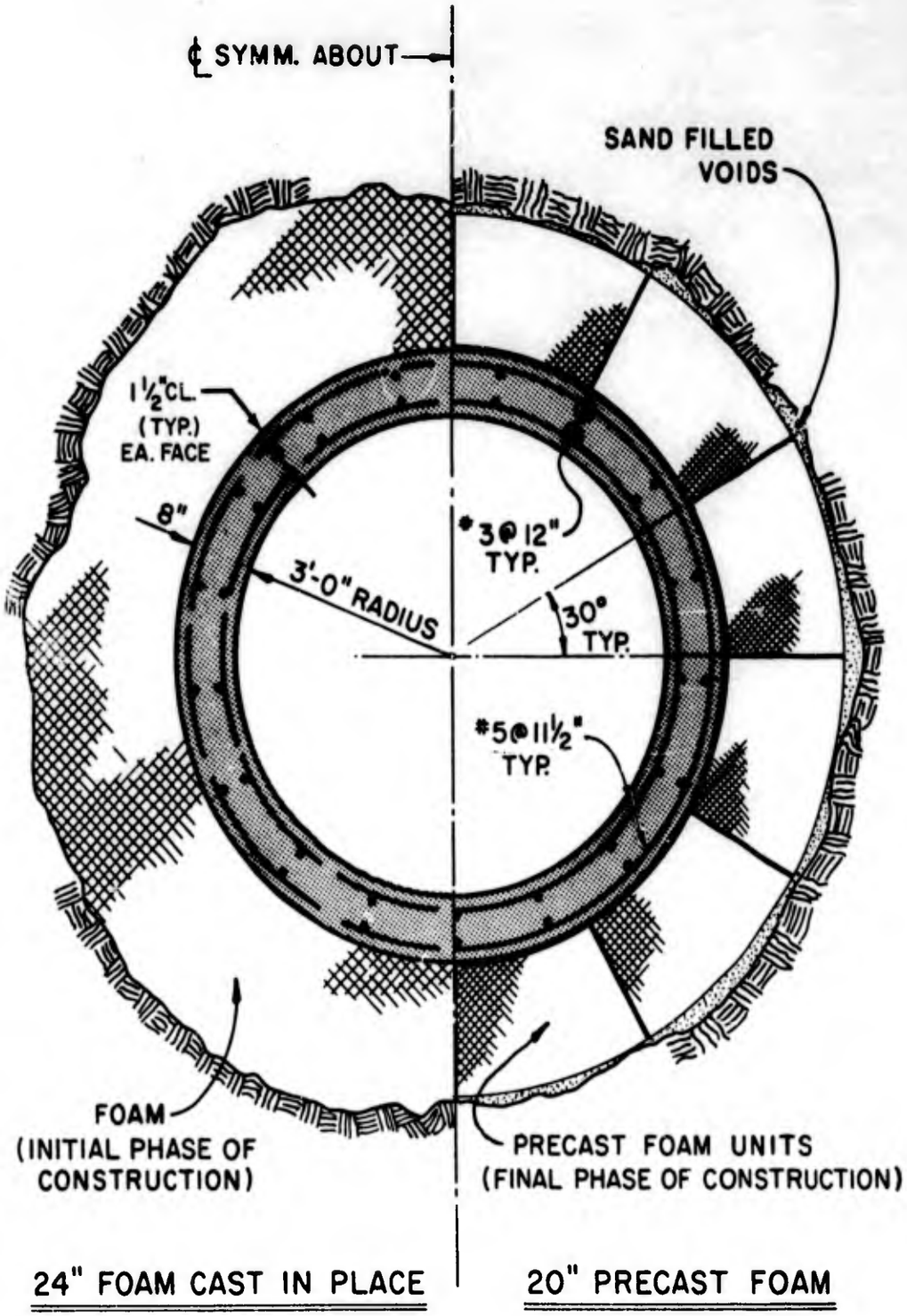

Figure 1.20 Half sections of two types of 8-inch reinforced concrete liners.

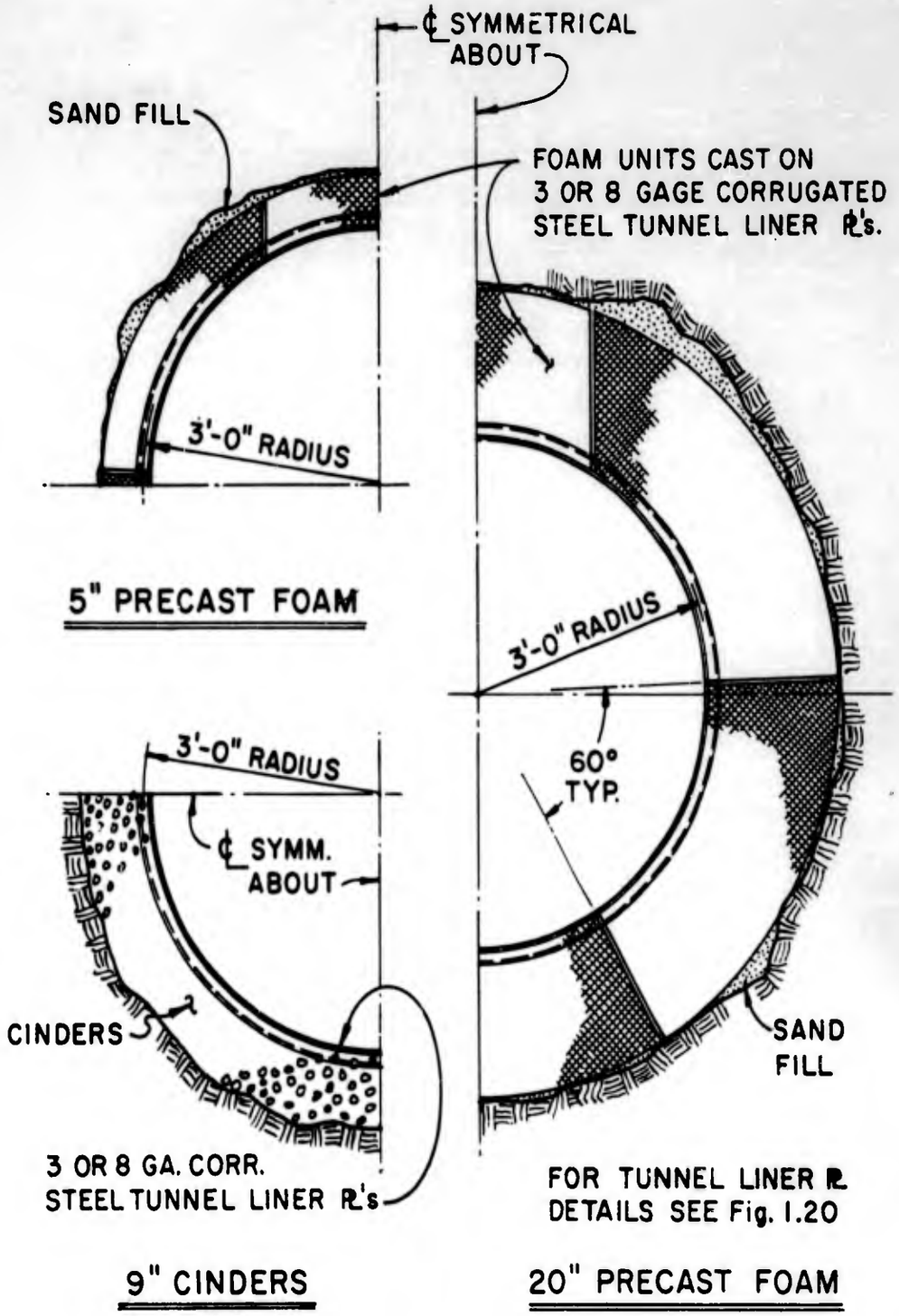

Figure 1.21 Partial sections of three types of corrugated steel tunnel liners.

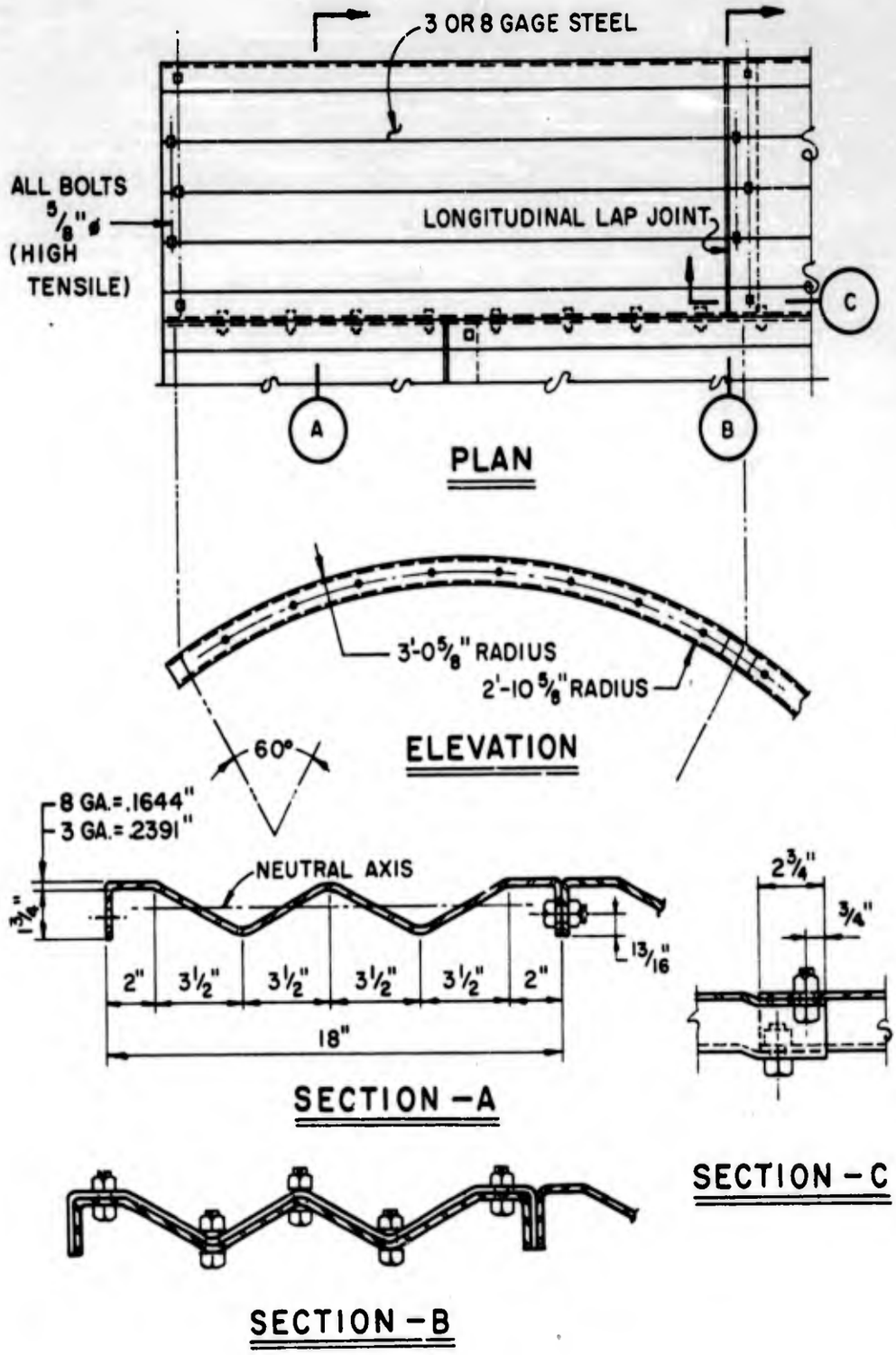

Figure 1.22 Details, corrugated steel tunnel liner.

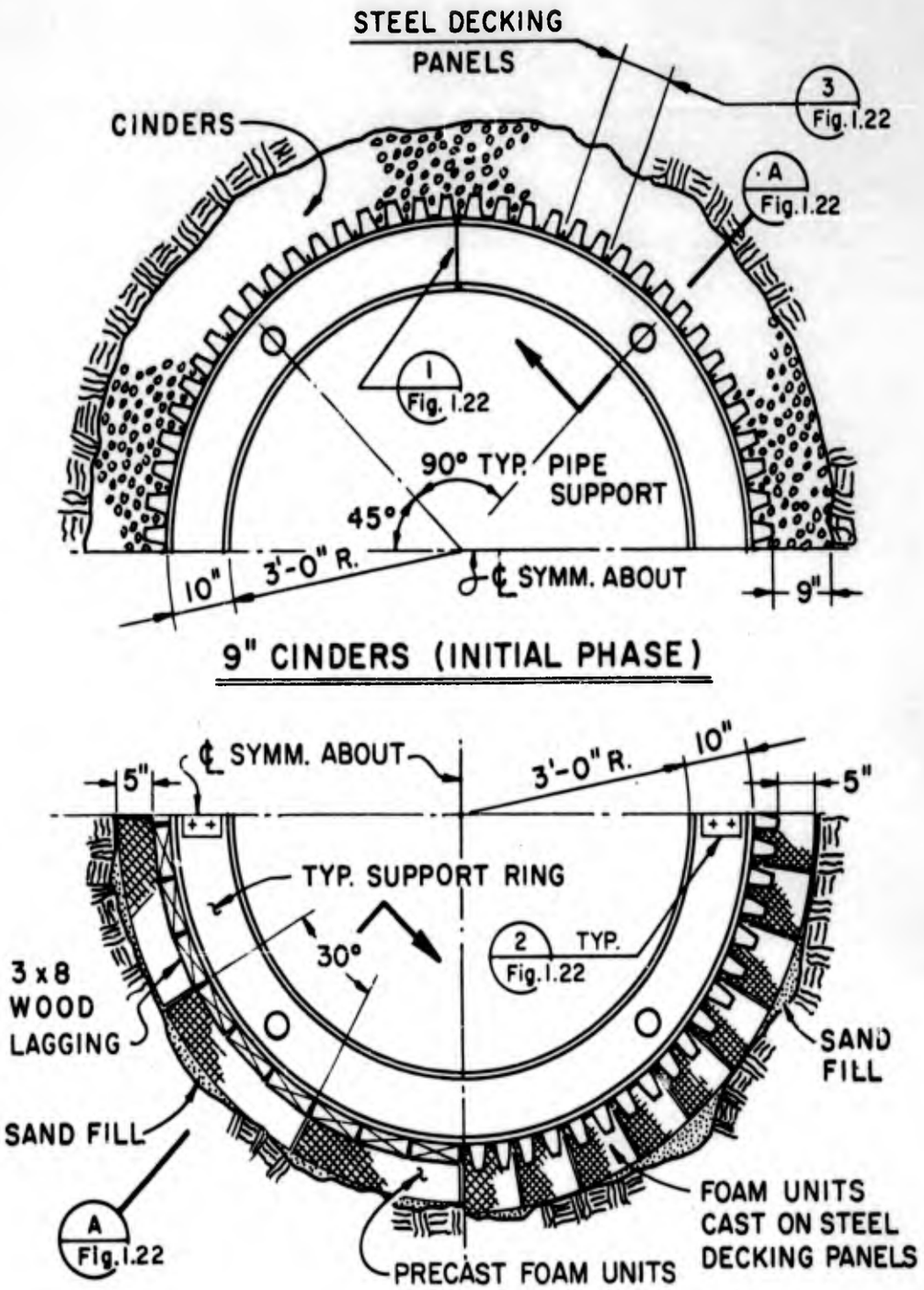

Figure 1.23 Partial sections of three types of liners with wide flange rings.

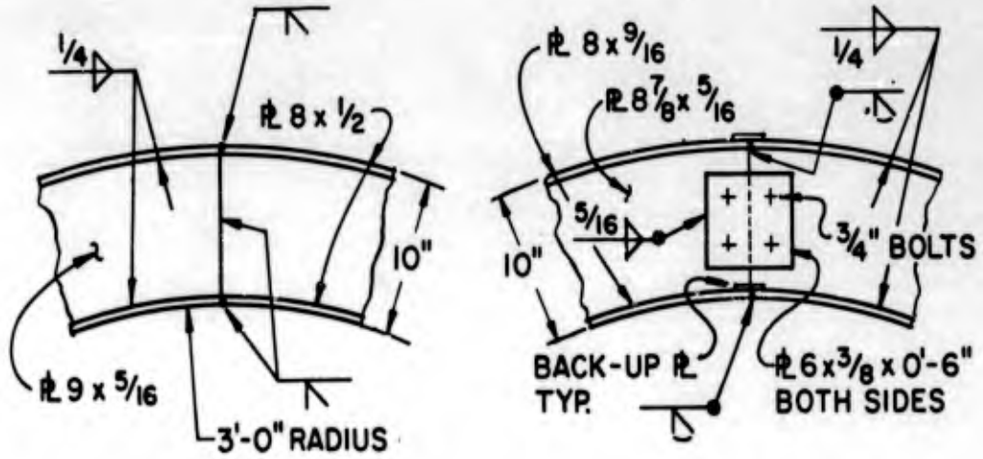

DETAIL-1 DETAIL-2

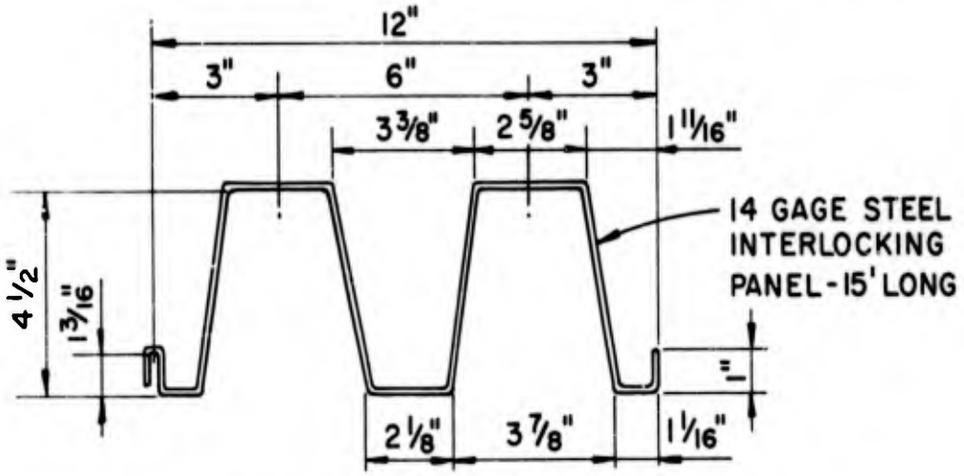

STEEL DECKING DETAIL-3

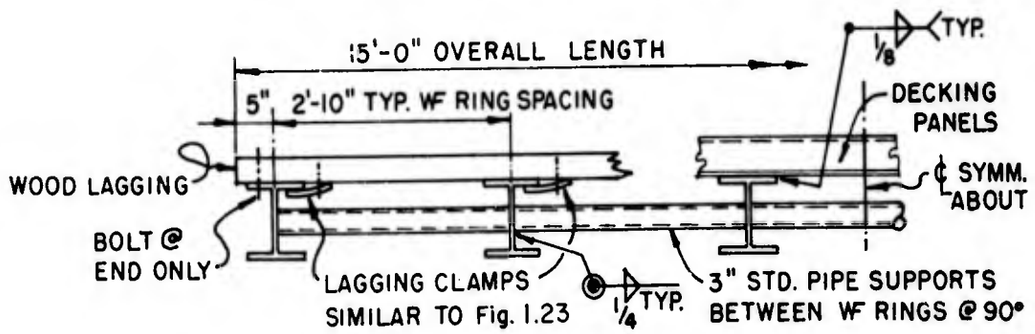

TYPICAL SECTION - A

Figure 1.24 Details, wide flange rings.

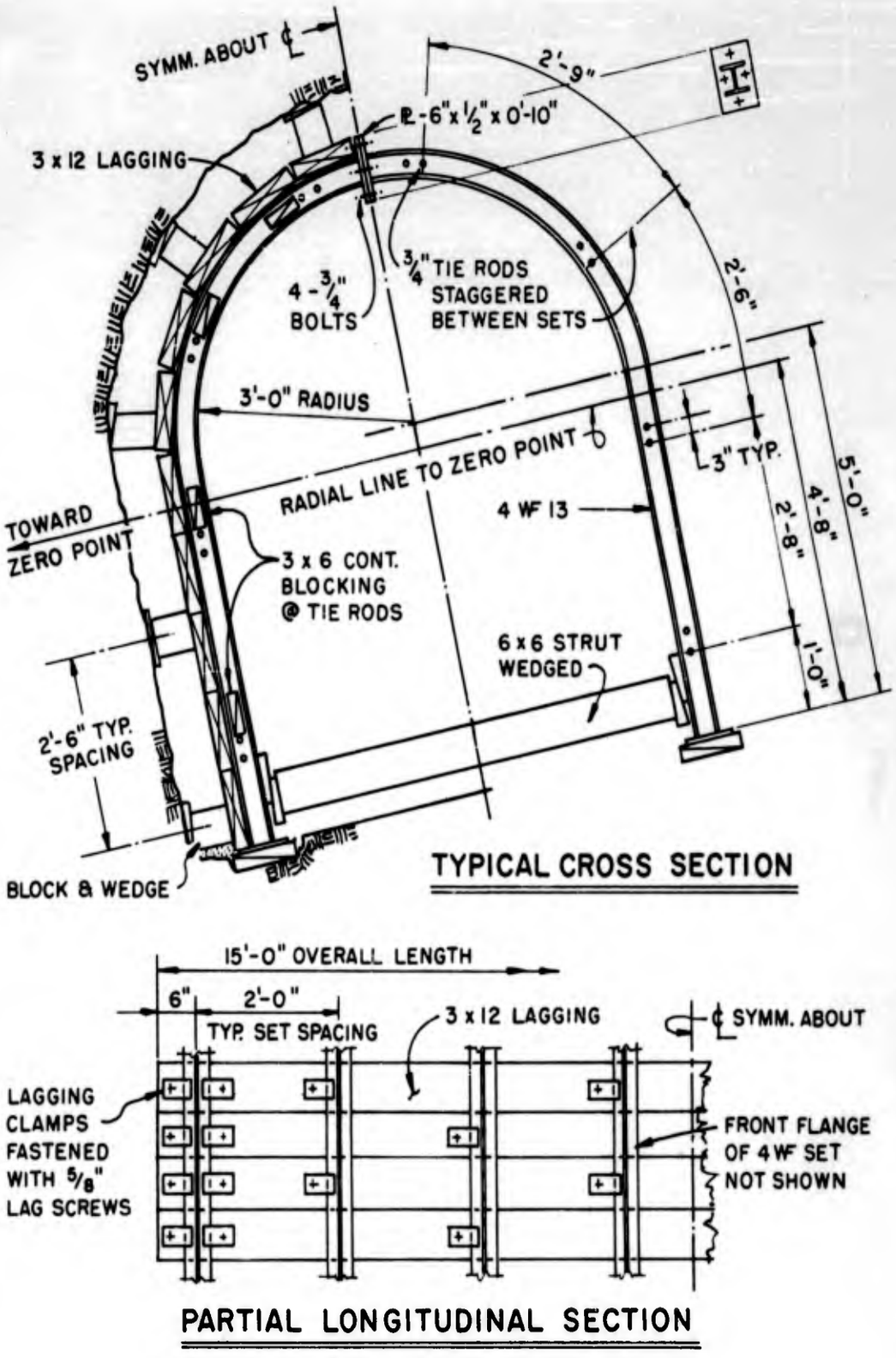

Figure 1.25 Horseshoe sets with wood lagging.

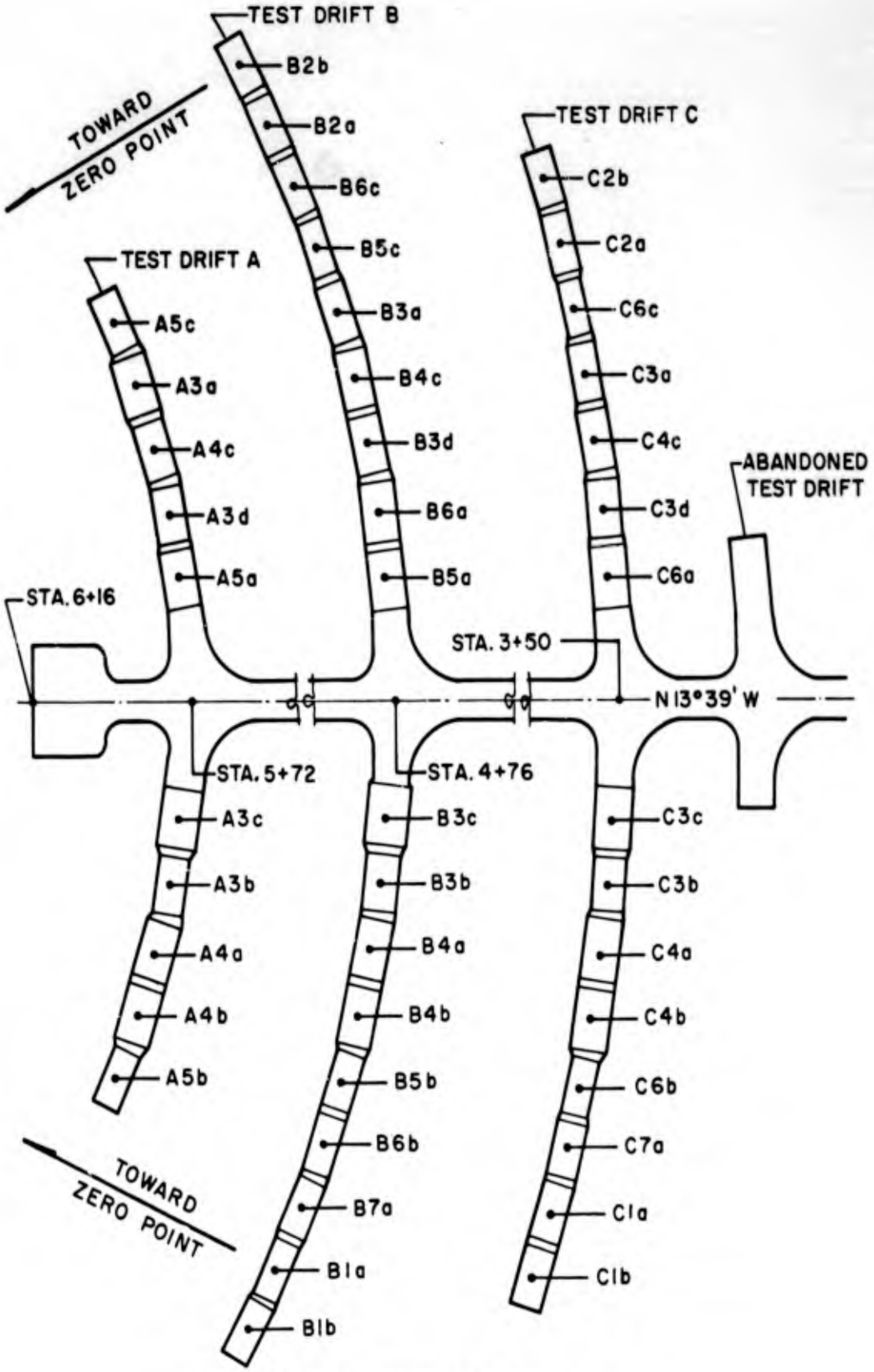

Figure 1.26 Plan view of test sections.

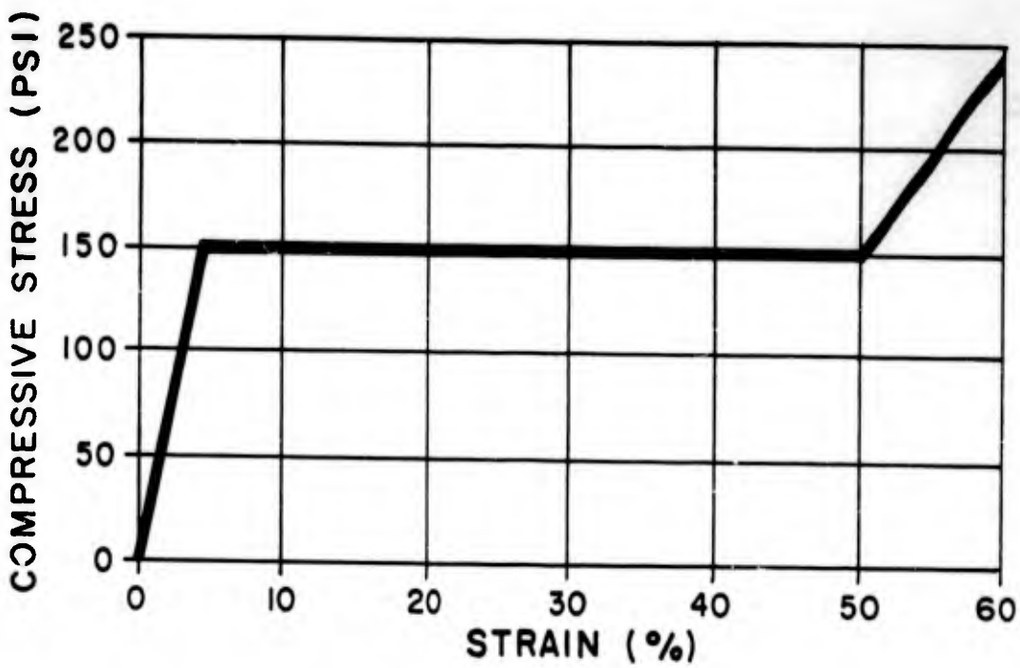

Figure 1.27 Assumed stress-strain relationship of polyurethane foam.

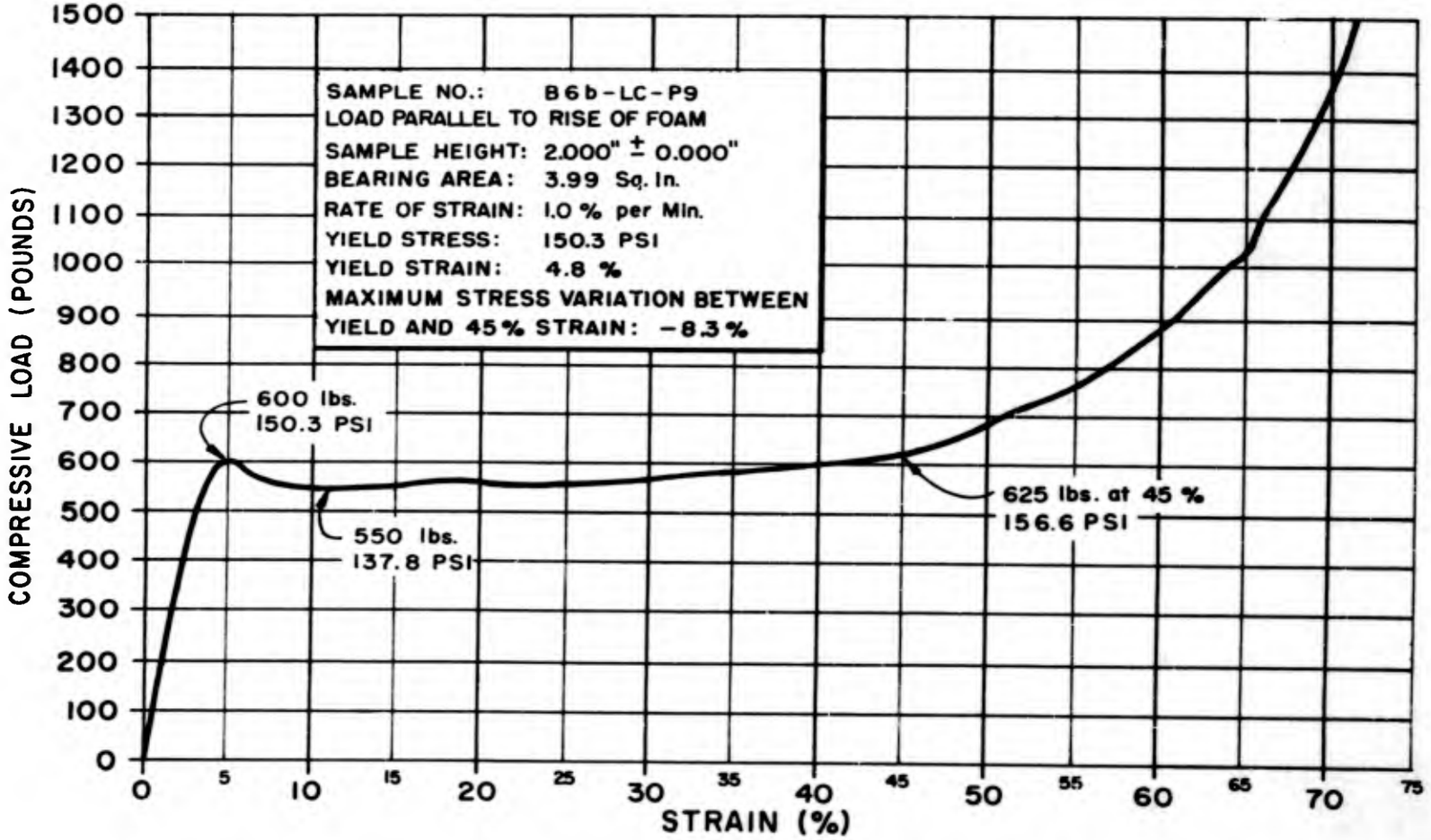

Figure 1.28 Sample stress-strain curve from unconfined compression test for precast foam sections.

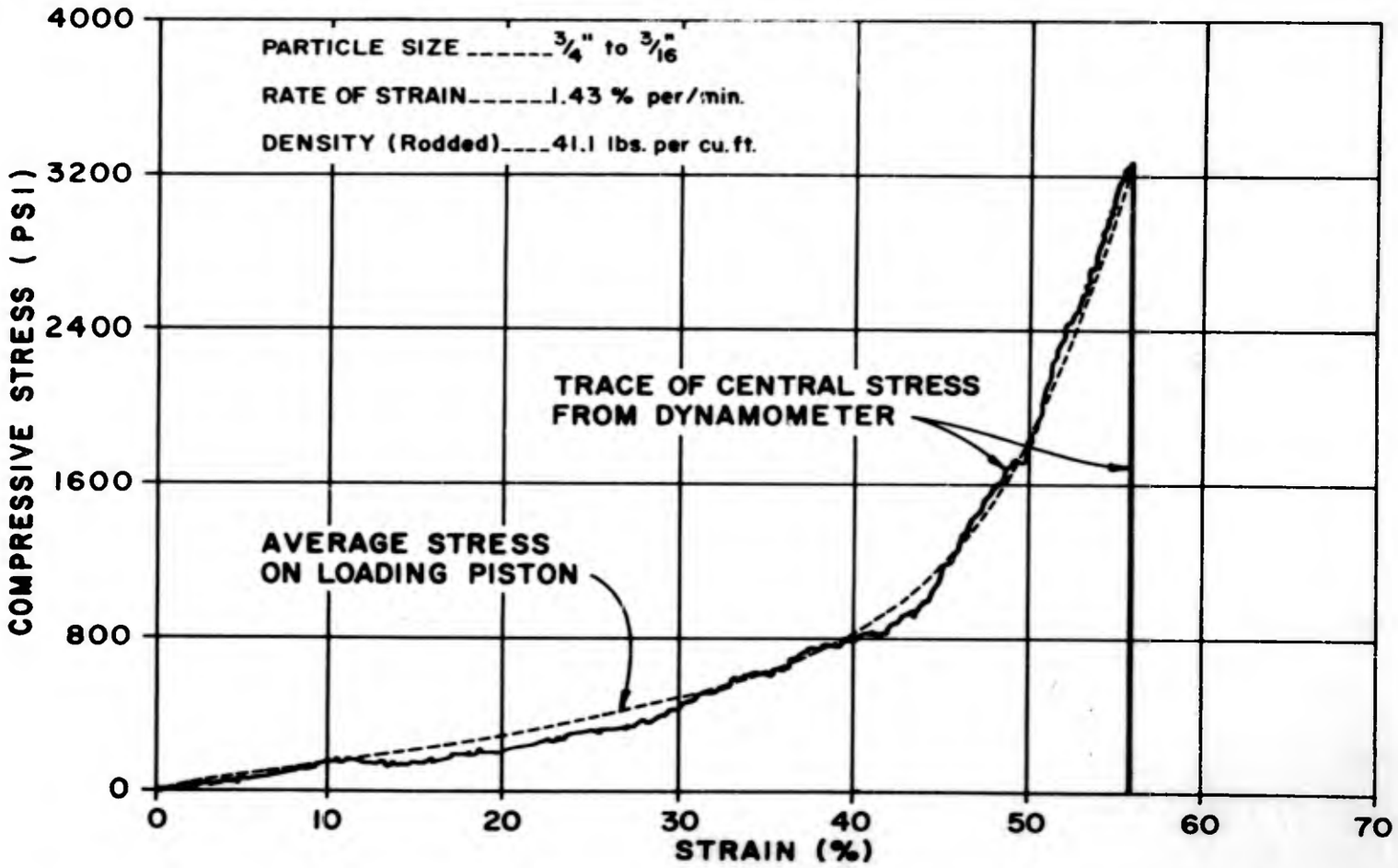

Figure 1.29 Stress-strain curves from confined compression test on volcanic cinders used for backpacking material.

CHAPTER 2

PROCEDURES

2.1 CONSTRUCTION

A lump-sum contract was awarded for the construction of the Station 1500 complex, and work was started in November 1959. The scope of the contract included construction of the vertical shaft, the access tunnel, and the three test drifts complete with liners and backpacking.

As a result of difficulties encountered in producing polyurethane foam of acceptable properties by foaming-in-place methods, construction was incomplete when work was suspended in October 1960. At that time, sixteen of the twenty liners requiring polyurethane foam backpacking were incomplete or were filled to some extent with unacceptable foam. In the spring of 1961, all liner materials and foam were removed from these sixteen sections.

In November 1961, the construction of these remaining sixteen liners was resumed by the NTS cost-plus-fixed-fee (CPFF) contractor. Precast foam units were installed as backpacking

in lieu of foaming-in-place. All tunnel liner construction was completed in January 1962.

Because the construction had been suspended and resumed, the whole construction program has been separated into two phases for purpose of discussion in this report. The initial phase includes the complete excavation and the construction of the first 27 test sections. The final phase refers to the installation of the last sixteen liners.

2.1.1 Initial Phase.

Excavation. Excavation of the vertical access shaft at Station 1500 was started in November 1959. Conventional shaft sinking techniques were used. Standard shaft drill round patterns, using vee cuts for relief, were drilled with jackhammers. The rounds were generally drilled six feet deep. A Cryderman shaft-mucking machine was used to load the broken rock into a self-dumping skip with a capacity of 75 cubic feet. Figure 2.1 shows the skip being dumped at the surface.

As excavation proceeded, the shaft lining was installed about twenty feet behind the advancing rock face. The shaft lining was of conventional design and included hoisting, manway, and utility compartments. Details of the lining are shown in Figure 2. 2.

In February 1960, the shaft construction was completed, and the access tunnel was started. The access tunnel as well as the test drifts were driven without roof support. Jackleg rock drills were used for drilling, Eimco Model 630 mucking machines for loading, and Scootcretes for hauling the broken material to the shaft for hoisting.

When the access tunnel reached the proposed location of C Drift, a fault zone was encountered, approximately eighteen feet wide and trending roughly at right angles to the access tunnel. This zone consisted of three approximately parallel fault strands, averaging 1/2 inch thick, and dipping steeply to the south. The rock between the strands was lightly brecciated. The rock

condition appeared to be suitable for test purposes. Considering the desirability of retaining the drift in its original proposed location, it was decided to excavate as planned. Also, the undulating nature of the fault strands and the limited exposure made it difficult to project the fault easterly or westerly.

Upon advancing the drift a short distance each way, low-angle cross-faulting was encountered at the top of the western drift. The rounds tended to break to these faults, causing excessive enlargement of the drift over the desired dimensions. Accordingly, C Drift was relocated to its present position, forty feet northerly of the original location. The B Drift location was shifted ten feet northerly to maintain its location as the geometric mean of the distances from the detonation point to A Drift and the relocated C Drift.

The excavation tolerances for test drifts are shown in Figure 2.3. In general, the contractor drilled the test drift rounds using the A

minus three-inch line as a guide. It was believed that this method would result in a minimum of overbreaking beyond the A plus five-inch line.

The rough excavation of all drifts was completed in May 1960. Following this, the walls of the test drifts were smoothed by removing projections inside the minus three-inch line and guniting the areas broken outside of the plus five-inch excavation line. The contractor backfilled the sections requiring polyurethane foam backpacking with gunite to the minus three-inch line to reduce the volume of foam required. As a result, the test sections designated as having nominal foam thickness of 24 or 9 inches now had an annular gap of approximately 21 inches or 6 inches, respectively.

Lining Installation. Generally, the liners for the various test sections were installed in sequence from the extremities of the drifts toward the access tunnel. In sections requiring cinder backpacking, the cinders were installed after each liner was completed. In sections

requiring polyurethane foam, with the exception of those requiring concrete liners, the liners remained supported by erection beams until several liners had been accumulated. This procedure permitted a more continuous foam placement operation.

Corrugated steel tunnel liner sections were pre-assembled on the surface into eighteen-inch wide rings which were then transported underground. The first ring was bolted to the far end bulkhead, and subsequent rings were aligned and bolted together to form the completed section. When the last ring was installed, the section was bolted to the near end bulkhead, and the temporary blocking supports removed. In this condition, the liner was quite rigid and supported normal foot traffic with little deflection. Figures 2.4, 2.5, 2.6, and 2.7 illustrate several stages in the assembly of a corrugated steel tunnel liner.

Wide flange rings (to support the corrugated steel decking or three-inch by eight-inch wood lagging) were shop fabricated into one piece and taken underground in this form. A section of steel rails, laid upon the floor, supported the rings for spacing and alignment. The rings were then connected by welding three-inch standard pipe spacers between rings. When the connections were completed, the entire unit was raised to the proper elevation and aligned before an erection beam was installed. The wood lagging or corrugated steel decking was then installed. Following this, the final end bulkheads, which would contain the foam or cinder backpacking, were installed and the cinders or foam emplaced.

The erection beam was then withdrawn, permitting the weight of the liner to be transferred to the backpacking material. Figures 2.8, 2.9, 2.10, 2.11, and 2.12 illustrate a typical section of wide-flange rings with corrugated steel decking in various stages of construction. Note that the

corrugated steel decking was welded to the wide-flange rings. The method of fastening wood lagging to the wide-flange rings by means of metal clips and lag screws is shown in Figure 2.13.

The reinforced concrete sections in which polyurethane foam backpacking was to be placed were first provided with tongue-and-groove forms. These forms were covered on the outer surface with polyethylene film to facilitate removal of the forms after foam emplacement (see Figures 2.14 and 2.15). After the foam had been poured and allowed to cure for approximately 72 hours, the forms were removed (see Figure 2.16), and the reinforcing steel for the concrete liner was installed. The polyurethane foam served as the outer form for the concrete liner, and an inner form was installed. Figure 2.17 shows typical concrete form construction.

Concrete was pumped through a four-inch pipe inserted at the top of the end bulkhead, as shown in Figures 2.17 and 2.18. The pipe initially

extended the entire length of the test section. It was assembled in approximately five-foot lengths with irrigation pipe couplings to facilitate disassembly. As concrete filled the forms, the pipe was gradually withdrawn and finally removed.

Concrete sections requiring cinder backpacking were constructed in essentially the same manner as the sections with polyurethane foam backpacking. Forms for the cinders were installed in the same manner as the forms for the foam, except that polyethylene film was not applied. The same forms were used for the emplacement of the cinders and concrete and remained in place after the concrete was cast. The presence of the wood was not considered objectionable from the test standpoint, as the compressive strength of wood perpendicular to the grain is comparable to that of the cinders.

A bond-breaking solution was first applied to the tunnel surface in test sections which were to have the concrete cast directly against the rock.

The various steps involved in this type of liner are shown in Figures 2.19, 2.20, 2.21, and 2.22.

The horseshoe sets used in this experiment were conventional tunnel supports and presented no particular problems in erection. The alignment of these sets was unusual, however, in that they were inclined toward the zero point in order to be normal to the direction of the stress wave (see Figure 2.23). No backpacking was used around these sets in order that a correlation between this test and previous tests, Hardtack Phase II, could be obtained. As shown in Figure 2.23, intermittent wood blocking to the rock face was installed.

The sections designated to receive mesh lining were lined with four-foot by eight-foot sheets of No. 10 expanded metal, held in place by rock bolts. This mesh is quite rigid and difficult to install, because it did not readily conform to the irregular rock wall surfaces. Because of this, and the need to place rock bolts at the points where the sheets

overlapped, it was necessary to vary the spacing of the rock bolts from the planned three-foot spacing. Figures 2.24 and 2.25 show typical features of this type of liner.

Backpacking Installation. Cinders were blown into the annular spaces between the rock walls and liners, or forms, by use of the same machine used for pumping concrete. This machine had a regulator which allowed the air pressure to be varied over a wide range, and it was established, by trial and error, that a pressure of approximately forty psi produced optimum results. It was found that cinders would flow around and fill irregularities in the liners, and a minimum of fines would be produced by attrition.

Several holes were provided in the end bulkheads to permit introduction of the cinders. As the level of the cinders rose, the holes were covered. It is interesting to note that, upon inspection of the cinders through holes caused by later accidental damage to several bulkheads, no trace of

fine material was detected. Apparently, the small quantity of dust produced by attrition was carried through the section and emitted through small gaps in the far bulkhead.

The placement of polyurethane foam was the most difficult operation in the initial construction phase of the experiment. Two subcontractors failed to install satisfactory foam around the liners, although one made satisfactory pours in one-cubic-foot pasteboard containers and in a simulated test section in the abandoned C Drift. The reasons for this difficulty are not completely clear at this writing, although it appears that the methods of emplacemnt, i.e., pumping the components through small holes in the liners, with no opportunity to observe the foaming reaction, contributed greatly to the problem. As a result of the difficulties in this operation, only four of the twenty test sections requiring polyurethane foam backpacking had been completely filled with foam of usable quality on the date of the termination of the initial construction contract.

There were many variations in the techniques of mixing the components and in the compositions of the foam formulations. The following procedures were common to both subcontractors.

The components were prepared and then pumped through separate hoses to a mixing nozzle. The nozzle was inserted in 1/2- to 1-inch-diameter holes, previously drilled through the liner in horizontal rows. The ratio of the components was varied by adjusting the speeds of the two pumps, and the foam was placed in 1- to 2-foot-deep lifts extending the length of the test section. Some difficulty was experienced in filling the crown of each section, because the plastic foam was quite fluid before the foaming reaction started and flowed out of the access holes as the nozzle was withdrawn.

2.1.2 Final Phase. In August 1961, a plastic foam manufacturer was engaged by H&N to develop formulations and techniques for installing foam of specified properties behind

the remaining sixteen test liners. The scope of the program included placement tests in simulated test sections constructed in the manufacturer's shop, followed by field placement test in one of the test drifts of Station 1500.

Various methods of foam placement were investigated, including spraying and casting-in-place by either machine pouring or batch pouring. At the end of the laboratory investigation, the foam manufacturer recommended that batch pouring was the most feasible method of depositing foam behind the liners, meeting the required physical properties.

The recommended method was to construct the liners in successive vertical lifts from the invert to the crown. As the liner was installed, the annular gap would be divided into compartments, both radially and longitudinally, by means of wood forms. Foam components would be mixed and then poured into each compartment. Because of the irregular surfaces of the tunnel walls, and to produce a slight backpressure considered necessary for control of the foam properties, an excess of the calculated volume of foam would be poured into each compartment, and the excess allowed to extrude from the form.

The urgency of resuming construction of the tunnel liners precluded the field placement tests. When reviewed by H&N, the recommended foaming method was deemed tedious for the following reasons: (1) the irregular rock surface of the test drift would cause undue difficulty in fitting and sealing the wood forms; (2) several crews (crafts) such as carpenters, steel workers, and plastic foam technicians, would be required to be in the same test section at the same time. The resulting congestion would create a highly inefficient operation; and (3) the existing liners, installed during the initial phase of the construction, would impede the movements of foaming equipment and chemicals.

In view of the above difficulties, inherent in the cast-in-place method, it was decided to install precast foam units in the remaining sixteen test sections. Collateral benefits of the precast method were as follows: (1) quality control would be better in the manufacturer's shop than if the foam were produced in the tunnels; (2) in view of the anisotropic properties of the foam, it was considered desirable, from a structural analysis standpoint, that the foam rises radially relative to the longitudinal axis of the

test section. If the foam were cast in place, the direction of rise could not be controlled and probably would be in a vertical direction.

In preparation for the precast foam installation, the rock surfaces of the sixteen test sections were trimmed, as necessary, to provide a minimum one-inch radial clearance between the rock surface and the foam. This was necessary to provide sufficient space for assembly purposes. It had previously been determined that, in order to avoid excessive trimming of rock surfaces, the optimum thickness of foam would be 20 inches and 5 inches, corresponding to the nominal specified thicknesses of 24 inches and 9 inches, respectively.

Wide Flange Ring Sections. During the final phase of the construction, it became necessary to pass all materials through existing liners. To facilitate the installation of the lagging and foam, it was necessary to fabricate the rings in halves and weld them together within the test section.

The corrugated steel decking had foam cast directly to each panel in the shop, and the panels were

assembled within the test section (see Figure 2.26). In general, the sequence of assembly for this type of liner was as follows: (1) sand was installed in the bottom of the drift and smoothed to the proper configuration; (2) an erection beam was then installed to facilitate handling the wide flange rings within the test section; (3) two rings were brought in, assembled, and suspended from the erection beam, at opposite ends of the test section; (4) two or three panels were placed upon the sand, interlocked, and blocked to conform to the proper radius, and additional sand was added at the sides as needed; (5) the remaining panels were brought into the test section and arranged around the two rings in succession from the bottom to the top. The panels were temporarily held against the rings by means of wooden wedges inserted between the foam and the rock surface; (6) the remaining rings were then moved into the section, positioned, and assembled for welding; and (7) bulkheads were fitted at the ends of the liner to seal the annular gap, and sand was blown in.

Figures 2.26, 2.27, 2.28, and 2.29 show various steps in the assembly of one of these sections.

Liners With Wood Lagging and Foam. The assembly techniques for the liners with wide flange rings, wood lagging, and foam were essentially the same as for the liners with corrugated steel decking. The foam backpacking consisted of twelve units, such as those in Figure 2.30. The wood lagging and foam units were installed around the end rings in the same sequence as that described for the corrugated steel decking.

Lag screws and steel clips were used to fasten the wood lagging to the flanges of the wide flange rings. Typical views of a liner of this type in various stages of completion are shown in Figures 2.31, 2.32, and 2.33.

Corrugated Tunnel Liners. All corrugated tunnel liner plates were cast with either five inches or twenty inches of polyurethane foam, in the shop. Prefoamed plates with twenty inches of foam, as

delivered to the site, are shown in Figure 2.34. These individual plates were transported underground and assembled in place upon a bed of sand. It was necessary to locate the first plate precisely to ensure that the completed liner would be centered within the rock walls, and that all plates with gage mounts were properly oriented with respect to the zero point. Figure 2.35 shows the first plates of one of these sections being aligned.

When the plates had all been assembled, the end bulkheads were installed, and the annular gap was filled with sand. A completed liner of this type is shown in Figure 2.36.

Reinforced Concrete Liners. Foam for concrete liners was cast in twelve annular units of 30 degrees each. The twenty-inch-thick units were cast five feet in length to facilitate shipping and handling within the test drifts. The five-inch-thick units were cast in fifteen-foot lengths.

The sequence of construction for concrete liners with precast foam was as follows: (1) the

foam was fastened to the test drift walls in the proper orientation by means of rock bolts. All gaps between adjacent pieces of foam were filled with felt; (2) end bulkheads were installed, and the annular space between the foam and the rock walls was filled with sand. Reinforcing bars and concrete forms were then installed in approximately the same manner as was followed during the initial construction phase. As the installation of the concrete form progressed, fabricated chairs were installed between the foam and the inside of the concrete form to permit removal of the rock bolts which had been holding the foam in position. In this manner the foam was supported by the concrete form to prevent shifting or sagging during the pour. Typical form construction can be seen in Figure 2.37.

2.1.3 Preshot Preparation for Reentry During the final phase of tunnel liner construction, a detailed plan for reentry was prepared. The primary purpose of this plan was to provide for safe, economical, and expeditious postshot recovery of data and observations of test drift damage.

The Station 1500 re-entry plan included the requirement for a system of stemming consisting of two bulk sand plugs, each thirty feet in length, and a 75-psi blast door. The two sand plugs were centered on Stations 4+35 and 5+27, and the door was located at Station 0+37. The effect of the stemming system was to divide the underground openings into several compartments. In the event of venting of radioactive, explosive, or toxic gases into the underground openings, it would be possible, upon re-entry, to purge the individual compartments in sequence. In that manner, rehabilitation of the shaft and access tunnel and re-entry to the test drifts could be conducted, step by step, within a safe atmosphere.

During the development of the re-entry plan, H&N was requested to evaluate the response of the more critical surface facilities and equipment to the anticipated levels of shock. In accordance with the recommendations of this study, the headframe, hoist, and ventilation blower at Station 1500 were removed before the shot.

2.2 INSTRUMENTATION

2.2.1 General. The plan of instrumentation was developed by the U of I in collaboration with SRI and H&N. The general objective of the plan was to obtain as much significant information on the loading and response of the tunnel liners as possible within the budgeted time and funds.

It was recognized that transient measurements of loading and liner deformation, recorded by electronic instrumentation, would provide the most useful information for purposes of analysis. However, cost limitations and the availability of electronic gages dictated that the majority of the measurements be made with passive instrumentation. Accordingly, the final instrumentation plan specified 749 static or mechanical measurements, as well as 108 electronic measurements. The distribution of these measurements is shown in Figure 2.38, which is a schematic presentation of the instrumentation plan.

For the purpose of assigning locations for gages, all test sections were given angular notations in the circumferential direction. The position designated as 0^{o} was directed toward the point of detonation, as shown in the lower right hand corner

of Figure 2.38. The same system was used to describe postshot damage.

Most of the electronic gages were concentrated in B Drift. This distribution was based on the prediction that B Drift would receive significant damage and would therefore yield the most useful information on liner response. Static or mechanical measurements were designated for all test sections, irrespective of drift location.

At the start of user-occupancy, representatives of Projects 3.1 and 3.2 jointly assigned locations for all instruments and measurement points in each test section. Electronic instruments were assigned the most desirable locations, as near the mid-point of the liner as possible. The instruments were grouped in such a manner that complementing measurements would be made in as nearly the same vertical plane as practical. As examples, velocity gages were mounted close to diameter-change gages, and compression-of-filler gages (i.e., compression of backpacking material) were installed near gages measuring pressure on the lining (Carlson gages).

Static or mechanical measurements were generally taken in close proximity to like electronic measurements to obtain a correlation of these measurements.

SRI, Project 3.2, incorporated gages for the measurement of pressure exerted on the linings, changes in liner diameter, circumferential and longitudinal strain in liner structural components, compression of the backpacking material, lining velocity, and circumferential and radial strain measurements in the rock adjacent to the test sections.

H&N and U of I took pre-shot measurements for longitudinal strains in the liners, compression of the backpacking, and diameter change in the liners, using extensometers and scratch type gages. Precise pre-shot surveys by H&N to locate all test sections in an absolute sense were also made.

STL, Project 3.12, utilized reed gages within some of the liners and in canisters at various locations in the tunnel floor to obtain displacement response spectra. These gages were of the same design as used in previous test operations.

EG&G, Project 3.11, was responsible for motion-picture determinations for fly-rock velocities and trajectories.

Measurements of considerable importance to this project were the dynamic free-field measurements made by Sandia Corporation, Project 3.3. A portion of these measurements was made at the bottom of six 100-foot holes, drilled at intervals in the floor of the access tunnel. Other measurements, to determine the dynamic strain concentration around the tunnel, were made in short holes which had been drilled radially around the tunnel at two locations.

APRL/USBM, Project 3.6, determined static stress profiles around bare rock sections at two or more locations.

2.2.2 Transient Measurements.

Electronic Strain Gages. Circumferential and radial strains developed in the walls of the tunnels by the pressure pulse were determined by the use of SR-4 type strain gages mounted upon rock cores. The cores were grouted into NX size diamond-drilled holes extending radially from selected test sections. Strains were measured at depths of zero, one, and two tunnel radii from the rock surface. It was expected that these measurements could be compared

with corresponding free-field measurements to establish strain concentrations around the tunnel openings.

Circumferential and longitudinal strains in the linings were also measured with SR-4 type strain gages mounted on liner components (see Figure 2.39).

Pressure Gages. Pressures transmitted from the rock to the lining through the backpacking material were measured by Carlson pressure gages. These gages were mounted through the liners so as to protrude slightly into the backpacking. Figures 2.40 and 2.41 show pressure gages installed.

Displacement Gages. Transient determinations of changes in diameter were made on several liners by the use of Sandia-SRI relative displacement gages. This gage consists of a potentiometer and a spring-driven spool or drum attached to a common shaft. A piano wire is wound around the drum and extends across the liner on a

diameter. An electronic displacement gage may be seen in Figure 2.42.

Compression of the backpacking was determined at two orientations in one liner by use of the displacement gages described above. For this application, the wires were fastened to the ends of rock bolts which were anchored in the rock wall (see arrow in Figure 2.43).

Velocity Gages. Lining velocity was measured by standard SRI velocity gages modified for this experiment. This gage, described as an over-damped accelerometer, was used to measure liner velocity radially with respect to zero point. A typical velocity gage installation is shown with an arrow in Figure 2.44.

For more detailed information on the operation and construction of the various electronic gages, the reader is referred to Reference 10.

Photographic Stations. EG&G, Project 3.11, installed three stereo motion-picture

cameras at locations shown in Figure 2.38. The purpose of this photography was to record tunnel deformation and to determine fly-rock trajectories and velocities.

The three camera stations were self-contained, shock-mounted units, designed and fabricated for this experiment by EG&G. A typical installation is shown in Figure 2.45.

The stations in test sections B6c and C6c each contained two 16-mm Fairchild (Red Devil) cameras, capable of operating at 500 frames per second, and two Gun-Sight-Aiming-Point (GSAP) cameras, capable of 64 frames per second. The unit in test section B5a was similar but contained only one GSAP camera.

2.2.3 Mechanical Measurements. Compression of the backpacking was measured by compression-of-filler gages, assembled from standard rock bolts and pipe fittings. The magnitude of the relative motion between the rock wall and the liner

was recorded by the length of scratches on the rock bolts. The initial and final positions of the end of the pipe nipple, with respect to the rock bolt, indicated the permanent deformation of the backpacking. A compression-of-filler gage is indicated by an arrow in Figure 2.46. For details of the construction of this type of gage see Figure 2.47.

Diameter changes of the liners were measured by diameter-change gages fabricated from pipes and pipe fittings. Operation of these gages is similar to that of the compression-of-filler gages described in the preceding paragraph. See Figures 2.49, 2.50, and 2.51 for details of the construction of this type of gage. A typical installation is shown in Figure 2.48.

Reed gages were installed on all concrete liners, on one of the sections having wide-flange rings lined with corrugated steel decking, and in canisters grouted into the floor of the access tunnel at approximate ranges of 250, 340, 460, and 723 feet from the shot point. Each gage consisted of ten masses on cantilever reeds ranging in natural frequency from approximately three to 300 cycles per second. The maximum displacement of each mass relative to its mounting is determined by the length

of scratch scribed on a recording plate; the displacement response spectrum is plotted from these results.

The reed gage is capable of measuring the displacement shock spectrum in one direction. In this experiment, some of the gages were oriented so as to respond to shock in a radial direction with respect to the shot point. Others were mounted transverse to this direction. The reed gage shown in Figure 2.52 is mounted radially, while the gage in Figure 2.53 is oriented to respond to the transverse component. Gages installed in canisters may be seen in Figures 2.54 and 2.55.

By comparing the data derived from gages mounted in canisters with the response of gages mounted on tunnel liners at the same range, a measure of the shock attenuation provided by the various backpacking materials could be obtained.

DeForest scratch gages were installed for measuring circumferential strains in the liner components. These gages were manufactured by Baldwin-Lima-Hamilton Corporation and are no longer available in the market. According to the manufacturer's specifications, this gage, consisting of a scratch arm and polished scratch plate (target), is capable of recording

deformations ranging from 0.0001 to 0.05 inch over its gage length of two inches.

In the concrete liners, circumferential strains were measured by deForest gages mounted on the circumferential reinforcing steel through access holes provided during the construction. Typical deForest gage installations are shown by the arrow in Figure 2.56 and Figure 2.57.

2.2.4 Static Measurements. Measurements of permanent circumferential and longitudinal strains in liner components were made by drilling gage holes approximately two inches apart, then measuring the exact spacing by means of a Whittemore extensometer or similar direct-reading gage. The readings were repeated after the test to determine the permanent strain. By careful preparation of the gage points and proper manipulation of the gage, accuracy of approximately 0.0005 inch could be obtained. These measurements supplemented the measurements of strain made by deForest gages.

A precise pre-shot traverse was made from remote points on the surface down the access shaft and into the test drifts to locate each test section in an absolute sense. An equivalent

postshot survey was made to determine the gross displacements of the test sections.

At the end of the excavation phase, detailed cross sections of the test drift walls were made. These measurements were repeated after the liners had been installed to determine variations in thickness of the backpacking materials and to determine precisely the as-built dimensions of the liners. Permanent distortion of liners as well as determinations of rock breakage in unlined sections were obtained by comparing the pre- and postshot cross sections.

2.2.5 Variation from Instrumentation Plan. Minor departures were made from the instrumentation plan during the course of the instrumentation phase. For example, measurements of circumferential strain by both deForest and Whittemore gages were eliminated in test sections B7a and C7a. It was agreed that the locations of maximum strain in the sets were readily predictable, i.e., corresponding to the points of blocking, and the deflection of the sets would be most readily obtained from comparison of the pre- and postshot cross sections of the sets. The ten deForest gages allotted to these liners were accordingly reassigned to other liners.

The number of survey measurements made considerably exceeded the planned minimum for each type. Approximately 2,500 separate measurements were involved in the as-built transit survey of the tunnel liners. Also more than 1,000 sets of Whittemore gage points were established on tunnel liner components.

At the end of the instrumentation phase, as-built drawings showing exact locations of all gages and measurement points were prepared.

Figure 2.1 Dumping muck at Station 1500 during shaft excavation. (H&N-AEC 60-738-4, 1960).

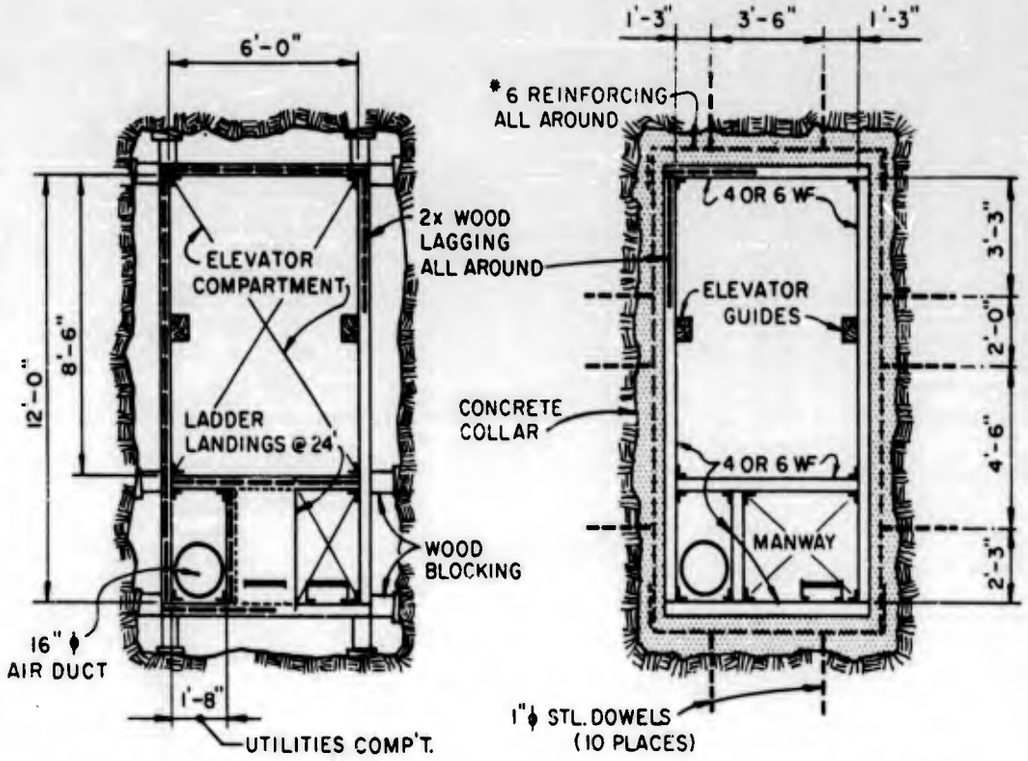

PLAN AT STANDARD SET

PLAN AT BEARING SET

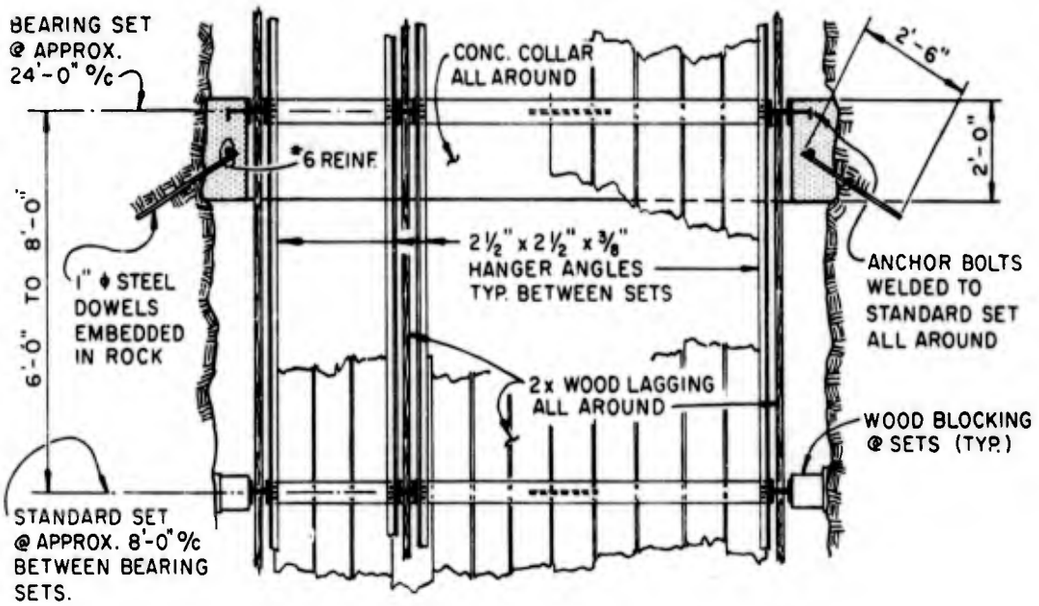

LONGITUDINAL CROSS SECTION

Figure 2.2 Details, shaft lining, Station 1500.

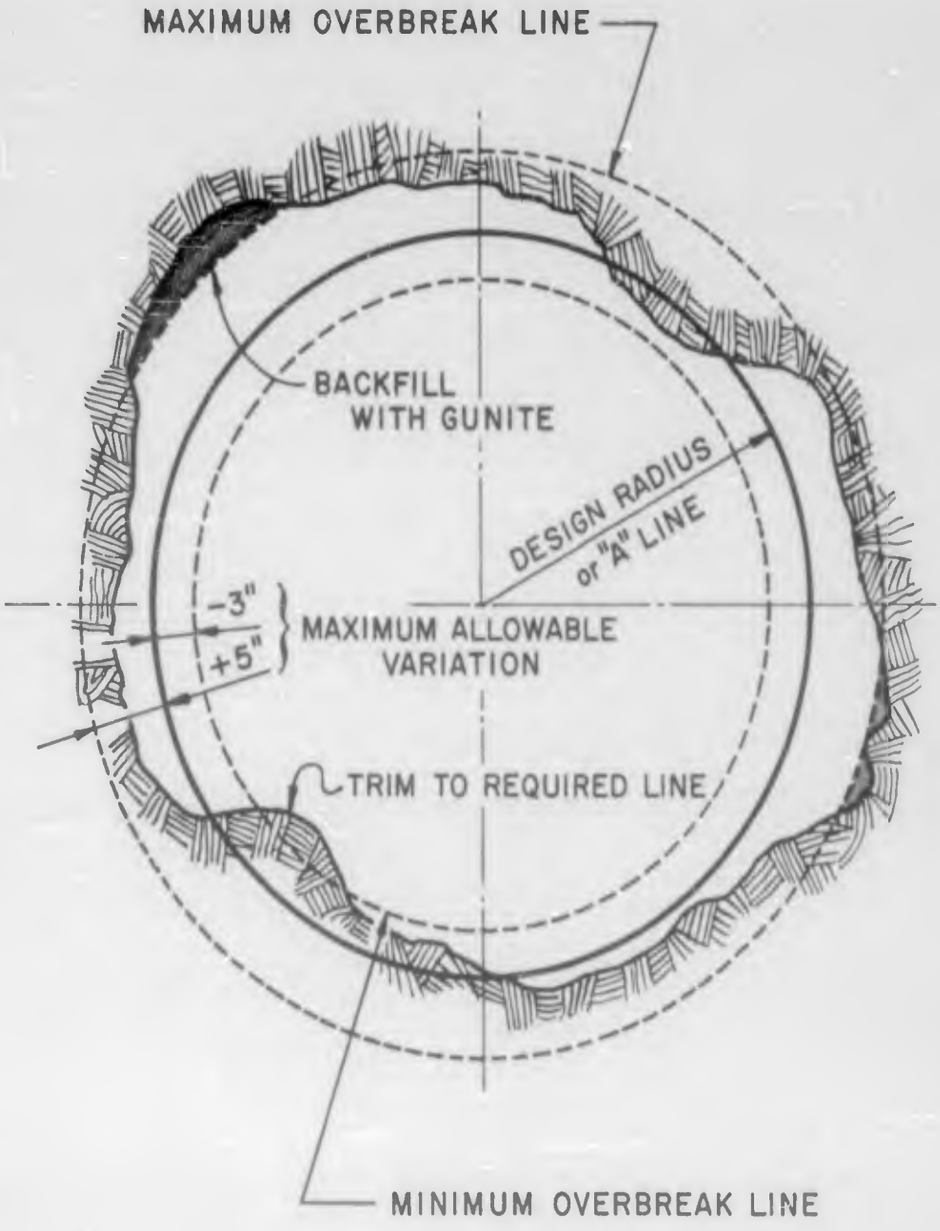

Figure 2.3 Excavation tolerances.

Figure 2.4 Assembling of corrugated steel tunnel liner. (H&N-AEC 792-10, 1960).

Figure 2.5 Tightening of bolts connecting one ring of corrugated steel tunnel liner to the next ring. (H&N-AEC 796-5, 1960).

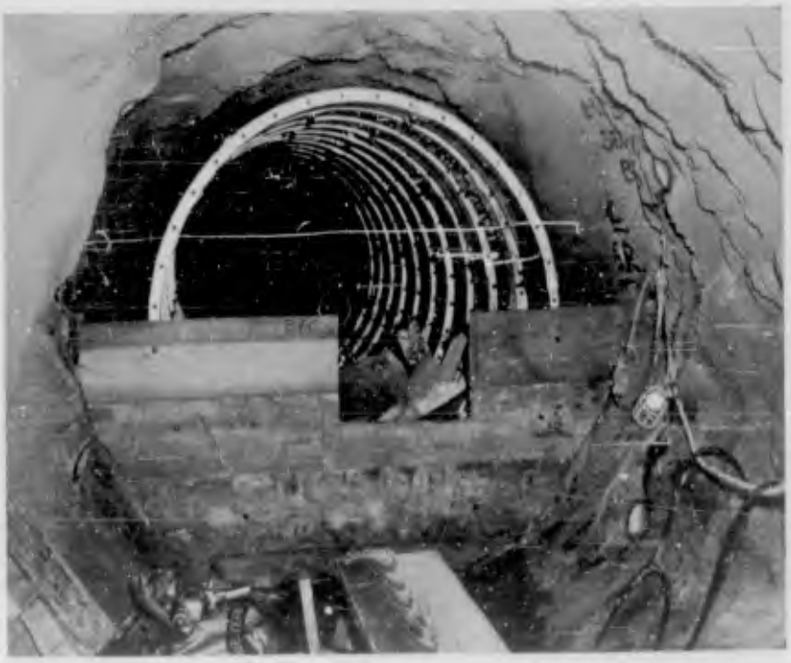

Figure 2.6 End bulkhead for corrugated steel tunnel liner partially installed. (LRL Photo, 1960).

Figure 2.7 Corrugated steel tunnel liner completed. (LRL Photo, 1960).

Figure 2.8 Assembling wide-flange rings on rails. (H&N-AEC 805A-5, 1960)

Figure 2.9 Wide-flange rings suspended on erection beam. (H&N-AEC 709-3, 1960).

Figure 2.10 Welding corrugated steel decking to wide-flange rings. (LRL Photo, 1960).

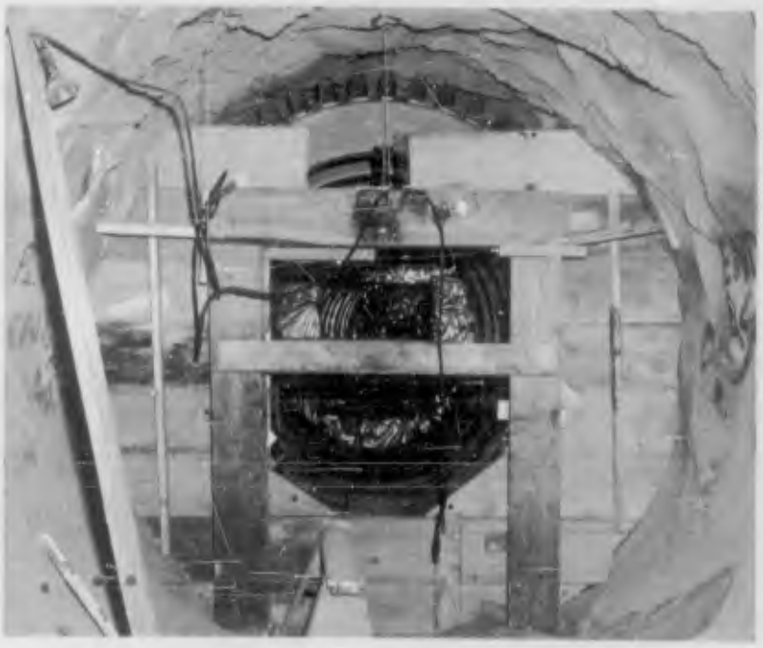

Figure 2.11 Installing end bulkhead, wide-flange rings with corrugated steel decking. (H&N-AEC 789-4, 1960).

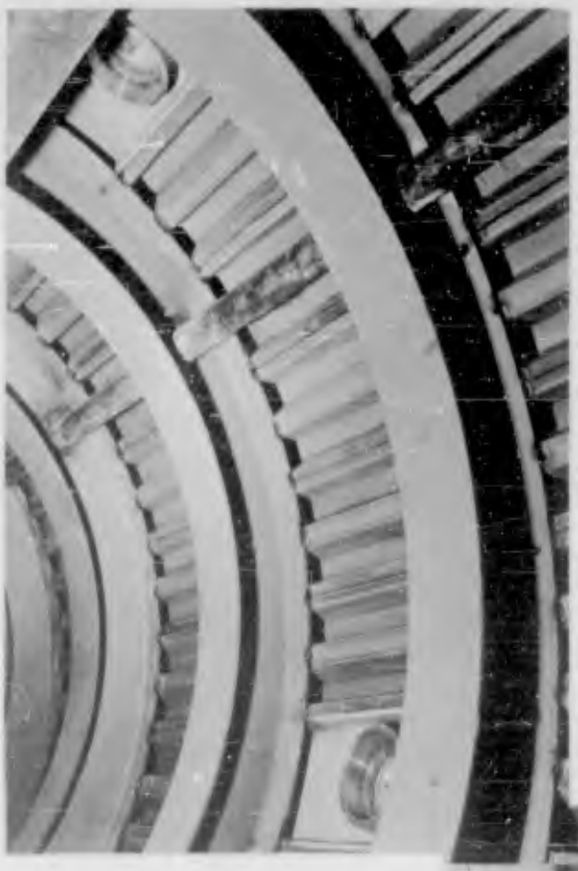

Figure 2.12 Details, wide-flange rings with corrugated steel decking. (H&N-AEC 805A-8, 1960).

Figure 2.13 Details, wide-flange rings with wood lagging. (H&N-AEC 805A-2, 1960).

Figure 2. 14 Installing polyethylene film which lined forms for polyurethane foam. (H&N-AEC 805A-1, 1960).

Figure 2. 15 Installing tongue-and-groove forms for polyurethane foam. (H&N-AEC 789-1, 1960).

Figure 2.16 Stripping tongue-and-groove forms after foaming. (H&N-AEC 60-829-7, 1960).

Figure 2.17 Typical concrete form construction. (H&N-AEC 789-8, 1960).

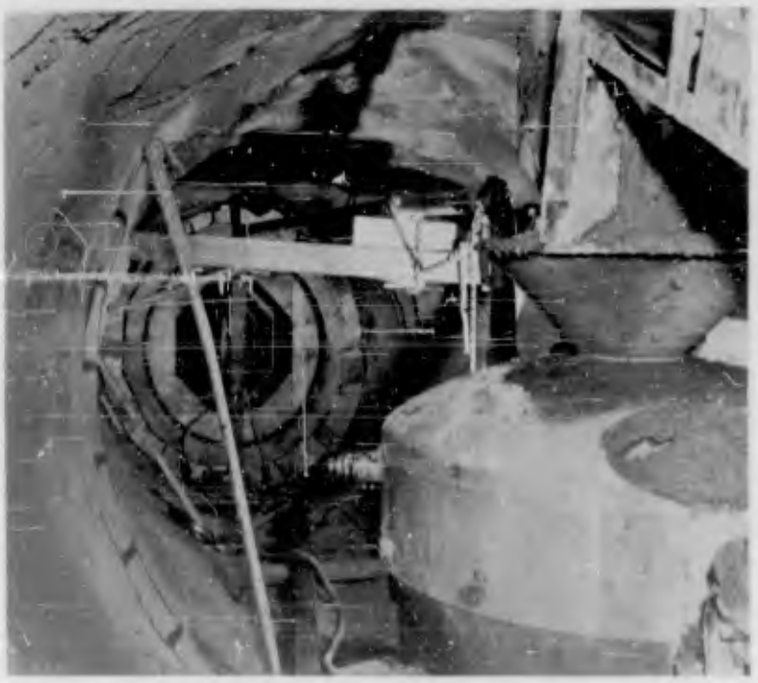

Figure 2.18 Equipment for pumping concrete (H&N-AEC 789-9, 1960).

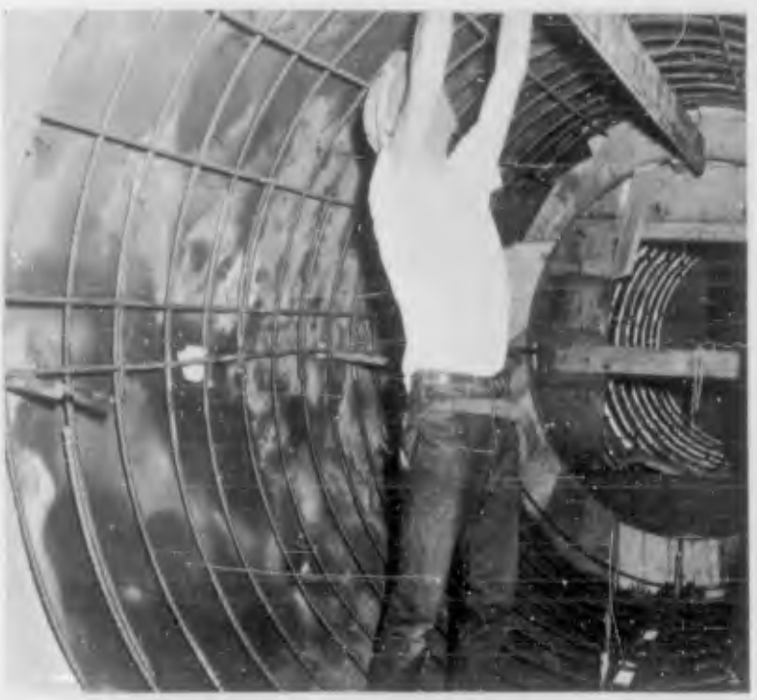

Figure 2.19 Installing reinforcing steel for concrete liner cast against rock. (H&N-AEC 60-788-8, 1960).

Figure 2.20 Reinforcing steel installed, ready for concrete form; concrete liner cast against rock. (LRL Photo, 1960).

Figure 2.21 Concrete liner, forms installed. (H&N-AEC 789-2 1960).

Figure 2.22 Concrete liner, formwork removed. (H&N-AEC 60-788-8, 1960).

Figure 2.23 Steel horse-shoe sets with wood lagging. (LRL Photo, 1960).

Figure 2.24 Typical installation, rock bolts and mesh, circular test section. (LRL Photo, 1960).

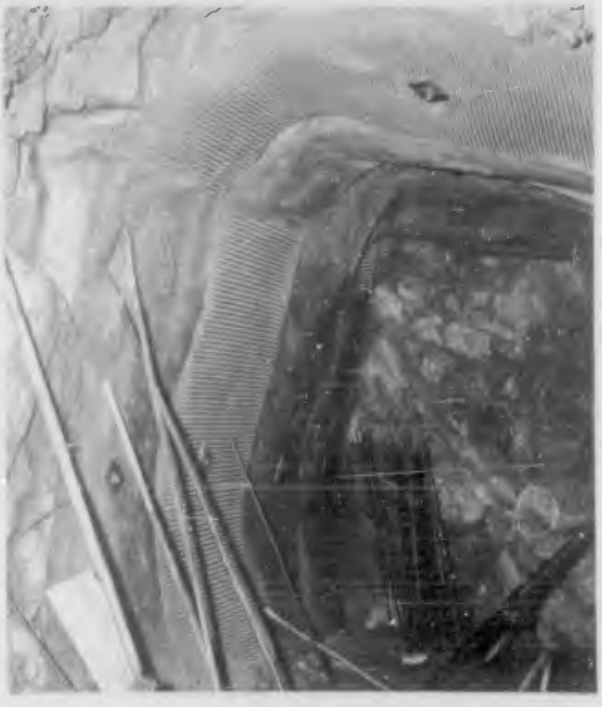

Figure 2.25 Rock bolt installation, square test section. (H&N-AEC 60-779-7, 1960).

Figure 2.26 Corrugated steel decking panels with precast foam prior to installation around wide-flange rings (DASA - NOU 038-08 NTS-62).

Figure 2.27 Panels installed at invert. Note sand bed and wood blocks holding panels against wide-flange rings (DASA - NOU 044-08 NTS-62).

Figure 2.28 Panels installed at side. Note wood blocking in annular gap between foam and test drift wall (DASA - NOU 044-05 NTS-62).

Figure 2.29 Wide flange rings installed, ready for welding (DASA - NOU 043-10 NTS-62).

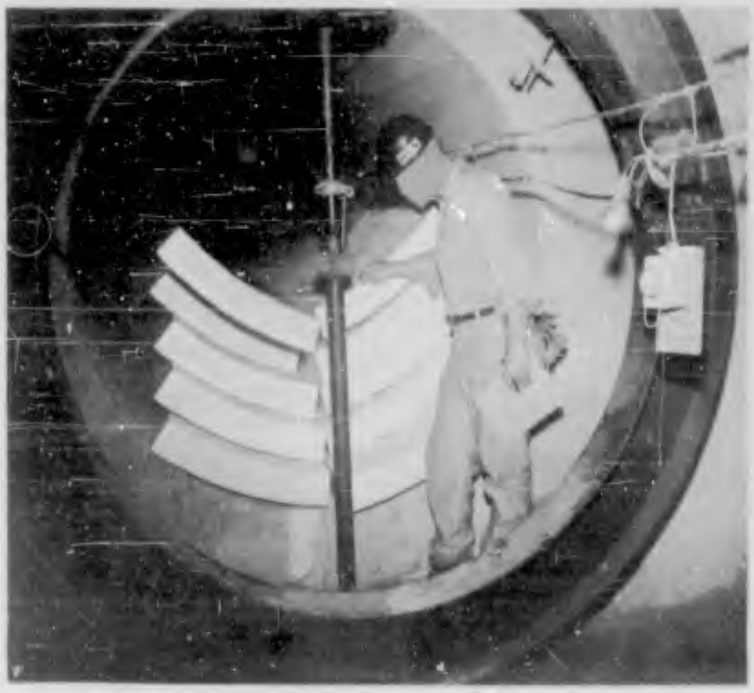

Figure 2.30 Foam units for liner of wide-flange rings with wood lagging (DASA - NOU 039-02 NTS -62).

Figure 2.31 Erection beam installed. End wide-flange ring installed (DASA - NOU 039-03 NTS-62).

Figure 2.32 Installing wood lagging between wide-flange rings and foam units (DASA - NOU 037-12 NTS-62).

Figure 2.33 Welding wide-flange rings (DASA - NOU 044-07 NTS-62).

Figure 2.34 Prefoamed tunnel liner plates, as delivered to site (DASA - NOU 037-10 NTS-62).

Figure 2.35 Assembling tunnel liner plates in test section (DASA - NOU 048-07 NTS-62).

Figure 2.36 Completed liner composed of tunnel liner plates and precast foam (DASA - NOU 082-02 NTS-62).

Figure 2.37 Form for concrete liner with precast foam (DASA - NOU 039-09 NTS-62).

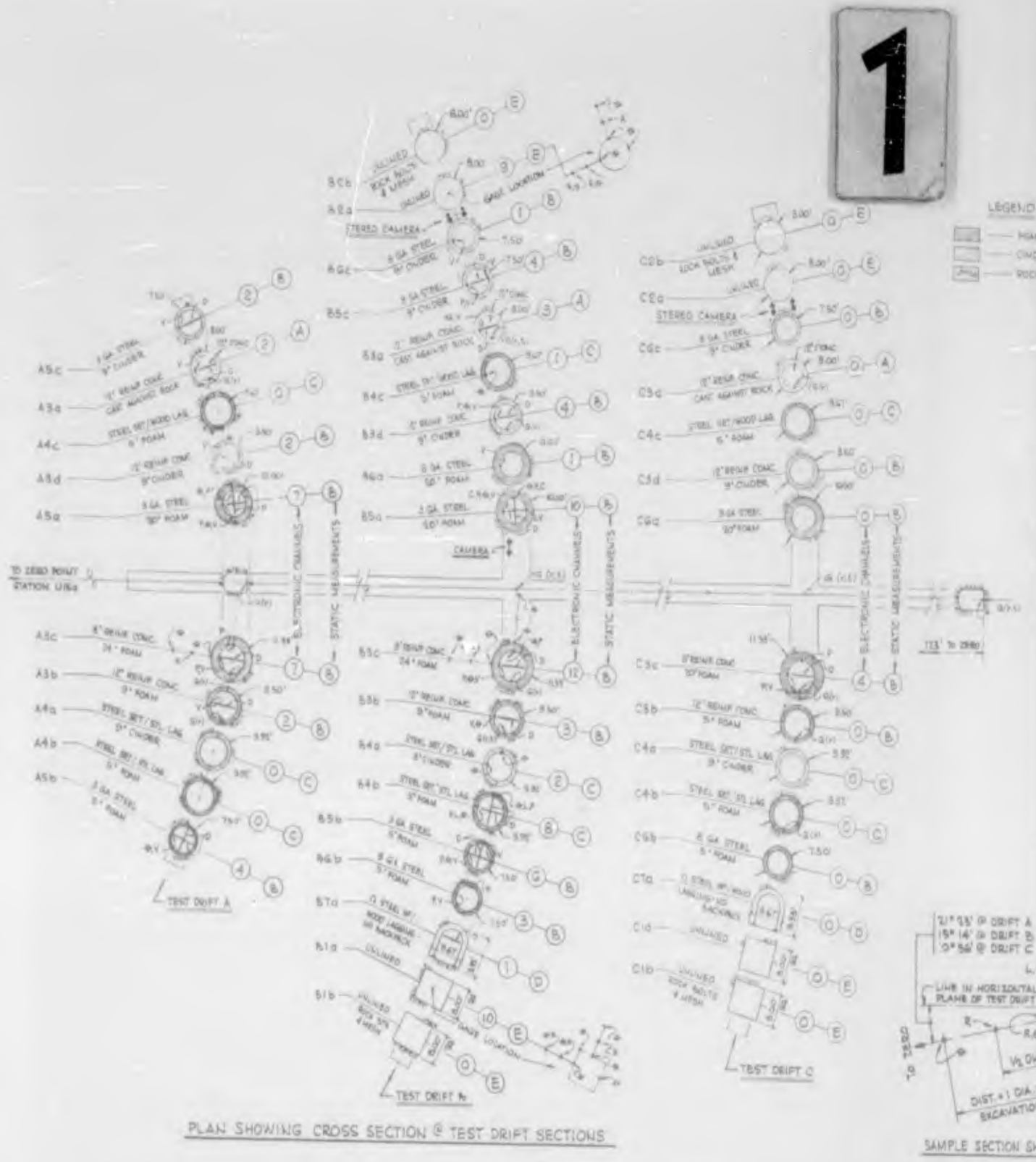

Figure 2.38 Instrumentation plan.

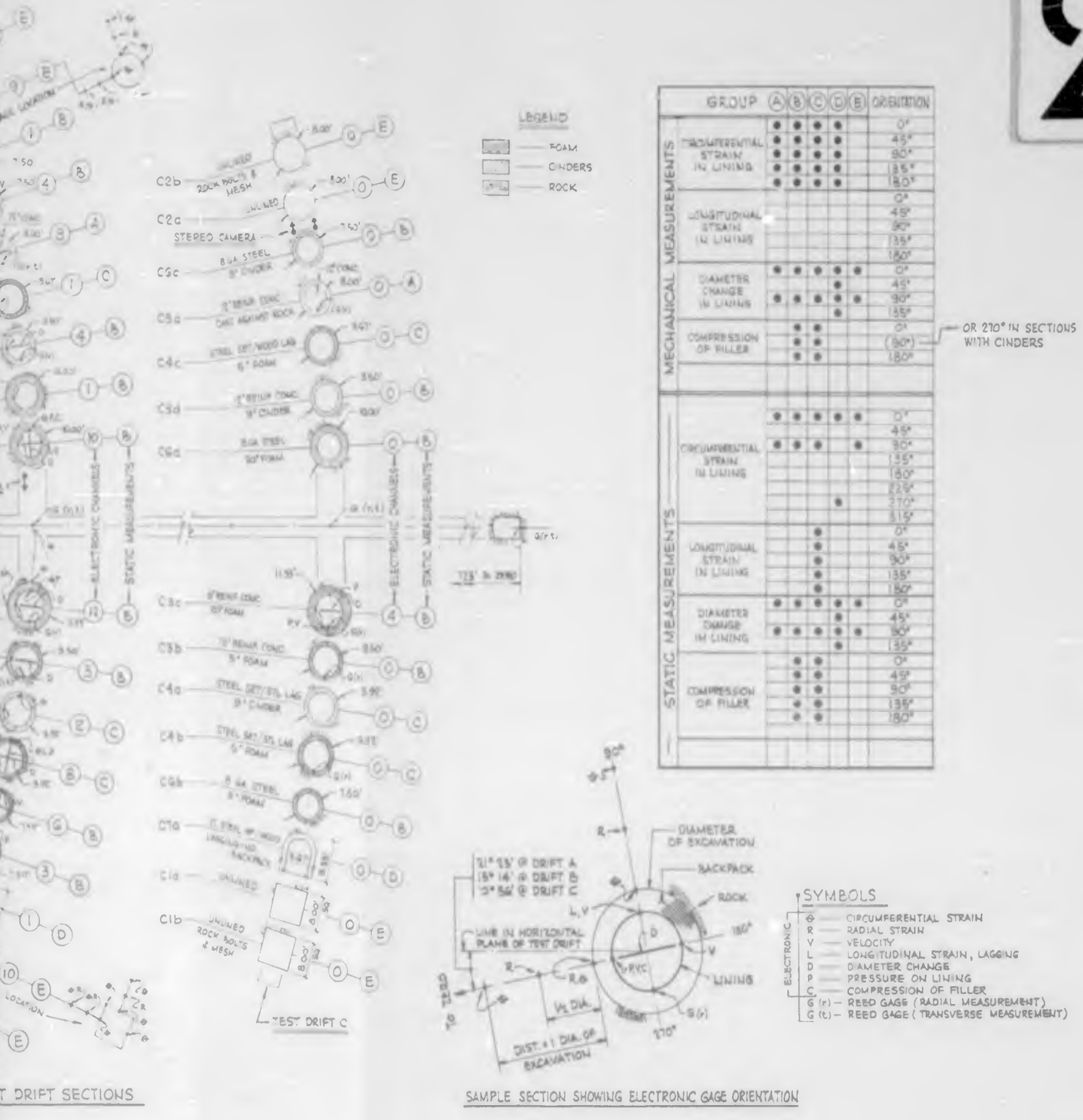

Figure 2.38 Instrumentation plan.

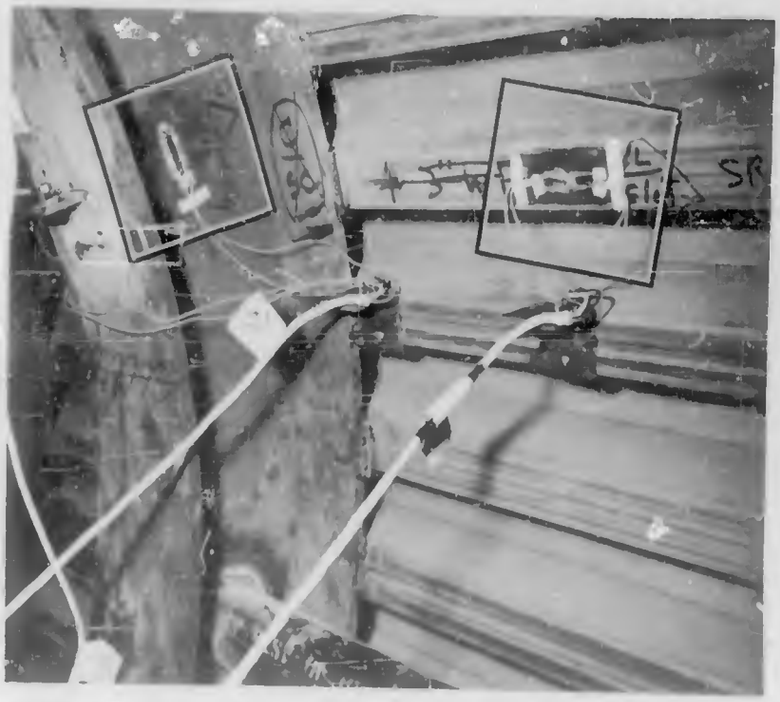

Figure 2.39 Electronic strain gages mounted to measure longitudinal strain in lining (right), and circumferential strain in wide-flange ring (left) (DASA - NOU 084-04 NTS-62).

Figure 2.40 Pressure gage installed in reinforced concrete liner (DASA - NOU 082-03 NTS-62).

Figure 2.41 Pressure gage installed in corrugated steel liner (DASA - NOU 072-04 NTS-62).

Figure 2.42 Electronic displacement gage mounted to measure diameter change (DASA - NOU 084-05 NTS-62).

Figure 2.43 Electronic displacement gage installed to measure compression of backpacking material (DASA - NOU 073-10 NTS-62).

Figure 2.44 Velocity gage installed on reinforced concrete liner (DASA - NOU 082-02 NTS-62).

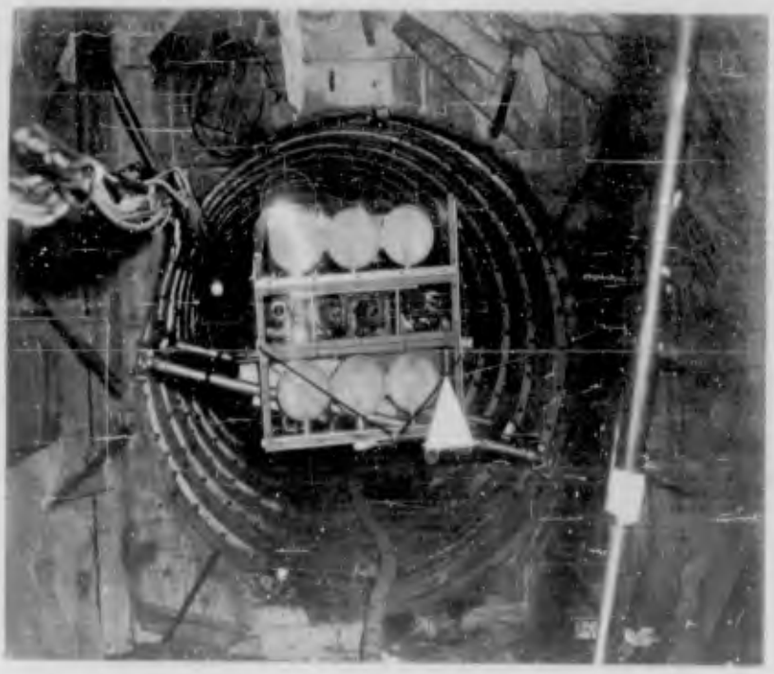

Figure 2.45 Stereographic motion-picture camera station, Test Section B6c, for observing fly-rock in Test Sections B2a and B2b (DASA - NOU 082-08 NTS-62).

Figure 2.46 Mechanical compression-of-filler gage installed through wood lagging (DASA - NOU 070-11 NTS-62).

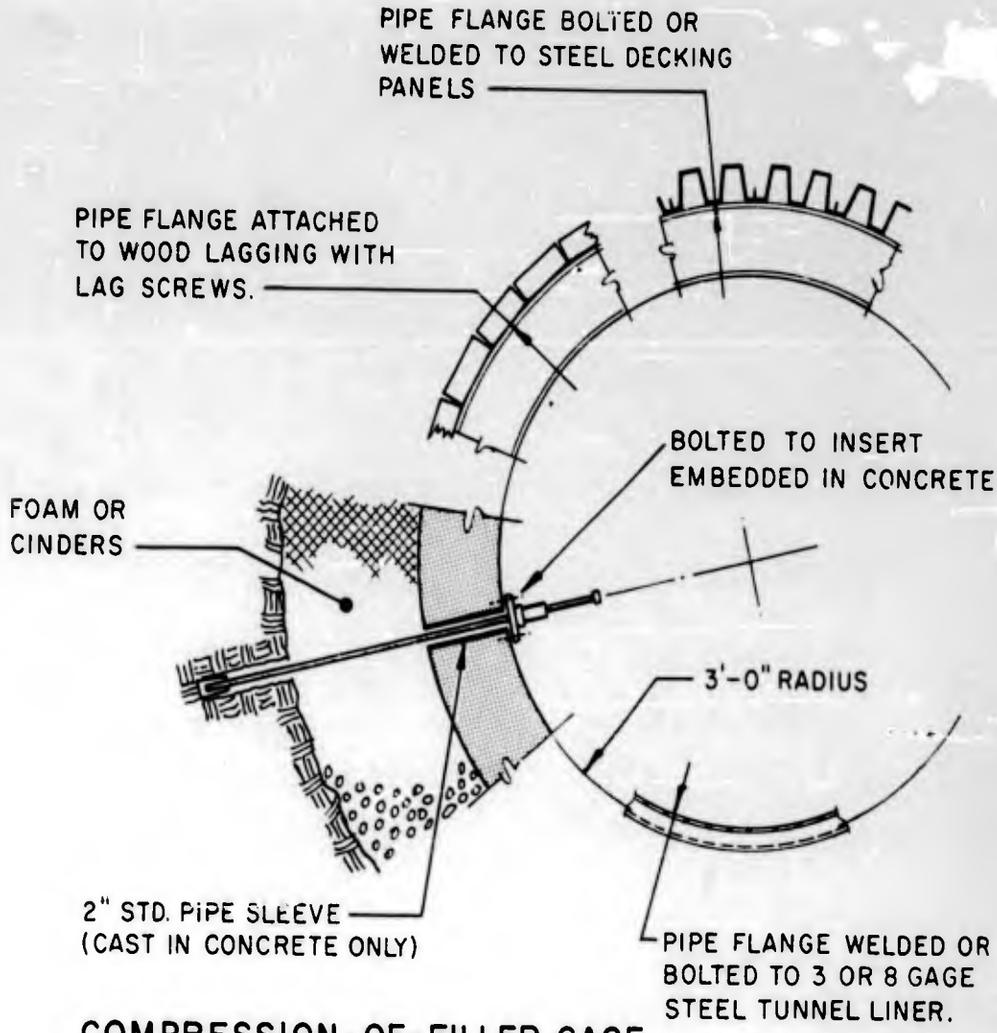

COMPRESSION-OF-FILLER GAGE

USED IN CONC., WOOD & STEEL LINING

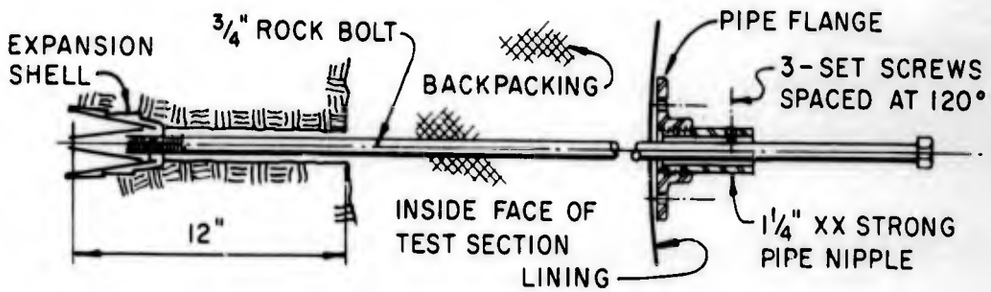

GAGE DETAIL

Figure 2.47 Details, compression-of-filler scratch gage.

Figure 2.48 Mechanical diameter-change gages installed on wide-flange rings (DASA - NOU 071-06 NTS-62).

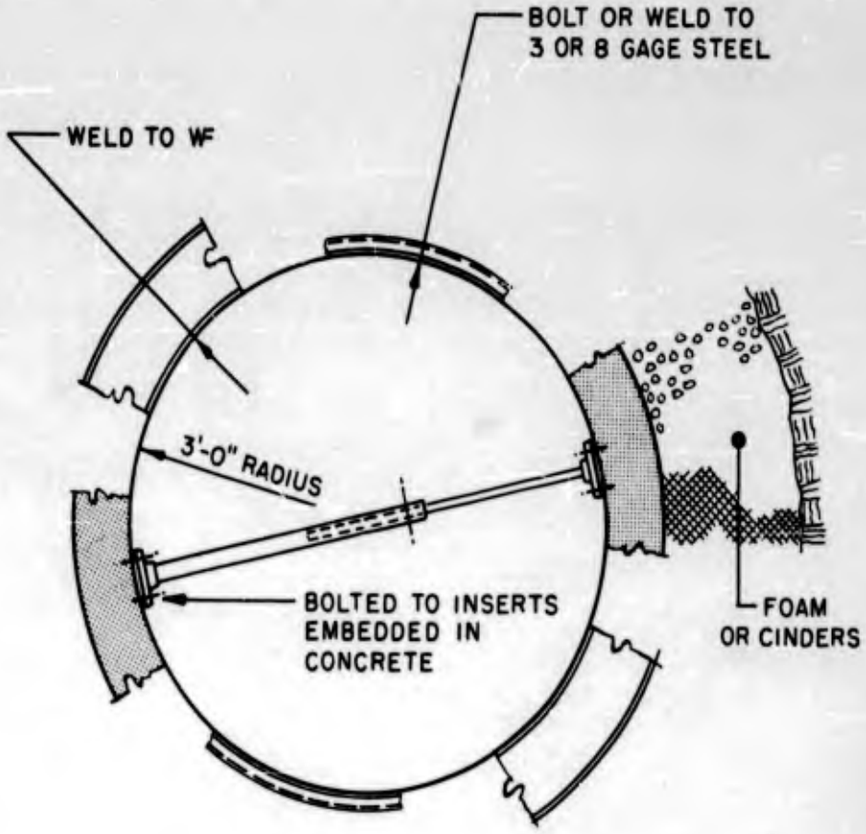

DIAMETER-CHANGE GAGE

USED ON CONC, WF SETS & 3 OR 8 GA. STEEL

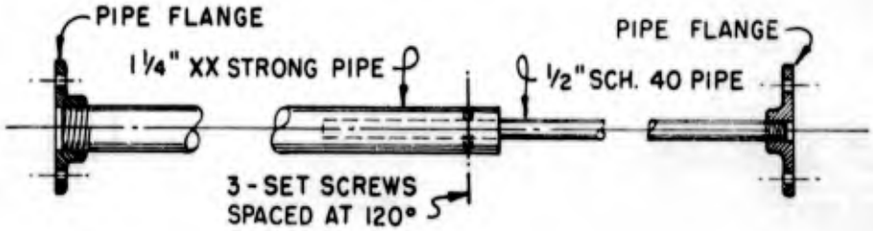

GAGE DETAIL

Figure 2.49 Details, diameter-change scratch gage, lined circular sections.

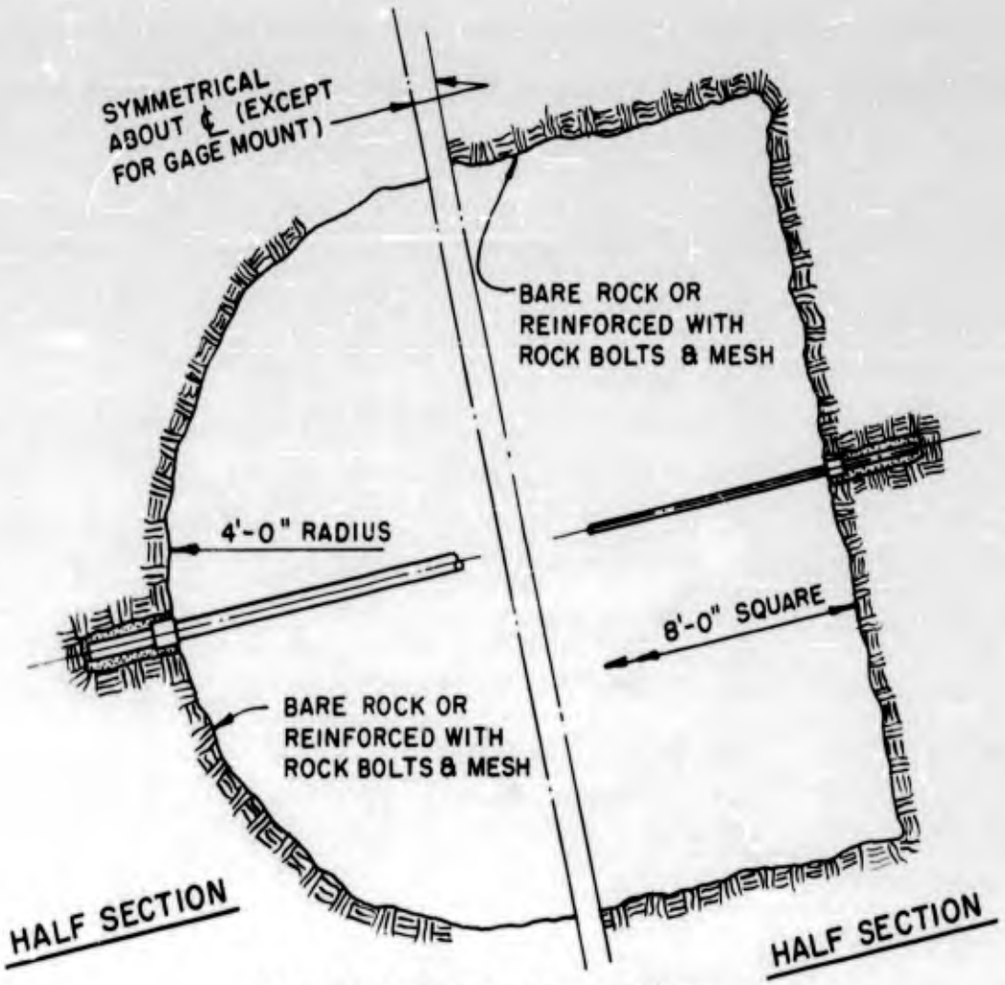

DIAMETER-CHANGE GAGE
USED ON UNLINED TEST SECTIONS

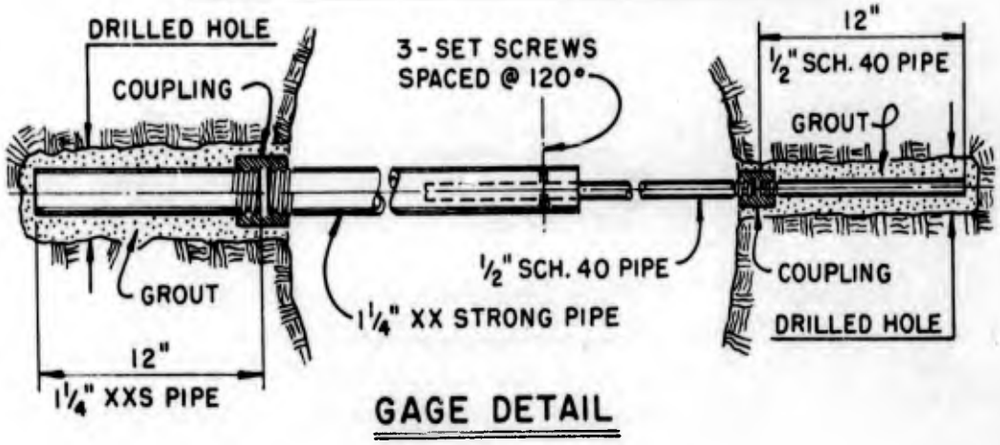

GAGE DETAIL

Figure 2.50 Details, diameter-change scratch gage, unlined sections.

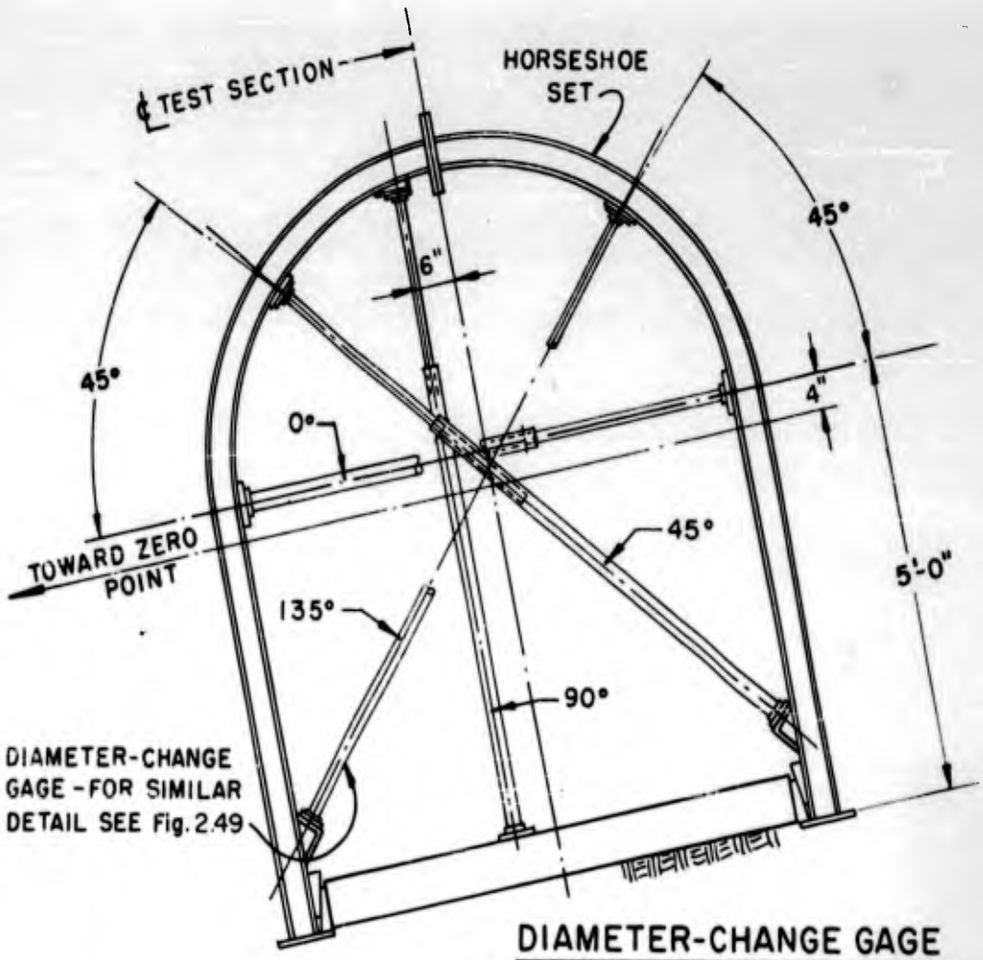

DIAMETER-CHANGE GAGE USED ON HORSESHOE SETS

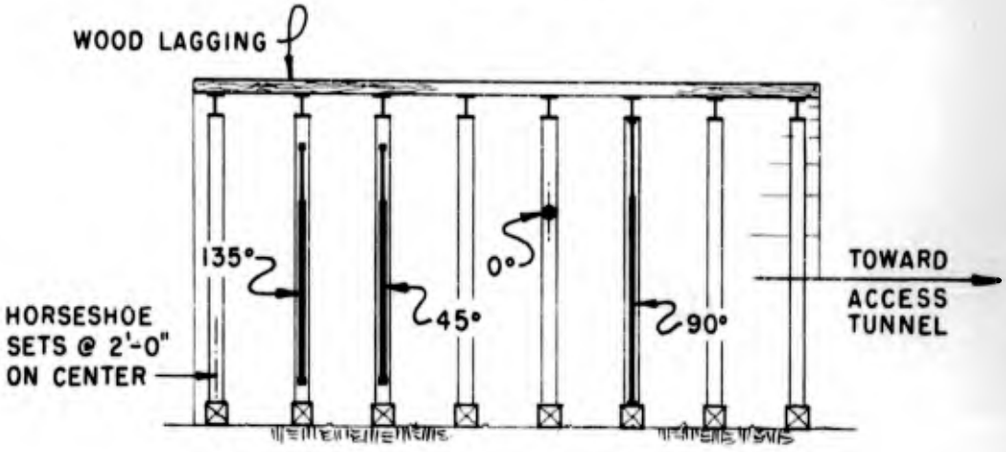

LONGITUDINAL SECTION SHOWING GAGE LOCATIONS

Figure 2.51 Details, diameter-change scratch gage, horeshoe sets.

Figure 2.52 Reed gage mounted on liner to respond to radial (horizontal) shock (DASA - NOU 082-06 NTS-62).

Figure 2.53 Reed gage mounted on liner to respond to transverse (vertical) shock (DASA - NOU 082-05 NTS-62).

Figure 2.54 Reed gage in canister. Gage oriented to measure transverse (vertical) component of shock (DASA - NOU 083-02 NTS-62).

Figure 2.55 Reed gage in canister, oriented to measure radial (horizontal) component of shock (DASA - NOU 083-04 NTS-62).

Figure 2.56 DeForest gage installed on wide flange ring to measure circumferential strain (DASA - NOU 071-05 NTS-62).

Figure 2.57 DeForest gage installed on reinforcing steel in concrete liner to measure circumferential strain (DASA - NOU 074-01 NTS-62).

CHAPTER 3

RESULTS

3.1 RE-ENTRY

The Hard Hat detonation took place on 15 February 1962, at 1000 hours P S T. The shot was essentially completely contained, i.e., the gaseous and particulate products of the detonation were initially contained in the cavity created by the detonation.

A low level of radiation was first detected at Ground Zero at 1100 hours P S T. At 2105 hours, the cavity began to collapse. Between midnight and 0630 hours of the next morning, and following the cavity collapse, the radioactivity levels at the surface and within the tunnel increased markedly. The readings dropped to the normal background level in approximately two days at the surface and within one week in the tunnel.

Restoration of the concrete foundations preparatory to the replacement of the hoist, headframe, and related facilities was started 17 February 1962. On 23 February 1962, two members of the re-entry party were lowered to the bottom of the Station

1500 shaft in a small, free-swinging cage to ascertain the physical condition of the shaft and utilities and to monitor for radiation and explosive or toxic gases. It was found that the atmosphere was free of radiation or obnoxious gases, but the shaft was in need of repair. All utilities were apparently intact. Accordingly, on 28 February 1962, shaft rehabilitation was started. This work was completed 9 March 1962.

On 10 March 1962, the re-entry party tested the atmosphere, opened the blast door, and then proceeded on foot to Tunnel Station 2+40. The tunnel was observed to be completely closed by a rock fall at Station 2+75. Tunnel rehabilitation started on 12 March 1962.

3.1.1 Damage to Access Shaft, Station 1500. Postshot damage was noted at all depths of the shaft. In general, it was noted that the upper half of the shaft sustained heavier damage than the lower half. Many of the bearing sets (see Figure 2.2) were permanently distorted, as shown in Figures 3.1, 3.2, and 3.3. Some of the standard sets were distorted, due to loads imposed by broken rock from the walls. The latter sets generally returned to their original shape upon removal of the broken rock.

Several sets were displaced horizontally, resulting in misalignment of the shaft as shown in Figure 3.4. Differential vertical motions between sets caused tension in the hanger angles. As a result, many of the hanger angles sheared the bolts at points of connection to bearing sets. Because of the resulting postshot misalignment between the bolt holes in the sets and in the hanger angles, it was necessary to weld the hanger angles to the sets, as can be seen in Figures 3.5 and 3.6.

The permanent deflection and misalignment of sets made it necessary to reduce the dimension between the elevator guides from 62 inches to 50 inches. The elevator cage was correspondingly reduced in size.

3.1.2 Damage to Access Tunnel. Rehabilitation of the first 200 feet of access tunnel involved the removal of occasional rock falls, minor re-alignment of the track, and repairs to utilities. The tunnel was completely blocked by broken rock at Station 2+75 and again at Station 2+90. The blockage, starting at Station 2+90, was continuous to Station 3+40, and in this interspace, the floor was raised upward approximately four and one-half feet. Open tunnel (passable on foot) was then encountered

until Station 4+00, where the final point of closure was located. North of this point, floor heave was constantly present, and no open access tunnel was encountered.

The damage profile through the access tunnel is depicted in Figure 3.7. This figure was based upon visual observations of damage as well as cross section survey data. The rock failure observed in the first 200 feet of tunnel was typical of Zone 4 damage as described in Chapter 1, i.e., most of the fallen rock consisted of previously loosened slabs and material derived from minor fault zones exposed by the tunnel, as shown by Figure 3.8. The heavy damage between Stations 2+90 and 3+40 resulted from the presence of the strong fault zone centered on Station 3+10. This was the location originally planned for C Drift, which was relocated as described in Subsection 2.1.1 to avoid this fault zone.

Generally, the broken rock was found to be more finely crushed as the re-entry advanced to the north, as seen by comparing the average size of material in Figure 3.9 with that in succeeding photographs. The exceptions to this observation occurred at the intersections of the access tunnel with B and C

Drifts. At these intersections large slabs were encountered along with finer material. Figures 3.10 through 3.23 are comparative photographs (pre- and postshot) illustrating the damage at various points in the access tunnel. It should be noted that the apparent changes of rock color between some of the pre- and postshot photographs are due to differences in photographic techniques followed. The rock did not change in appearance as a result of the detonation.

3.2 VISUAL OBSERVATIONS OF TEST SECTION DAMAGE

The documentation of test section damage was started 16 April and completed 2 June 1962. This work was conducted in a step-by-step manner and generally involved the following sequence:

Step 1--before a test section was entered, photographs were taken from the entrance to record evidence of the immediate postshot condition. Close-up photos were taken of points of interest within the liners.

Step 2--scratch gages were recovered, and postshot strain measurements were made.

Step 3--notes were taken describing the liner condition.

Step 4--end bulkheads were removed, and debris was removed from within the liner and at the ends of sections.

Step 5--cracks were marked in concrete liners and in foam units. It should be noted that pre-shot shrinkage cracks were marked in a different color than that used for postshot marking. These pre-shot cracks were not included in the sketches referred to in Step 7.

Step 6--additional photographs were then taken as necessary to document damage details revealed by Steps 4 and 5.

Step 7--sketches were made to record features such as concrete cracks which would not be obvious from the postshot photographs and surveys.

The postshot surveys were started 13 May 1962 and continued throughout the remainder of the data-recovery phase. The underground portion of the survey included cross-sectioning the access tunnel at approximately ten-foot intervals from Station 2+00 to Station 5+60, cross-sectioning all accessible portions of the test drifts including the transition zones, and precisely locating each accessible test section liner.

The information presented below is based upon visual observations and sketches made of the test sections.

In C Drift, fourteen test sections were viewed. One test section was not accessible because of heavy damage. In B Drift, an additional thirteen test sections were available, and five were inaccessible. Because of the extremely heavy damage sustained by A Drift, only three of its test sections were accessible.

3.2.1 Summary, C Drift. In summary, all C Drift test sections with liners survived and were readily accessible. Although test sections C2a and C2b were heavily damaged, they were passable on foot. Figure 2.38 in Chapter 2 shows the relative locations of these test sections. Section C1a was completely closed, and C1b is assumed to be similarly damaged. The heavy damage to the latter two test sections is attributed to the presence of intense faulting in that area, as can be seen in Figures 1.3 through 1.5. Test Section C7a apparently experienced a disproportionate amount of damage because of its proximity to the same fault zone. The liners with backpacking (either foam or cinders) were less severely damaged than liners without shock isolation, such as C3a and C7a.

Test Sections C4a and C4b provided a good visual comparison between the behavior of foam and cinders, because the

corrugated steel decking deforms readily. The decking in the test section having cinder backpacking (C4a) was noticeably more distorted than the decking in the section having foam backpacking (C4b).

The observed damage to the accessible test sections in C Drift is given below. Pre- shot photographs in most cases are not included in this report, because the postshot photos were considered sufficient to illustrate the effects of the shot on the condition of test liners.

Left, C Drift. The following sections are on the left-hand side of the main access tunnel. The zero point is to the right of each section when entering. The test sections are presented in sequence.

(1) C3c, Eight-Inch Reinforced Concrete Liner With Twenty-Inch Precast Foam Backpacking. This liner exhibited very little damage. Fine hairline cracks were noted on the concrete surface. The cracks were marked with a dye marking pen to accent the crack pattern for

photography and sketching. When the bulkheads were removed, exposing the ends of the liner, these cracks were found to extend about four inches into the liner, as shown in Figure 3.24. Note the cracks radiating from the inside surface between 45° and 90° (see Subsection 2.2.1 for convention). Cracks between 225° and 270° were hidden by the muck pile in the foreground. Note the cracks radiating from the outside surface near 180°. A similar set (not shown) was found diametrically opposite at 315° to 360°. The majority of the cracks found on the inside liner surface were in two groups between 45° to 90° and 225° to 270°, respectively. Figure 3.26 shows the crack pattern on the inside surface of the liner.

The foam units exhibited no significant signs of crushing, although some cracking of the brittle foam skin was evident. These observations were made by inspection of the foam panels at the ends of the test section.

The rock surrounding the opening appeared to be well supported by the foam. There was little evidence of rock breakage around the test section. As a possible indication of the rock breakage, the unlined portion of tunnel leading up to this test section (i.e. the transition zone) is shown in Figure 3.25. Note that the breakage pattern was oval shaped, with the major axis at approximately 60° to 70°. It is inferred that the rock breakage pattern behind the foam would be similar.

The diameter-change gage spanning the 90° to 270° direction was bent toward zero point. The gage oriented at right angles to the first gage appeared not to have been bent.

(2) C3b, Twelve-Inch Reinforced Concrete Liner With Five-Inch Precast Foam Backpacking. This test section suffered little or no damage. Figure 3.27 illustrates the postshot condition. The canister in the foreground was used to house an STL reed gage. The diameter-change gage spanning 90° to 270° was bent toward

zero about 2-1/4 inches, while the gage spanning 0^{o} to 180^{o} (parallel to the radial line to zero point) remained straight.

At the time the Figure 3.27 photograph was taken, the cracks in the concrete had not yet been marked with the dye marking pen. Hairline cracks were present predominantly between 60^{o} to 100^{o} and between 225^{o} to 260^{o}, with the highest frequency between 60^{o} to 100^{o}. The crack pattern on the inside concrete surface is shown in Figure 3.29.

When the bulkheads were removed, the crack pattern at the ends was found to be similar to C3c, shown in Figure 3.24.

(3) C4a, Steel Wide-Flange Rings With Corrugated Steel Decking and Nine-Inch Cinder Backpacking. The steel wide-flange rings were apparently undamaged. Preliminary strain measurements by Whittemore gage indicated that these rings received no measurable permanent strain. The

steel decking, however, exhibited a significant amount of plastic deformation.

Figure 3.28 is an overall view of the post-shot condition of the steel rings, and Figure 3.30 shows typical failure of the steel decking. The crushing of the corrugations was apparent near 45°, while the corrugations near 0° showed little distortion. A sectional view between two steel wide-flange rings (center of span) is shown in Figure 3.32. A typical sectional view through a steel wide flange ring, showing the distortion of the steel decking, is given in Figure 3.33. This distortional pattern of the decking shown in these two figures is indicative of the manner of loading on the liner.

In Figure 3.28, note that the 90° to 270° diameter-change gage was bent toward zero about 1-1/4 inches, and the 0° to 180° gage was bent toward 270° about one-half inch.

(4) C4b, Steel Wide-Flange Rings With Corrugated Steel Decking and Five-Inch Precast

Foam Backpacking. Figure 3.31 illustrates the postshot condition of the steel wide-flange rings and the corrugated steel decking panels. Figure 3.34 is a close-up view of a portion of the steel decking, showing plastic deformation typical of this test section. The yielding of the decking in this test section was generally less pronounced than in C4a, as can be seen by comparing Figures 3.30 and 3.34.

The deformational patterns of the decking in C4b are shown in Figures 3.36 and 3.37. Figure 3.36 shows the deformation of the decking at the centerline of the test section (between rings). Figure 3.37 illustrates the deformation of the decking at a wide flange ring. This deformation pattern is indicative of the type of loading sustained by the liner.

Another indication of the loading is shown in Figure 3.31, where the diameter-change gages are seen to have bent toward the zero point about two inches and toward 270° about 1-1/2 inches.

(5) C6b, Eight-Gage Steel Liner Plates With Five-Inch Precast Foam Backpacking. A post-shot view of this test section can be seen in Figure 3.35. At the far (west) end of the liner, the last four rings (there are ten total) showed signs of distortion between approximately 45° and 90°. The liner was bulged inward by approximately two to three inches at these points. The two rings adjacent to the midsection were distorted in the same manner but not quite so pronounced.

Removal of the wood bulkheads at the ends revealed no signs of crushing of the foam. Some surface cracking of the brittle foam skin was noted. Some cracks are visible in the exposed foam panels in Figure 3.35.

At the far (west) end of this test section, the liner plate at 90° was bent inward about 1-1/2 inches. The rock around this test section was not as competent as the rock in the first four test sections of the drift. The damage observed in C6b may be attributed to this local rock condition.

The diameter-change gage spanning 90° to 270° was bent toward zero point about 3-1/4 inches, and the gage spanning 0° to 180° was bent downward about 1-3/4 inches.

(6) C7a, Horseshoe Sets With Wood Lagging, No Backpacking. Figure 3.38 is a preshot view of this test section. The steel sets were blocked against the tunnel opening. There was no backpacking behind the three-inch-thick wood lagging. The bottom of each set was blocked and wedged by six-inch by six-inch timber struts, as shown.

Figure 3.39 shows the postshot condition of the test section. The floor had heaved upward, dislodging the timber struts. All the diameter-change scratch gages were severely damaged. The top of the muck pile was approximately three feet from the crown of this set, indicating that the floor heave was five feet or more. The bearing plates at the crown of each set separated, causing failure

of the bolts. The timber lagging was generally in good condition with little breakage.

The last three horseshoe sets received somewhat greater damage at the crown than the first five sets. This heavier damage was induced by the collapse of the next test section, C1a. Rock bolts and chain link mesh had been installed as roof support in C1a and the west half of C7a during construction because of the weak rock in this area. The collapse of C1a transferred some load back to the horseshoe sets, through the mesh.

The broken rock behind the liner consisted of large blocks bounded by joints, mixed with smaller pieces two to four inches in size. Many large slabs were found in the material derived from the floor heave. Generally, the broken rock became more highly crushed at the far (west) end of C7a.

(7) · C1a, Unlined Square Section and C1b, Unlined Square Section Reinforced With Rock Bolts and Mesh. The pre-shot view of these

two test sections is shown in Figure 3.40. The test section in the foreground, C1a, was intended to be completely unlined. The rock bolts and chain link mesh at the top were installed during construction for personnel safety because of the incompetency of the rock in this area. The section in the background, C1b, was a square section reinforced with rock bolts and expanded metal. The string in the photograph is a plumb line and represents the true vertical line. The diameter-change scratch gages are at 0^{o} and at 90^{o}. This photograph provides a comparison between the expanded metal mesh and the chain link mesh.

Figure 3.41 is a postshot view of C1a from the end of C7a, showing the complete closure of C1a. Note that the floor had heaved and was in contact with the chain link mesh. The mesh had dropped approximately two feet. The broken rock in C1a was highly crushed.

Since re-entry was not made through C1a, the postshot condition of the next test section, C1b,

is unknown. It is assumed, however, that C1b is completely closed.

Right, C Drift. The following test sections are on the right-hand side of the access tunnel. Zero point is to the left when entering. The presentation is given in sequence as seen upon re-entry.

(1) C6a, Eight-Gage Steel Liner With Twenty-Inch Precast Foam Backpacking. Figure 3.42 is a pre-shot view of this section. The outline of the transition drift between the main access tunnel and the first test section can also be seen in this photograph.

The postshot condition of the transition zone and the test section is shown in Figure 3.43. The rock outline in the transition zone assumed an oval shape, with the major axis oriented at about 60°. The same rock breakage pattern was noted in the transition zone on the left hand side of C Drift (see description of C3c above).

The steel liner did not appear to be distorted. When the bulkheads were stripped to inspect the condition of the precast foam panels, a few minor surface cracks were noted. Most of these surface cracks were found near 180°. They were several inches long, radiating from the inside surface. There were no signs of significant crushing of the foam panels.

The diameter-change scratch gage spanning 90° to 270° was bent toward zero point about 2-5/8 inches. The gage at 0° to 180° remained essentially straight.

(2) C3d, Twelve-Inch Reinforced Concrete Liner With Nine-Inch Cinder Backpacking. A postshot photograph of this section is shown in Figure 3.44. Fine hairline cracks were found on the inside concrete surface. These cracks were finer than those observed in any of the other concrete liners in C Drift. Figure 3.46 illustrates the crack pattern observed on the inside surface of the liner.

The tongue-and-groove timber form containing the cinders was crushed. Figure 3.45 illustrates the crushing between 0° to 45°. At the opposite side, near 180°, there was also evidence of crushing of the timber form.

The diameter-change scratch gage spanning 0° to 180° was bent slightly toward 270°. The diameter-change gage at 90° to 270° was bent away from the zero point about 2-1/2 inches. This gage was the only one observed to have bent away from zero. All others in C Drift were bent towards the zero point.

(3) C4c, Steel Wide Flange Rings With Wood Lagging and Five-Inch Precast Foam Backpacking. Figure 3.47 illustrates the postshot condition of C4c. The steel wide-flange set suffered no visible distortion. The three-inch-thick wood lagging exhibited minor cracks at several locations. The cracks were concentrated between 30° to 60° and 180° to 225°.

Some minor cracking of the brittle foam skin was seen when the bulkheads were removed. There was little evidence of crushing of the pre-cast foam panels.

The diameter-change scratch gage at 0° to 180° appeared straight. However, the scratch gage spanning 90° to 270° broke off at both ends. This gage was found in the position shown in Figure 3.47.

(4) C3a, Twelve-Inch Reinforced Concrete Liner Cast Against Rock. The postshot condition of this liner is shown in Figure 3.48. The diameter-change scratch gage from 90° to 270° broke off at the top and came to rest about six inches closer to the zero point. It had also bent toward zero about 2-1/2 inches. The gage was found in the position shown in the photograph. The 0° to 180° gage was bent approximately 1-1/2 inches toward 270°.

The concrete liner was crushed at 90° and 270°, exposing the reinforcing bars. Some buckling of the reinforcing bars was noted.

Figure 3.49 illustrates the crack and breakage pattern on the inside surface of the liner.

Inspection of the ends showed that some rock breakage occurred between 80° and 135°. This breakage was about one foot in thickness.

(5) C6c, Eight-Gage Steel Liner Plate With Nine-Inch Cinder Backpacking. Figure 3.50 shows a postshot view of this test section. The diameter-change scratch gages behaved in the same manner as did most of the other gages in C Drift, i.e., one bent about 1-5/8 inches toward zero, and the other bent about one inch toward 270°. There was no visible permanent distortion of the liner plates. In the background, one can see the stereo camera installed by Edgerton, Germeshausen and Grier, Inc. (EG&G) to record fly-rock, as delinated in Section 2.2.2.

Removal of the bulkheads revealed that the cinders were slightly compacted and crushed. At from 60° to 100°, some broken rock, about six-inch size, was seen.

(6) C2a, Unlined Circular Section and C2b, Unlined Circular Section Reinforced With Rock Bolts and Expanded Metal. Figure 3.51 shows a preshot view of test sections C2a and C2b. The postshot condition of these two test sections is shown in Figure 3.52. In the foreground, the outline of the opening and the muck pile can be seen. Some of the broken rock and cinders in the left foreground was derived from the clean-up of C6c. The immediate postshot surface of the muck pile spanned from approximately 0° upward through the center-line of the test section to about the 180° mark. The breakage appeared to attain a maximum at about 45°, where it was about 2-1/2 feet thick. The breakage at 0° was about one foot and at 90° was about 1-1/2 feet. There was no evidence of floor heave in either of these test sections.

Figure 3.53 is a close-up view of the damage in section C2b. The diameter-change scratch gages can be seen in the background, to the right of the mesh. Both gages were severely damaged. The expanded metal

mesh had torn loose from the rock bolts on the side toward zero point. The mesh was intact from about 90° to 315°. The broken rock held by the mesh ranged in size from two to six inches, or larger. The maximum amount of rock breakage appeared to be between 45° and 90°. This breakage was approximately 1-1/2 feet in thickness. All of the broken rock not supported by the mesh was subsequently removed from both C2a and C2b to prepare for stress determinations by APRL, Project 3.6, and to permit survey determinations of rock breakage.

3.2.2 Summary, B Drift. All test sections, except B3c, were heavily damaged and required the removal of debris from the interior to permit passage through the liners. In most cases, rock broken from the gaps between test sections completely blocked the ends of the liners.

The unlined test sections (B2a, B2b, B1a, and B1b) were not accessible and are assumed to be completely closed. This assumption is based upon the damage observed in the equivalent test sections in C Drift and the relative conditions of the lined

test sections in B and C Drifts. Efforts to gain entrance to B6c through B5c were unsuccessful, due to heavy damage. Floor heave was generally observed throughout the drift. Evidence of the heave was particularly prominent in all liners with wide flange rings (B4a, B4b, and B4c) and in the concrete liners located in B Drift, right (B3d and B3a).

In several test sections, particularly those with liners composed of wide flange rings, spaces of as much as two feet were noted between the liner or backpacking and the rock wall on the zero point side. In other words, the postshot rock wall was not in intimate contact with the liner or backpacking.

In contrast to the heavy damage sustained by all the other liners in B Drift, the undamaged condition of B3c was striking. Although the foam backpacking around B3c was highly compressed, the concrete liner was in as good condition as was C3c, located in C Drift.

Because of the extensive damage to B5a and B6a, the first two test sections in B Drift, right, it was necessary to bypass these two liners by means of a new drift. The bypass drift was ultimately extended to intersect the gap between B3a and B5c, as shown in Figure 3.54.

Left, B Drift. The following test sections are on the left-hand side of the access tunnel. The zero point is to the right of each test section when walking in. The test sections are presented in sequence.

(1) B3c, Eight-Inch Reinforced Concrete Liner With 24-Inch Cast-In-Place Foam Backpacking. Figure 3.55 is a pre-shot photograph taken from the transition zone looking into the test section. The barricade shown in the foreground was installed during the instrumentation phase to prevent unauthorized persons from entering the test sections. It was removed before shot time. Immediately within the test section the canister housing the STL reed gage can be seen at 270°. The two diameter-change gages, oriented at 0° to 180° and 90° to 270°, are shown in the background. After the shot, the transition zone from the access tunnel to the first test section was completely filled with broken rock. Much of the broken rock from the transition zone had been propelled into the liner. Figure 3.56 shows the test section when it was first uncovered by the mucking operations. Note the broken concrete at the edge, exposing the reinforcing bar at 90°, as well as the extreme compression of the foam backpacking near 45°.

Figure 3.57, a view looking into the test section, shows the postshot interior condition. Both diameter-change scratch gages were broken. The debris covering the floor consisted of broken rock from both ends of B3c, as well as broken concrete and pieces of foam from the next test section, B3b.

After clean-up, the liner was examined in detail and found to be in excellent condition. Although the foam was highly compressed, the concrete liner was no more damaged than its counterpart in C Drift, C3c. Figure 3.58, looking toward the access tunnel, shows the extreme compression of the foam observed at the end of the liner at approximately 20^{o}.

Figure 3.59 illustrates the cracks found at the ends of the concrete liner and the compression of the foam. The crack pattern on the inside concrete surface is illustrated by Figure 3.60. The majority of the longitudinal cracks were near the 0^{o} or 180^{o} points.

(2) B3b, Twelve-Inch Reinforced Concrete Liner With Nine-Inch Cast-In-Place Foam

Backpacking. A pre-shot view of this test section was previously shown in Figure 2.52. The postshot condition is shown in Figure 3.61. The concrete liner suffered heavy damage and was completely closed at the far (west) end. The reinforcing bars were exposed in many areas by crushing of the concrete. The heaviest damage occurred between 0° and 90°, exposing both layers of reinforcing steel. In some places, the reinforcing bars at 0° had broken loose and had been propelled across the liner. Severe buckling of reinforcing bars can be seen at 90° and at 225°. The foam backpacking was exposed over a large area of the far end of the liner, as shown in Figure 3.62. Note that the foam was essentially in place with only a few pieces broken away.

Another area of heavy damage was located between 180° and 270°. The floor was crushed, exposing reinforcing bars.

Figure 3.63 is a view of the liner after clean-up (mucking and cutting away the reinforcing bars). The liner had ovalled, with the major axis

oriented at approximately 135° to 315°. The major diameter was approximately six feet, four inches, and the minor diameter was about five feet, eight inches.

Figure 3.64 is a sketch showing the compression of the foam backpacking and the shape of the concrete at the east end of the liner.

Both diameter-change scratch gages were heavily damaged. The STL reed gage canister at the far end of the liner was broken free from the concrete. The one at the near (east) end is shown in Figure 3.61.

(3) B4a, Steel Wide-Flange Rings With Corrugated Steel Decking and Nine-Inch Cinder Backpacking. A pre-shot view of the test section is shown in Figure 3.65. In the foreground, two diameter-change scratch gages can be observed mounted on the third wide-flange ring. Two additional diameter-change scratch gages are shown in the background on the fifth set. These were at 45° to 255° and 135° to 315°. Compression-of-filler scratch gages can be seen at 0° and 270°, next to the third wide-flange ring.

Figure 3.66 shows the postshot condition of the test section. The wide-flange rings were considerably distorted throughout. The rings were most severely damaged in the two quadrants nearest zero point, as shown in Figure 3.67. The steel decking in these two quadrants was severely bent, and in many cases it was sheared off at the supports. The cinders were highly compressed, and the steel decking corrugations were crushed at the supports (see Figure 3.68). In the two quadrants away from zero, the steel decking had bowed inward, with some shearing at the wide flange supports.

The shape of each wide flange ring was sketched after removing the debris from around the rings. These sketches are shown in Figure 3.69. The solid line represents the approximate postshot configuration of the inside flange of the ring. The outside flange was not plotted. An assumed centerline was used in determining the postshot configurations.

(4) B4b, Steel Wide Flange Rings With Corrugated Steel Decking and Five-Inch Precast Foam Backpacking. Figure 3.70 is a pre-shot view of this test section. The diameter-change scratch gages are on the second

wide flange ring in the foreground, spanning the 45° to 225° and 135° to 315° axes. In the background, at the fourth ring, the 0° to 180° and 90° to 270° gages can also be seen.

A postshot photograph of the test section is shown in Figure 3.71. The steel rings were heavily damaged in a manner similar to that in B4a. The rings were severely buckled, and the decking failed by bending and shear at the rings.

The postshot profile of each wide flange ring is shown in Figure 3.72. As in Figure 3.69, these sketches are drawn from an arbitrary centerline. Neither this liner nor the remaining liners in this drift (B Drift, left) were accessible to the survey crew because of the limited space.

(5) B5b, Three-Gage Steel Liner Plate With Five-Inch Precast Foam Backpacking. An overall pre-shot view of this test section is shown in Figure 3.73. Section B6b can also be seen in the background. Figure 3.74 is a postshot view of the interior of B5b, taken from the same

direction. An overall postshot view from the opposite end may be seen in Figure 3.75. In this figure, the zero point is to the left of the test section.

The bolts failed along the circumferential and longitudinal joints in the 45° to 90° region, and the liner plates were overlapped, as shown in Figure 3.75 (the 90° line had overlapped the 45° line). Overlapping was noted throughout the length of the liner. The width of the opening at the end, toward the access tunnel, was approximately two to three feet, and the height was about three to four feet. At the opposite end (foreground in Figure 3.75) the liner was approximately four feet high and five feet wide.

The foam exposed at the ends did not appear to have been significantly compressed; however, evidence of shearing and buckling of the foam panels was noted. This was the result of the telescoping of the foam units over each other when the liner plates failed at the joints. Sketches were made to depict the shape of the liner in lieu of surveying because of the limited access. These sketches are shown in Figure 3.76.

(6) B6b, Eight-Gage Steel Liner Plate With Five-Inch Precast Foam Backpacking. A preshot view of this test section is shown in the background of Figure 3.73. The postshot condition is shown in Figure 3.77. The first ring of panels was severely damaged by fly-rock from the gap between the test sections. This damage was not typical of the rings near the center of the liner.

The next eight rings of panels were buckled longitudinally at 60° and 150°. The buckling was inward at 60° and outward at 150°. The average width of the opening was approximately four feet, and the average height was approximately five feet. Failure in this test section was predominantly plate failure. The bolts were generally intact throughout the test section, as shown in Figure 3.78. The shape of the liner is reflected in Figure 3.79.

Inspection of the near (east) end of test section at the first ring of panels revealed that the foam was not appreciably compressed in the radial direction.

Closure of the last two rings of the liner prevented an inspection of the liner from the far (west) end.

(7) B7a, Horseshoe Sets With Wood Lagging, No Backpacking. This test section was completely closed. The damage was similar in nature to that observed in C7a but more severe. The wood lagging was broken between sets, and the sets were severely distorted. Figure 3.80 is a postshot view of B7a.

(8) B1a, Unlined Square Section. This test section was inaccessible due to heavy damage in the previous test sections. It is assumed to be completely closed.

(9) B1b, Unlined Square Section Reinforced With Rock Bolts and Mesh. This test section was inaccessible due to heavy damage in the previous test sections. It is assumed to be completely closed.

Right, B Drift. The following test sections are located on the right-hand side of the access tunnel. Zero point is to the left. The test sections are described in sequence:

(1) B5a, Three-Gage Steel Liner With Twenty-Inch Precast Foam Backpacking. Figure 3.81 is a pre-shot view of the interior of this test section. After completion of construction, a stereo camera was installed at the near (west) end of this test section to record the fly-rock phenomena in the transition zone. Figure 3.82 is a view from the access tunnel, showing the transition zone and the stereo camera in place. The barricade was removed before the shot.

A postshot view of the test section is shown in Figure 3.83. Most of the bolts failed, allowing the liner plates to telescope. The broken bolts from longitudinal and circumferential joints were found scattered about the liner. Inspection of the bolts showed that they failed in a brittle manner, as exhibited by smooth, broken surfaces. The size of the opening was about 2-1/2 to three feet in diameter. The foam was not appreciably compressed.

The stereo camera mounted within the section was heavily damaged. All scratch gages were damaged to the extent that no recovery was made.

(2) B6a, Eight-Gage Steel Liner Plate With Twenty-Inch Precast Foam Backpacking. A pre-shot view of B6a is shown in the background of Figure 3.81. After the shot, this test section was completely closed. The bypass drift exposed the end of the test section facing B3d, as shown in Figure 3.84. In this photograph, zero point is to the right. The foam, as seen from this vantage point, showed some crushing. This crushing, however, was not extensive but was somewhat localized and may have been aggravated by the blasting involved in driving the bypass drift. Bolts in this test section generally did not fail. Instead, the liner plate failed at the bolt holes.

(3) B3d, Twelve-Inch Reinforced Concrete With Nine-Inch Cinder Backpacking. Figure 3.85 is a pre-shot photograph of this test section. The postshot view is shown in Figure 3.86. This picture was taken from the bypass drift excavated for re-entry purposes. The floor heaved and almost closed the liner opening. Less than two feet remained

between the floor line and the crown of the liner. Many of the circumferential reinforcing bars were sharply buckled at 90°, as shown in Figure 3.87. Figure 3.88 is a view of the liner looking toward the access tunnel. Zero point is to the right in this photograph. An STL reed gage canister is visible on the left side of the liner. The top of the canister had been cut open to recover the reed gage. Some of the reinforcing bars along the top of the muck pile had been cut and removed to provide a crawl space.

As can be seen in Figure 3.89, the cinder backpacking was compressed from an original nominal nine-inch thickness to approximately two to four inches. This crushing occurred over all the visible portions of the concrete liner.

(4) B4c, Steel Wide Flange Rings With Wood Lagging and Five-Inch Precast Foam Backpacking. A preshot photograph of this test section is given in Figure 3.90. The postshot condition of the test section is shown in Figure 3.91. This is a view from B3d. Figure 3.92 is a view from within B4c, looking back toward the access tunnel.

The timber lagging generally failed by flexure at mid-span between wide flange rings. The foam backpacking was not highly compressed. Most of the debris seen within the liner in Figure 3.91 was broken foam and wood. Most of the fly-rock was contained behind the lagging. Figure 3.93 is a view of the only significant rock breakthrough observed.

Sufficient debris was removed from around the second and third wide flange rings to permit sketches to be made. The approximate shape of these two rings is shown in Figure 3.94.

(5) B3a, Twelve-Inch Reinforced Concrete Cast Against Rock. Figure 3.95 is a pre-shot view looking into this test section. B5c can be seen in the background. Because of the heavy damage in this test section, as observed from B4c, the bypass drift (Figure 3.54) was extended to this test section and intersected the east end. Figure 3.96 is a view of B3a at left and B5c at right, as encountered by the bypass drift. This test section, B3a, was completely

closed. The mode of failure was similar to B3d but much more pronounced. The floor had heaved up against the top of the liner, and fly-rock had broken through the liner at 0°. The reinforcing bars were severely buckled at 90°, and many were broken.

A view of the upper half of this test section as seen from B5c is shown in Figure 3.97. The zero point is to the right in this view.

(6) B5c, Three-Gage Steel Liner Plate and Nine-Inch Cinder Backpacking. A view of this test section from the bypass drift was shown previously in Figure 3.96. B5c failed in a manner similar to the other three-gage steel liners in B Drift, i.e., the bolts failed and allowed the liner plates to telescope. The cinders were moderately compressed. The average size of the opening was approximately two feet wide by three feet high.

Figure 3.98 shows the interior of B5c as first viewed upon re-entry. The two liner plates in the foreground were completely free and were removed by hand after the photograph was taken.

(7) B6c, Eight-Gage Steel Liner Plate With Nine-Inch Cinder Backpacking. No recovery was made, due to heavy damage at this test section. Attempts to gain access through B5c were unsuccessful. The gap between this test section and B5c was completely filled with broken rock, which could not be removed through the small passageway afforded by B5c. Considering the heavy damage to the other B Drift liners of this type, it was decided that further extension of the by-pass drift was not warranted.

(8) B2a, Unlined Circular Section, and B2b, Unlined Circular Section Reinforced With Bolts and Mesh. Heavy damage in previous test sections prevented re-entry to these test sections. Both test sections are assumed to be completely closed.

3.2.3 Summary, A Drift. The primary objective of the A Drift re-entry effort was to observe the condition of Test Section A3c. Based upon the relative performances of the corresponding test sections in B Drift, A3c appeared to be the only test section in A Drift with a chance of survival. It

was also considered necessary to determine the manner in which A3c failed, regardless of how heavily damaged it may have been.

A3c was found to be heavily damaged but not completely closed. The next test section in A Drift, left, A3b, was completely closed, however.

The first test section to the right of the access tunnel, A5a, was also uncovered and found to be completely closed. In view of the extremely heavy damage to the foregoing three test sections, re-entry work in A Drift was suspended. All remaining test sections are assumed to be completely destroyed.

Left, A Drift. The test sections observed in the left side of the access tunnel are described below. Zero point is to the right.

(1) A3c, Eight-Inch Reinforced Concrete With 24-Inch Cast-in-Place Foam Backpacking. Figure 3.99 is a pre-shot view of A3c. A postshot view is shown in Figure 3.100. The liner was more heavily damaged on the side toward zero point. At 0°, the rock had broken through the liner and intruded the reinforcing bars and foam into the liner. Many large pieces of foam were found intermixed with the broken rock and concrete within the liner, as can be seen in Figure 3.101, which is a

view looking toward the access tunnel from the west end. Zero point is to the left. Much of the rock found within the liner was derived from the transition zone on the east end of A3c. This material displaced the exposed reinforcing bars and scratch gages to the west. The reed gage canister shown in Figure 3.100 was crushed by this effect.

The half of the liner away from zero point was severely fractured, although there was no breakthrough of the concrete. Many severe cracks and much broken concrete were evident on this side. Figure 3.102 illustrates the deformation of the liner and the foam backpacking.

(2) A3b, Twelve-Inch Reinforced Concrete With 9-Inch Cast-in-Place Foam Backpacking. A3b appeared to have failed in the same manner as A3c. The foam was highly compressed, and the liner was completely filled with broken rock and concrete, as can be seen in Figure 3.103. Re-entry to the left side of A Drift was terminated at the east end of A3b.

Right, A Drift. The only test section uncovered in the right side of A Drift was A5a, the first test section from the access tunnel. A description of this test section is given below:

A5a, Three-Gage Steel Liner Plate With Twenty-Inch Precast Foam Backpacking. Figure 3.104 is a post-shot view of A5a taken from the access tunnel. The liner was completely closed, and the foam backpacking was highly distorted. The foam appeared to have deformed plastically around the collapsed tunnel liner plates. The rock outline, originally a nominal ten feet in diameter, was reduced to approximately four feet. Recovery work in the right side of A Drift was suspended at this point. All other test sections in the right side of A Drift are assumed to be closed.

3.3 INSTRUMENTATION DATA

3.3.1 Transient Measurements, Test Section Response Data, Project 3.2 (SRI). The measured peak values of liner and tunnel response as well as their interaction that were obtained by the SRI electronic gages in accordance with the instrumentation

plan are tabulated in Table 3.1. The detailed records are given in Reference 10.

Project 3.2 assigned a code to designate the type of gage and its orientation and location within the test section. The nomenclature used was as follows:

First Character:

D	Diameter change
V	Liner velocity
P	Backpacking pressure
SC	Circumferential strain
SR	Radial Strain in rock
F	Compression of backpacking

Second Character:

R	Radial at 0^{o}
P	Perpendicular at 90^{o}
0	At 0^{o}
90	At 90^{o}
180	At 180^{o}

Third Character:

0	At tunnel surface
1	At one radius depth
2	At two radii depth
L	On liner

For example, Gage SC0-1 in Test Section B2a is a circumferential strain measurement at 0^{o} at one radius depth in rock. Gage PP in Test Section A3c is a pressure measurement on the foam backpacking at the 90^{o} point on the reinforced concrete liner.

The following sign convention was used by Project 3.2 for designating the positive or negative peaks listed in Table 3.1:

DR	A decrease in diameter is positive
DP	An increase in diameter is positive
VR	Motion away from zero point is positive
PR	Recorded pressure is positive
PP	Recorded pressure is positive
FR	Compression of the backpacking is negative
FP	Compression of the backpacking is negative

For all strain measurements, either on a liner or in the rock, an elongation of the gage (i.e. tension) is considered positive.

The locations of these electronic gages are shown in Figure 2.38 in Chapter 2. A postshot examination of the gages in the test sections of B and C Drifts was made to determine their general condition. The gages in C Drift were found to be intact. The majority of the gages in B Drift were found to be loose or battered due to the heavy damage in the drift. The gages uncovered in Test Section A3c were heavily damaged. It is assumed that all of the remaining gages in A Drift are also heavily damaged.

The positive and negative peak values of liner and tunnel response listed in Table 3.1 are also plotted in Figures 3.105 through 3.113. The pre-shot estimates by U of I from Table 1.4, used for setting the ranges of gages, are also shown in these figures. It should be noted that the estimates for the compression of foam were based upon the use of either nine inches or 24 inches of foam, while in most test sections the foam installed was either five inches or twenty inches in thickness.

3.3.2 Transient Measurements, Particle Motion Data, Project 3.3 (Sandia Corp.).

Free-Field Data. The peak values of free-field effects obtained by Project 3.3 from electronic records are given in Table 3.2. The complete records, including detailed time histories of the measured quantities, may be found in Reference 11.

The gage designation used by Project 3.3 reflects the type of measurement and orientation used to record the shock effects. The following nomenclature was used by Project 3.3:

First Letter(s):

D, DI	Displacement
U	Velocity
A	Acceleration
F	Stress
L	Strain

Second Letter:

V	Vertical
T	Tangential (perpendicular to direction of shock)
R	Radial (parallel to direction of shock)

The locations of the free-field measurements are given in Figure 3.114. Comparisons of the measured peak values with the pre-shot estimates are shown in Figure 3.115.

Access Tunnel Strain Data. The measurements of dynamic strain around the access tunnel, also made by Project 3.3, were located as shown in Figures 3.114. These measurements were made to allow comparisons of dynamic strains concentrations around the access tunnel with similar measurements by Project 3.2 around several test section openings. The peak values of recorded strain, as interpreted by Project 3.3, are listed in Table 3.3 and are plotted in Figures 3.116 and 3.117. The gage designation symbols used are defined as follows:

S refers to Section S at Station 5+30

T refers to Section T at Station 4+30

N refers to gage response normal (radial) to the tunnel axis

C refers to gage response circumferential with respect to tunnel surface

Additional data, including complete curves, may be found in Reference 11.

3.3.3 Fly-Rock Photography, Project 3.11 (EG&G). Only two of the three camera stations were recovered. The cameras in Test Section C6c were apparently intact when recovered. The cameras from the station in Test Section B5a were also recovered; however, some damage was noted. The film from both stations was badly fogged by radiation, and no data was obtained. The third camera station, in Test Section B6c, was not recovered.

For additional information on the fly-rock motion picture photography, see Reference 12.

3.3.4 Mechanical Measurements. The results of the mechanical gage measurements in C and B Drifts are given in Tables 3.4 and 3.5, respectively. No gages were recovered in A Drift due to the severe damage.

Circumferential Strain. The deForest gage targets recovered from known locations are listed in Tables 3.4 and 3.5. A few other targets were reduced at the U of I by reading the coordinates of critical points on the records by means of a microscope with a micrometer-driven platform. The

ordinates of the points were converted to strain by dividing the trace deflections in inches by the two-inch gage length. The abscissas of the points were the measured horizontal distances from the starting point. The peak measured values of circumferential strain from these records are shown in Figure 3.118.

The curves shown in Figure 3.119 (3 pages) were plotted from the reduced data. It should be noted that the abscissas of these curves are in units of length of scratch arm cross travel rather than arbitrary time units. Also, because the rate of scratch arm cross travel for each gage is a function of the pressure developed between the scratch arm and the target, it is not possible to relate quantitatively the abscissa of one gage with that of another gage.

Diameter-Change Scratch Gages. The diameter-change measurements are given in terms of the permanent displacement and transient peak(s). In some of the gage readings, it was possible to determine the direction of first motion from the width of the scribed mark on the gage. The scribed mark in these cases started out as a fine scratch. As the point of the setscrew wore

against the pipe or rock bolt, the width of the scratch increased, giving an indication of the first and last motions. Where it was possible to determine the first motion, this was annotated in the tables.

The majority of the scratch gages in B Drift were damaged beyond recovery. None were recovered in A Drift.

The measured peak values of diameter-change and the ranges of the pre-shot estimates are shown in Figure 3.120. The sign convention used for these measurements is as follows:

(+) indicates an increase in liner diameter, and

(-) indicates a decrease in liner diameter.

Compression-of-Filler Scratch Gages. The results from the scratch readings are given in terms of the permanent displacement and transient peak(s). In several instances, the direction of first motion was readily evident from the width of the scratch mark. These are annotated in the tables.

The measured peak values of compression-of-filler and the ranges of the pre-shot estimates are shown in Figures 3.121, 3.122, and 3.123. The positive (+) values represent increases in the annular gap between the liner and the rock, i.e., apparent elongation of the backpacking thickness. Negative (-) values are true compression of the backpacking.

Reed Gage Data, Project 3.12 (STL). A summary of the postshot condition of the 21 STL reed gages is given in Table 3.6. The records recovered from twelve gages are presented in Figures 3.124 through 3.135. For detailed descriptions see Reference 13.

3.3.5 Static Measurements

Survey Measurements. The postshot survey consisted of repetition of the appropriate pre-shot as-built survey measurements, such as internal liner dimensions, liner location, and cross sections of unlined tunnels and test sections. Comparisons of the pre- and postshot measurements were made to

determine liner deformation and translation as well as rock breakage patterns around the unlined underground openings. The information obtained from these comparisons is presented in the following paragraphs.

(1) Liner Deformation. The survey methods used to determine liner deformation and translation are depicted in Figure 3.136. It can be seen that the internal liner dimensions, both pre- and postshot, were determined by measuring distances, within vertical planes, from the design centerline to points on the liners. In the pre-shot survey, these points were marked on the liner at 45° intervals starting from 0° which designates the point on the liner closest to the shot point. The postshot measurements were made from the same centerline to the same points on the liner surface irrespective of the new locations of the points. Because of liner translation, the postshot measurements were not true radii.

Within concrete liners, the cross sections were taken at horizontal intervals of twelve inches along the middle third of the liner and at intervals of thirty inches within each outer third of the liner length. Liners with

tunnel liner plates were cross sectioned at the center of each ring of plates, i.e., on eighteen-inch intervals. Liners with wide flange rings were cross sectioned at the center of the inner flange of each ring and at the center of each span of lagging.

When the pre- and postshot cross sections were plotted and compared, it was apparent that the distortions of B3c and of many of the liners in C Drift were too slight to be reliably detected by the order of accuracy of the survey. Also, the deformations noted were often not consistent with the permanent deformations indicated by the diameter change scratch gages. Therefore, supplemental postshot measurements of liner diameter were made.

By rationalization of the data from the translation surveys, deformation surveys, and the supplemental diameter measurements, the liner shapes shown in Figure 3.137 were developed. Consideration was also given to the scratch gage data and to observed indications of liner shape such as crack patterns in concrete liners and distortion of tunnel liner plates. Therefore, the deformation patterns shown in Figure 3.137 are considered typical for the liners shown.

(2) Liner Translation. The pre-shot location of each liner was determined by surveying four reference points near each end of the inner surface of the liners, as shown in Figure 3.136. The reference points were located at the extremities of vertical and horizontal axes located within planes normal to the longitudinal axis of the liners. In metal liners, punch marks were used for the reference points. Lead inserts and tacks were provided in concrete liners.

Each of the eight points within each liner were surveyed pre-shot to determine the North and East coordinates and elevation. All undamaged points were resurveyed postshot when accessible.

The liner translations given in Table 3.7 were developed by comparing the pre- and postshot location surveys. It should be noted that all liners surveyed, with the exception of A3c, had pronounced eastern components of displacement. Also, all liners moved upward more steeply than would have resulted from a purely radial translation.

The directions of translation of the liners are depicted vectorially in Figure 3.138. The more prominent faults taken from Figure 1.3 are also shown to illustrate

the apparent influence of the northwesterly trending faults on the horizontal components of the measured displacements in B Drift and C Drift. It can be seen that the liner translations tended to be parallel to this system of faults. The vectors for each liner shown in Figure 3.138 were derived by eliminating points in areas of extreme liner distortion and then averaging the displacements of the remaining points. Therefore, the vectors represent the approximate rigid body translations of the liners.

(3) Rock Breakage. The as-built survey of the underground complex included cross sectioning of the access tunnel and of the test drifts before liners were installed. The appropriate parts of the as-built survey were repeated postshot to obtain information on rock breakage around the access tunnel and around the accessible, unlined portions of the test drifts. The superimposed pre- and postshot cross sections (corrected for translation) are presented in Figures 3.139 (2 pages), 3.140, and 3.141. The apparent poor match between the pre- and postshot access tunnel floors from

Station 2+10 to Station 3+40 resulted from the fact that rail haulage was installed after the completion of the pre-shot survey. An excess of ballast was placed under the ties between those stations to provide a uniform overall grade for the railroad.

Commencing with Station 3+40, the pre-shot access tunnel outlines were shifted easterly and vertically with respect to the postshot outlines by an amount consistent with the translations noted in the test drifts. The translations of pre-shot cross sections of C2a and C2b, Figure 3.141 were developed from the measured translation of C6c before superimposing the postshot outlines. Similarily, the pre-shot outlines of the transition zones of C Drift, Figure 3.138, were shifted on the basis of the translations noted for test sections C3c and C6a.

Access tunnel rock breakage data derived from comparisons of the pre- and postshot cross sections are presented in Figure 3.142 wherein the cumulative volumes and ratios of cross sectional areas are given.

Whittemore Measurements. Measurements were taken to obtain the postshot distance between the two-inch (nominal spacing) Whittemore gage points installed before the shot. The postshot readings were compared with the corresponding pre-shot readings to determine the residual circumferential or longitudinal strain. These results are tabulated in Table 3.8 for C and B Drifts. The locations of the measure points on the wide-flange rings and on the corrugated steel tunnel liner panels are shown in Figures 3.143 and 3.144.

Few postshot measurements were taken in B Drift due to heavy damage in the test liners. Efforts to make these readings were abandoned because of limited accessibility. Also, in view of the extreme distortions of the liners, measurements of strain would be meaningless. No measurements were taken in A Drift because of heavy damage.

The measured values of residual circumferential and longitudinal strain in liners are plotted in Figures 3.145 and 3.146. Positive values represent elongation or tension in the liners.

TABLE 3.1 RESPONSE MEASUREMENTS IN TEST SECTIONS FROM ELECTRONIC INSTRUMENTS (PROJ. 3.2)

TEST SECTION	GAGE	POSITIVE PEAK	TIME OF PEAK	NEGATIVE PEAK	TIME OF PEAK	REMARKS	END OF RECORD
A3a	DR	5.98 in	.026s	2.49 in	.030s		.031s
A3b	DR	1.11 in	.024				.055
	VR	2.77 fps	.023	4.26 fps	.025		.026
A3c	PP	480 psi	.021			Partial Positive Peak	.021
A3d	DR	4.21 in	.027	2.86 in	.029		.042
	VR	4.17 fps	.020	3.96 fps	.026		.028
A5a	DR	1.12 in	.024	>3.9 in	.025	Partial Negative Peak	.025
	DP	9.2 in	.030	1.7 in	.025	Partial Positive Peak	.030
	PR	468 psi	.026			Partial Positive Peak	.026
	PP	145 psi	.020				.024
	VR	16.8 fps	.018	3.2 fps	.021		.024
	SCO-L			3.39 ppk*	.016	Partial Negative Peak	.016
	SC90-L			11.6 ppk	.021	Partial Negative Peak	.021
A5b	DR	1.69 in	.025				.045
	DP	4.41 in	.019				.027
A5c	DR	14.4 in	.017	2.6 in	.024		.032
	VR	5.2 fps	.018			Partial Positive Peak	.018
B1a	SC 180-0	0.53 ppk*	.028			Partial Positive Peak	.028
	SR 90-1	1.10 ppk	.017	1.89 ppk	.022	Partial Negative Peak	.022
B2a	SCO-1			.27 ppk	.020		
	SRO-1	3.92 ppk	.026				.027
	SR 90-1	0.78 ppk	.024	0.17 ppk	.018		.032
B3a	DR	2.37 in	.031			Partial Positive Peak	.031
	VR	56.2 fps	.039	1.7 fps	.045		.061
B3b	DR	4.01 in	.052	2.16 in	.078		.098
	VR	13.1 fps	.029	5.8 fps	.093		.103
	SCO-L			2.92 ppk	.027		.038
B3c	DR	1.48 in	.074	3.91 in	.076		.116
	PR	144 psi	.036				.105
	PP	592 psi	.033				.325
	VR	16.6 fps	.040				.103
	SCO-0	>0.2 ppk	.022	.19 ppk	.020	Partial Positive Peak	.022
	SRO-1	0.61 ppk	.021				.021
	SCO-L	0.69 ppk	.040	1.03 ppk	.025		.049

* ppk - parts per thousand

TABLE 3.1 (CONTINUED)

TEST SECTION	GAGE	POSITIVE PEAK	TIME OF PEAK	NEGATIVE PEAK	TIME OF PEAK	REMARKS	END OF RECORD
B3d	DR	1.53 in	.042s	3.51 in	.040s		.093s
	VR	10.5 fps	.026	10.5 fps	.066	Partial Negative Peak	.066
	SCO-L	1.71 ppk*	.024	0.59 ppk*	.033		.036
B4a	SC90-L	0.85 ppk	.030	0.64 ppk	.027	Partial Positive Peak	.030
B4b	DP			1.18 in	.030	Partial Negative Peak	.030
	PR	170 psi	.028				.038
	PP	309 psi	.038	54 psi	.047		.065
	SC90-L	0.43 ppk	.029				.030
	SCO-L	2.37 ppk	.024				.025
B5a	DR	1.92 in	.038				.050
	DP	9.4 in	.057	4.8 in	.064		.065
	FR	1.69 in	.034				.035
	FP	1.89 in	.029	0.88 in	.049		.097
	PR	359 psi	.047				.092
	PP	192 psi	.026				.055
	VR 180	3.53 fps	.017	25.7 fps	.027		.027
	SC90-L			1.58 ppk	.026		.026
B5b	DR	4.56 in	.034	1.34 in	.048		.072
	DP	1.43 in	.028				.050
	PR	202 psi	.024	70 psi	.030		.038
	VR	22.0 fps	.032	17.4 fps	.055		.067
	VR 180	21.9 fps	.030	6.2 fps	.034		.113
B5c	DR	2.24 in	.042	1.36 in	.061		.068
	PR	320 psi	.022				.026
	VR	5.88 fps	.024				.030
	VR 180	1.48 fps	.030				.300
B6a	VR	8.8 fps	.028	4.5 fps	.034		?
B6b	PP	83 psi	.023			Partial Positive Peak	.023
	VR	11.7 fps	.037	6.9 fps	.033		.049
B6c	VR	7.7 fps	.029				.032
B7a	DR	2.39 in	.030				.088
C3c	PR	38.7psi	.043				.089
	PP	124 psi	.041				.500
	VR	9.7 fps	.042	.92 fps	.069		.300

* ppk - parts per thousand

TABLE 3.2 RECORDED SHOCK EFFECTS FROM ELECTRONIC INSTRUMENTS (PROJ. 3.3)

GAGE NUMBER	HORIZ. RANGE (feet)	TIME OF ARRIVAL (msec)	PEAK ACCEL. (G's)	PEAK VELOCITY (ft/sec)	PEAK DISPL. (inch)	PEAK STRESS (psi)	PEAK STRAIN %	SET RANGE
4-A	256	14.1	4226	56.5*	–	–	–	6,000
6-A	306	17.1	1946	60.6	6.4(5.5)	–	–	1,500
6-U	306	18.5	–	51.3	1.4(1.3)	–	–	150
6-F	306	17.0	–	–	–	14,036	–	30,000
6-L	306	17.1	–	–	–	–	0.15	3.0
8-A	396	22.0	493	30.1	8.5(5.2)	–	–	700
8-U	396	23.1	–	30.0	7.1(3.4)	–	–	60
8-DI	396	23.0	–	–	3.9	–	–	10
8-F	396	21.9	–	–	–	13,051	–	20,000
8-L	396	–		–	–	–	No Data	0.3
9-A	505	28.0	215	21.4	5.6	–	–	200
9-U	505	28.8	–	8.0	2.5	–	–	50
9-DI	505	28.5	–	–	6.8	–	–	6
9-F	505	28.3	–	–	–	2,230	–	12,000
9-L	505	28.7	–	–	–	–	0.16	0.2
11-AR	604	33.0	46.0	6.0	1.8(0.19)	–	–	100
11-AV	604	33.6	22.3	1.9	4.9	–	–	100
11-AT	604	33.0	57.2	10.2	1.4	–	–	100
11-UR	604	36.1	–	5.2	0.7	–	–	40
11-UV	604	35.2	–	2.2	4.4	–	–	40
11-UT	604	34.6	–	11.0	3.8	–	–	40
11-DI	604	35.0	–	–	6.7(0.5)	–	–	6
11-F	604	33.5	–	–	–	4,423	–	10,000
11-L	604	33.3	–	–	–	–	0.037	0.1
12-AR	784	42.5	32.7	5.7	1.98	–	–	80
12-AV	784	42.5	12.4	1.5	0.13	–	–	80
12-AT	784	42.6	23.9	4.1	0.62	–	–	80
12-UR	784	43.7	–	7.4	2.6(1.5)	–	–	20
12-UV	784	–		No Data	–	–	–	20
12-UT	784	44.6	–	3.9	1.05	–	–	20
12-D	784	44.7	–	–	1.05 (0.2)	–	–	16

* Not a true peak
( ) Values in parenthesis are residuals

TABLE 3.3 STRAIN MEASUREMENTS IN ACCESS TUNNEL
FROM ELECTRONIC INSTRUMENTS (PROJ. 3.3)

GAGE NUMBER	SECTION *	DEPTH (ft)	TIME OF ARRIVAL (msec)	STRAIN %	SENSE	DIRECTION **	CABLE BREAK (msec)	SET RANGE %
SN-W4	S	4	15.7	2.1	TENS.	RADIAL	22.0	1.3
SC-W4	S	4	15.3	0.50	COMPR.	CIRCUM.	22.6	1.0
SN-W8	S	8	18.0	0.20	TENS.	RADIAL	21.5	1.3
SC-W8	S	8	15.4	0.16	COMPR.	CIRCUM.	18.7	1.0
SN-D4	S	4	15.2	2.1	TENS.	RADIAL	21.6	1.3
SC-D4	S	4	15.8	0.37	COMPR.	CIRCUM.	28.5	1.0
SN-D8	S	8	15.8	0.99	TENS.	RADIAL	23.7	1.3
SC-D8	S	8	13.0	0.20	COMPR.	CIRCUM.	23.5	1.0
SN-B4	S	4	15.3	0.26	COMPR.	RADIAL	22.8	1.3
SC-B4	S	4	15.0	0.34	COMPR.	CIRCUM.	23.7	1.0
SN-B8	S	8	15.4	0.14	COMPR.	RADIAL	19.0	1.3
SC-B8	S	8	15.8	0.074	COMPR.	CIRCUM.	19.1	1.0
TC-W2	T	2	21.8	0.51	TENS.	CIRCUM.	156	1.0
TN-W4	T	4	23.0	2.0	TENS.	RADIAL	158	1.3
TC-W4	T	4	21.8	1.2	TENS.	CIRCUM.	152	1.0
TN-W8	T	8	27.0	0.90	TENS.	RADIAL	174	1.3
TC-W8	T	8	21.9	0.54	TENS.	CIRCUM.	167	1.0
TC-B2	T	2	NO RECORD		-	CIRCUM.	-	1.0
TN-B4	T	4	21.8	0.05	TENS.	RADIAL	35	1.3
TC-B4	T	4	23.0	0.04	COMPR.	CIRCUM.	32	1.0
TN-B8	T	8	24.9	1.4	TENS.	RADIAL	-	1.3
TC-B8	T	8	22.6	0.23	COMPR.	CIRCUM.	-	1.0

* For location of tunnel Cross-Section see Figure 3.114

** The directions of strain listed in this column are all referred to the longitudinal axis of the Access Tunnel.

TABLE 3.4 MECHANICAL GAGE MEASUREMENTS IN C DRIFT

	CIRCUMFERENTIAL STRAIN IN LINING (%)					DIAMETER CHANGE IN LINING (INCHES)				COMPRESSION OF FILLER (INCHES)			
TEST SECTION	0°	45°	90°	135°	180°	0°	45°	90°	135°	0°	90°	180°	270°
C3c	R	Rta	—	Rtf	—	+1/8 P	—	-1/16 P	—	+15/16 P	-7/16 P	-1/4 P	—
						-5/16* + 7/16 M	—	-3/16 + 1* M	—	+1 7/8 M	-13/16 M	-7/8 + 15/16* M	—
C3b	—	—	R	Rt	Rta	+1/16 P	—	0 PB	—	-1/2 P	-5/16 PQ	-1/2 P	—
						-1/16* + 3/8 M	—	+ 7/16 MB	—	-15/16 M	-5/16 M	-3/4 M	—
C4a	R	R	R	Rt	Rt	0 PB	—	-1/8 PB	—	-5/8 P	—	+3/4 P	+9/16 P
						+7/16 MB	—	-1/4 MB	—	-3/4 M	—	+3/8 M	-1/4 + 11/16 M
C4b	Rta	Rt	R	Rt	Ra	0 PB	—	0 PB	—	-1/16 P	-3/4 P	+5/16 P	—
						-1/8* + 3/8 MB	—	+1/8 MB	—	-1/2 M	-1 1/8 M	+1/2 M	—
C6b	N	N	N	Ra	N	-3/8 PB	—	-3/4 PB	—	+1 1/8 P	N	-5/16 P	—
						-3/4 MB	—	-13/16 + 1/8 MB	—	+1 1/4 M	N	-1/2 + 1/4* M	—
C7a	—	—	—	—	—	-7 13/16 P	-3 7/8 P	-17 7/16 P	+1 1/4 P	—	—	—	—
						-7 13/16 M	-4 3/16 + 15/16* M	-17 7/16 + 1/16 M	-4 1/16 + 1 11/16 M	—	—	—	—
C1a, C1b & C2a	—	—	—	—	—	N	—	N	—	—	—	—	—
						N	—	N	—	—	—	—	—
C6a	N	N	R	R	R	+5/16 PB	—	-1/2 PB	—	0 P	-1/16 P	-3/8 P	—
						-1/8* + 3/4 MB	—	-5/8 + 5/8 MB	—	-5/8 M	-3/8 M	-5/8 + 1/4 M	—
C3d	—	Rt	R	R	R	0 P	—	+1/16 PB	—	+1 1/16 P	—	-1 3/8 P	0 P
						-1/16 + 1/16 M	—	+1/2 MB	—	-1/8* + 1 5/16 M	—	-1 7/8 + 1/8 M	-1/8 M
C4c	Rt	N	Rt	N	—	0 P	—	+3/8 PQ	—	0 P	-1/8 P	-1 1/4 P	—
						-1/8* + 1/4 M	—	+5/16 MQ	—	+3/16 M	-7/16 M	-1 5/16 M	—
C3a	Rt	N	.t	—	Rt	-1/2 PB	—	-1/16 PB	—	—	—	—	—
						-11/16 + 1/16* MB	—	-1/16 + 5/16* MB	—	—	—	—	—
C6c	Ra	Ra	R	N	N	0 PB	—	0 PB	—	-3/8 PQ	—	+5/16 P	+3/8 P
						-7/16 + 1/8* MB	—	+1/2 MB	—	-9/16 MQ	—	+3/16 M	-3/8* + 11/16 M
C2b	—	—	—	—	—	-1/8 P	—	-1 1/8 P	—	—	—	—	—
						+3/16 - 11/16 MB	—	-1 5/16 MB	—	—	—	—	—

N – No Recovery because of Damage
Q – Gage Damaged, Questionable Reading
R – Gage Recovered, Data shown in Figures 3.118, 3.119

t – Target Loose
a – Arm Loose
ta – Arm and Target Loose, Found on Floor
tf – Target Loose, Found on Floor

M – Maximum Transient
P – Permanent
B – Gage Bent
— No Gage Installed

(-) – Compression
(+) – Elongation
(*) – First Motion

TABLE 3.5 MECHANICAL GAGE MEASUREMENTS IN B DRIFT

	CIRCUMFERENTIAL STRAIN IN LINING (%)					DIAMETER CHANGE IN LINING (INCHES)				COMPRESSION OF FILLER (INCHES)			
TEST SECTION	0°	45°	90°	135°	180°	0°	45°	90°	135°	0°	90°	180°	270°
B3c	—	Ra	—	—	N	+1⅞ PQ	—	N	—	-2⅜ P	-4¾ P	-1¼ P	—
						+1⅞ MQ	—	N	—	-2⅞ M	-5¼ M	-1¾ M	—
B3b	N	—	N	—	—	-5½ PQ	—	N	—	-7 11/16 P	N	-1 1/16 PQ	—
						-6½ PQ	—	N	—	-8¼ M	N	-2¾ M	—
B4a	N	N	N	N	N	-5⅛ PQ	—	N	—	N	—	N	N
						N	—	-3/16° MQ	—	N	—	N	N
B4b & B5b	—	N	N	N	N	N	—	N	—	N	N	N	—
						N	—	N	—	N	N	N	—
B6b	—	—	N	N	N	N	—	N	—	N	N	N	—
						N	—	N	—	N	N	N	—
B7a	—	—	—	—	—	N	N	N	N	—	—	—	—
						N	N	N	N	—	—	—	—
B1a & B1b	—	—	—	—	—	N	—	N	—	—	—	—	—
						N	—	N	—	—	—	—	—
B5a & B6a	—	N	—	N	N	N	—	N	—	N	N	N	—
						N	—	N	—	N	N	N	—
B3d	N	N	N	N	—	N	—	N	—	N	—	N	N
						N	—	N	—	N	—	N	N
B4c	N	N	N	N	N	N	—	N	—	N	N	N	—
						N	—	N	—	N	N	N	—
B3a	—	N	N	N	N	N	—	N	—	—	—	—	—
						N	—	N	—	—	—	—	—
B5c & B6c	N	N	N	N	—	N	—	N	—	N	—	N	N
						N	—	N	—	N	—	N	N
B2a & B2b	—	—	—	—	—	N	—	N	—	—	—	—	—
						N	—	N	—	—	—	—	—

N – No Recovery because of Damage
Q – Gage Damaged, Questionable Reading
a – Arm Loose
R – Gage Recovered, Data shown in Figures 3.118, 3.119

M – Maximum Transient
P – Permanent
B – Gage Bent
— No Gage Installed

(–) – Compression
(+) – Elongation
(°) – First Motion

TABLE 3.6 SUMMARY OF REED GAGE TEST DATA (PROJ. 3.12)

GAGE NO.	LOCATION	ORIENTATION	SLANT RANGE (feet)	NO. OF DATA POINTS	TEST RESULTS
1	SURFACE	VERTICAL	1340	4	SEE FIGURE 3.124
25	ACCESS TUNNEL	RADIAL	723	9	SEE FIGURE 3.125
16	ACCESS TUNNEL	VERTICAL	723	9	SEE FIGURE 3.126
20	ACCESS TUNNEL	RADIAL	457	8	SEE FIGURE 3.127
26	ACCESS TUNNEL	VERTICAL	457	6	SEE FIGURE 3.128
7	SECTION C3b	RADIAL	457	6	SEE FIGURE 3.129
21	SECTION C3c	RADIAL	457	7	SEE FIGURE 3.130
4	SECTION C3a	RADIAL	457	3	SEE FIGURE 3.131
8	SECTION C4b	RADIAL	457	7	SEE FIGURE 3.132
19	ACCESS TUNNEL	RADIAL	334	0	GAGE DAMAGED, NO DATA
22	ACCESS TUNNEL	VERTICAL	334	0	GAGE DAMAGED, NO DATA
24	SECTION B3a	RADIAL	334	0	GAGE DAMAGED, NO DATA
2	SECTION B3a	VERTICAL	334	-	INACCESSIBLE, NOT RECOV.
12	SECTION B3b	RADIAL	334	6	SEE FIGURE 3.133
5	SECTION B3b	VERTICAL	334	5	SEE FIGURE 3.134
15	SECTION B3c	RADIAL	334	5	SEE FIGURE 3.135
6	SECTION B3d	RADIAL	334	0	GAGE DAMAGED, NO DATA
27	ACCESS TUNNEL	VERTICAL	244	0	GAGE DAMAGED, NO DATA
23	SECTION A3a	RADIAL	244	-	INACCESSIBLE, NOT RECOV.
18	SECTION A3b	RADIAL	244	-	GAGE DAMAGED, NO DATA
13	SECTION A3c	RADIAL	244	0	GAGE DAMAGED, NO DATA

TABLE 3.7 LINER TRANSLATION

TEST DRIFT	TEST SECTION	THEORETICAL RADIAL TRANSLATION		MEASURED TRANSLATION			DIFFERENCE		AVERAGE DIFFERENCE	
		BEARING	* VERTICAL ANGLE	BEARING	* VERTICAL ANGLE	MAGNITUDE (FEET)	BEARING	* VERTICAL ANGLE	BEARING	* VERTICAL ANGLE
A-LEFT	A3c	S06°E	+21°	S06°E	+45°	2.3	0°	+24°	0°	+24°
B-LEFT	B3c	S08° E	+15°	S41° E	+38°	1.1	33°	+23°	33°	+24°
	B3b	S05°E	+15°	S36°E	+42°	1.2	31°	+27°		
	B4a	S02°E	+15°	S38°E	+37°	1.9	36°	+22°		
C-LEFT	C3c	S10°E	+11°	S59° E	+32°	0.7	49°	+21°	47°	+23°
	C3b	S08°E	+11°	S52°E	+30°	0.8	44°	+19°		
	C4a	S05°E	+11°	S57°E	+41°	0.8	52°	+30°		
	C4b	S03°E	+11°	S51°E	+34°	0.8	48°	+23°		
	C6b	S01°E	+11°	S44°E	+35°	0.8	43°	+24°		
C-RIGHT	C6a	S17°E	+11°	S51°E	+30°	0.7	44°	+19°	35°	+17°
	C3d	S20°E	+11°	S49°E	+25°	0.6	29°	+14°		
	C4a	S22°E	+11°	S58°E	+30°	0.7	36°	+19°		
	C3a	S24°E	+11°	S58°E	+27°	0.7	34°	+16°		
	C6c	S26°E	+11°	S56°E	+27°	0.7	30°	+16°		

* ANGLE MEASURED VERTICALLY FROM THE HORIZONTAL. A PLUS (+) ANGLE INDICATES AN UPWARD DIRECTION.

TABLE 3.8 WHITTEMORE STRAIN AND SURVEY MEASUREMENTS IN C AND B DRIFTS

			CIRCUMFERENTIAL STRAIN IN LINING (PPK)								LONGITUDINAL STRAIN IN LINING (PPK)								DIAMETER CHANGE IN LINING				COMPRESSION OF FILLER				
			0°	45°	90°	135°	180°	225°	270°	315°	0°	45°	90°	135°	180°	225°	270°	315°	0°	45°	90°	135°	0°	45°	90°	135°	180°
C DRIFT (60 FEET FROM ZERO)	C1c		0	—	—	—	—	0	+2.6	0	—	—	—	—	—	—	—	—									
	C1b		0	—	—	—	—	+0.6	-2.3	0	—	—	—	—	—	—	—	—									
	C4a*	1	0	0	0	0	0	0	-0.4	-0.3	+0.4	+9.1	+29.5	+1.3	0	+3.5	+10.3	0				ORDER OF SURVEY ACCURACY PRECLUDED PRECISE DETERMINATION OF SMALL DEFORMATIONS					
		2	-0.2	0	0	-0.5	-0.2	+0.2	-0.2	+0.2	—	—	—	—	—	—	—	—									
		3	-0.3	0	0	-0.2	0	-0.5	-0.5	+0.3	—	—	—	—	—	—	—	—									
	C4b*	1	-0.3	0	0	0	+0.3	+0.3	0	-0.3	+5.5	+1.7	-0.3	0	0	+1.1	+3.1	-0.3									
		2	0	0	0	-0.3	0	0	0	0	—	—	—	—	—	—	—	—									
		3	+0.4	+0.2	0	+0.2	0	-0.3	0	-0.2	—	—	—	—	—	—	—	—									
	C5c**	1	0	-2.0	-0.4	+0.2	-0.3	N	-2.6	-0.4	—	—	—	—	—	—	—	—									
		2	-0.2	0	0	0	+0.2	0	0	-0.6	—	—	—	—	—	—	—	—									
		3	N	+1.70	-0.6	N	-0.60	-1.0	+3.2	-0.4	—	—	—	—	—	—	—	—									
		4	-0.4	+0.4	0	-0.4	0	-0.6	-1.5	-0.2	—	—	—	—	—	—	—	—									
		5	0	-1.4	-0.5	0	-0.8	+0.7	-4.9	+0.2	—	—	—	—	—	—	—	—									
	C2c		—	—	—	—	—	—	—	—	—	—	—	—	—	—	—	—					—	—	—	—	—
	C1c		—	—	—	—	—	—	—	—	—	—	—	—	—	—	—	—	N	N	N	N	—	—	—	—	—
	C3b		—	—	—	—	—	—	—	—	—	—	—	—	—	—	—	—	N	N	N	N	—	—	—	—	—
	C4c**	1	+0.2	0	+0.3	+0.4	+0.3	-0.2	+0.5	+0.4	—	—	—	—	—	—	—	—									
		2	+0.2	0	0	0	0	+0.4	-0.40	0	—	—	—	—	—	—	—	—				ORDER OF SURVEY ACCURACY PRECLUDED PRECISE DETERMINATION OF SMALL DEFORMATIONS					
		3	-0.3	0	+0.20	+0.2	0	+0.20	+0.60	-0.6	—	—	—	—	—	—	—	—									
		4	0	0	+0.2	+0.2	0	+0.3	-0.6	0	—	—	—	—	—	—	—	—									
		5	+0.3	+0.3	-0.6	0	+0.2	0	-0.2	+0.2	—	—	—	—	—	—	—	—									
	C3d		—	—	—	—	—	0	-0.60	0	—	—	—	—	—	—	—	—									
	C4c*	1	N	+0.2	-0.3	-0.2	+0.3	+0.2	+0.3	-0.3	—	—	—	—	—	—	—	—									
		2	-0.2	+0.3	-0.4	0	-0.2	-0.2	0	0	—	—	—	—	—	—	—	—									
		3	0	0	+0.5	0	0	-0.5	0	+0.2	—	—	—	—	—	—	—	—									
	C2a		—	—	—	—	—	—	—	-0.5	—	—	—	—	—	—	—	—					—	—	—	—	—
	C4c**	1	0	-0.2	+0.3	+0.3	+0.30	+0.3	0	N	—	—	—	—	—	—	—	—									
		2	-0.3	-0.3	+0.3	-0.7	N	+0.4	-0.4	-0.8	—	—	—	—	—	—	—	—				ORDER OF SURVEY ACCURACY PRECLUDED PRECISE DETERMINATION OF SMALL DEFORMATIONS					
		3	+0.3	-0.30	+0.4	-1.00	-0.3	+0.8	0	0	—	—	—	—	—	—	—	—									
		4	0	0	0	0	+0.3	0	-0.4	-0.3	—	—	—	—	—	—	—	—									
		5	-0.8	-0.2	0	+0.3	+0.20	0	-0.5	N	—	—	—	—	—	—	—	—									
	C2c		—	—	—	—	—	—	—	—	—	—	—	—	—	—	—	—					—	—	—	—	—
	C3b		—	—	—	—	—	—	—	—	—	—	—	—	—	—	—	—					—	—	—	—	—
B DRIFT (304 FEET FROM ZERO)	B3c		—	—	—	—	—	—	+0.5	0	—	—	—	—	—	—	—	—	ORDER OF SURVEY ACCURACY PRECLUDED PRECISE DETERMINATION OF SMALL DEFORMATIONS.								
	B3b		—	—	—	—	—	N	-12.9	N	—	—	—	—	—	—	—	—									
	B4a*	1	-19.6	N	N	-0.4	-11.6	N	N	N	N	N	N	N	N	N	N	N	N	N	N	N	N	N	N	N	N
		2	N	N	N	+0.8	N	N	N	N	N	N	N	N	N	N	N	N	N	N	N	N	N	N	N	N	N
	B4b																		N	N	N	N	N	N	N	N	N
	B5b																		N	N	N	N	N	N	N	N	N
	B6b																		N	N	N	N	N	N	N	N	N
	B2a																		N	N	N	N	—	—	—	—	—
	B1a																		N	N	N	N	—	—	—	—	—
	B1b																		N	N	N	N	N	—	—	—	—
	B5a																		N	N	N	N	N	N	N	N	N
	B6a				NO DATA DUE TO HEAVY DAMAGE OF TEST SECTIONS						NO DATA DUE TO HEAVY DAMAGE OF TEST SECTIONS								N	N	N	N	N	N	N	N	N
	B5d																		N	N	N	N	N	N	N	N	N
	B4c																		N	N	N	N	N	N	N	N	N
	B3a																		N	N	N	N	—	—	—	—	—
	B5c																		N	N	N	N	N	N	N	N	N
	B6c																		N	N	N	N	N	N	N	N	N
	B2a																						—	—	—	—	—
	B3b																						—	—	—	—	—

PPK - PARTS PER THOUSAND
N - NO MEASUREMENT BECAUSE OF DAMAGE
Q - QUESTIONABLE READING
* - SEE FIGURE 3.143 FOR LOCATION OF MEASUREMENTS
** - SEE FIGURE 3.144 FOR LOCATION OF MEASUREMENTS

(-) - COMPRESSION
(+) - ELONGATION
— - NO MEASUREMENT PLANNED

Figure 3.1 Shaft Sta 3+75, NE corner of bearing set. (H&N-AEC 62-1241-2, 1962).

Figure 3.2 Shaft Sta 3+75, SE corner of bearing set. (H&N-AEC 62-1241-3, 1962).

Figure 3.3 Shaft Sta 1+35, NW corner of elevator compartment. Note deformation of WF set and hanger angles. (H&N-AEC 62-1241-6, 1962).

Figure 3.4 View looking up from Sta 1+48 in shaft. Note displacement of sets (DASA - NOU 150-02 NTS-62).

Figure 3.5 Shaft Sta 1+10, NW corner of bearing set. Note failure of hanger angles. (H&N AEC 62-1241-7, 1962).

Figure 3.6 Shaft Sta 1+35, SW corner of bearing set Note failure of hanger angles. (H&N-AEC 62-1241-5, 1962).

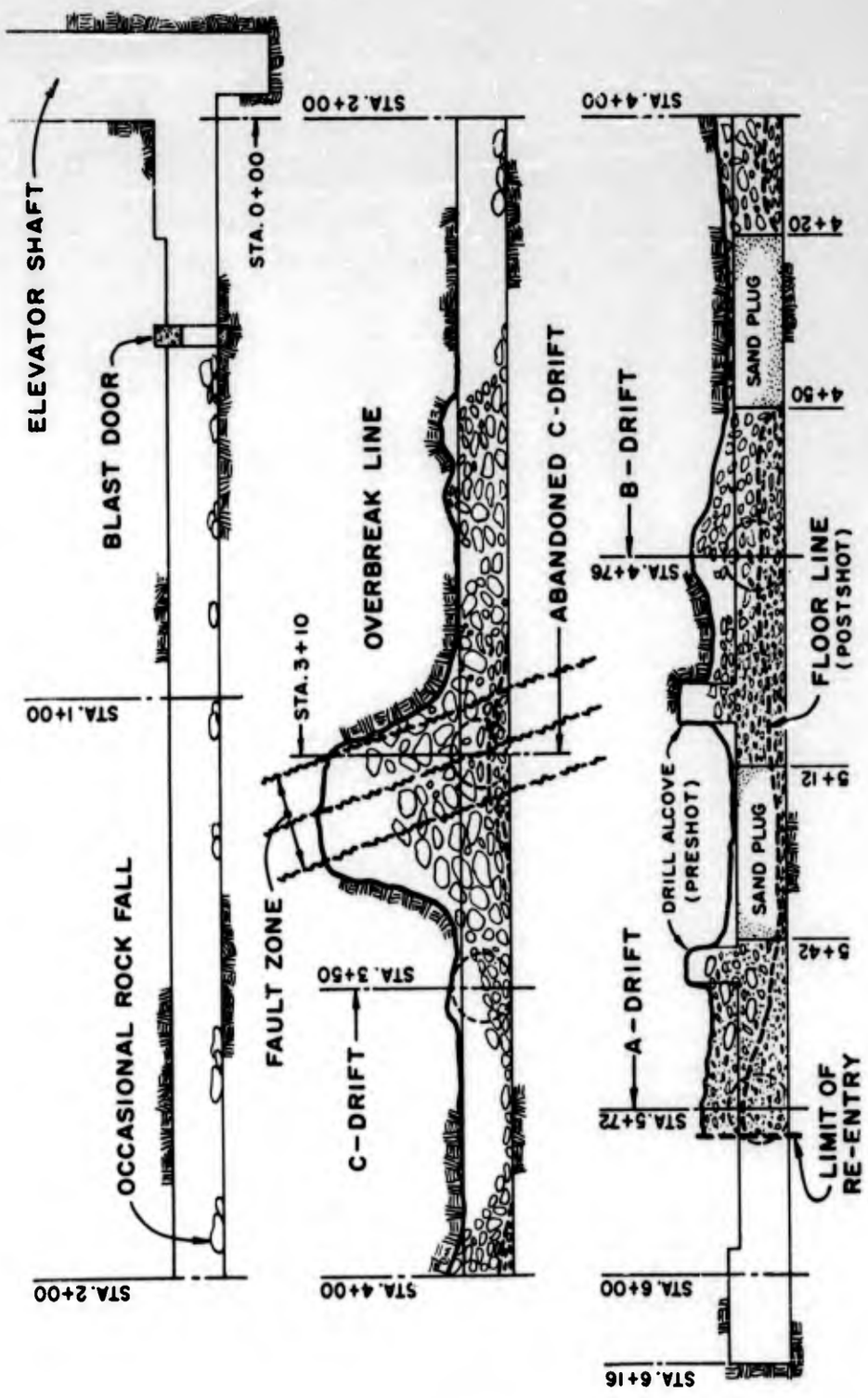

Figure 3.7 Damage profile through access tunnel.

Figure 3.8 Rock fall north side of blast door, Sta 0+42, approximately 760 feet from zero point, looking south (DASA - NOU 160-08 NTS-62).

Figure 3.9 Rock fall, Sta 2+60, approximately 545 feet from zero point, looking south (DASA - NOU 167-04 NTS-62).

Figure 3.10 Access tunnel from Sta 2+00, approximately 605 feet from zero point, looking north (preshot) (DASA - NOU 085-11 NTS-62).

Figure 3.11 Access tunnel from Sta 2+10, approximately 595 feet from zero point, looking north (postshot) (DASA - NOU 160-02 NTS-62).

Figure 3.12 Access tunnel from Sta 2+50, approximately 555 feet from zero point, looking north (preshot) (DASA - NOU 085-10 NT

Figure 3.13 Access tunnel from Sta 2+30, approximately 575 feet from zero point, view to north (postshot) (DASA - NOU 160-01 NTS-62).

Figure 3.14 Access tunnel from Sta 3+00, approximately 505 feet from zero point, view to north (preshot) (DASA - NOU 085-09 NTS-62).

Figure 3.15 Access tunnel from Sta 2+90, approximately 515 feet from zero point, view to north (postshot) (DASA - NOU 179-04 NTS-62).

Figure 3.16 Access tunnel from Sta 3+50, approximately 460 feet from zero point, view to north (preshot) (DASA - NOU 085-06 NTS-62).

Figure 3.17 Access tunnel from Sta 3+50, approximately 460 feet from zero point, view to north (postshot) (DASA - NOU 206-01 NTS-62)

Figure 3.18 Access tunnel from Sta 4+00, approximately 410 feet from zero point, view to north (preshot) (DASA - NOU 085-05 NTS-62).

Figure 3.19 Access tunnel from Sta 4+00, approximately 410 feet from zero point, view to north (postshot) (DASA - NOU 208-05 NTS-62).

Figure 3.20 Access tunnel from Sta 4+75, approximately 335 feet from zero point, view to north (preshot). Note timber sets (DASA - NOU 085-01 NTS-62).

Figure 3.21 Access tunnel from Sta 4+85, approximately 325 feet from zero point, view to north (postshot). Note crushed timber sets (DASA - NOU 365-05 NTS-62).

Figure 3.22 Access tunnel from Sta 5+00, approximately 310 feet from zero point, view to north (preshot) (DASA - NOU 084-12 NTS-62).

Figure 3.23 Access tunnel from Sta 5+00, approximately 310 feet from zero point, view to north (postshot) (DASA - NOU 377-01 NTS-62).

Figure 3.24 Test Section C3c (postshot) (DASA - NOU 339-09 NTS-62).

Figure 3.25 Transition zone, C Drift left. Note approximate rock breakage bounded by dotted lines (DASA - NOU 205-04 NTS-62).

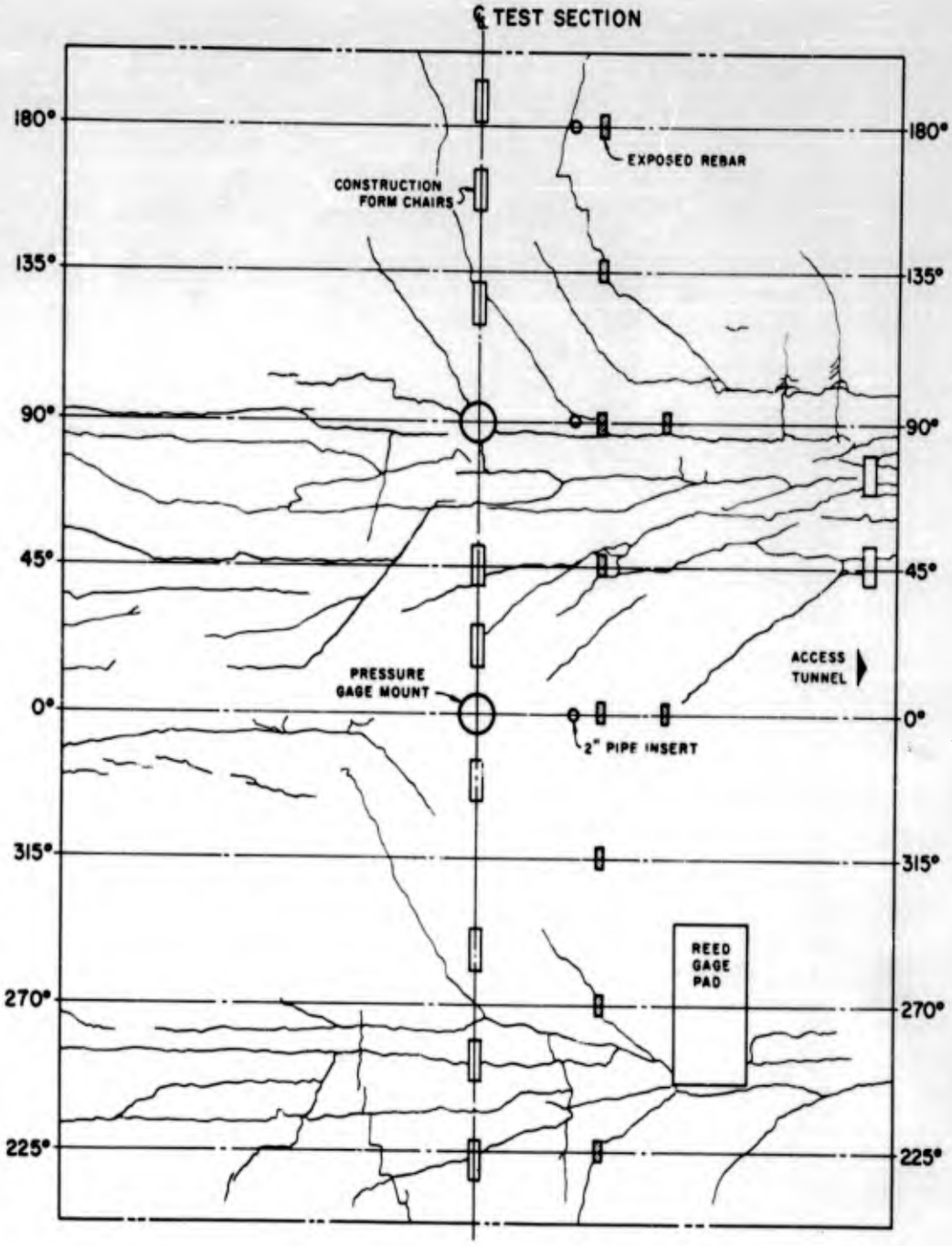

Figure 3.26 C3c, inside surface crack patterns

Figure 3.27 Test Section C3b (postshot) (DASA - NOU 229-04 NTS-62).

Figure 3.28 Test Section C4a (postshot) (DASA - NOU 227-09 NTS-62).

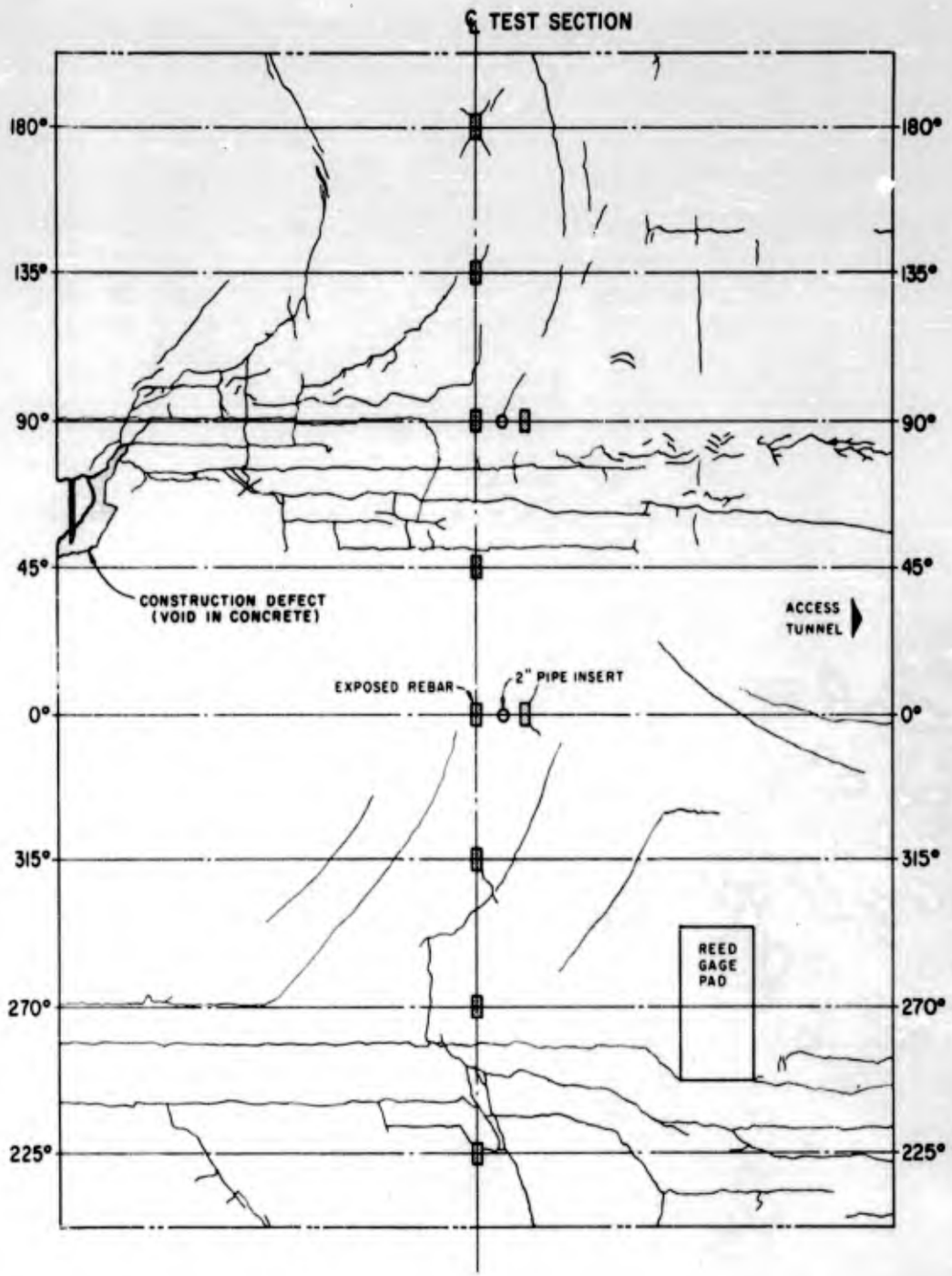

Figure 3.29 C3b, inside surface crack patterns.

Figure 3.30 Close-up C4a. Note distorted steel decking (DASA - NOU 227-10 NTS-62).

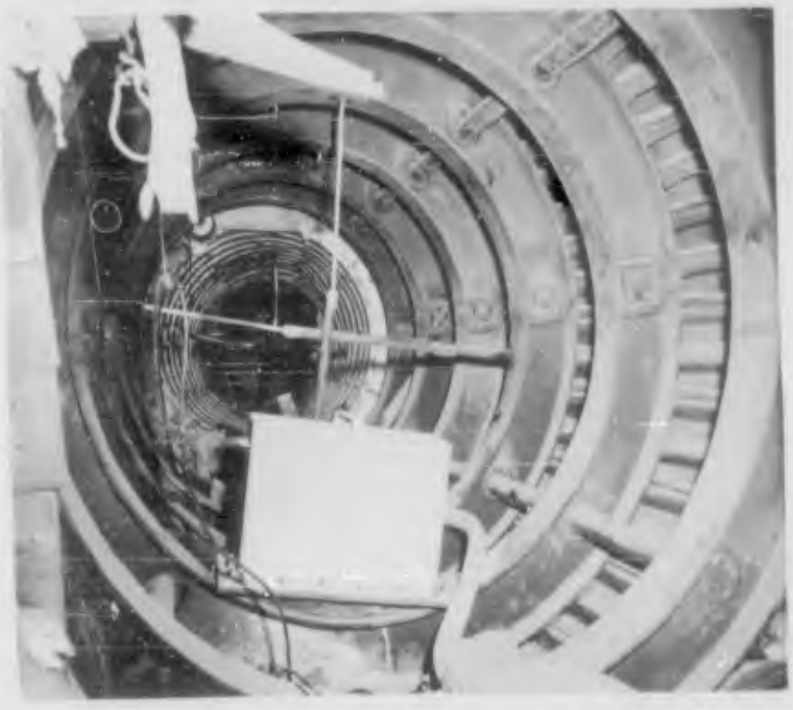

Figure 3.31 Test Section C4b (postshot) (DASA - NOU 227-11 NTS-62).

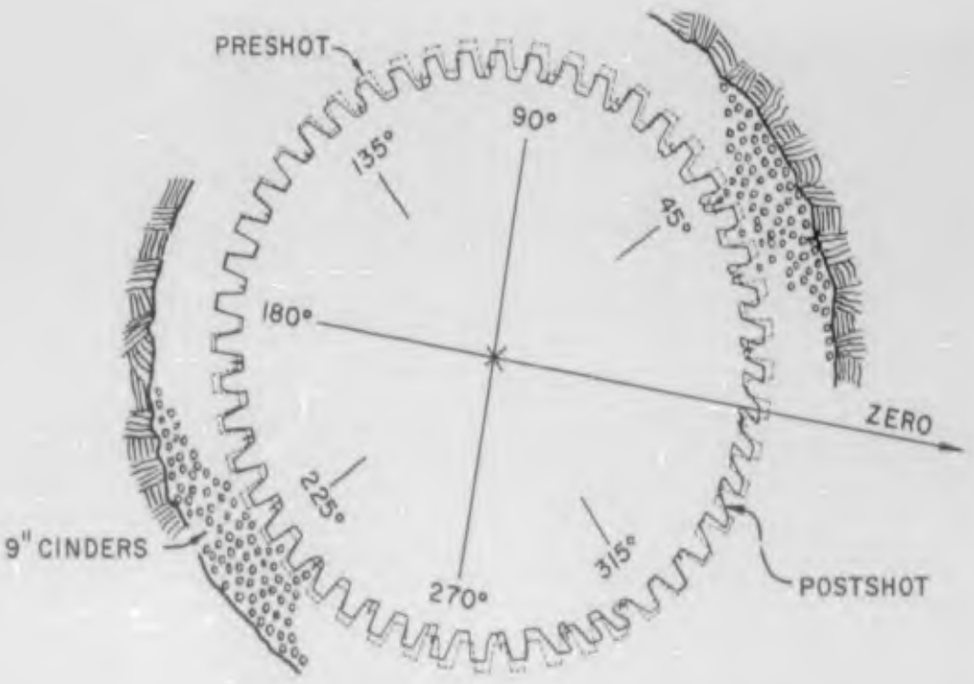

Figure 3.32 C4a, typical liner deformations at midspan between wide-flange rings.

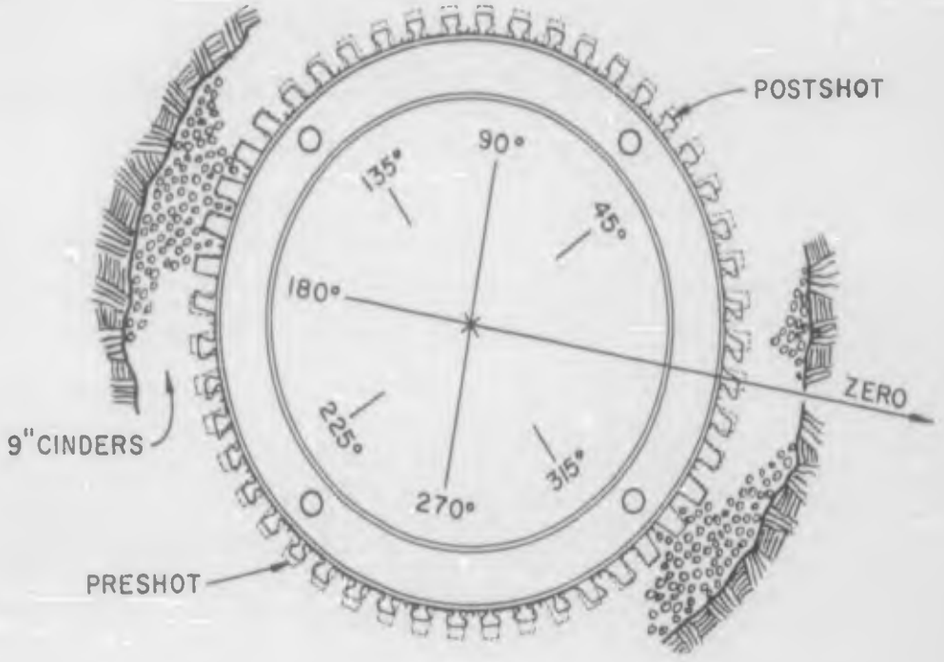

Figure 3.33 C4a, typical liner deformations at wide-flange rings.

Figure 3.34 Close-up C4b. Note distorted steel decking (DASA - NOU 228-01 NTS-62).

Figure 3.35 Test Section C6b (postshot) (DASA - NOU 227-12 NTS-62).

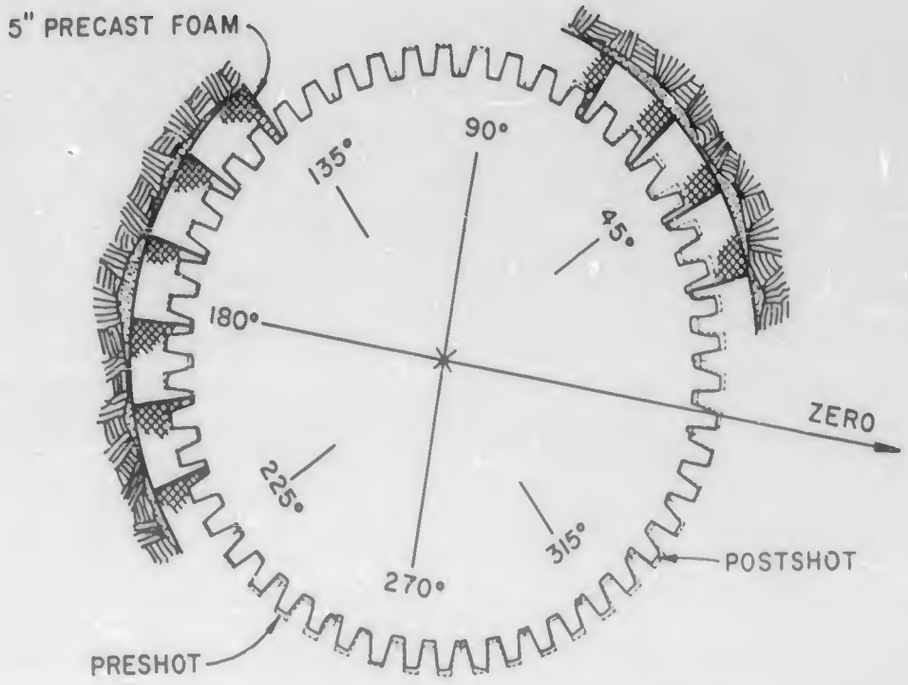

Figure 3.36 C4b, typical liner deformations at midspan between wide-flange rings.

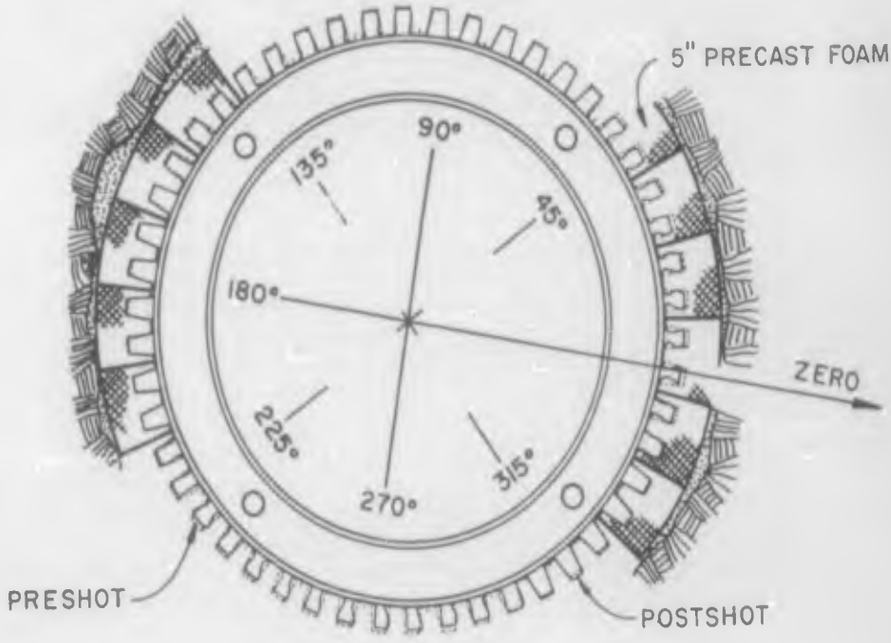

Figure 3.37 C4b, typical liner deformations at wide-flange rings.

Figure 3.38 Test Section C7a (pre-shot) (DASA - NOU 083-06 NTS-62)

Figure 3.39 Test Section C7a (postshot) (DASA - NOU 229-06 NTS-62).

Figure 3.40 Test Sections C1a and C1b (pre-shot) (DASA - NOU 038-05 NTS-62).

Figure 3.41 C1a from C7a (postshot) (DASA - NOU 229-05 NTS-62).

Figure 3.42 Test Section C6a (pre-shot). (DASA - NOU 085-08 NTS-62).

Figure 3.43 Test Section C6a and transition zone, C Drift right (postshot). Note approximate rock breakage bounded by dotted lines (DASA - NOU 206-04 NTS-62).

Figure 3.44 Interior C3d (postshot) (DASA - NOU 228-09 NTS-62).

Figure 3.45 West end C3d (postshot). Note broken tongue-and-groove boards (DASA - NOU 228-12 NTS-62).

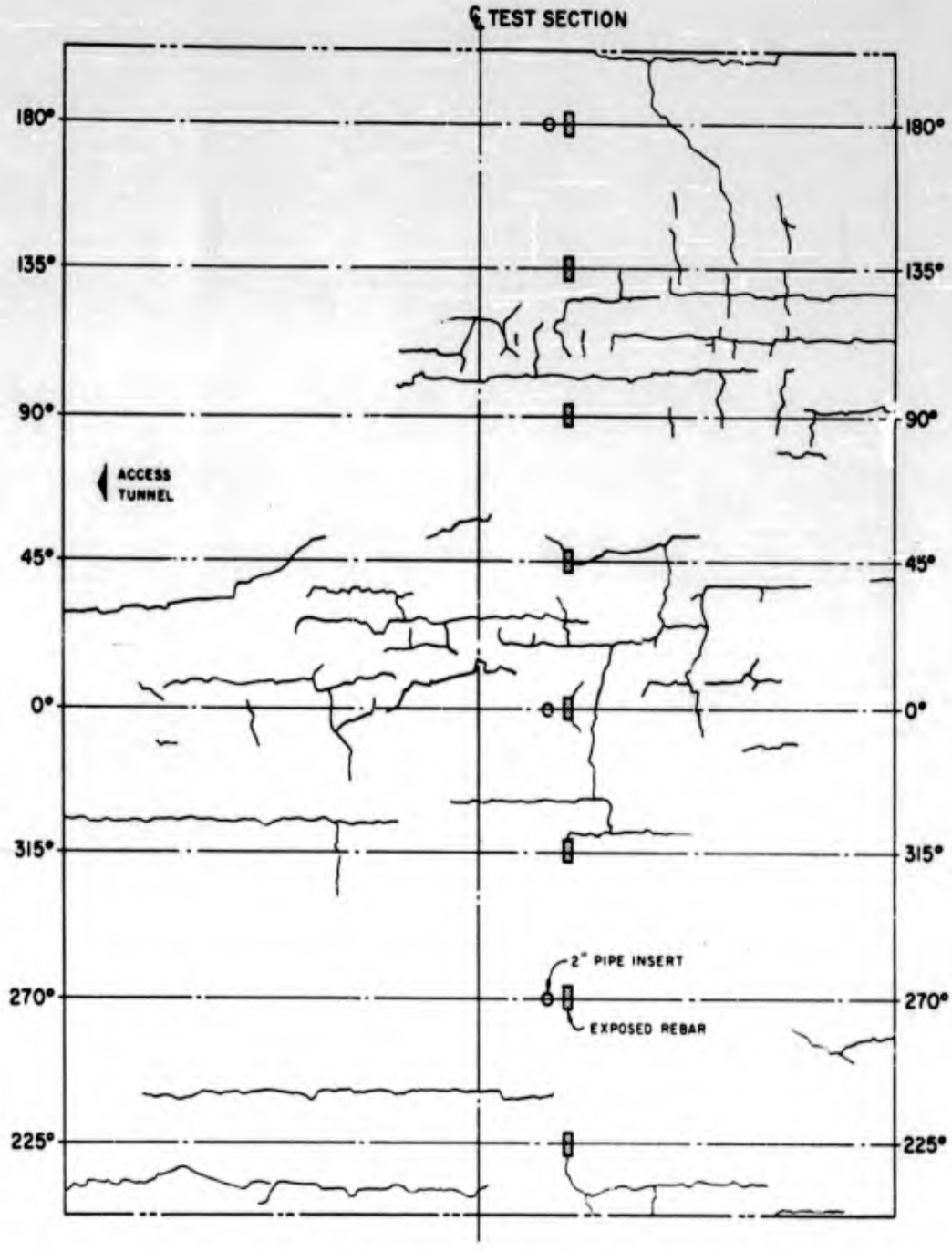

Figure 3.46 C3d, inside surface crack patterns.

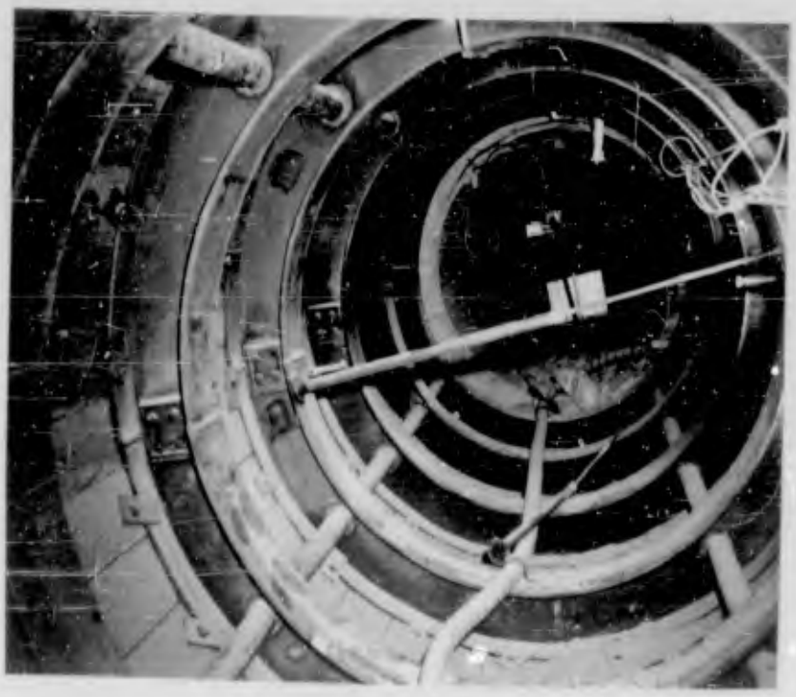

Figure 3.47 Test Section C4c (postshot) (DASA - NOU 228-08 NTS-62).

Figure 3.48 Test Section C3a (postshot) (DASA - NOU 228-06 NTS-62).

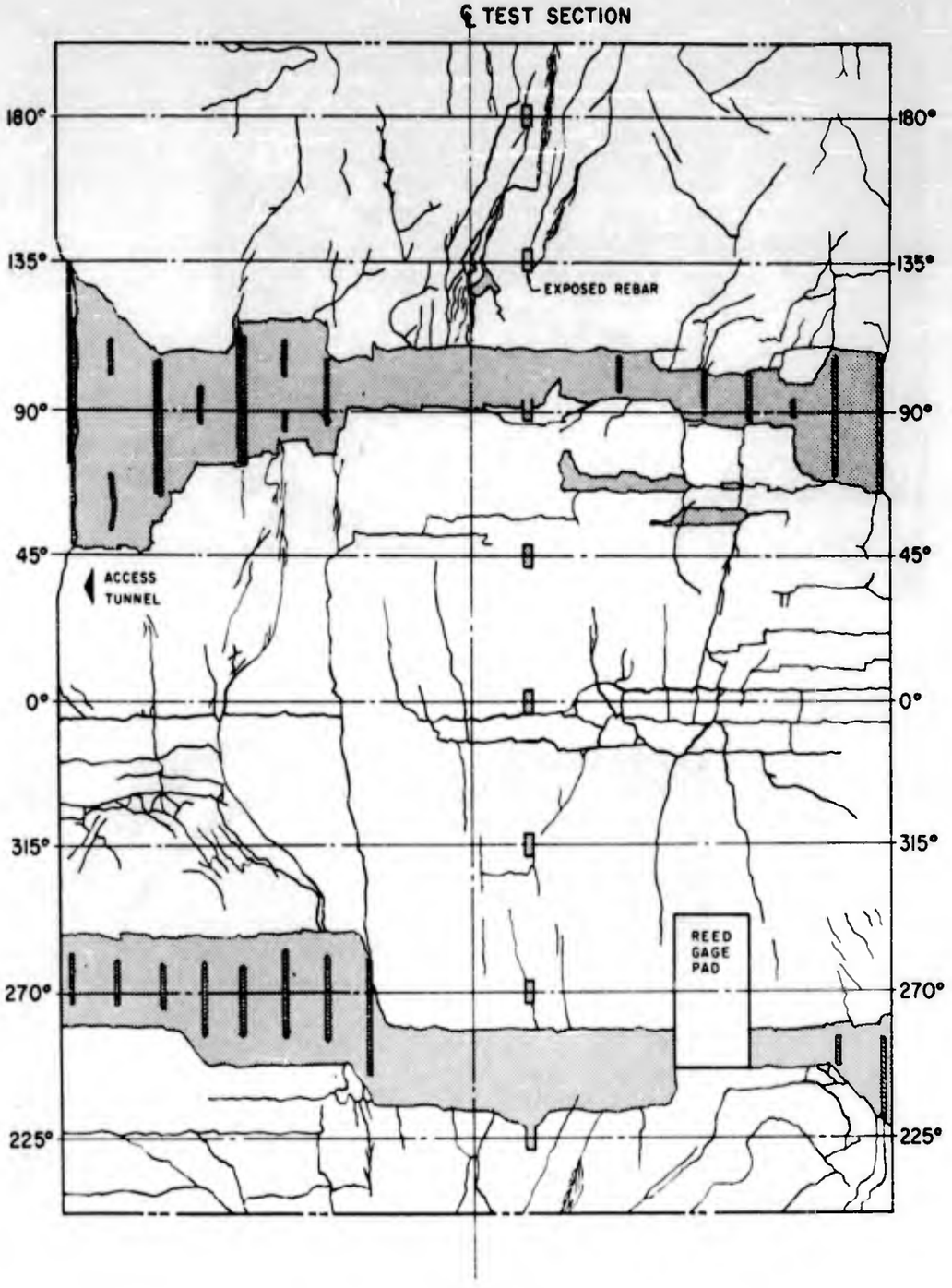

Figure 3.49 C3a, inside surface crack patterns.

Figure 3.50 Test Section C6c (postshot) (DASA - NOU 228-03 NTS-62).

Figure 3.51 Test Sections C2a and C2b (pre-shot) (DASA - NOU 074-02 NTS-62).

Figure 3.52 Test Sections C2a and C2b (postshot). Dotted line in foreground represents approximate surface of broken rock before clean-up (DASA - NOU 316-04 NTS-62)

Figure 3.53 Close-up view, Test Section C2b (postshot). Dotted line represents approximate pre-shot outline (DASA - NOU 316-06 NTS-62).

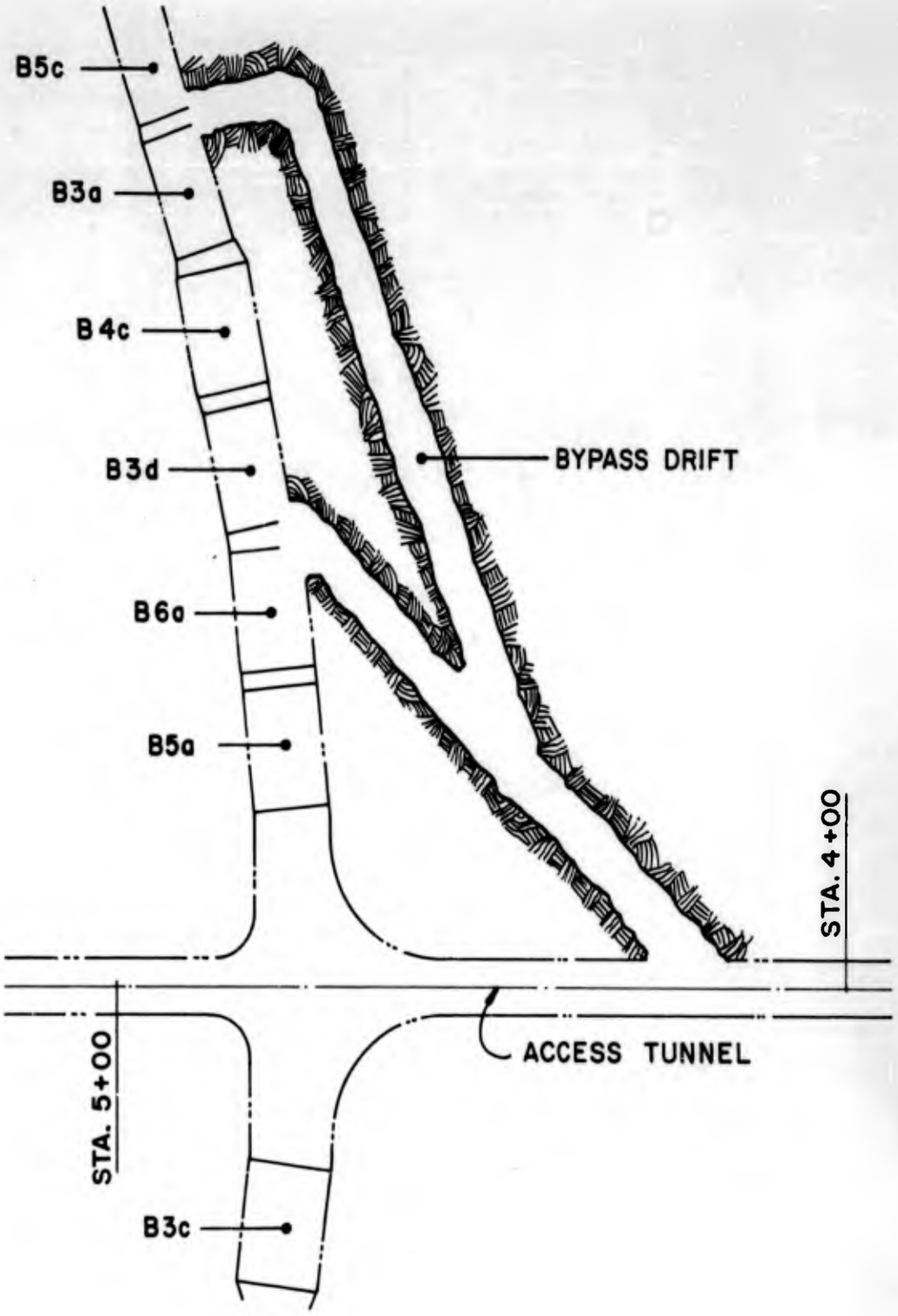

Figure 3.54 Re-entry bypass drift (B Drift right).

Figure 3.55 Test Section B3c (pre-shot) (DASA - NOU 085-03 NTS-62).

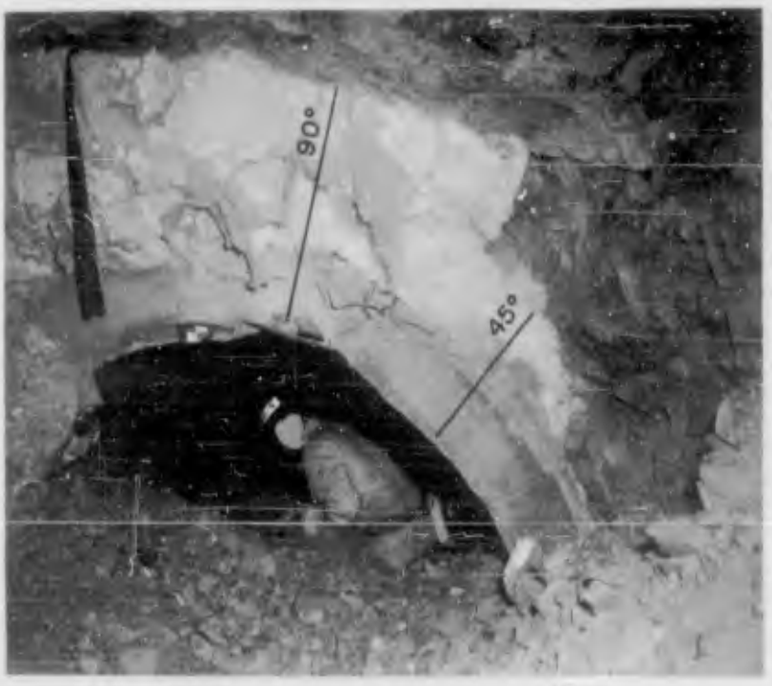

Figure 3.56 Test Section B3c (postshot) (DASA - NOU 238-12 NTS-62).

Figure 3.57 Interior B3c (postshot). (DASA - NOU 237-09 NTS-62)

Figure 3.58 West end B3c (postshot). Note thickness of polyurethane foam at 20°, as indicated by pencil (DASA - NOU 238-11 NTS-62).

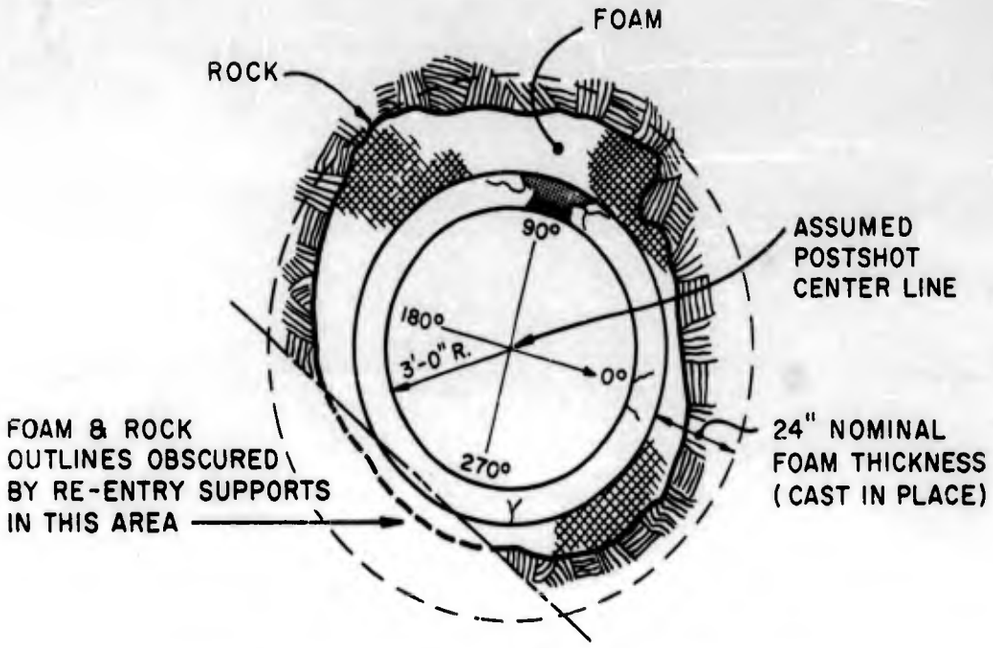

EAST END, VIEWED FROM ACCESS TUNNEL

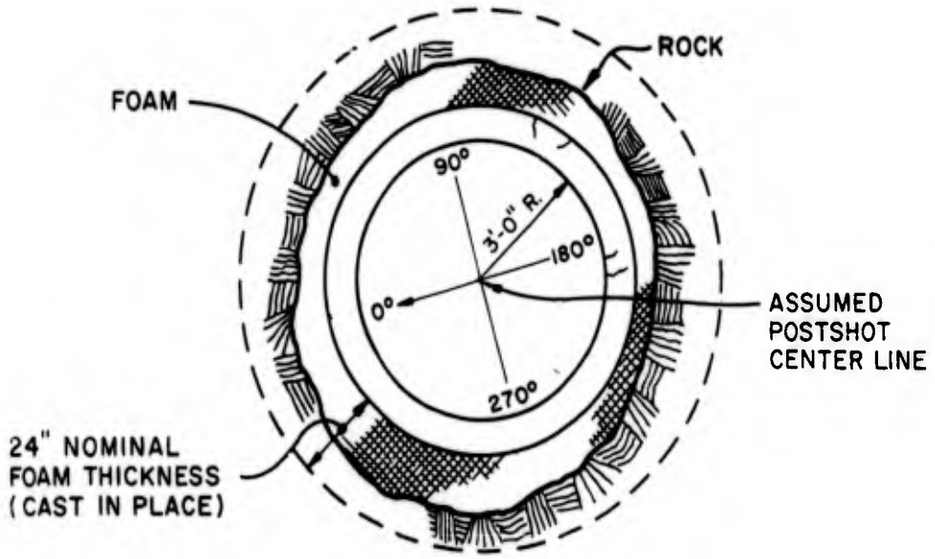

WEST END, VIEW TOWARD ACCESS TUNNEL

Figure 3.59 B3c, foam outline at ends of test section.

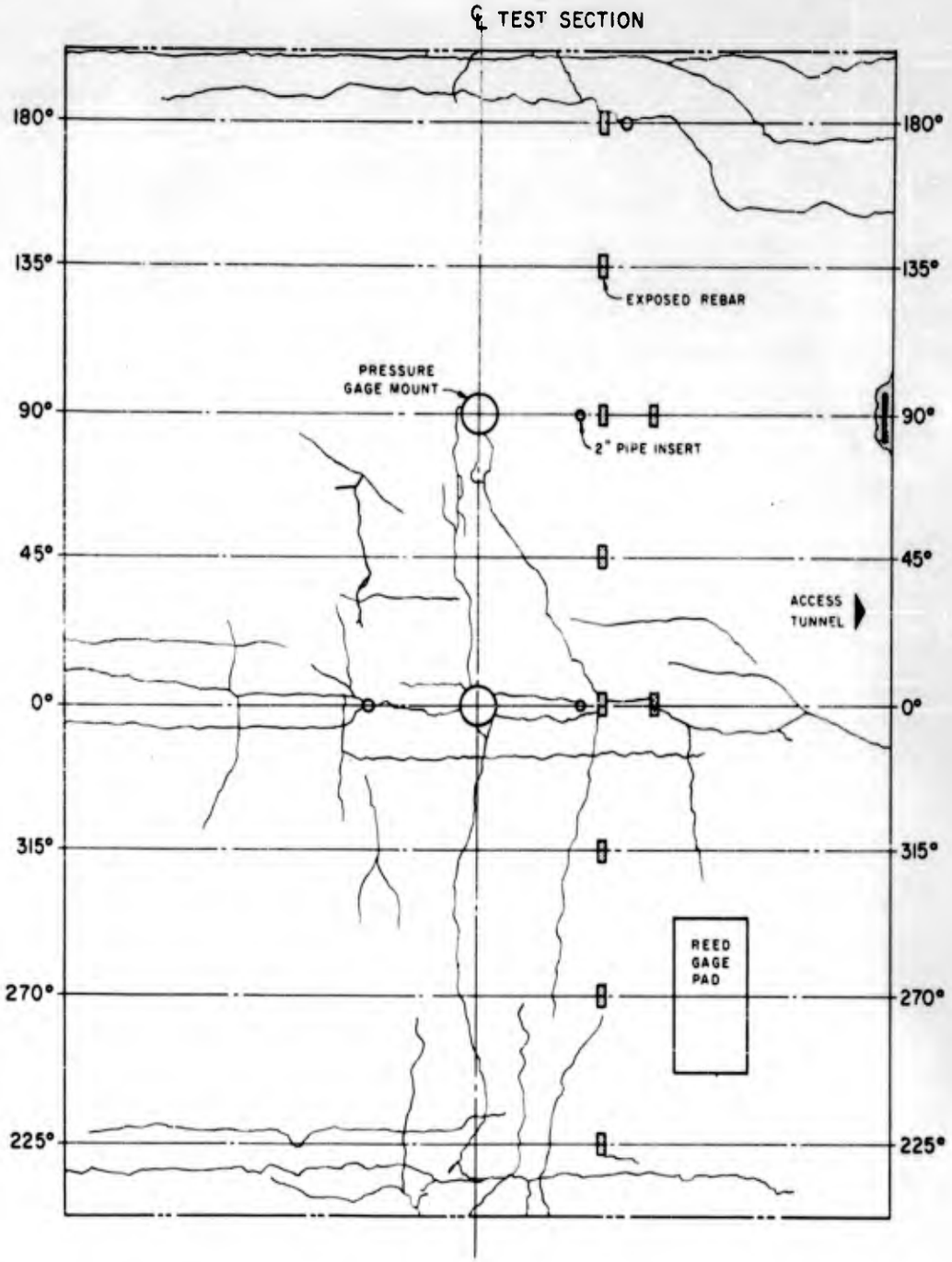

Figure 3.60 B3c, inside surface crack patterns.

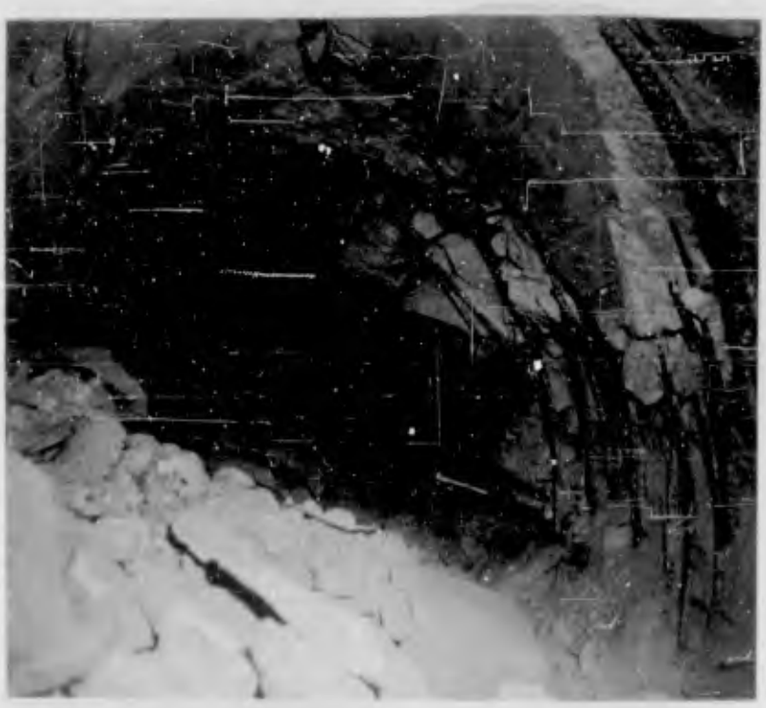

Figure 3.61 Test Section B3b (postshot) (DASA - NOU 237-11 NTS-62).

Figure 3.62 Close-up, west half B3b at 45° (postshot). Note exposed polyurethane foam behind reinforcing bars (DASA - NOU 237-12 NTS-62)

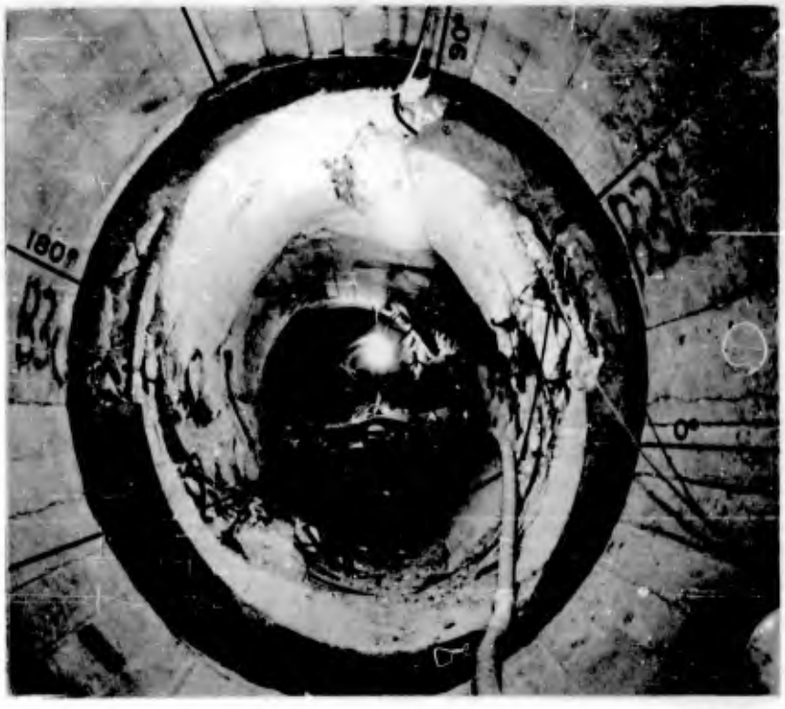

Figure 3.63 Overall view B3b after clean-up (post shot) (DASA - NOU 390-07 NTS-62).

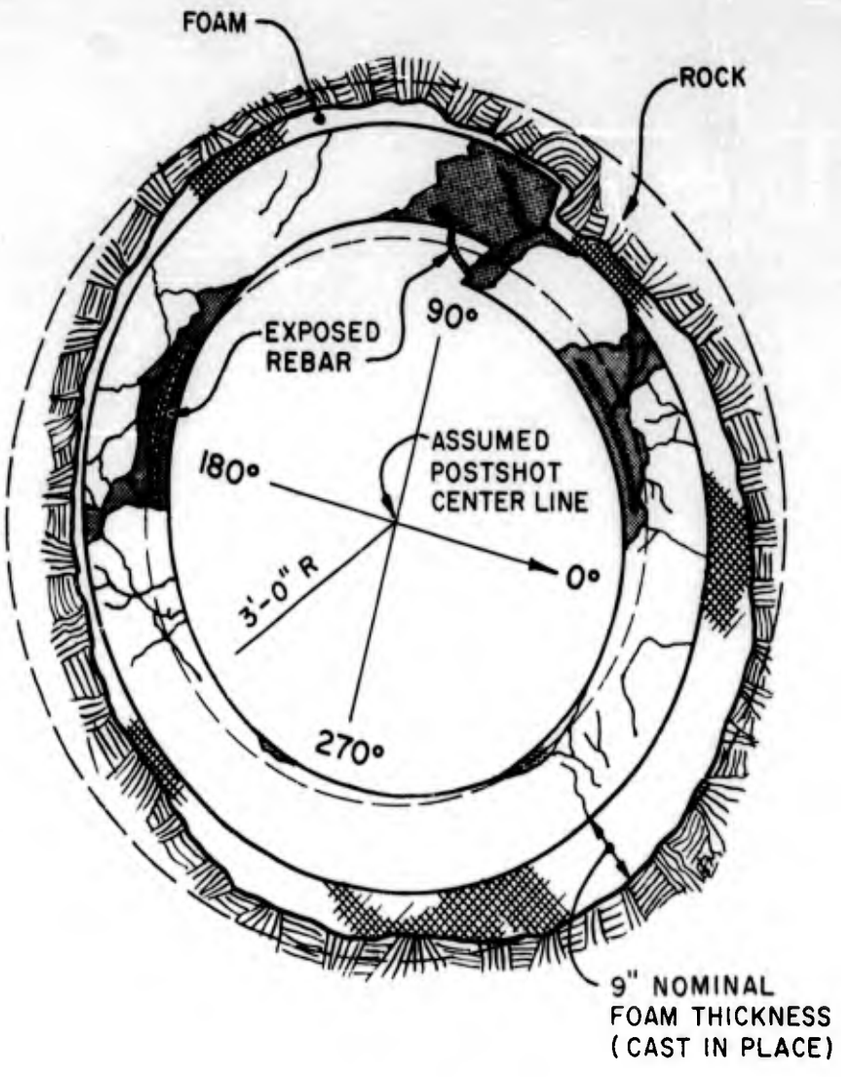

EAST END, VIEWED FROM ACCESS TUNNEL

Figure 3.64 B3b, foam outline at east end of test section.

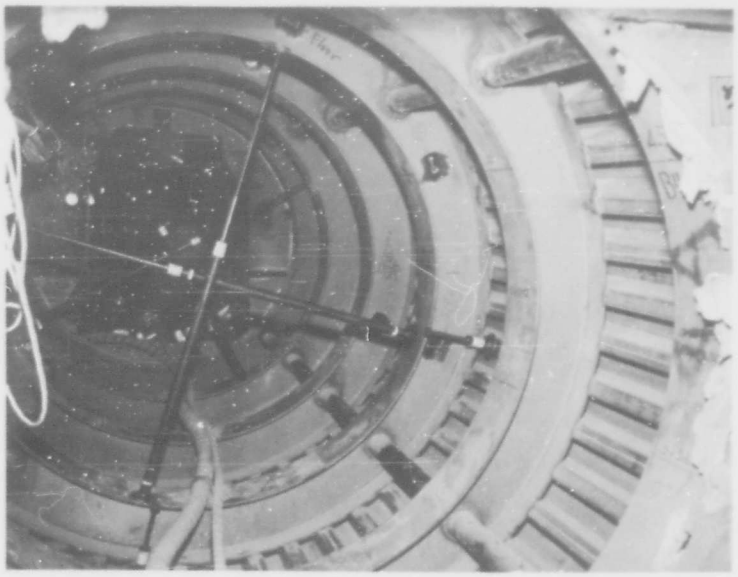

Figure 3.65 Test Section B4a (pre-shot) (DASA - NOU 072-06 NTS-62).

Figure 3.66 Test Section B4a (postshot) (DASA - NOU 323-07 NTS-62).

Figure 3.67 Close-up view B4a at 0° (postshot). Note buckling of wide flange ring (DASA - NOU 323-06 NTS-62).

Figure 3.68 East end B4a at 90° (postshot). Note compressed cinders and crushed steel decking (DASA - NOU 316-10 NTS-62).

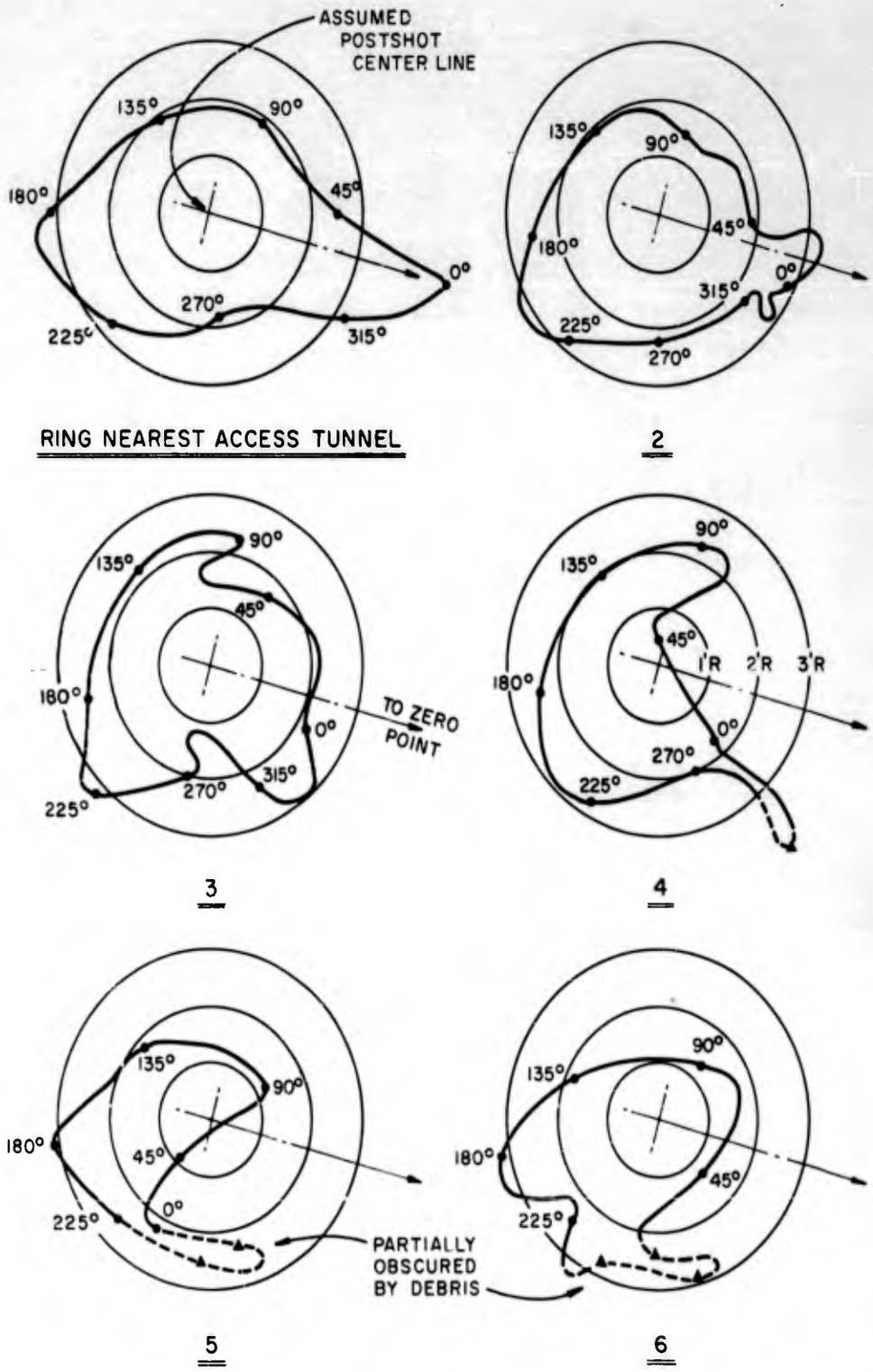

Figure 3.69 B4a, distorted shape of wide-flange rings (inside flanges only).

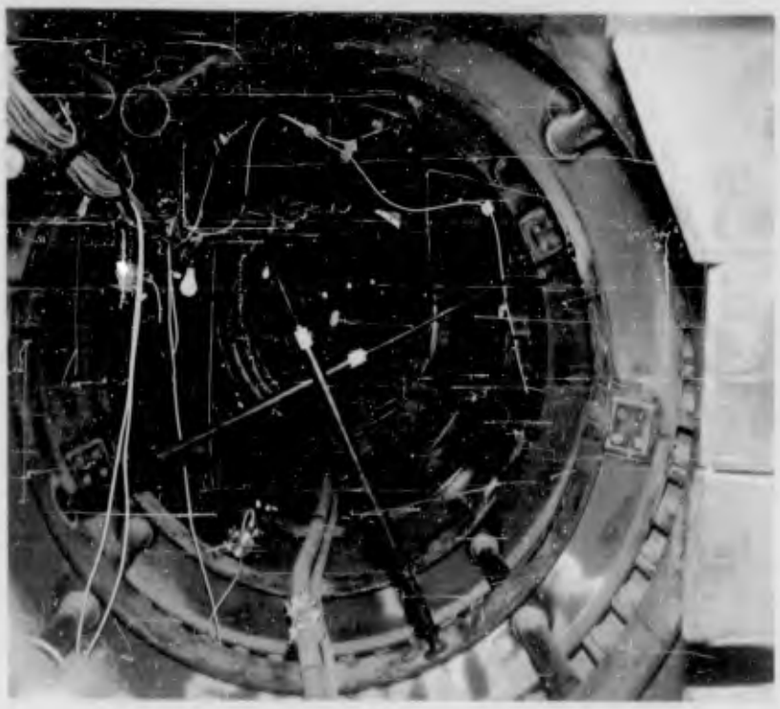

Figure 3.70 Test Section B4b (pre-shot) (DASA - NOU 072-05 NTS-62).

Figure 3.71 Test Section B4b (postshot) (DASA - NOU 390-06 NTS-62).

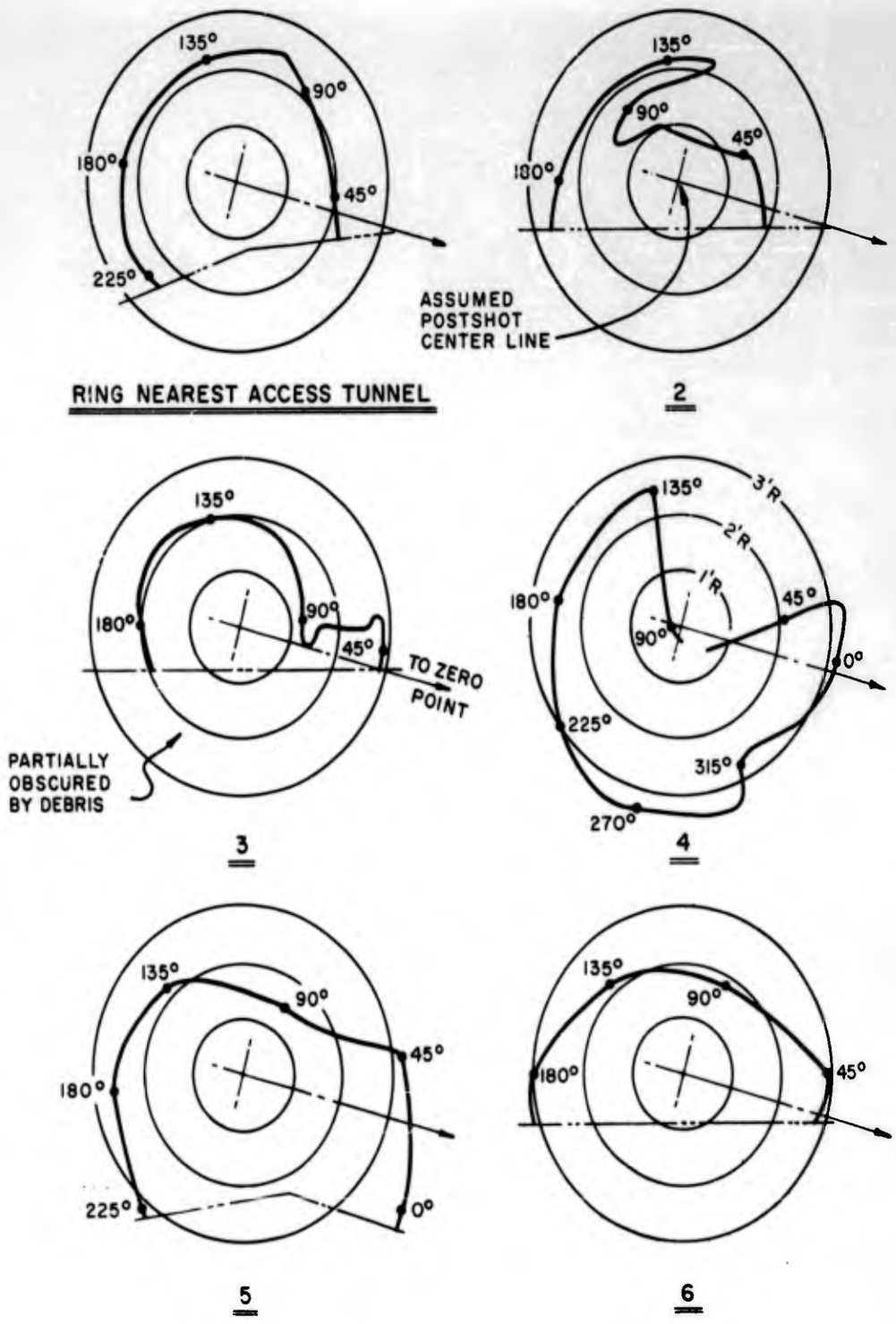

Figure 3.72 B4b, distorted shape of wide-flange rings (inside flanges only).

Figure 3.73 Test Section B5b (pre-shot). Test Section B6b can be seen in background (DASA - NOU 072-03 NTS-62).

Figure 3.74 Test Section B5b (postshot) (DASA - NOU 332-06 NTS-62).

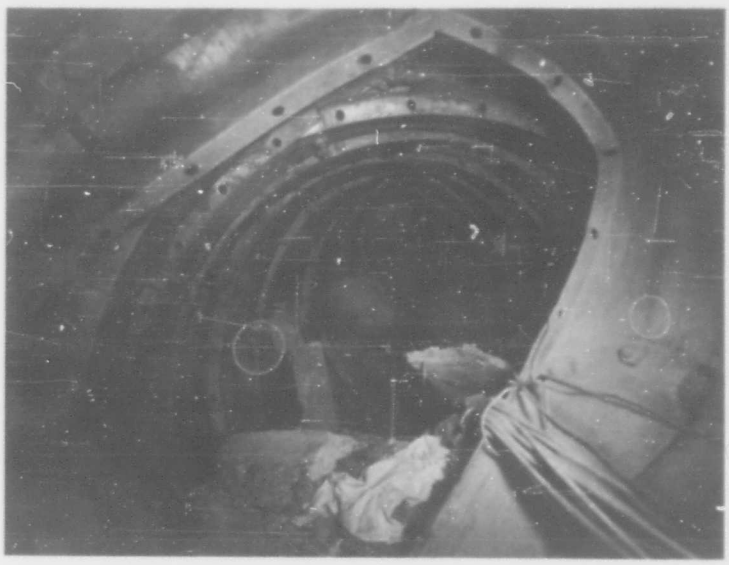

Figure 3.75 B5b from B6b (postshot). Note overlapped tunnel liner plates at the left (DASA - NOU 332-05 NTS-62).

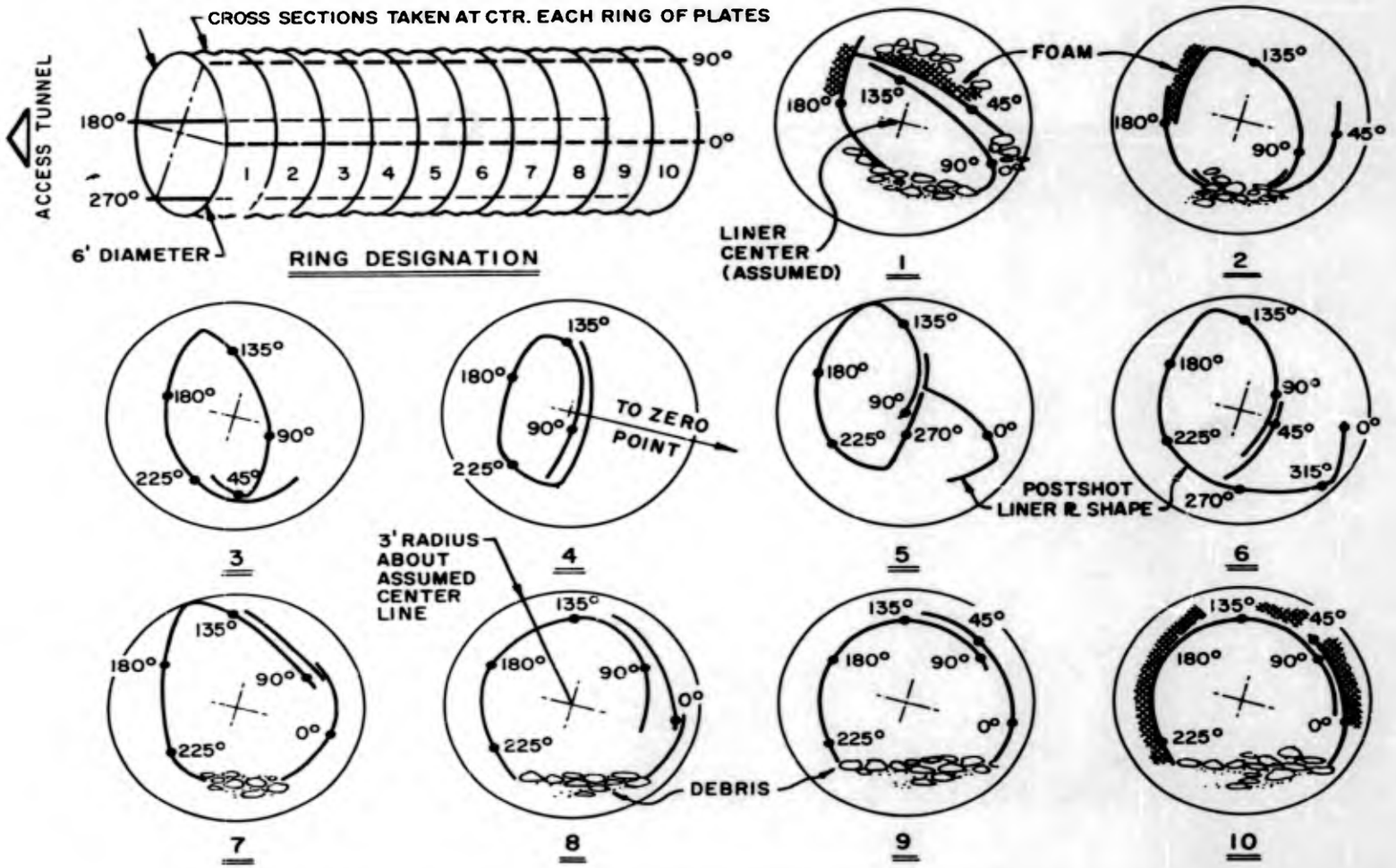

Figure 3.76 B5b, postshot condition of tunnel liner plates.

Figure 3.77 Test Section B6b (postshot) (DASA - NOU 332-04 NTS-62).

Figure 3.78 Close-up of interior of B6b during clean-up (postshot). Note failure of bolt holes in tunnel liner plates (DASA - NOU 482-02 NTS-62).

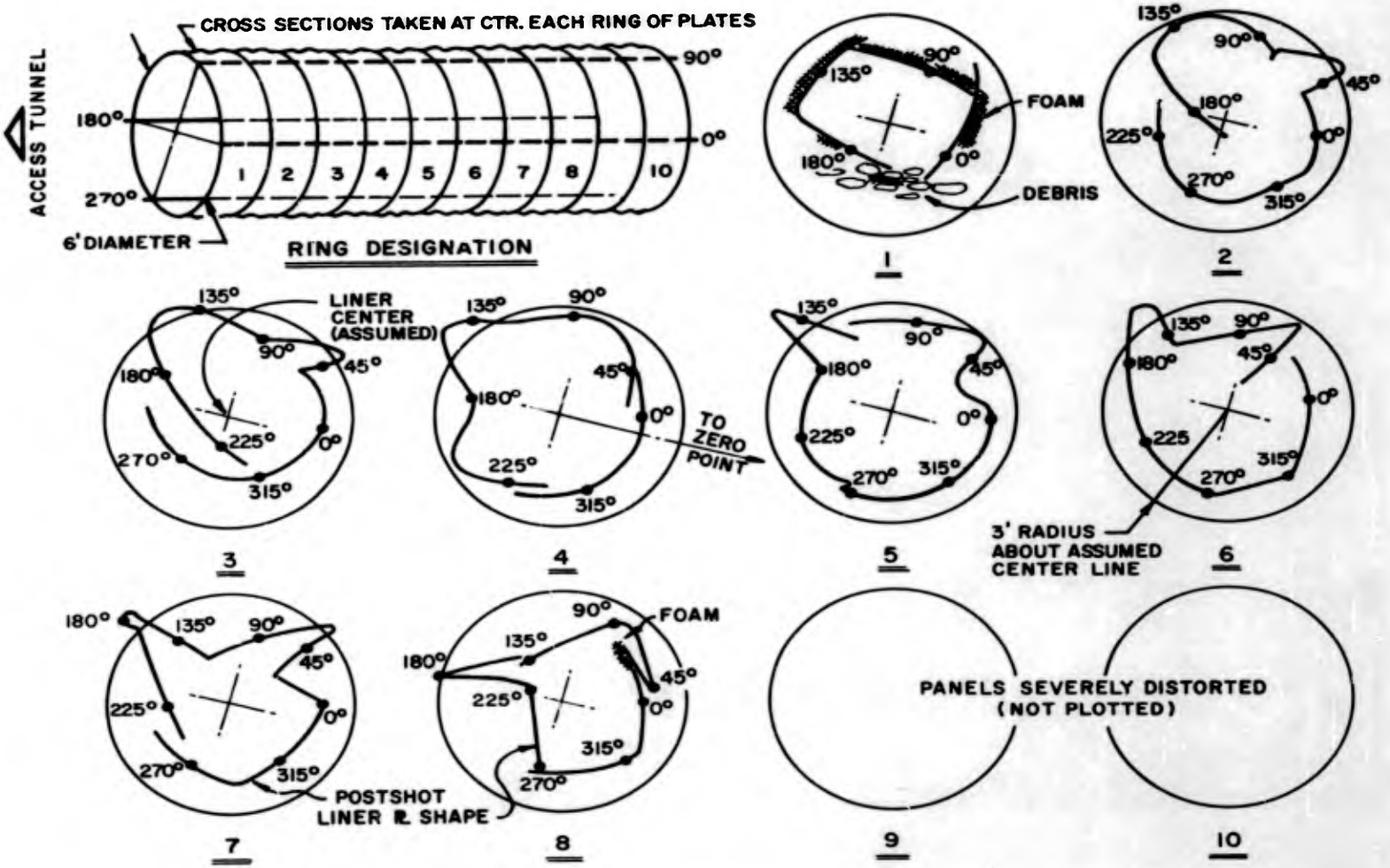

Figure 3.79 B6b, postshot condition of tunnel liner plates.

Figure 3.80 B7a as viewed from B6b (postshot) (DASA - NOU 482-01 NTS-62).

Figure 3.81 Interior view B5a (pre-shot) (DASA - NOU 073-11 NTS-62).

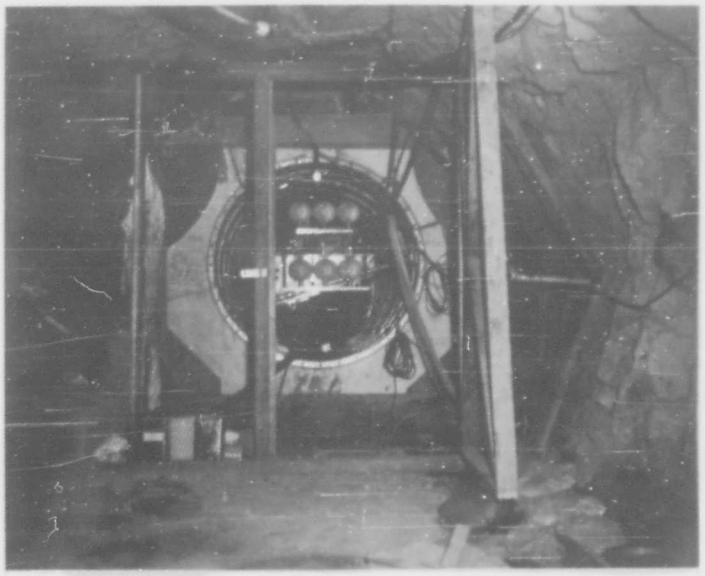

Figure 3.82 B5a from access tunnel (pre-shot). Note stereo camera station (DASA - NOU 085-02 NTS-62).

Figure 3.83 Test Section B5a (postshot). Damaged stereo camera station has been removed (DASA - NOU 316-07 NTS-62).

Figure 3.84 East end of B6a as viewed from B3d (postshot). Note collapsed tunnel liner plates (DASA - NOU 324-05 NTS-62).

Figure 3.85 Interior view B3d (pre-shot) (DASA - NOU 073-08 NTS-62).

Figure 3.86 West end B3d as viewed from bypass drift (postshot). Note floor heave (DASA - NOU 339-08 NTS-62).

Figure 3.87 Close-up view B3d (postshot). Note buckled reinforcing bars at 90° (DASA - NOU 324-03 NTS-62).

Figure 3.88 B3d as viewed from B4c (postshot) (DASA - NOU 365-01 NTS-62)

Figure 3.89 West end B3d at 90° (postshot). Note compression of cinders (DASA - NOU 324-04 NTS-62).

Figure 3.90 Test Section B4c (pre-shot) (DASA - NOU 073-06 NTS-62).

Figure 3.91 Test Section B4c (postshot) (DASA - NOU 365-03 NTS-62).

Figure 3.92 Interior B4c, view to west (postshot) (DASA - NOU 365-02 NTS-62).

Figure 3.93 Close-up rock break through B4c (postshot). Note broken wood lagging and compressed polyurethane foam (DASA - NOU 365-06 NTS-62).

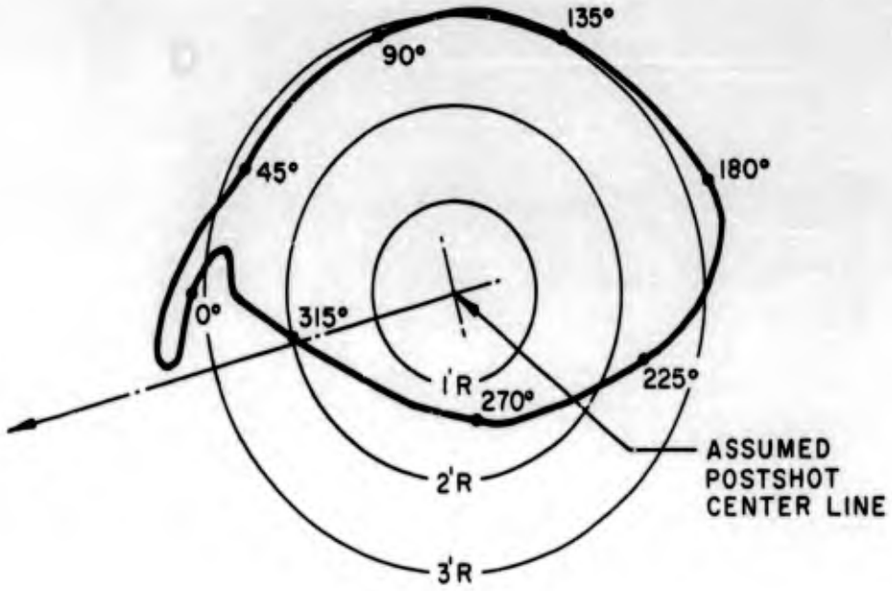

THIRD RING FROM ACCESS TUNNEL END

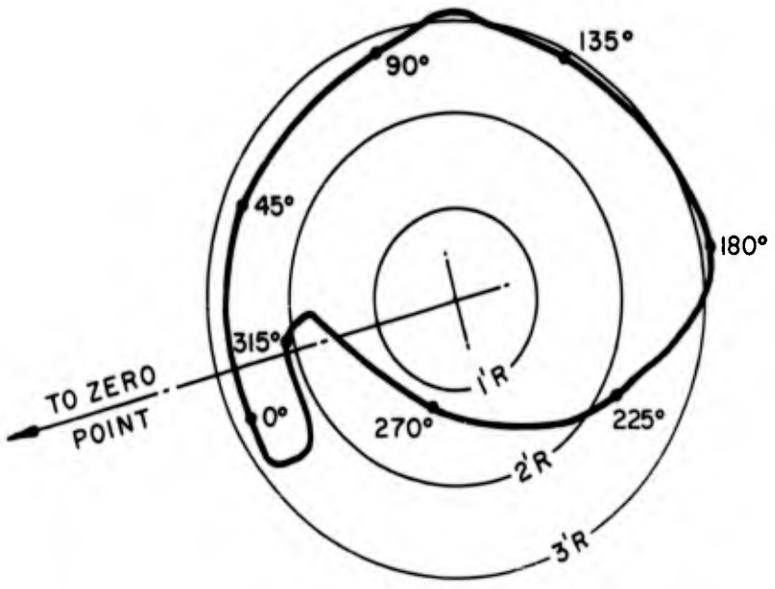

FOURTH RING FROM ACCESS TUNNEL END

Figure 3.94 B4c, distorted shape of wide-flange rings (inside flanges only).

Figure 3.95 Test Section B3a (pre-shot). B5c in background (DASA - NOU 073-05 NTS-62).

Figure 3.96 B5c (right) and B3a (left) as encountered by bypass drift (postshot) (DASA - NOU 390-09 NTS-62).

Figure 3.97 East end B3a as viewed from B5c (postshot) (DASA - NOU 390-08 NTS-62)

Figure 3.98 Interior view B5c (postshot) (DASA - NOU 390-03 NTS-62)

Figure 3.99 Interior view A3c (pre-shot), view from east (DASA - NOU 071-10 NTS-62).

Figure 3.100 Test Section A3c (postshot) (DASA - NOU 480-03 NTS-62)

Figure 3.101 Interior view A3c (postshot), view from west. Note large pieces of polyurethane foam (white) (DASA - NOU 480-02 NTS-62).

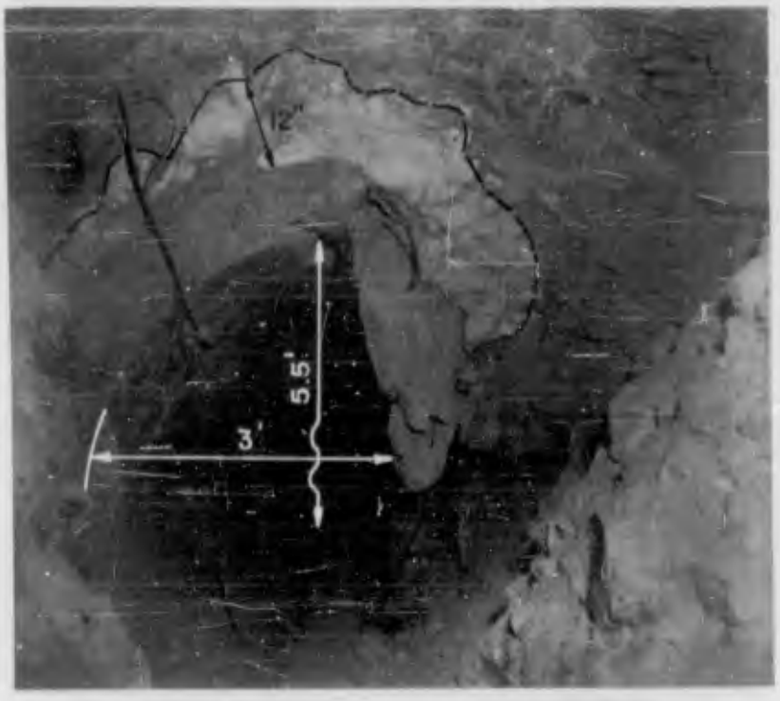

Figure 3.102 East end A3c (postshot). Note polyurethane foam outline and deformation of the concrete liner (DASA - NOU 467-03 NTS-62)

Figure 3.103 East end A3b as viewed from A3c (postshot) (DASA - NOU 482-03 NTS-62).

Figure 3.104 West end A5a (postshot). Note collapsed tunnel liner plates and distortion of polyurethane foam backpacking (DASA - NOU 494-02 NTS-62).

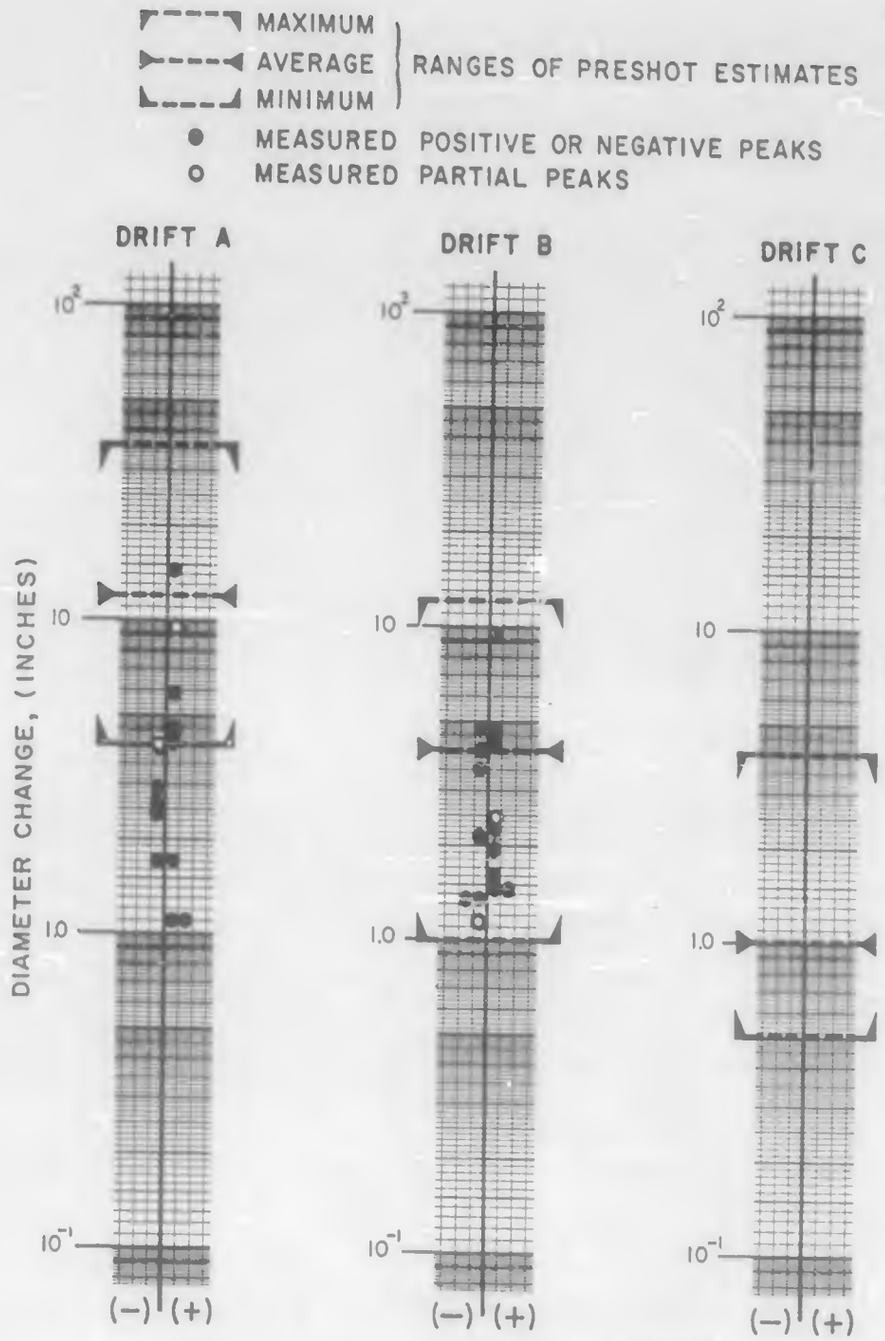

TEST DRIFTS	A	B	C
GAGES INSTALLED	9	12	1
RECORDS RECOVERED	8	11	0

Figure 3.105 Diameter change in lining (electronic).

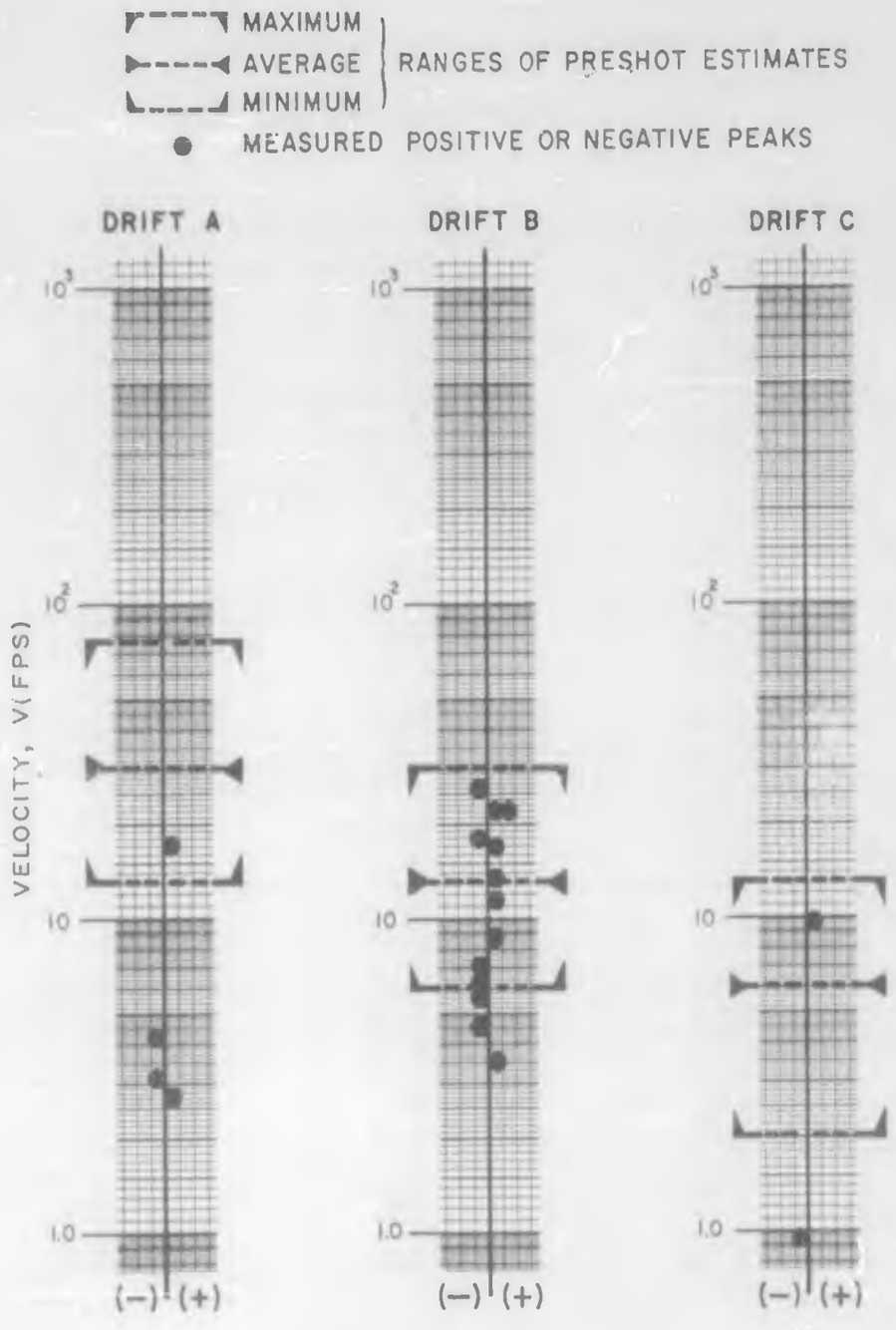

TEST DRIFTS	A	B	C
GAGES INSTALLED	4	8	1
RECORDS RECOVERED	2	7	1

Figure 3.106 Velocity of liner, foam backpacking (electronic).

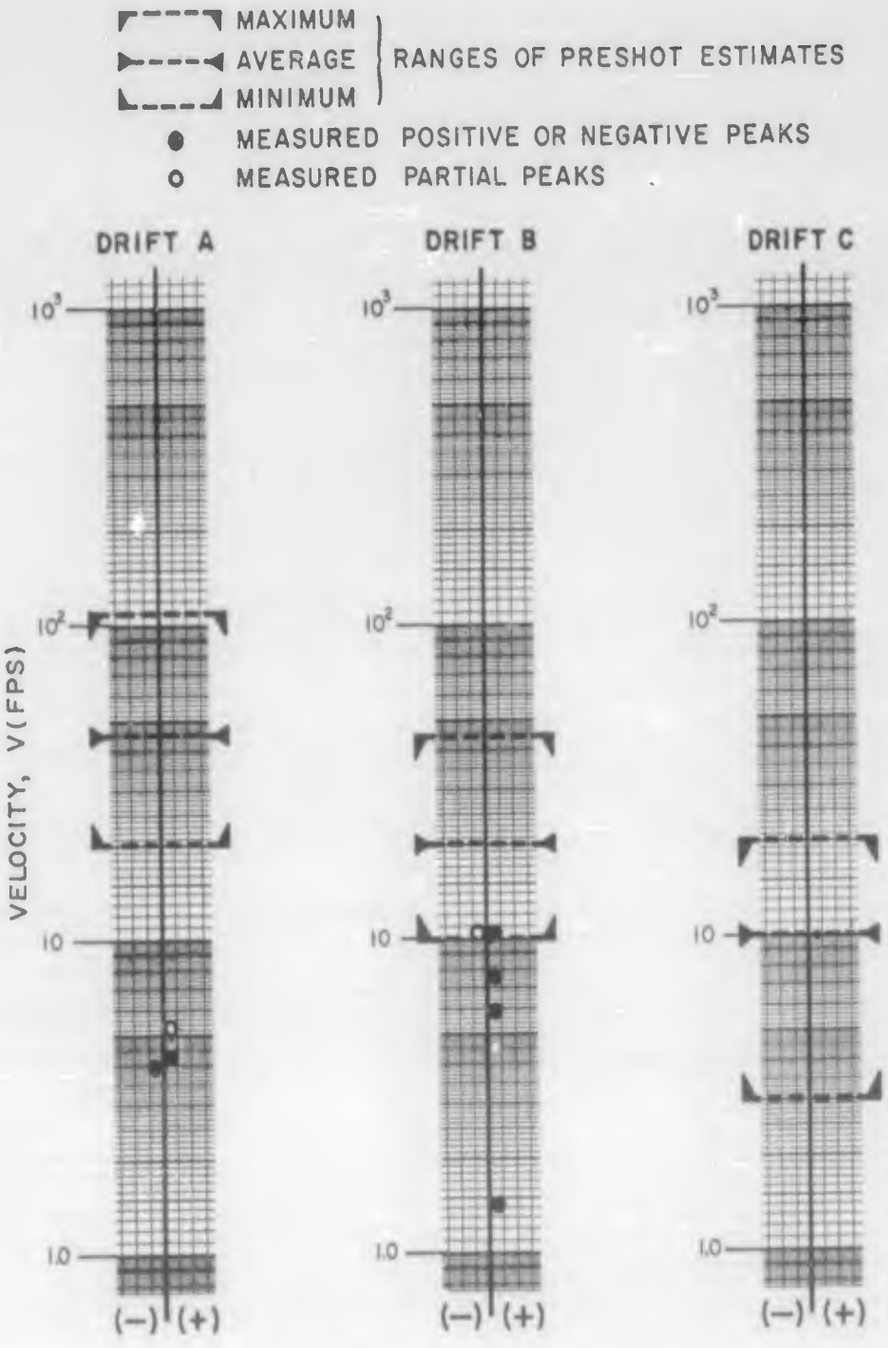

TEST DRIFTS	A	B	C
GAGES INSTALLED	2	4	0
RECORDS RECOVERED	2	4	—

Figure 3.107 Velocity of liner, cinder backpacking (electronic).

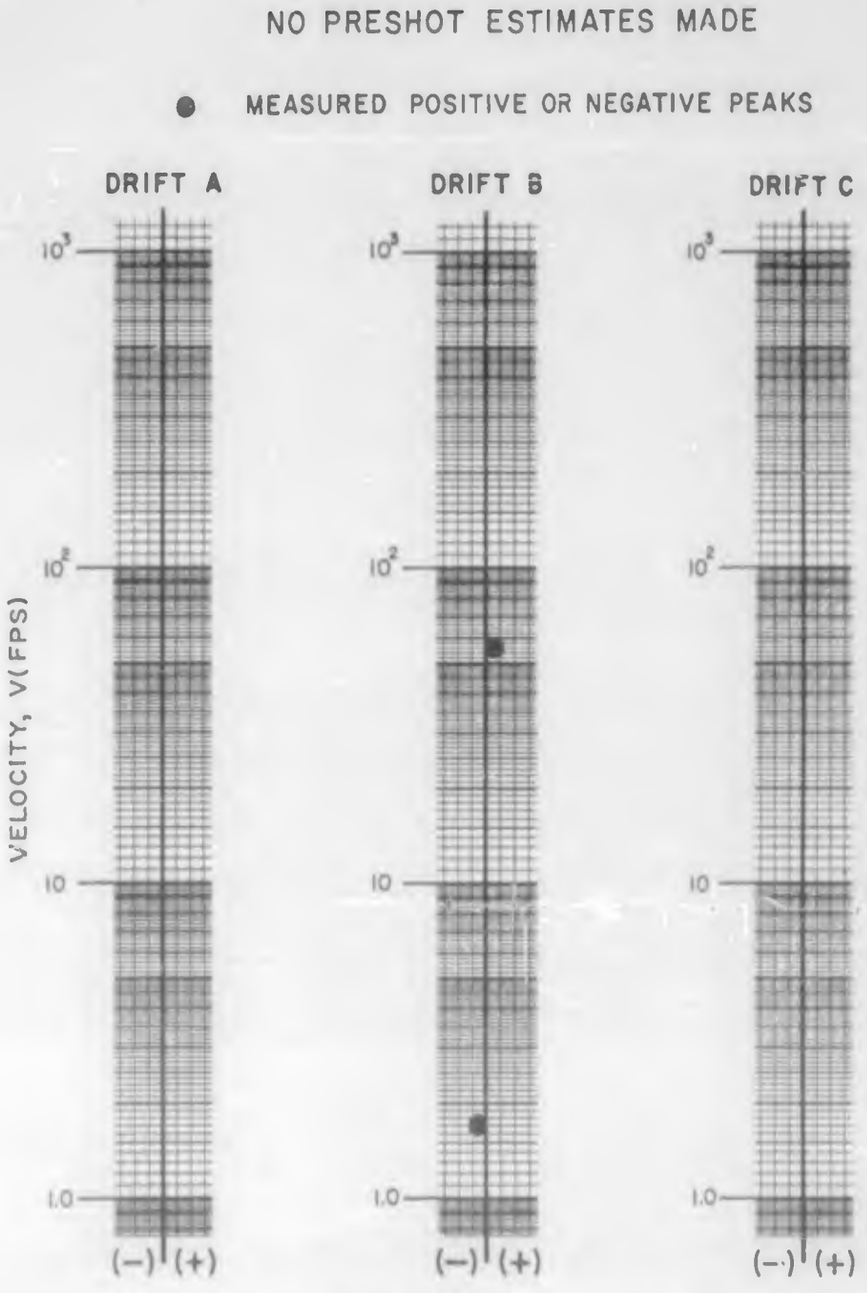

TEST DRIFTS	A	B	C
GAGES INSTALLED	1	1	0
RECORDS RECOVERED	0	1	-

Figure 3.108 Velocity of liner, concrete cast against rock (electronic).

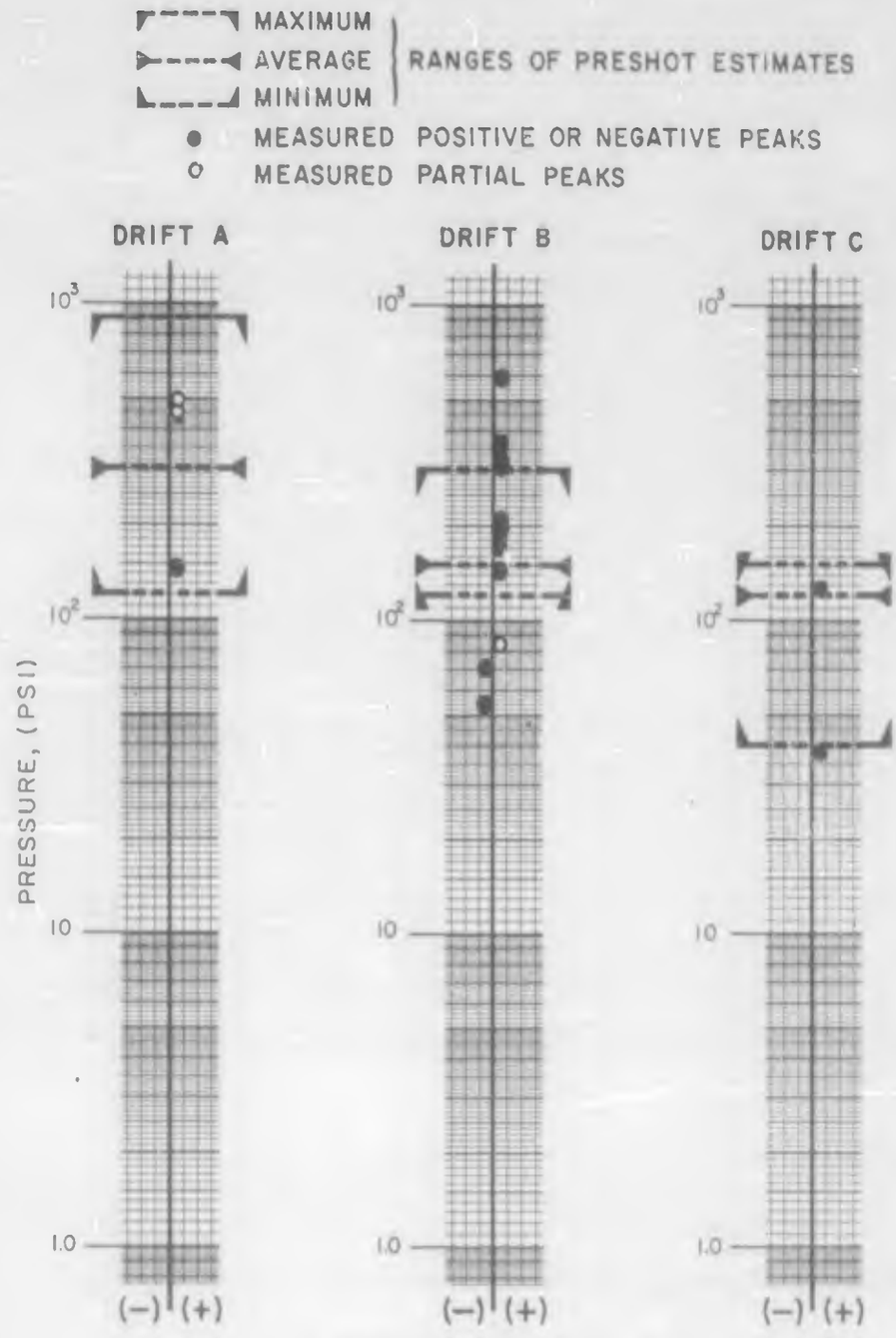

TEST DRIFTS	A	B	C
GAGES INSTALLED	4	11	2
RECORDS RECOVERED	3	9	2

Figure 3.109 Pressure on lining (electronic).

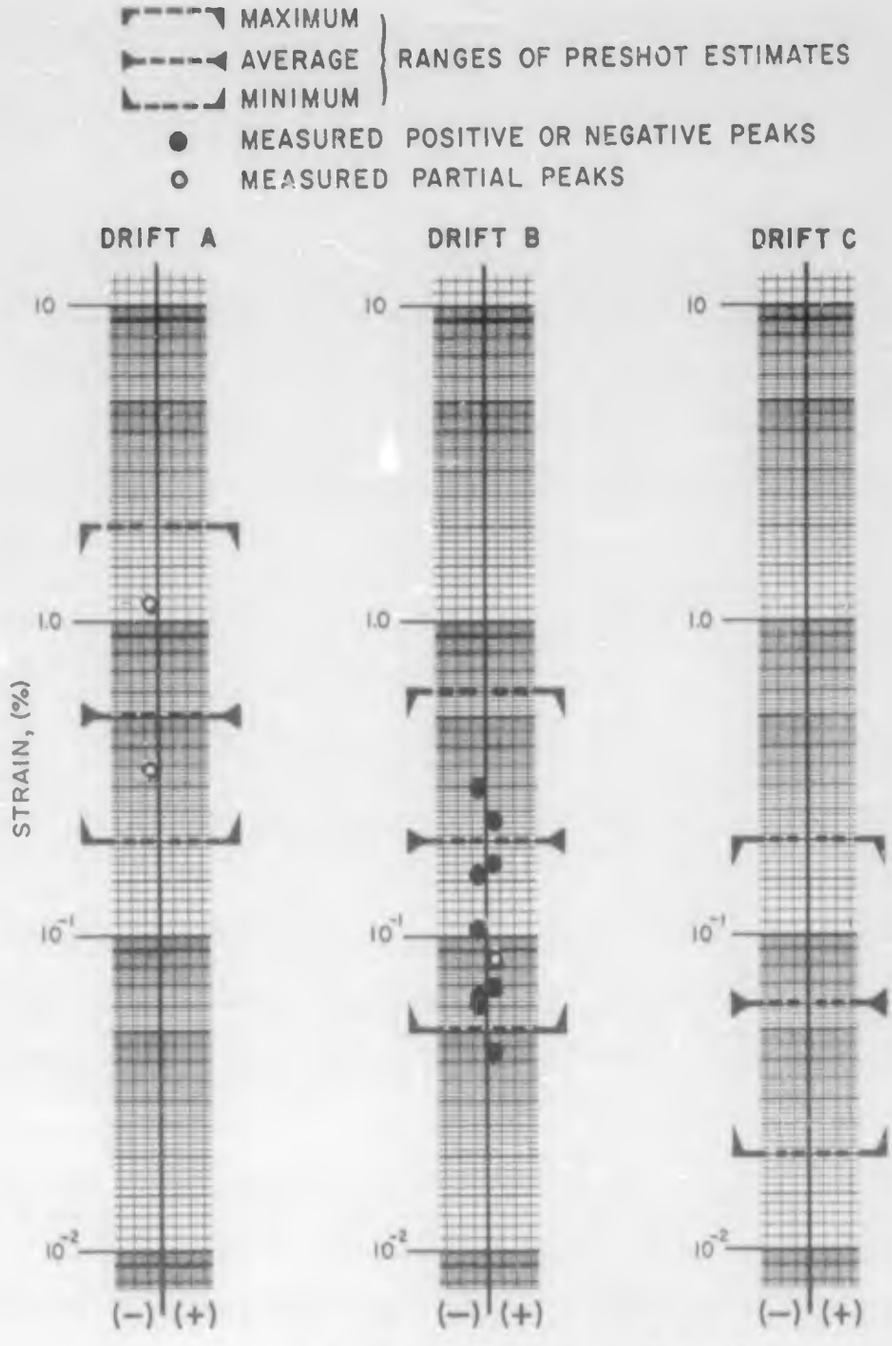

TEST DRIFTS	A	B	C
GAGES INSTALLED	3	13	0
RECORDS RECOVERED	2	7	–

Figure 3.110 Circumferential strain in lining (electronic).

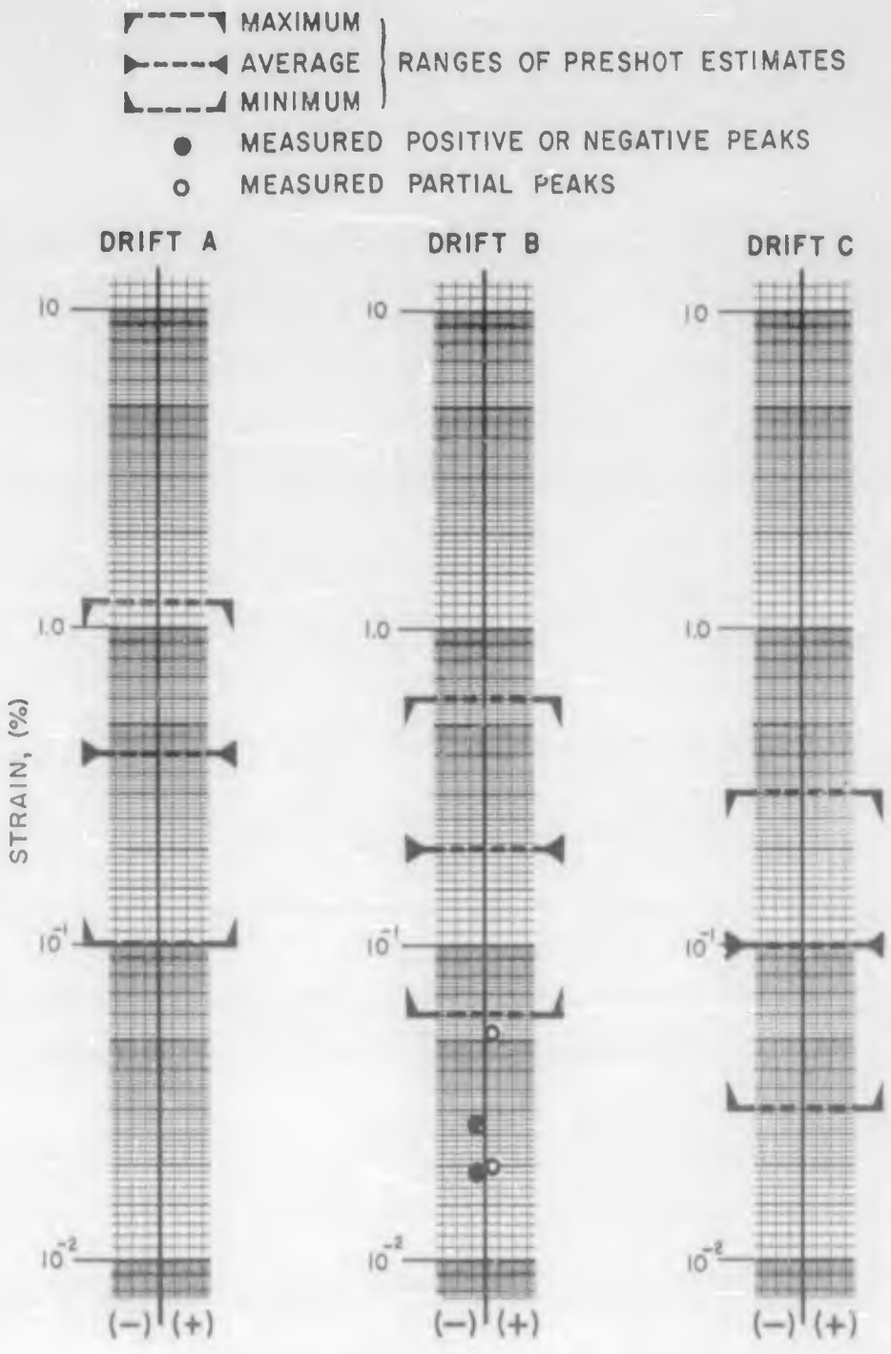

TEST DRIFTS	A	B	C
GAGES INSTALLED	2	18	0
RECORDS RECOVERED	0	3	–

Figure 3.111 Circumferential strain in rock (electronic).

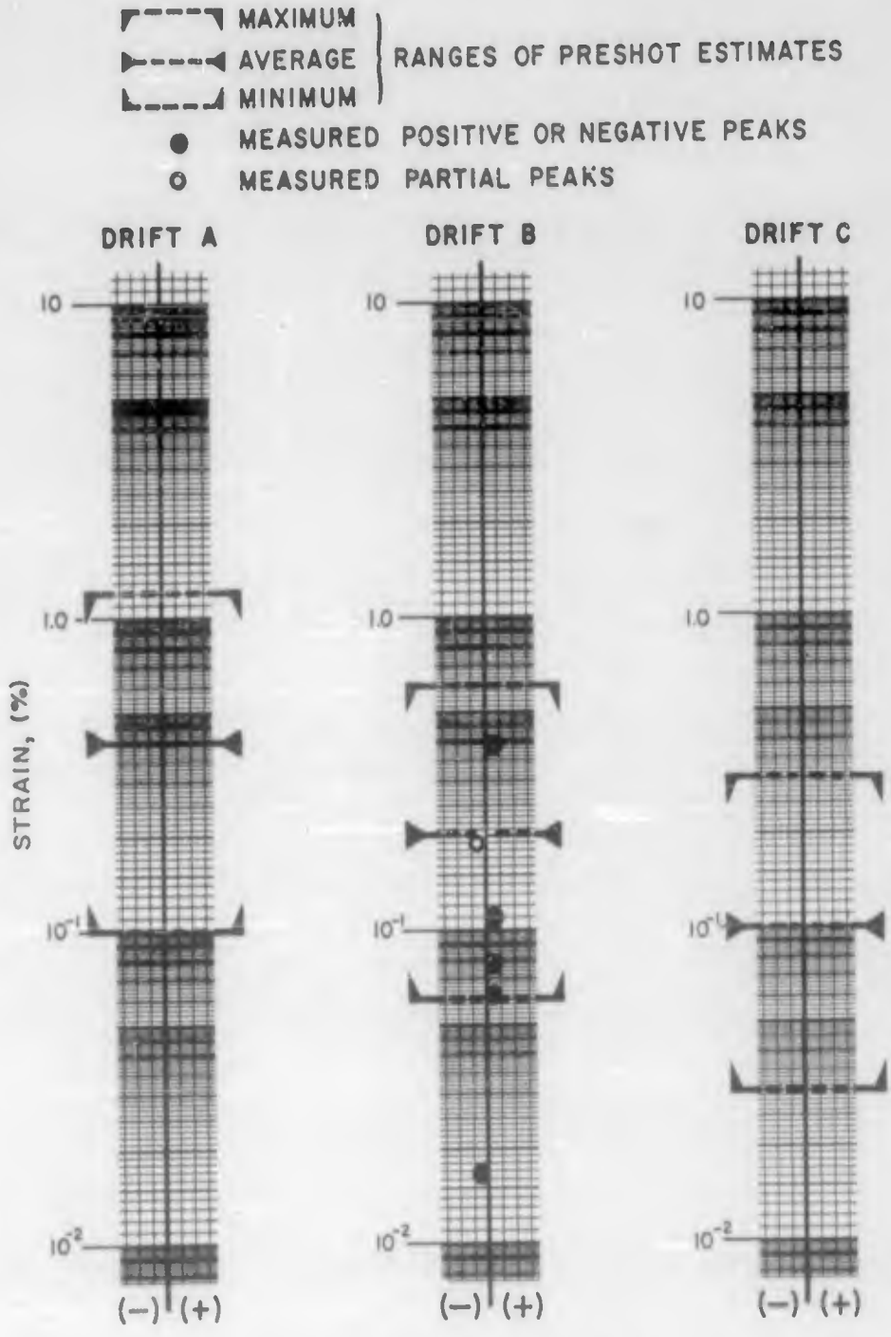

TEST DRIFTS	A	B	C
GAGES INSTALLED	1	7	0
RECORDS RECOVERED	0	4	–

Figure 3.112 Radial strain in rock (electronic).

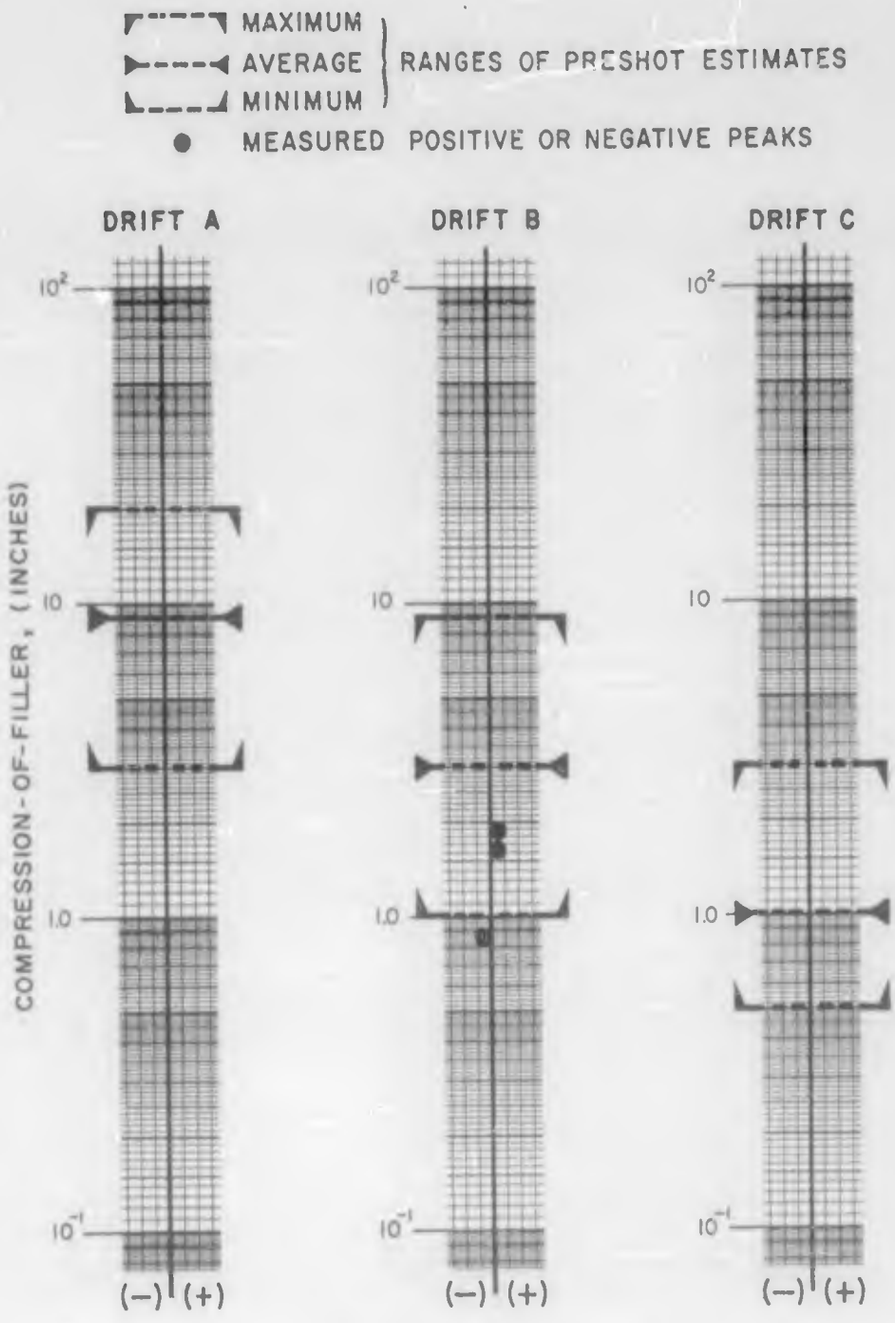

TEST DRIFTS	A	B	C
GAGES INSTALLED	0	2	0
RECORDS RECOVERED	–	2	–

Figure 3.113 Compression of filler, 20" foam (electronic).

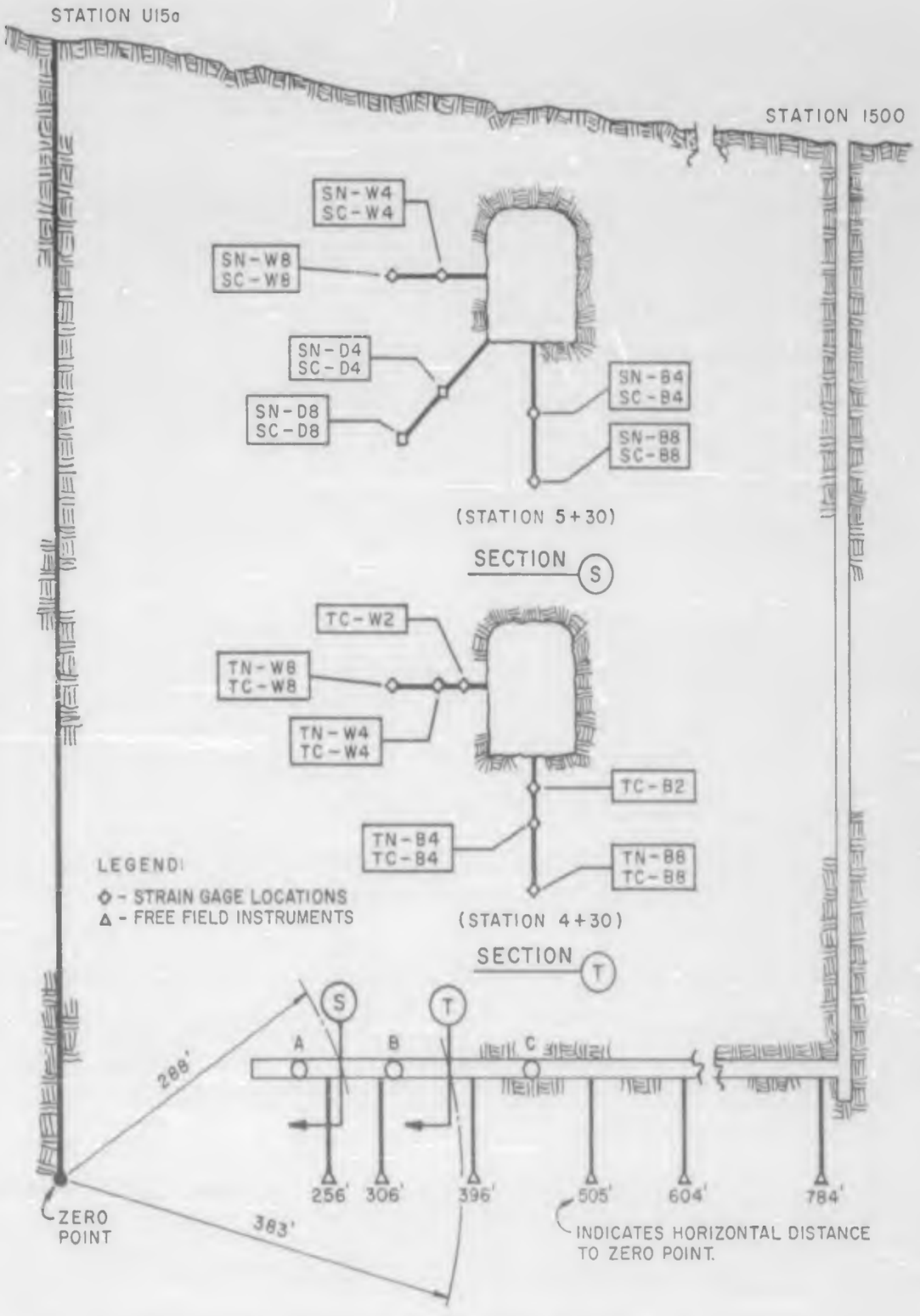

Figure 3.114 Instrumentation plan, Project 3.3, Particle Motion Studies.

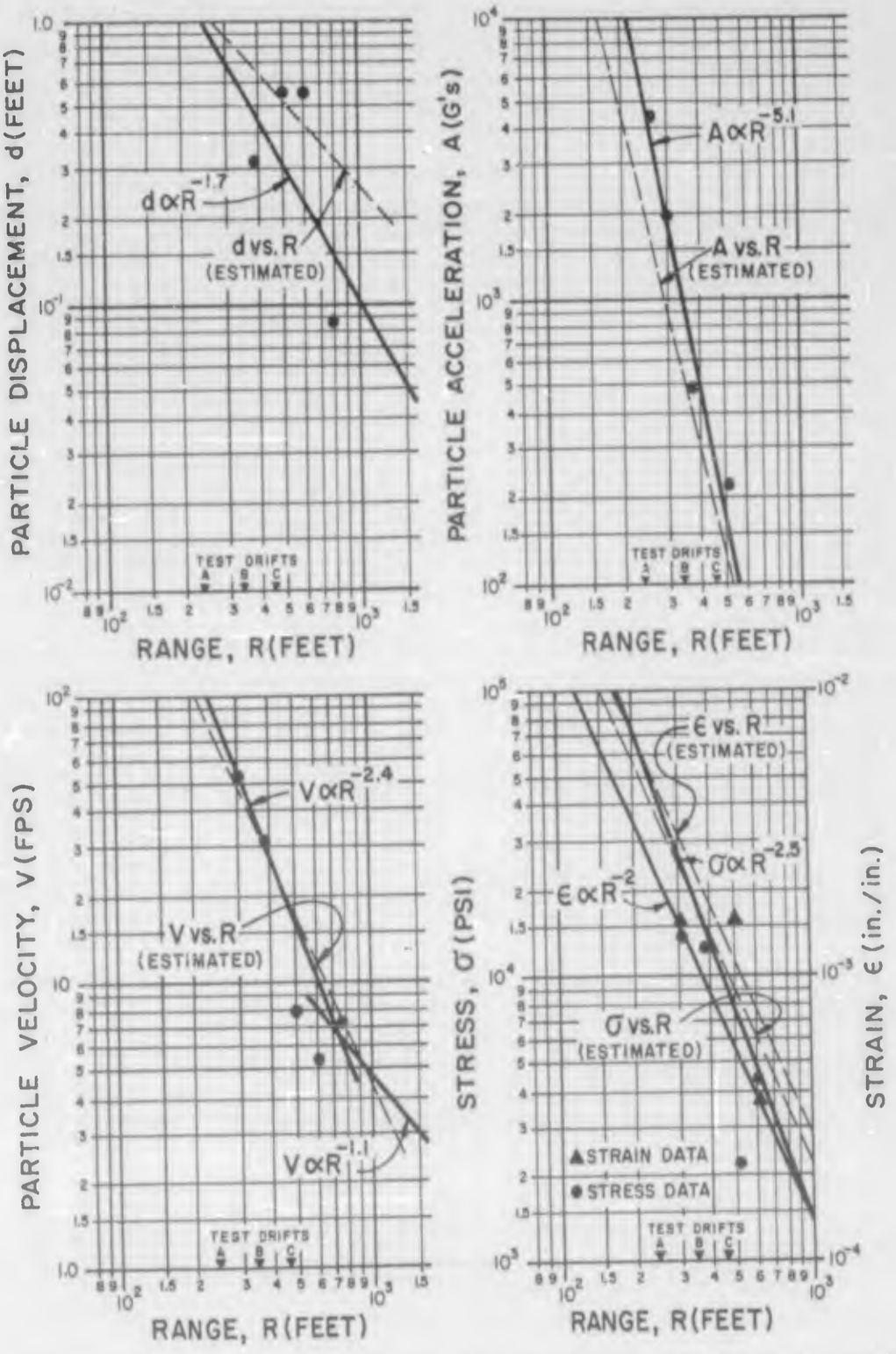

Figure 3.115 Free-field effects. Measured peak values versus preshot estimates.

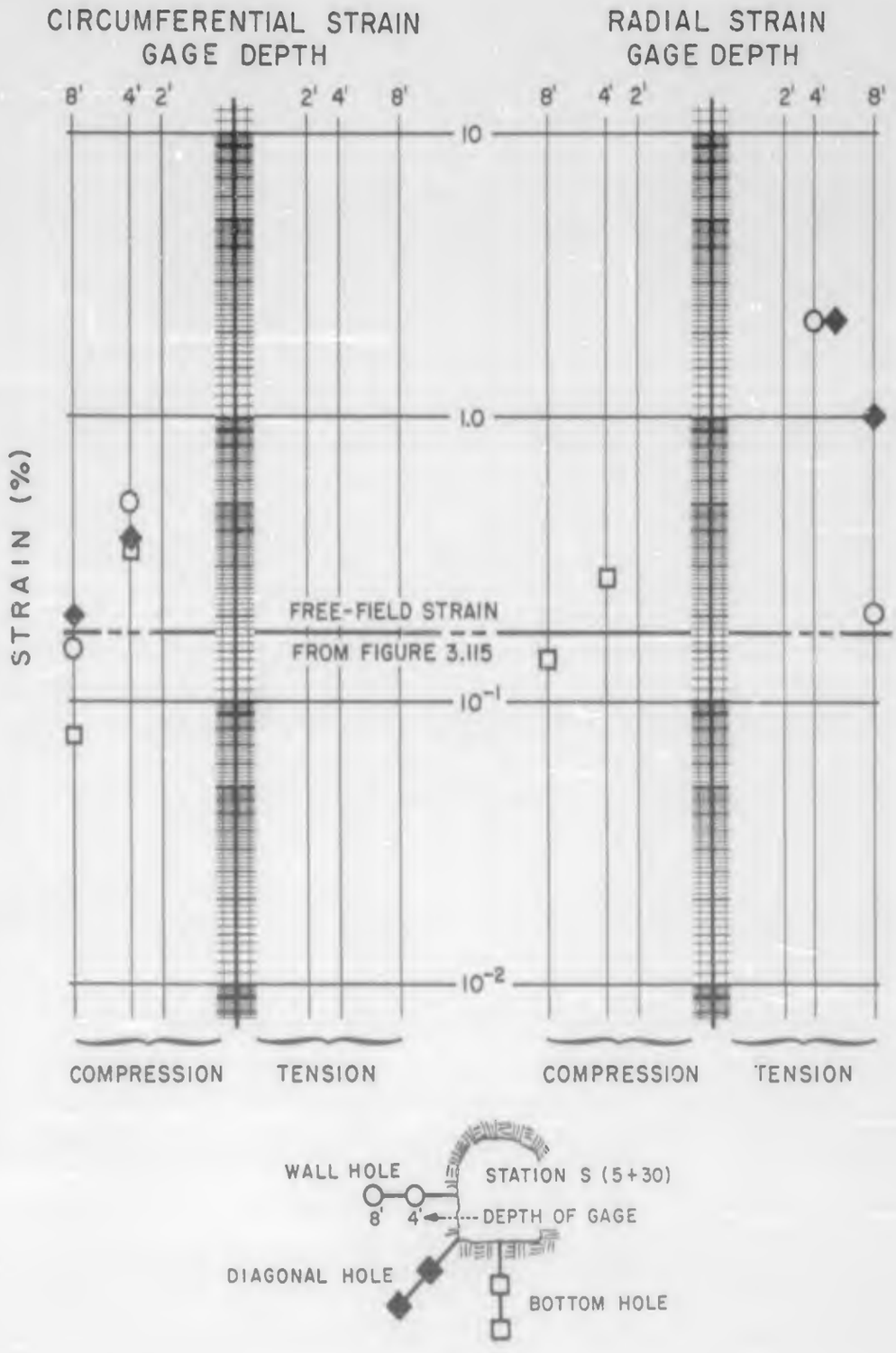

Figure 3.116 Measured peak strain values, access tunnel at Station S.

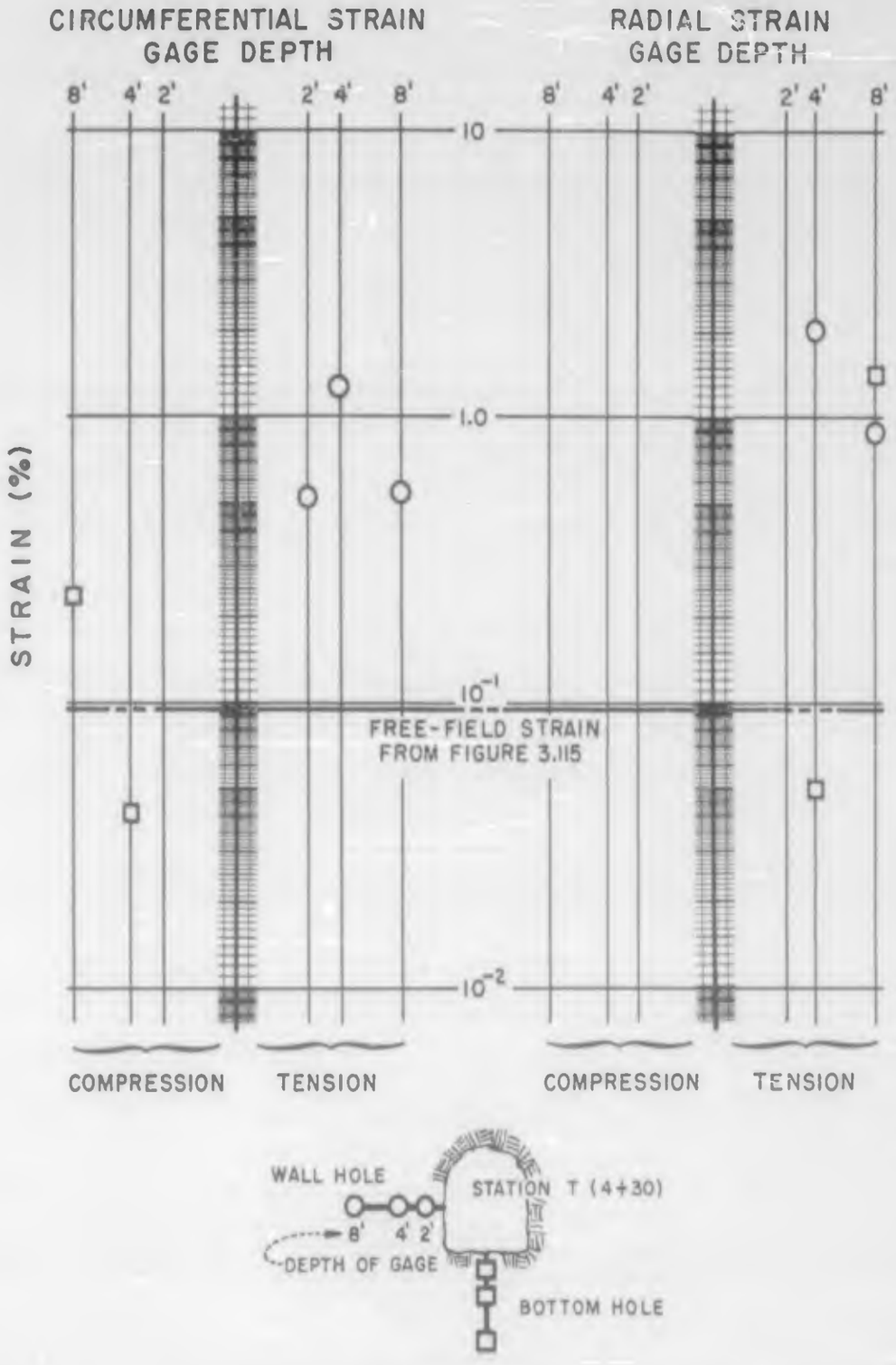

Figure 3.117 Measured peak strain values, access tunnel at Station T.

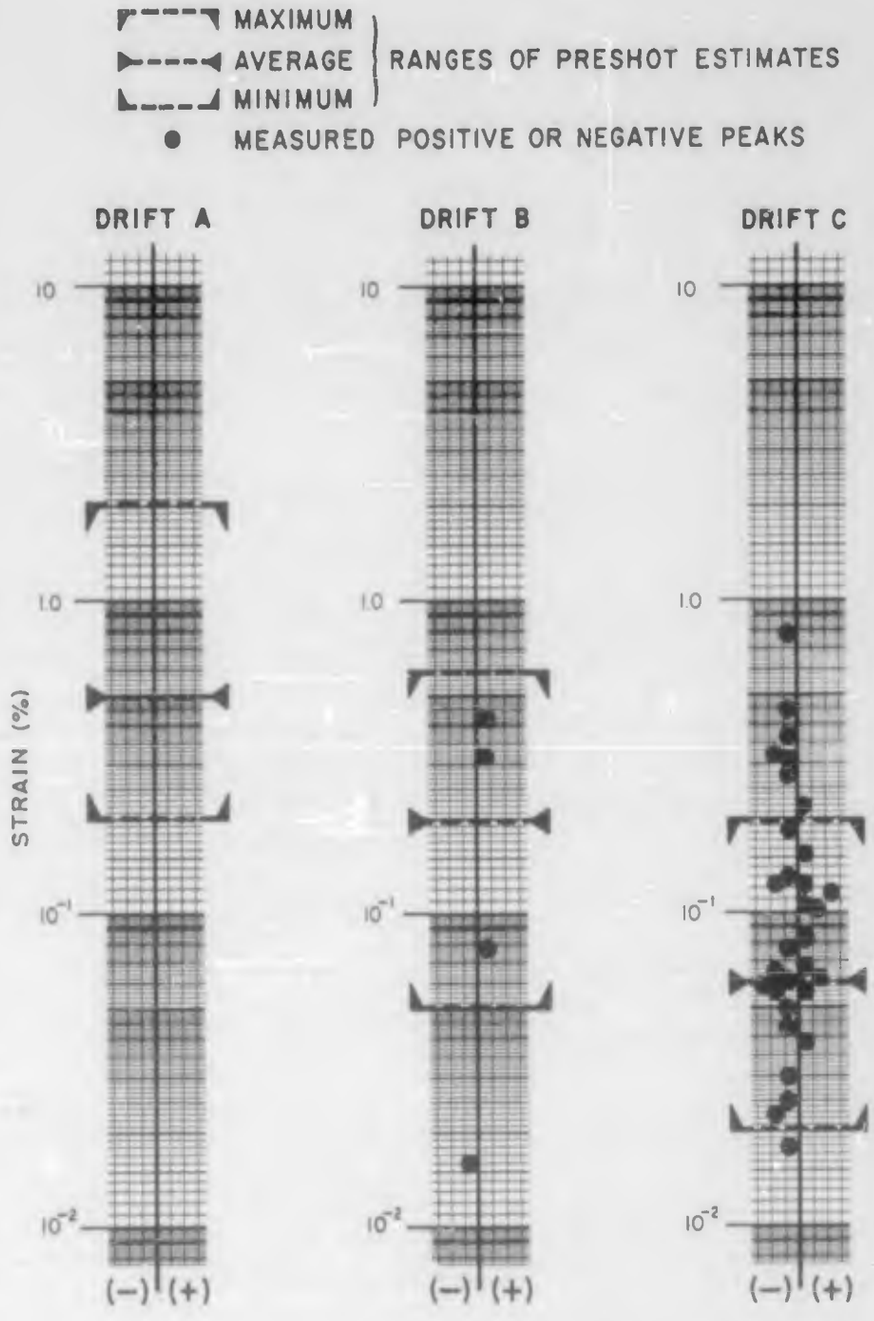

TEST DRIFTS	A	B	C
GAGES INSTALLED	50	44	43
RECORDS RECOVERED	0	4	31

Figure 3.118 Circumferential strain in lining (mechanical).

SECRET

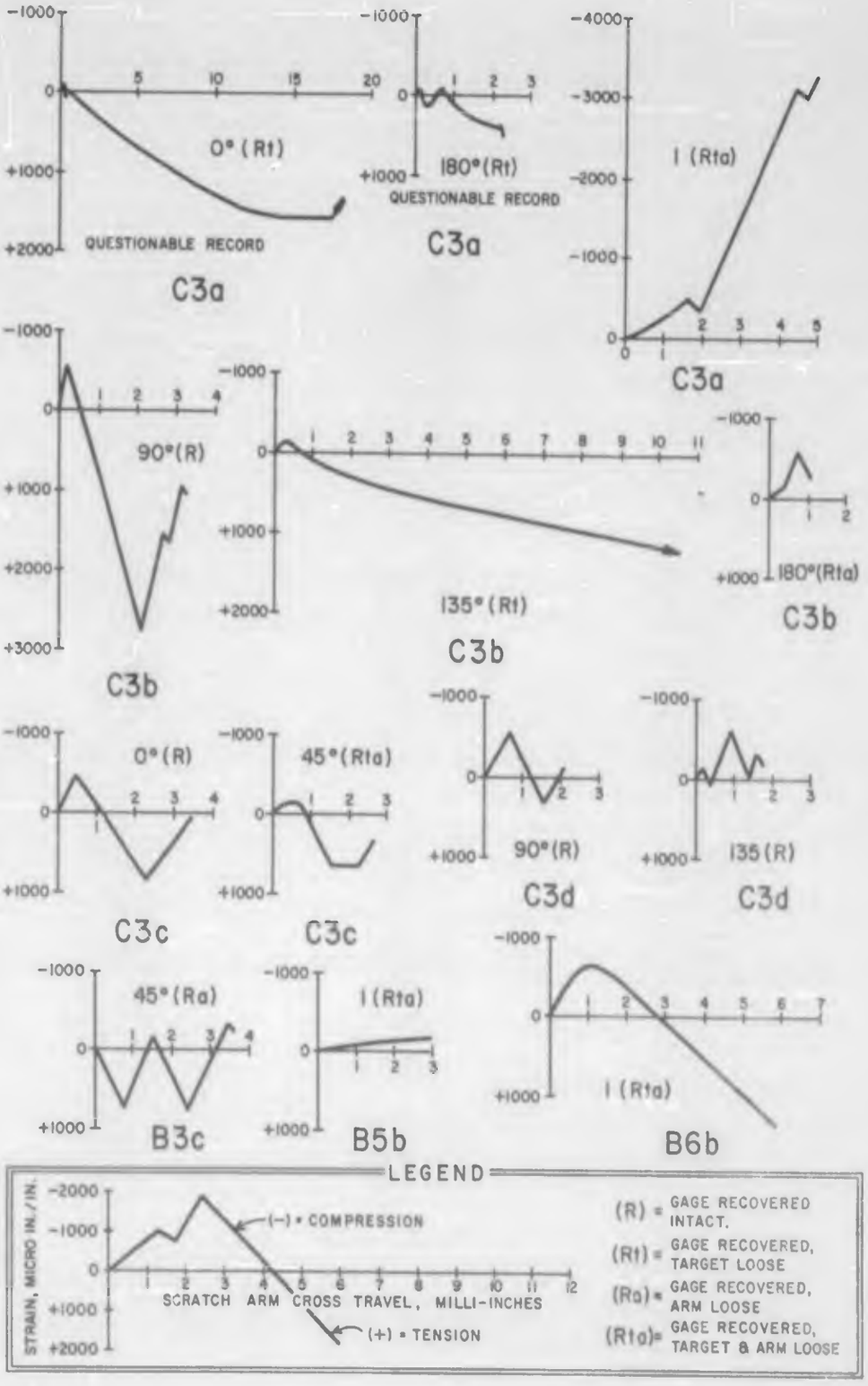

Figure 3.119 Records from deForest gage targets.

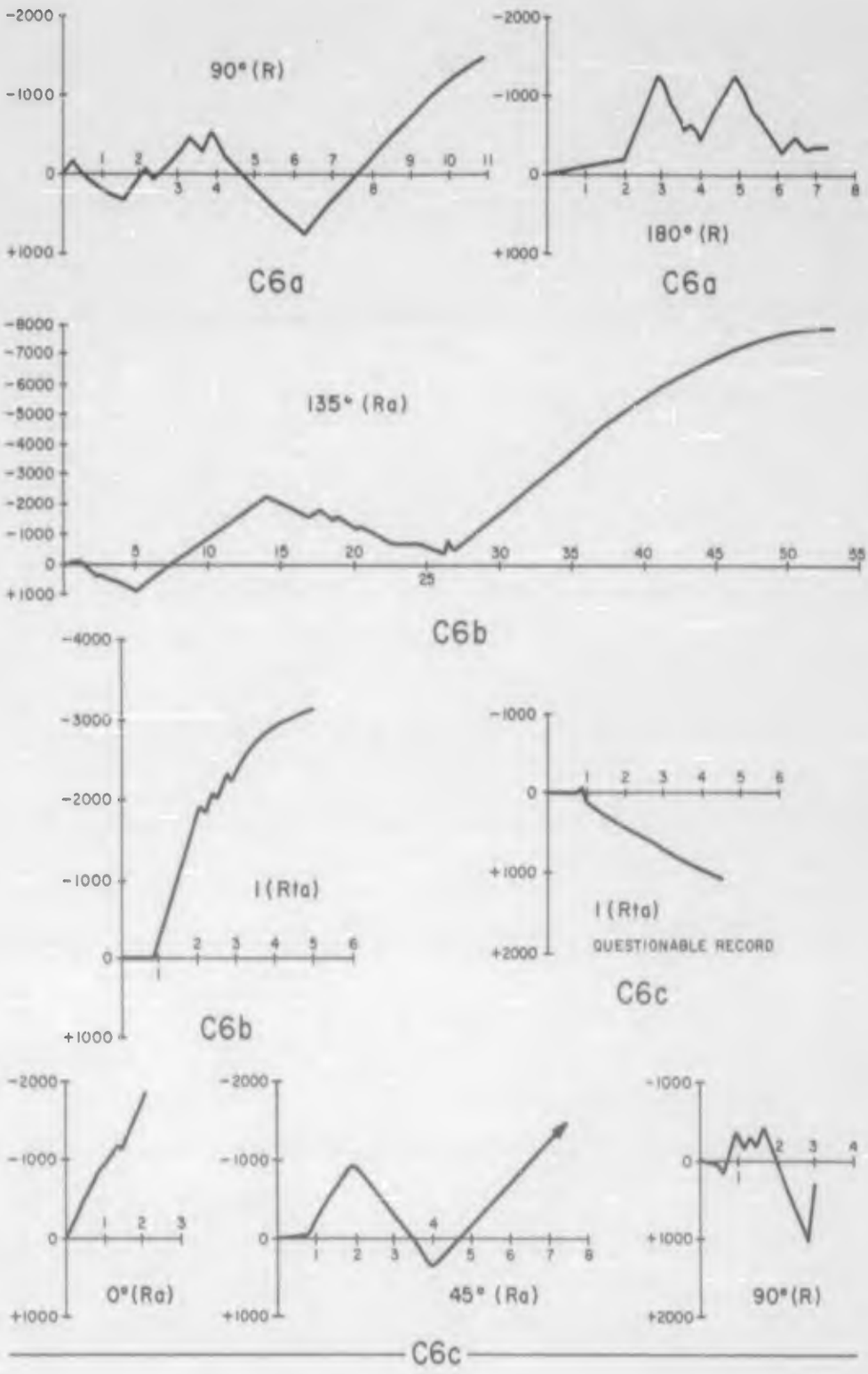

Figure 3.119 Continued

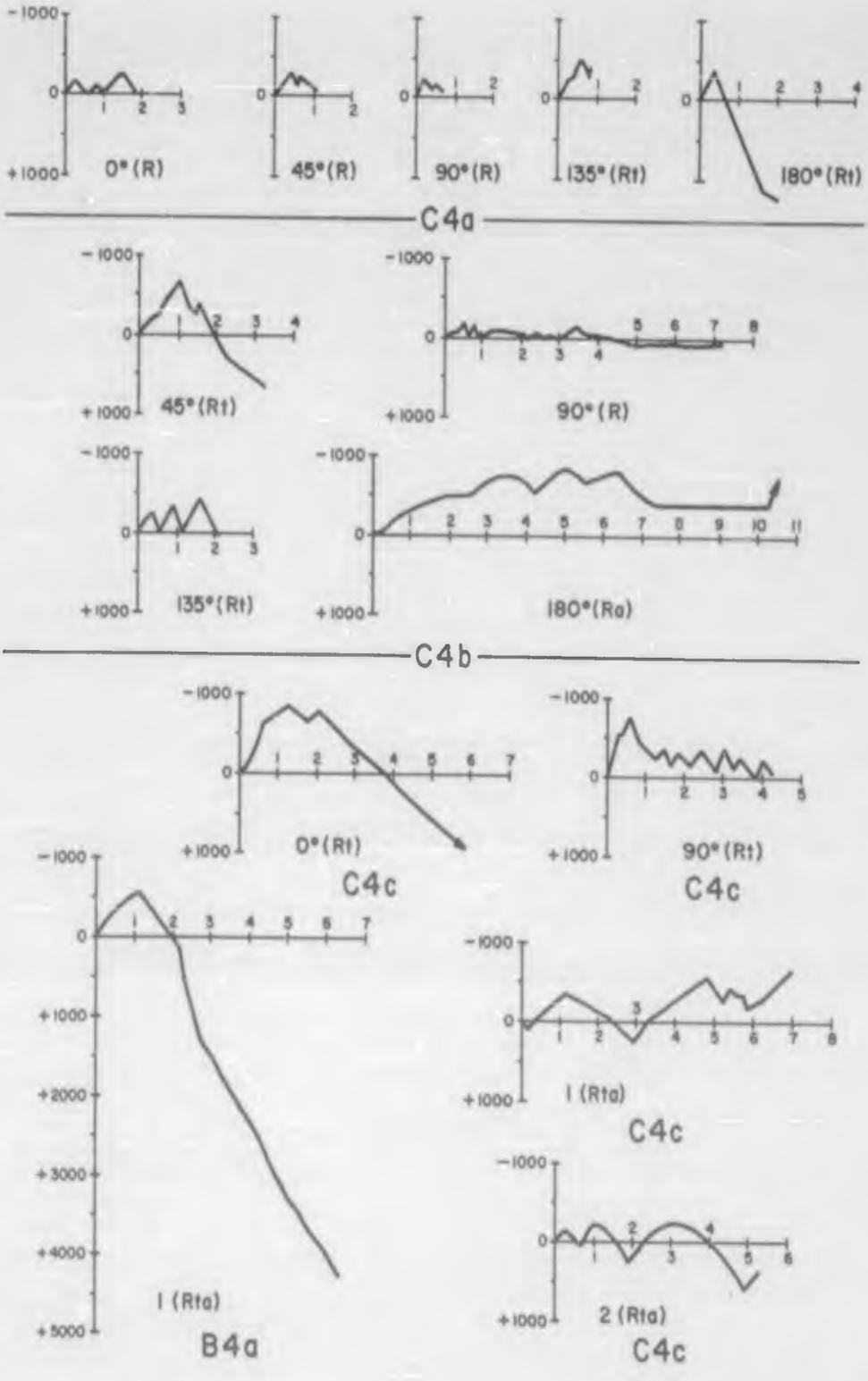

Figure 3.119 Continued

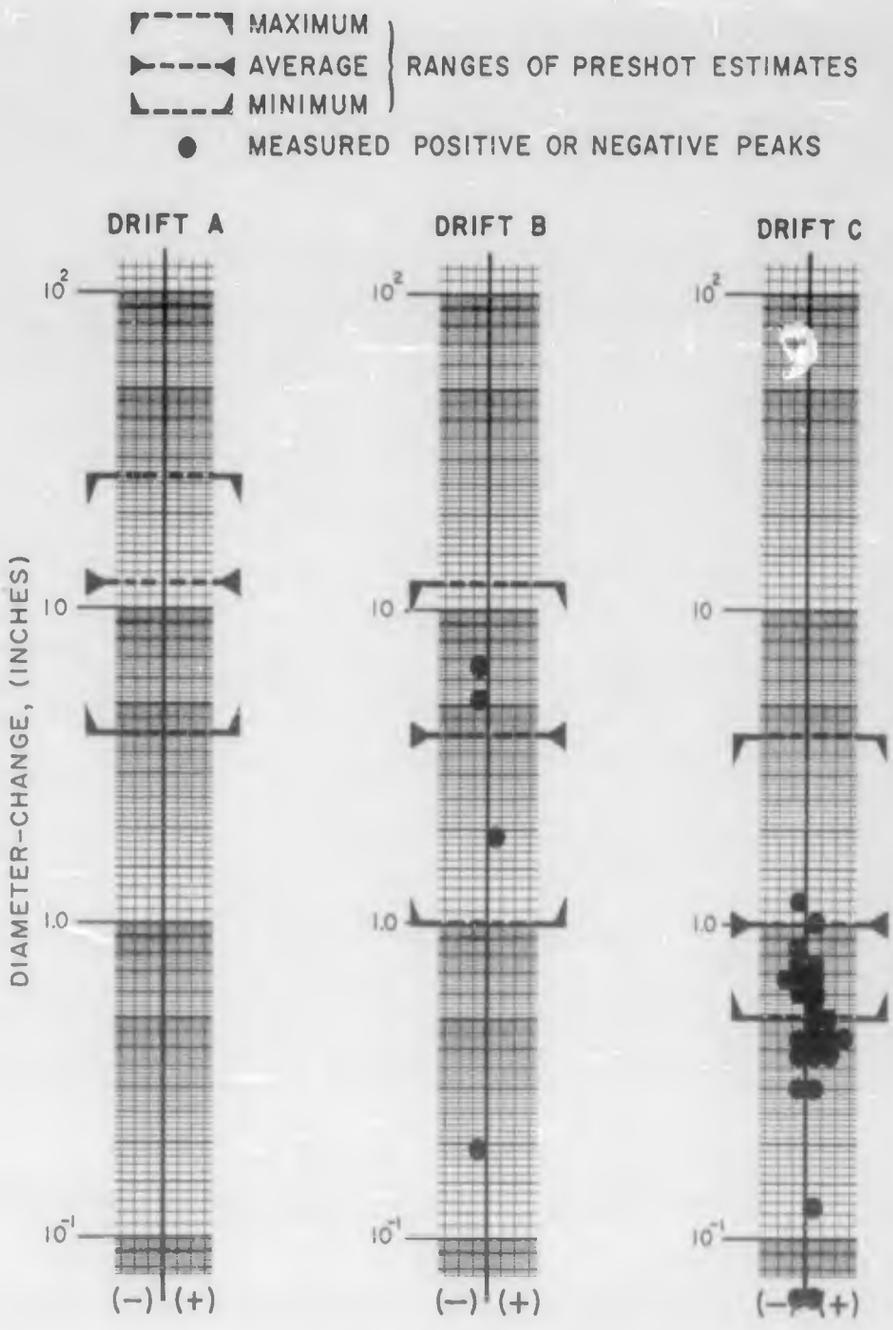

TEST DRIFTS	A	B	C
GAGES INSTALLED	20	38	32
RECORDS RECOVERED	0	4	26

Figure 3.120 Diameter change in lining (mechanical).

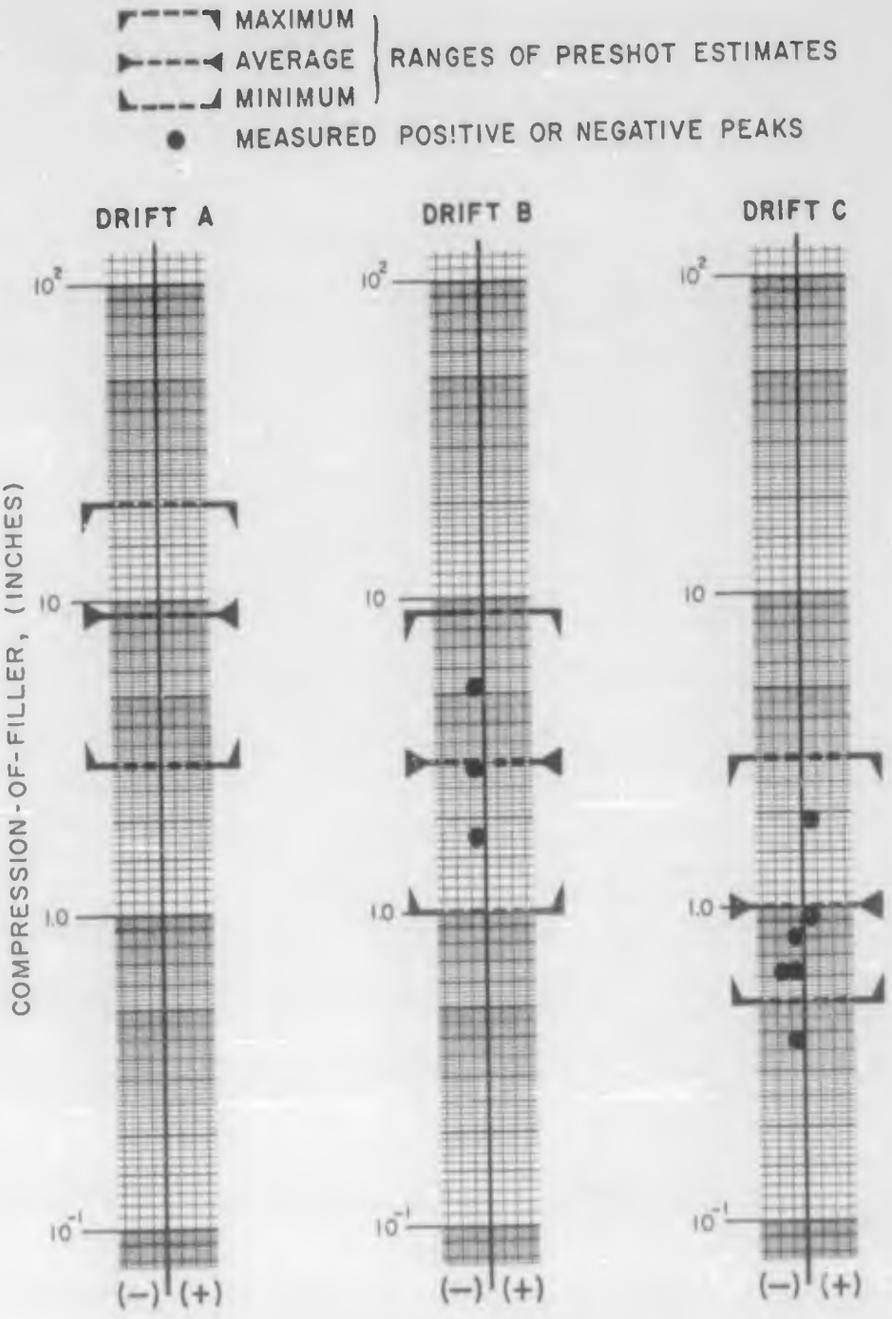

TEST DRIFTS	A	B	C
GAGES INSTALLED	6	9	6
RECORDS RECOVERED	0	3	6

Figure 3.121 Compression of filler, 20- and 24-inch foam (mechanical).

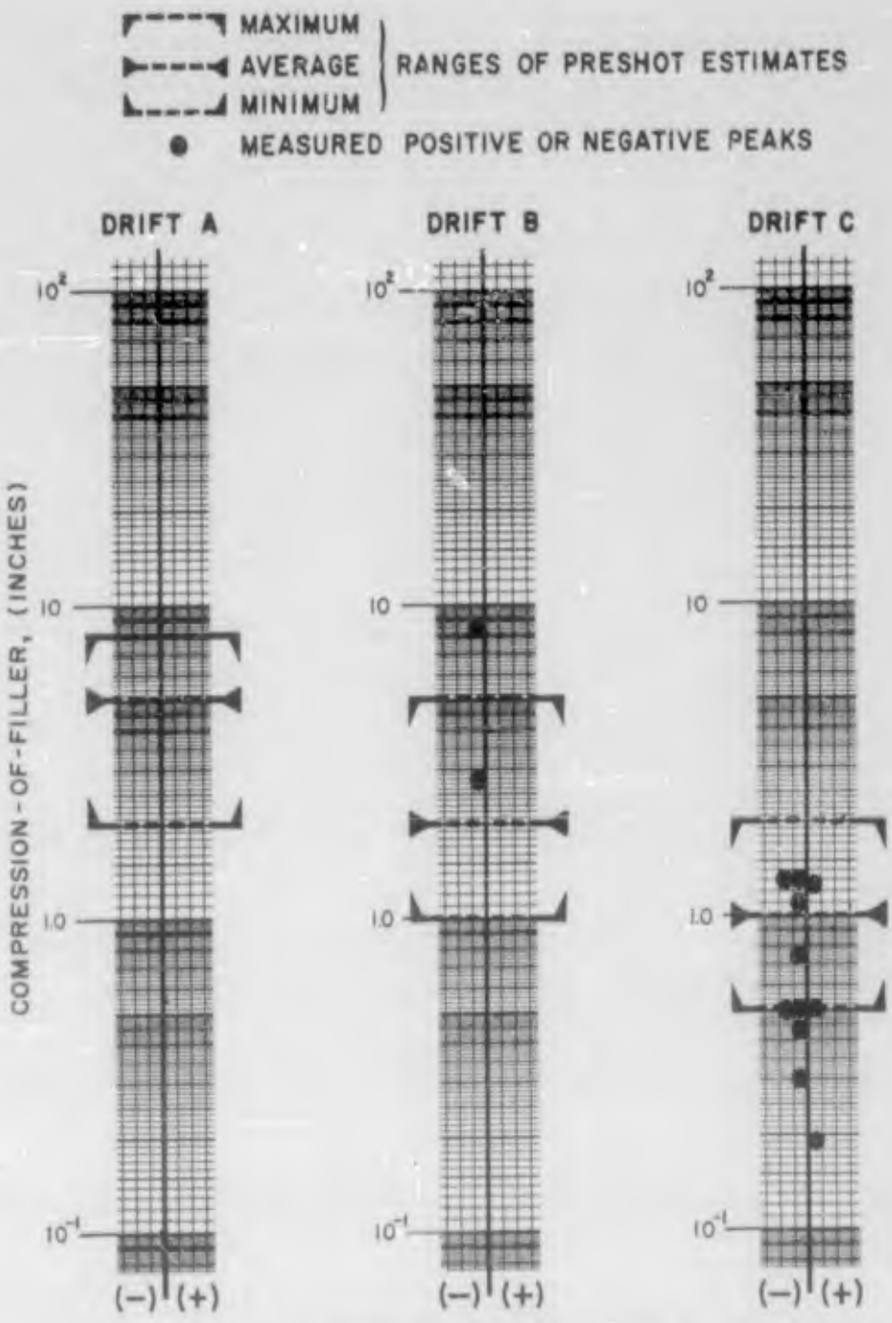

TEST DRIFTS	A	B	C
GAGES INSTALLED	12	15	12
RECORDS RECOVERED	0	2	11

Figure 3.122 Compression of filler, 5- and 9-inch foam (mechanical).

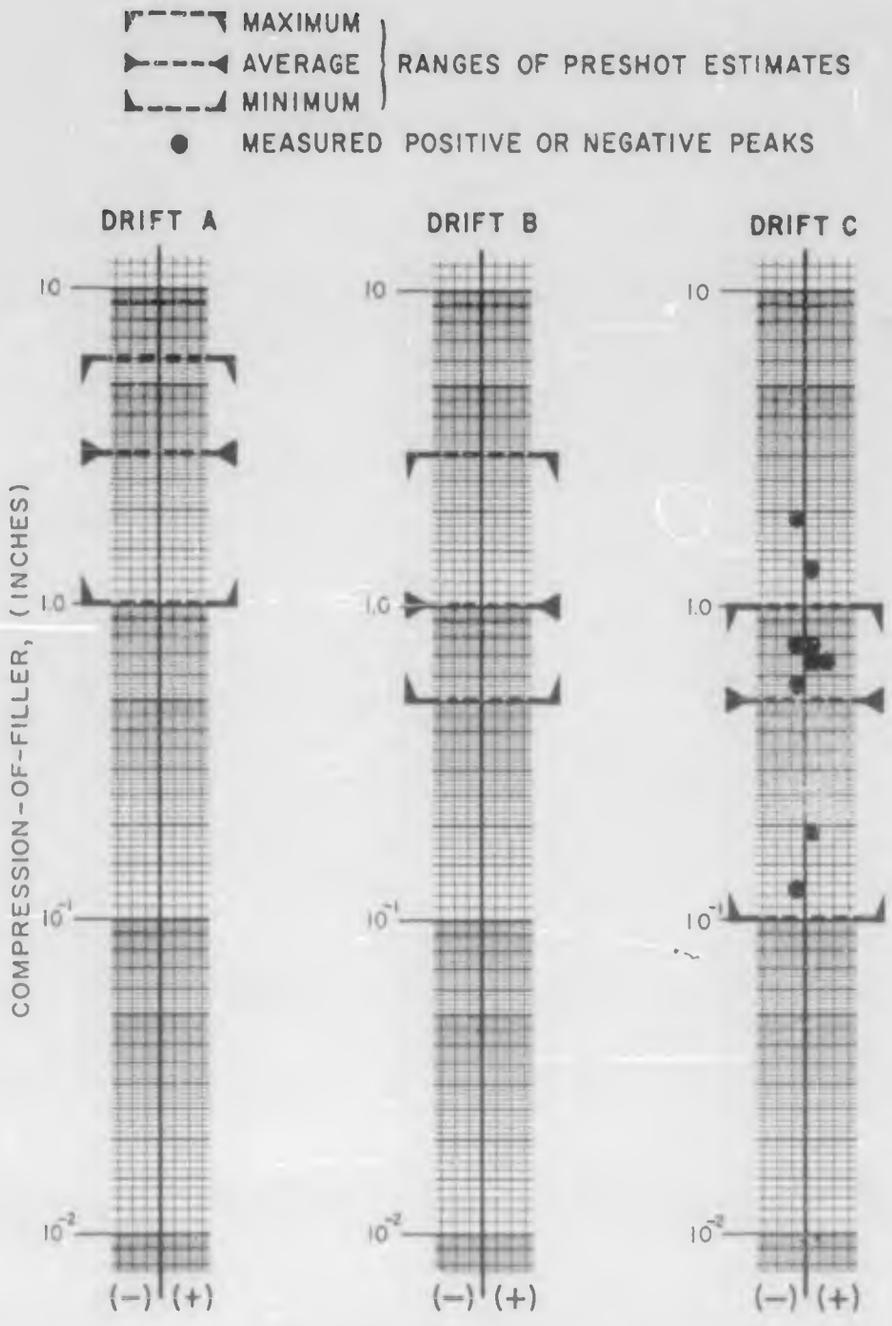

TEST DRIFTS	A	B	C
GAGES INSTALLED	9	12	9
RECORDS RECOVERED	0	0	9

Figure 3.123 Compression of filler, 9-inch cinder (mechanical).

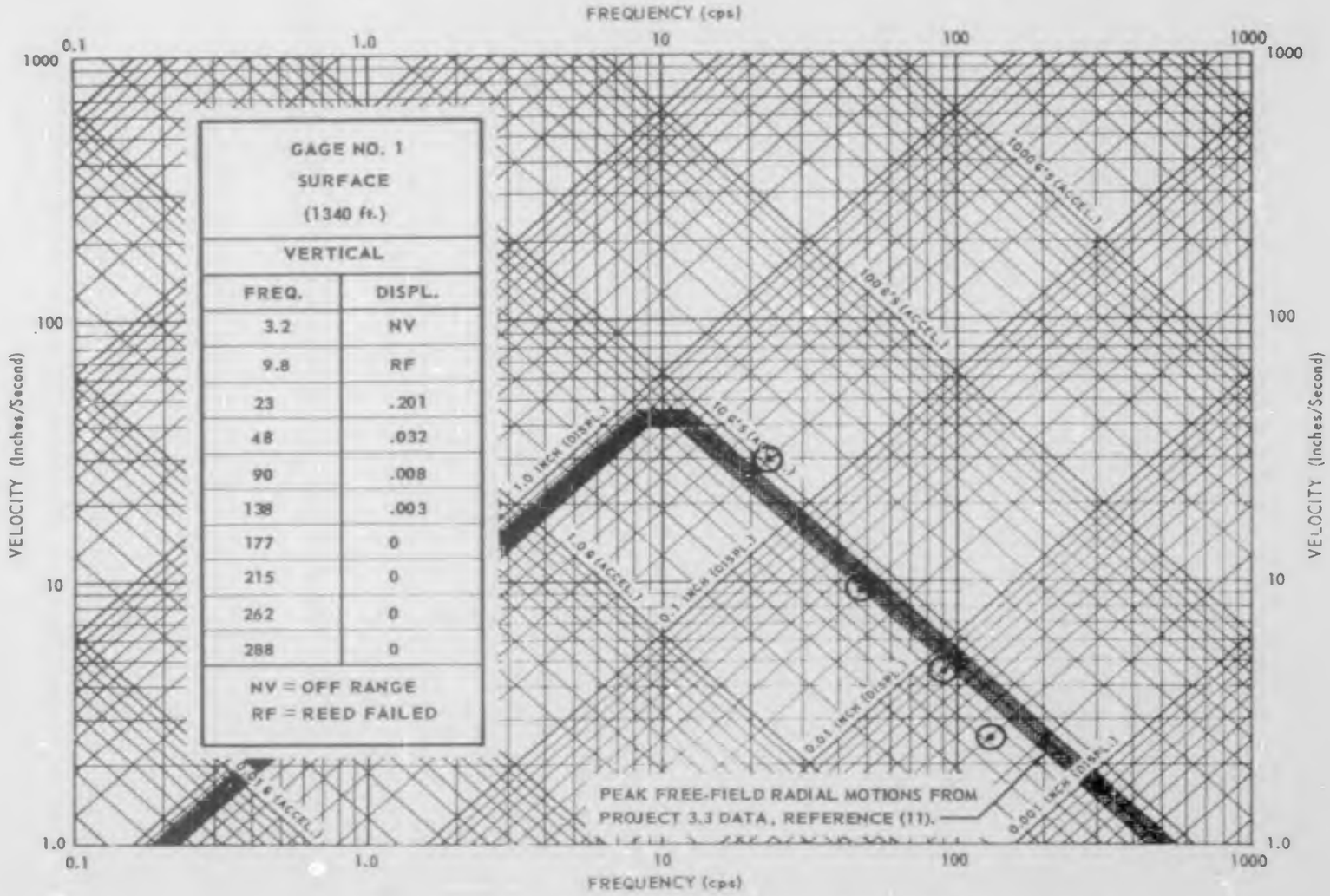

Figure 3.124 Surface shock spectra (STL).

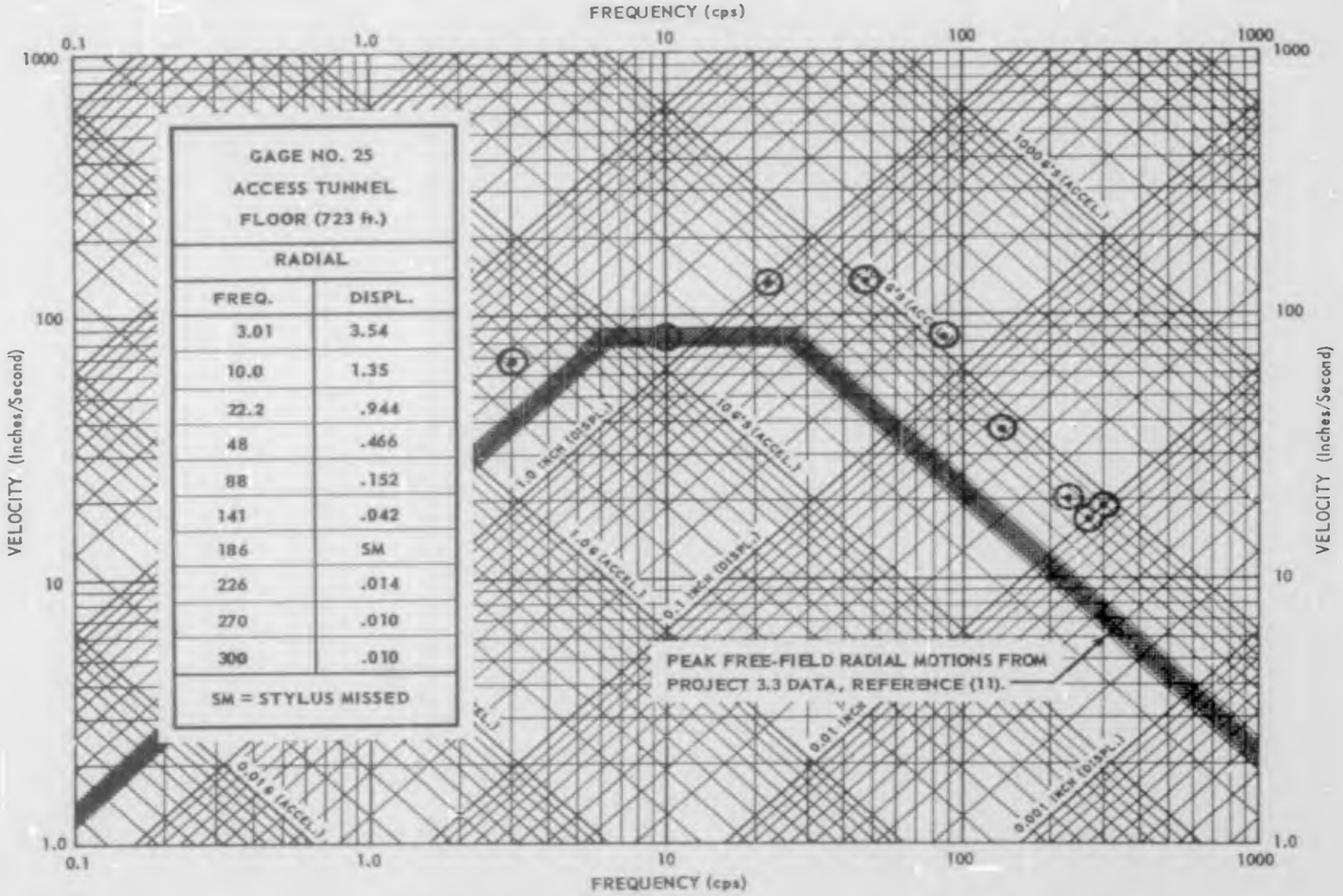

Figure 3.125 Access tunnel floor, shock spectra (STL), Gage 25.

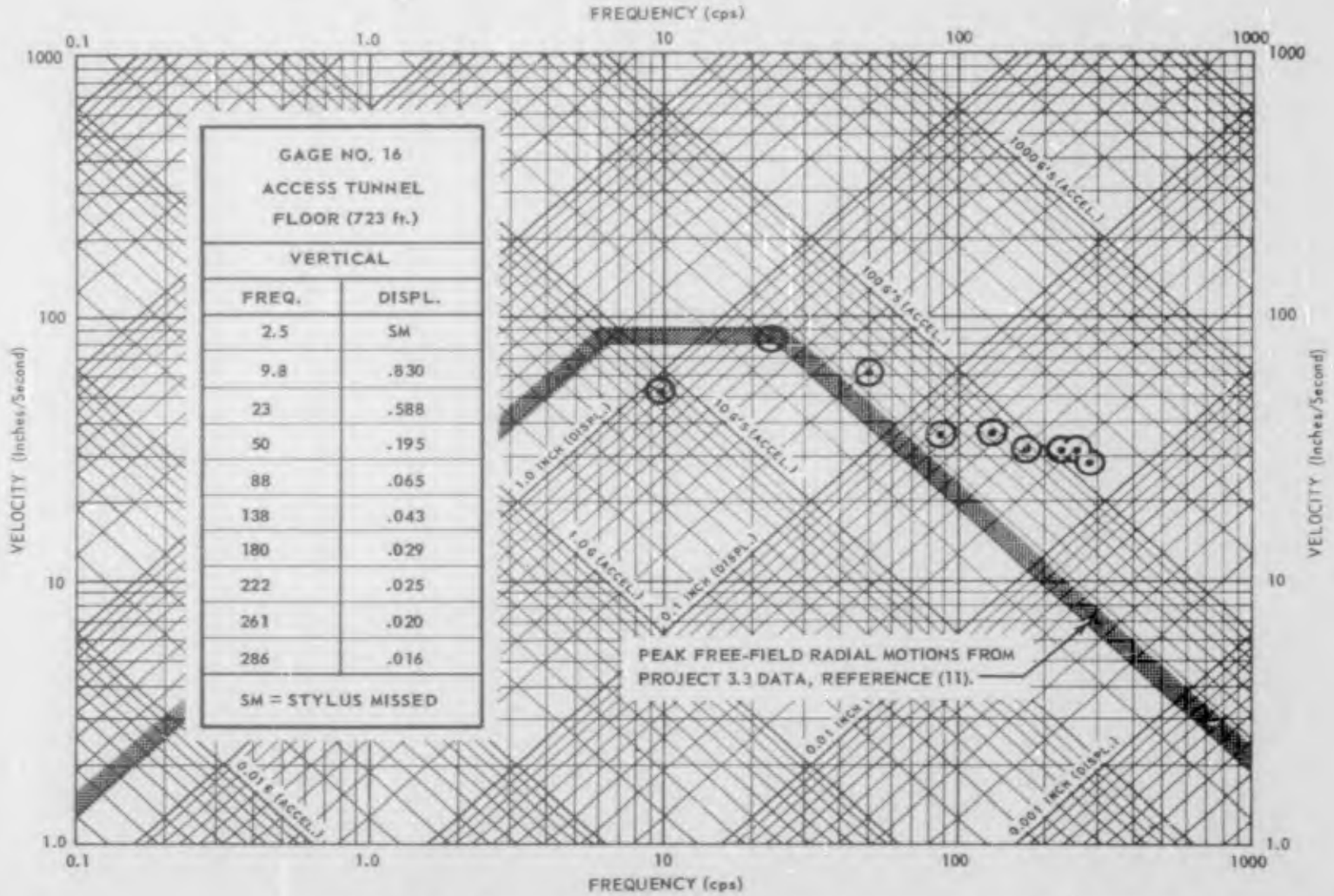

Figure 3.126 Access tunnel floor, shock spectra (STL), Gage 16.

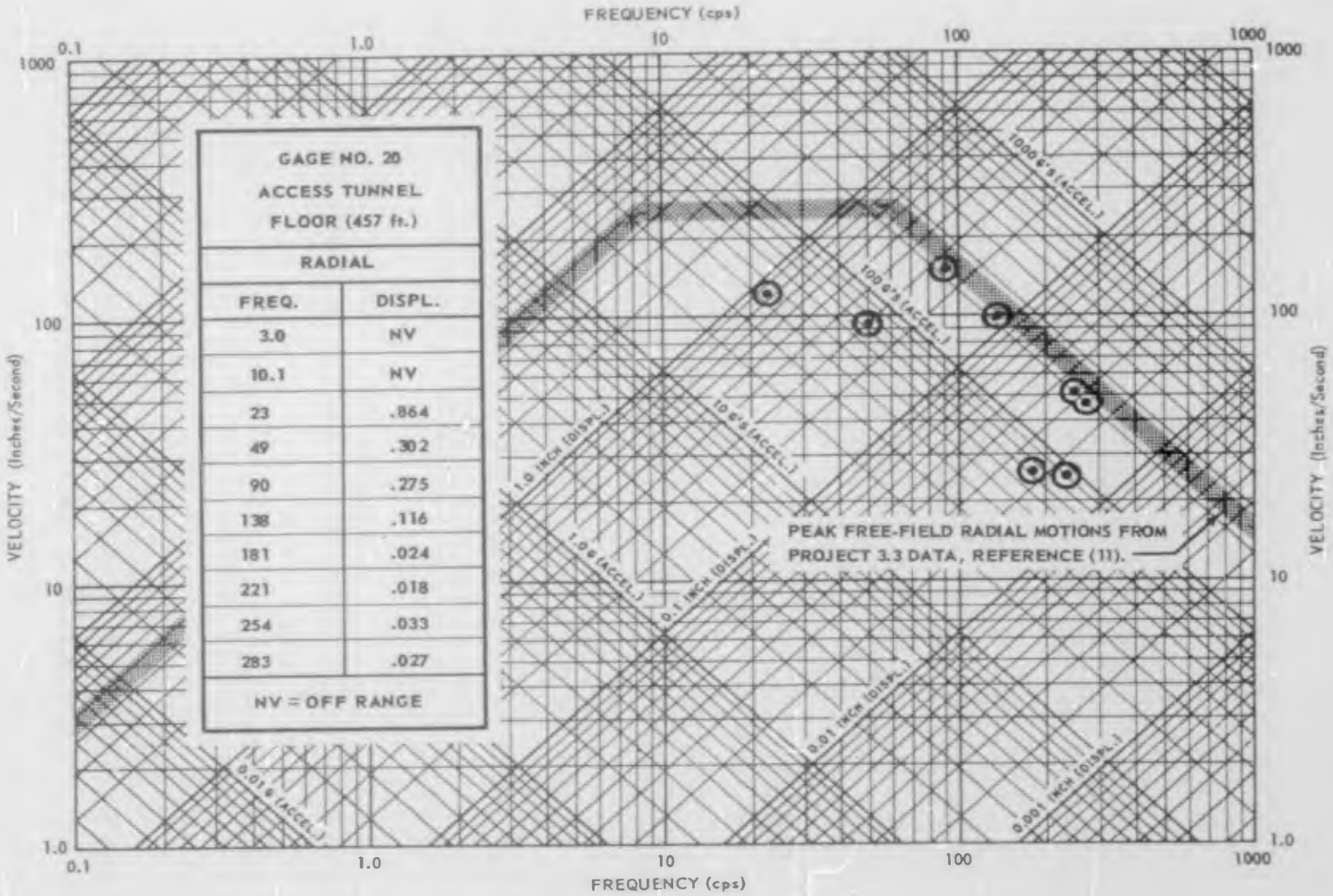

Figure 3.127 Access tunnel floor, shock spectra (STL), Gage 20.

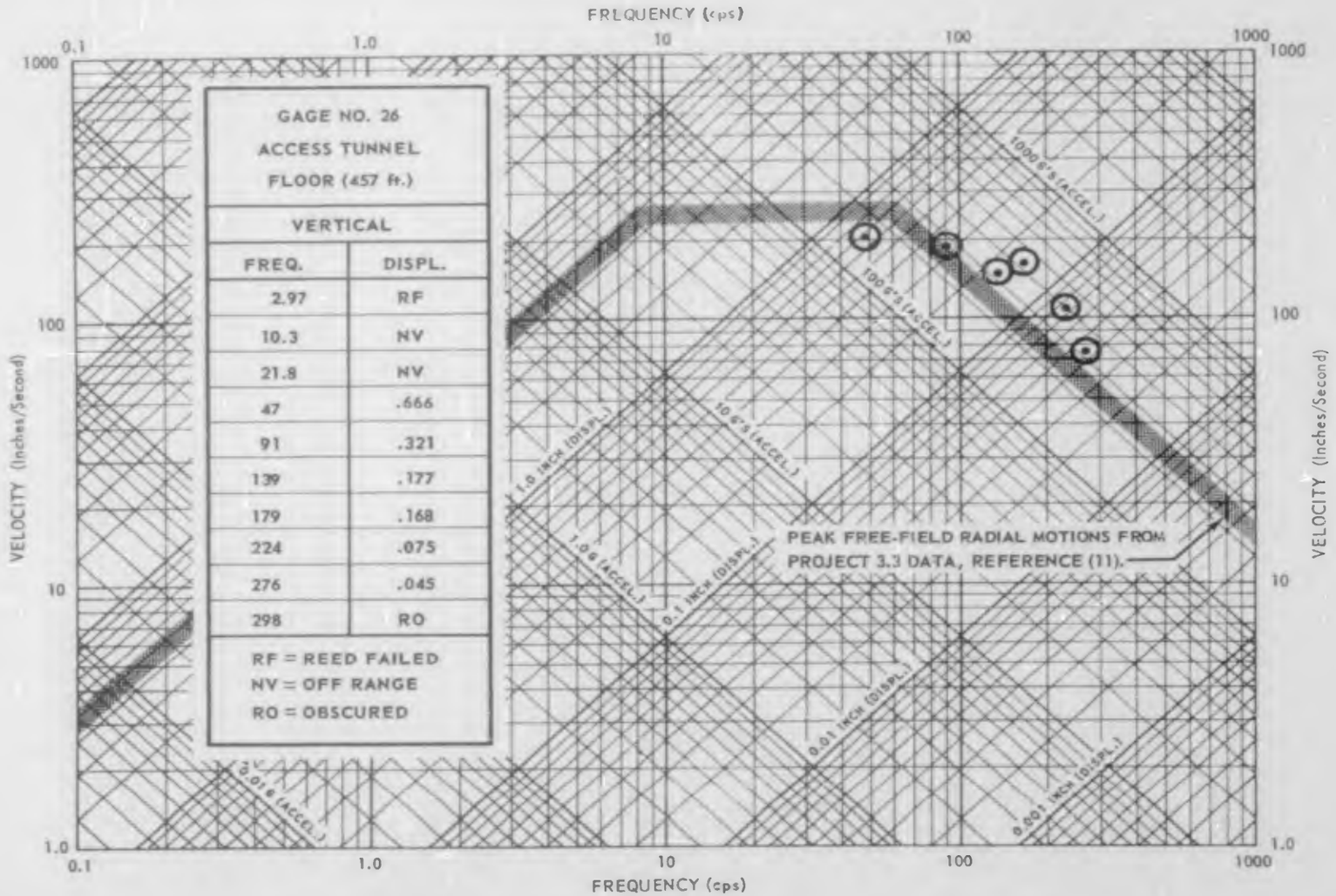

Figure 3.128 Access tunnel floor, shock spectra (STL), Gage 26.

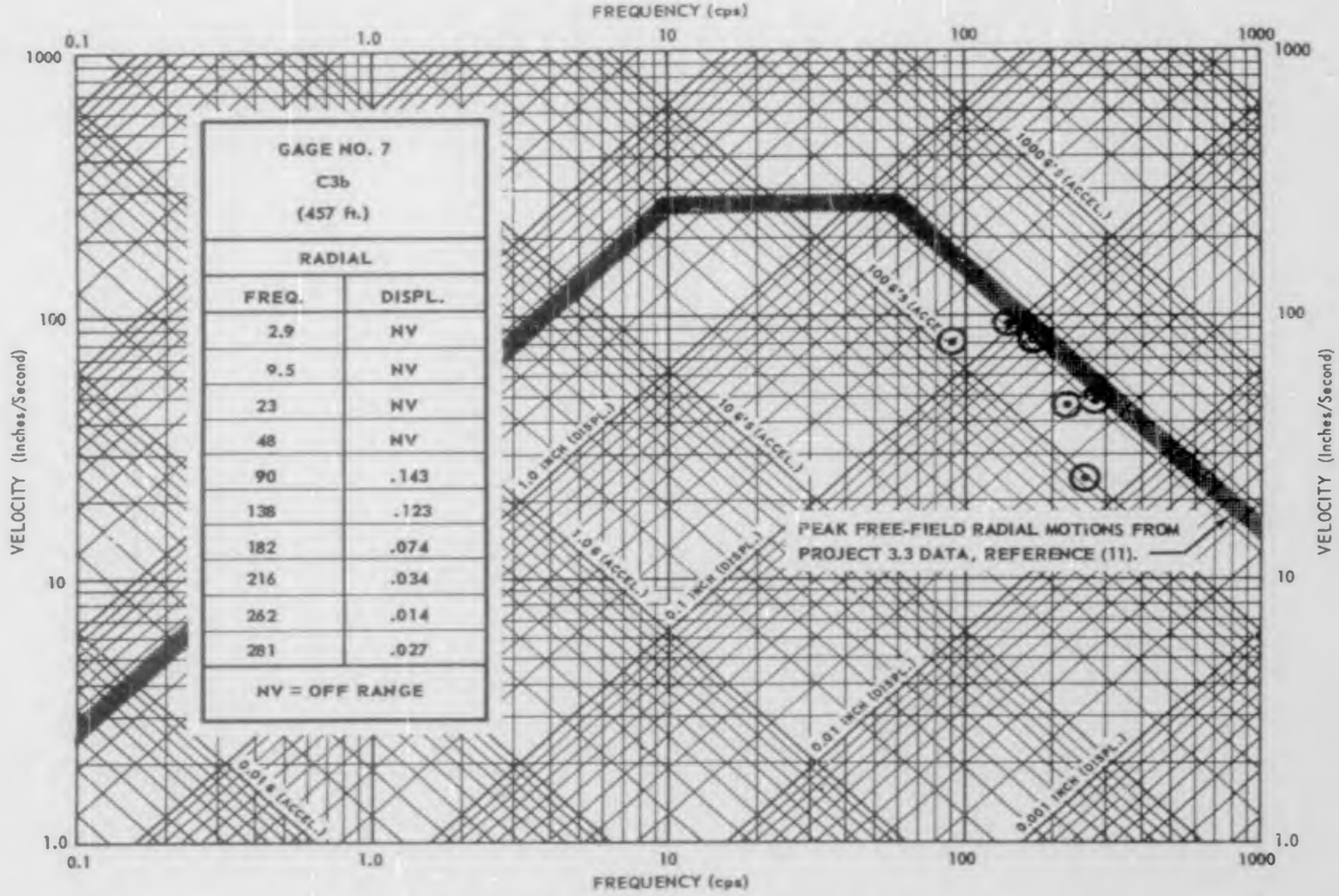

Figure 3.129 C3b, shock spectra (STL).

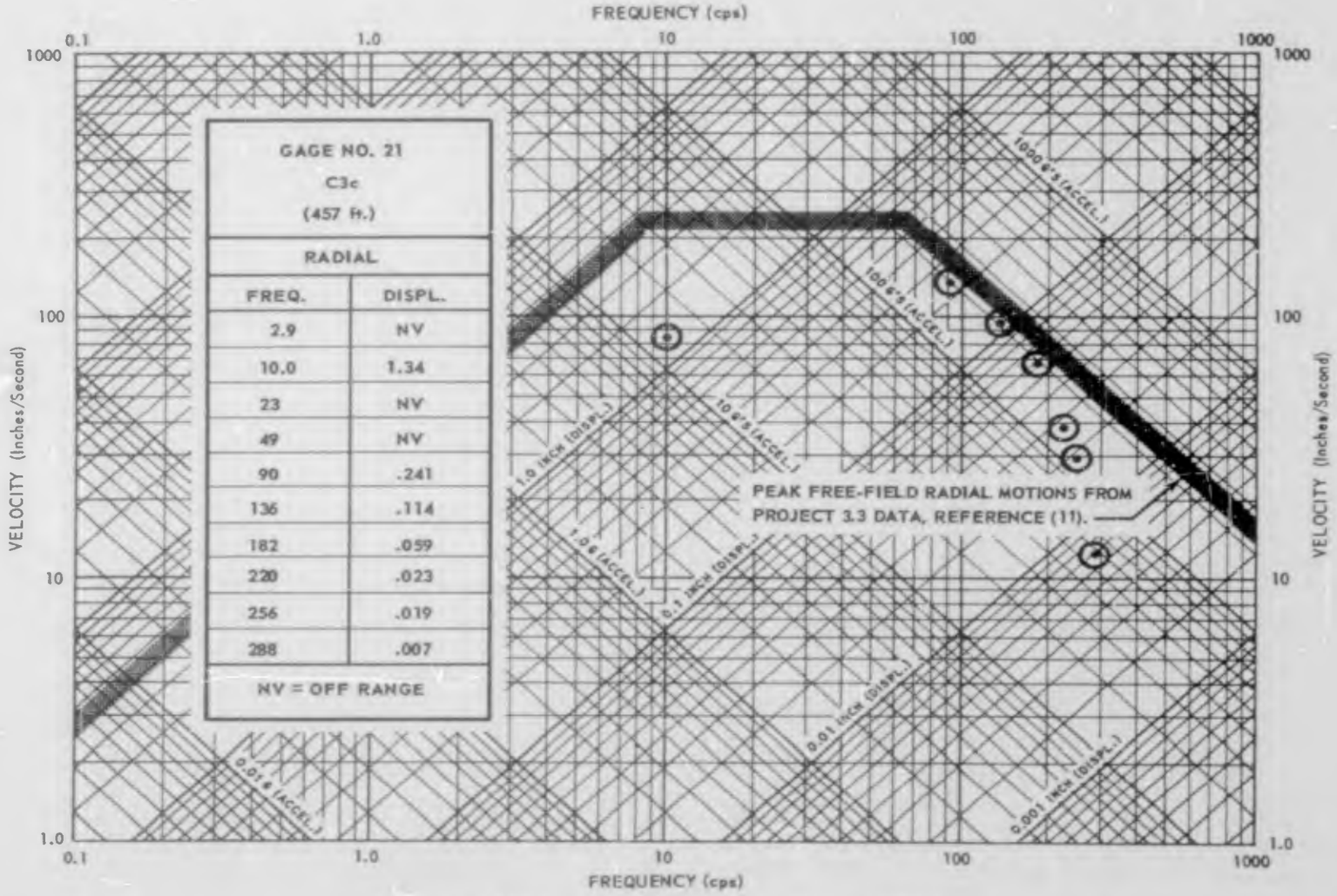

Figure 3.130 C3c , shock spectra (STL).

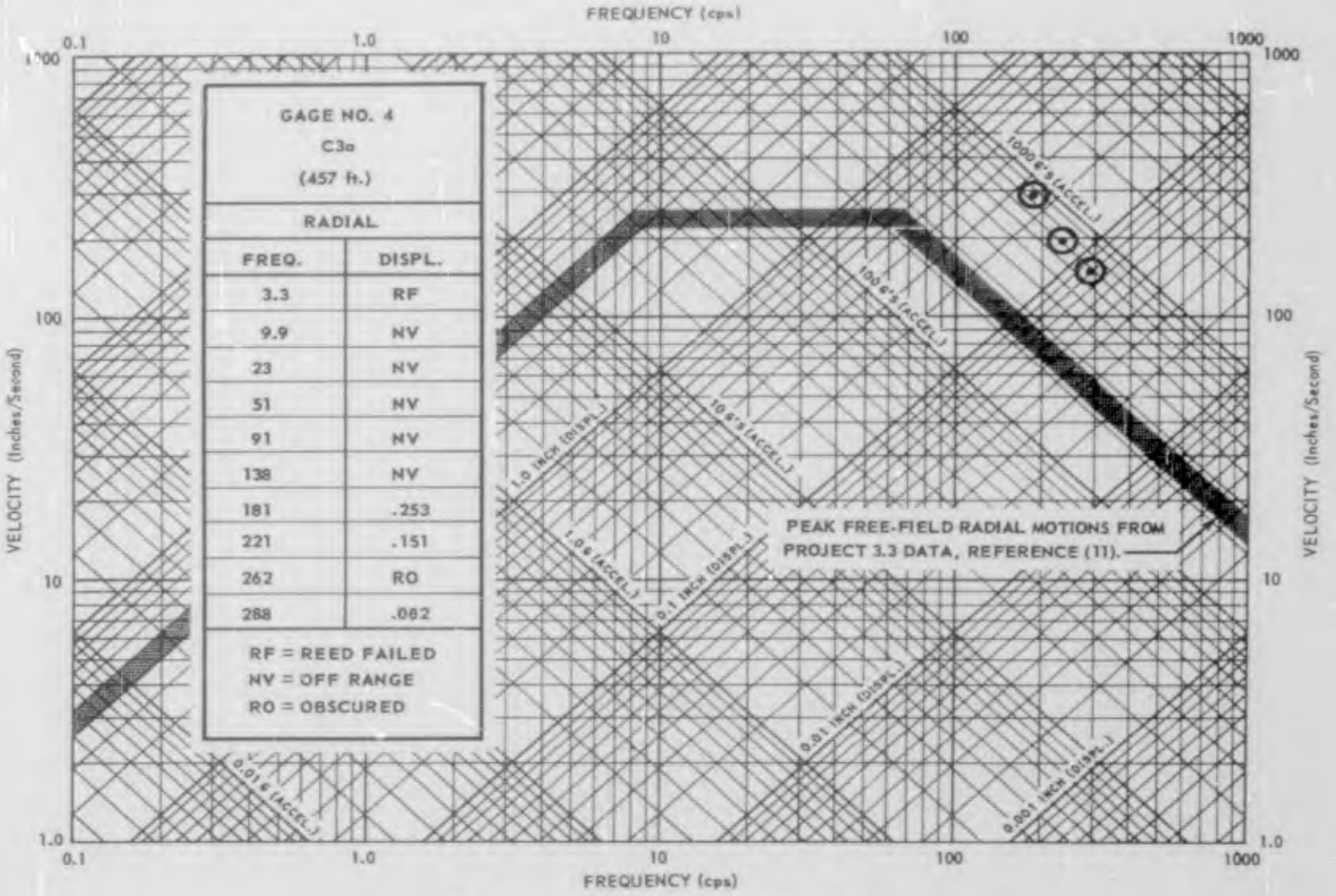

Figure 3.131 C3a , shock spectra (STL).

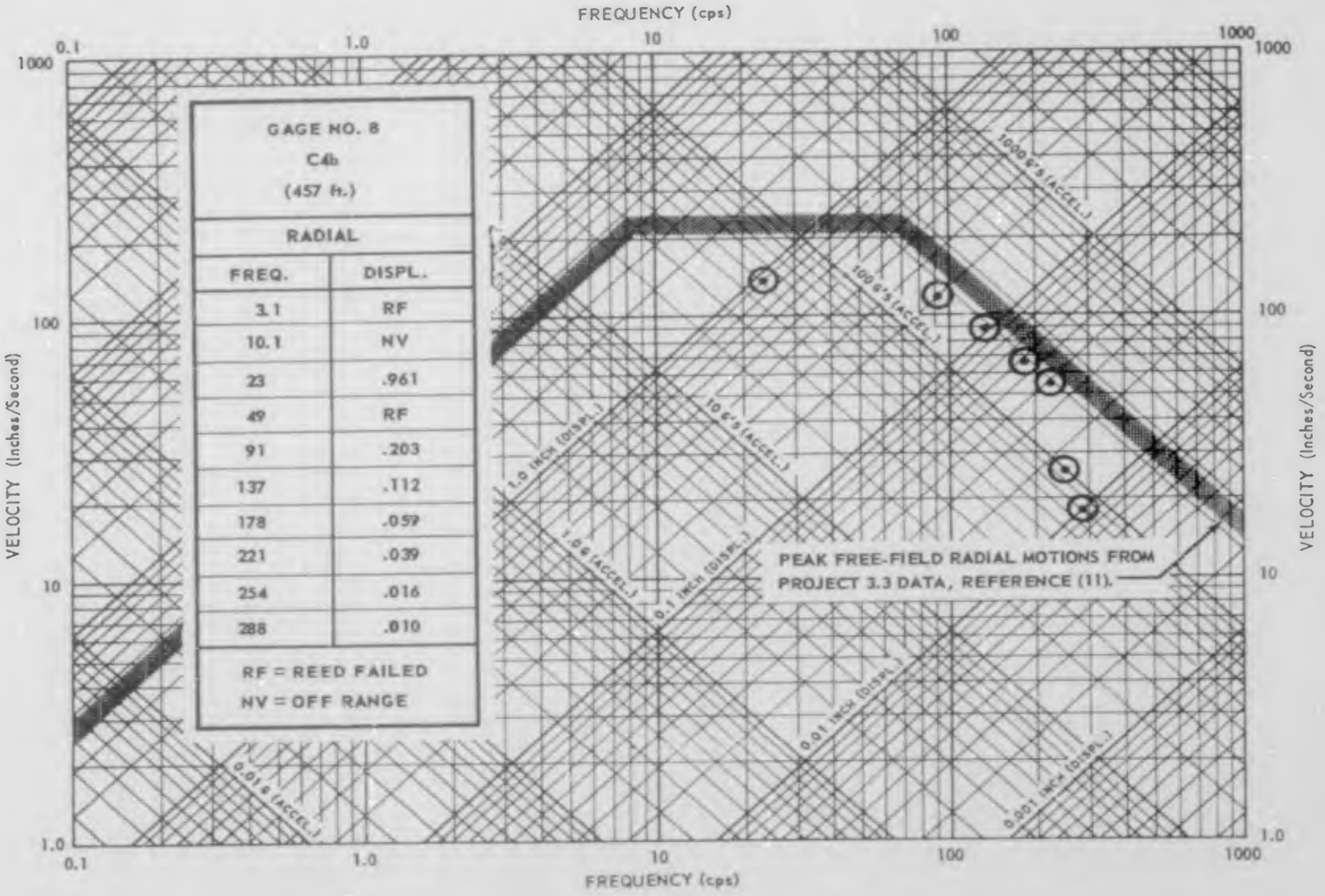

Figure 3.132 C4b , shock spectra (STL).

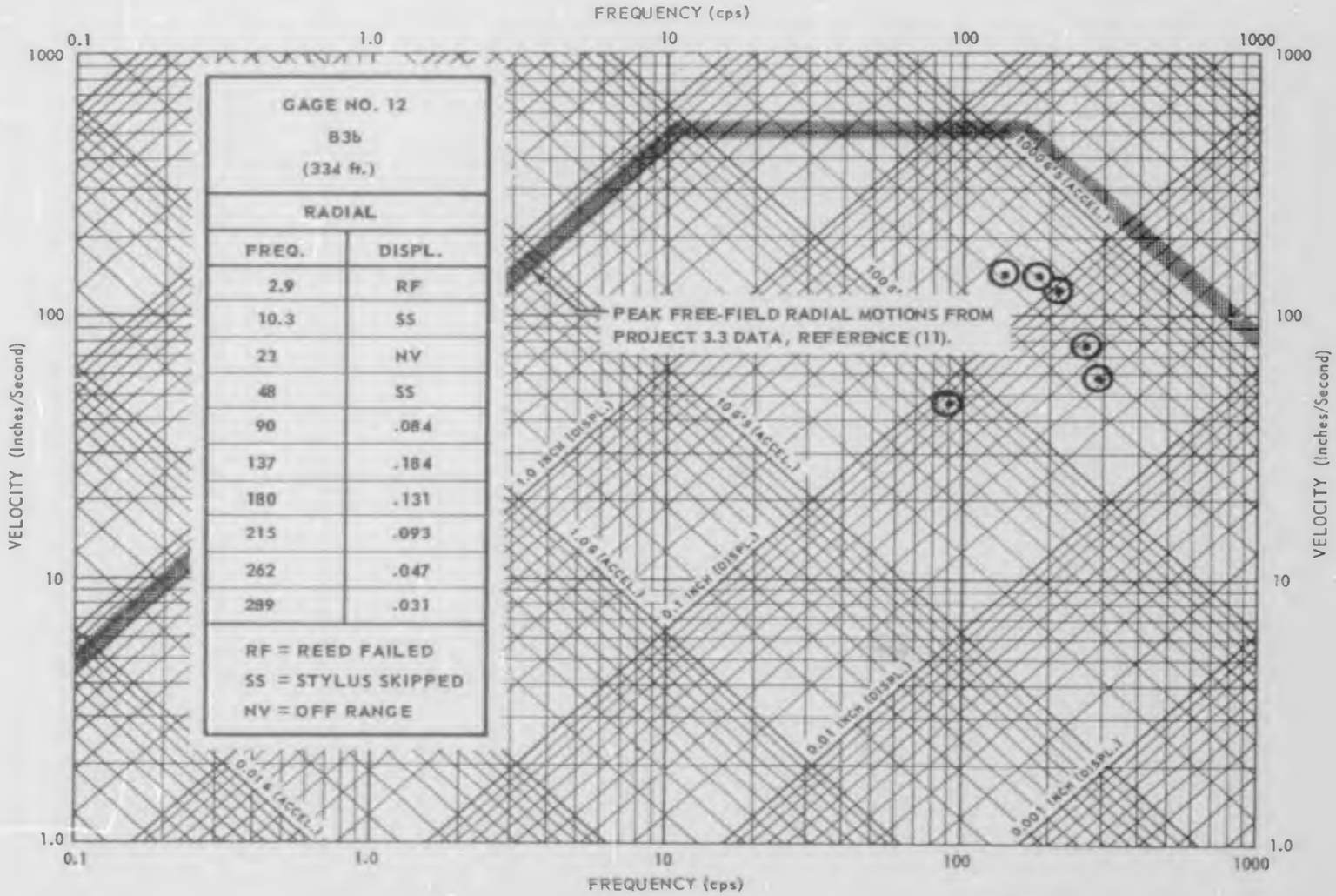

Figure 3.133 B3b , shock spectra (STL), Gage 12.

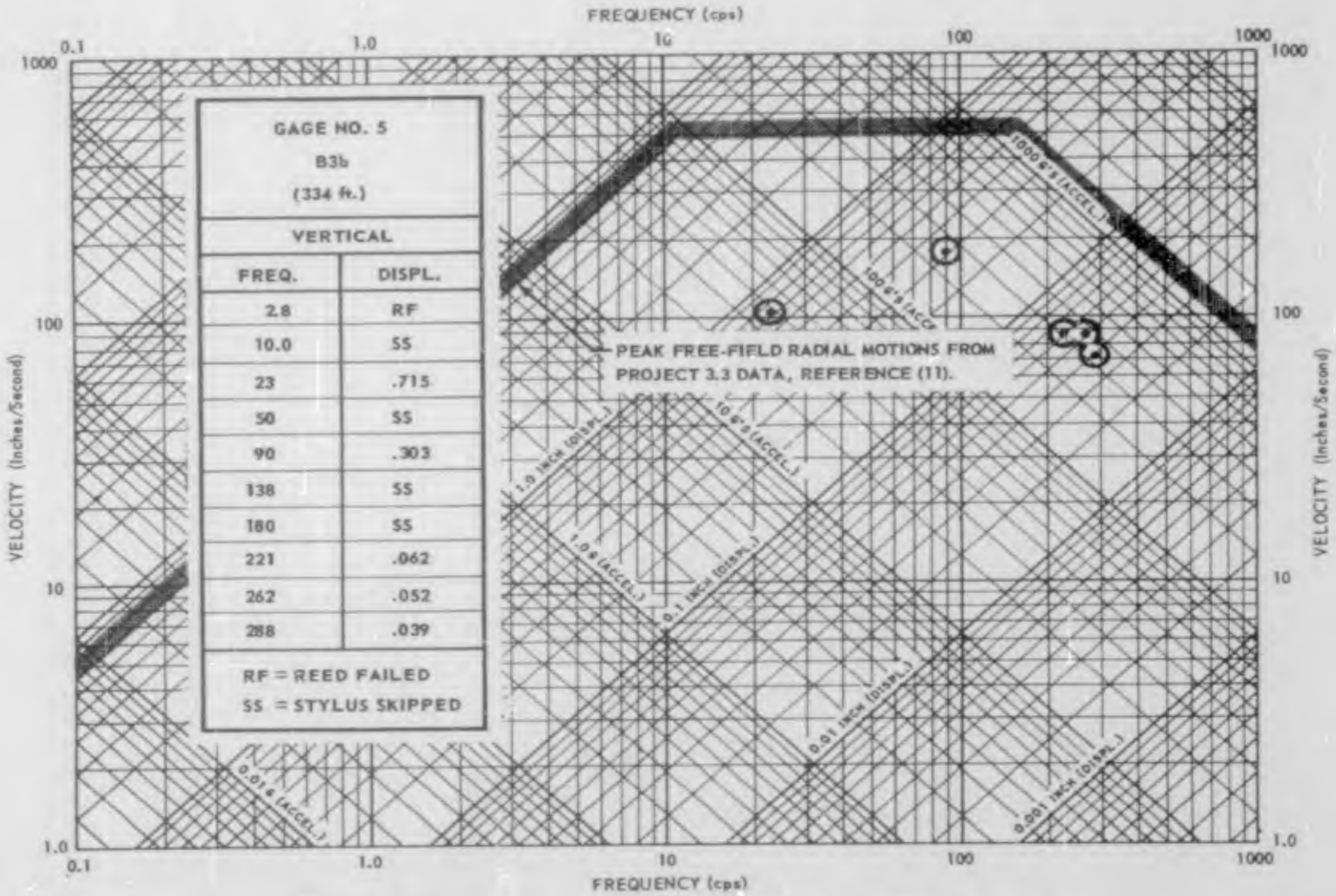

Figure 3.134 B3b, shock spectra (STL), Gage 5.

SECRET

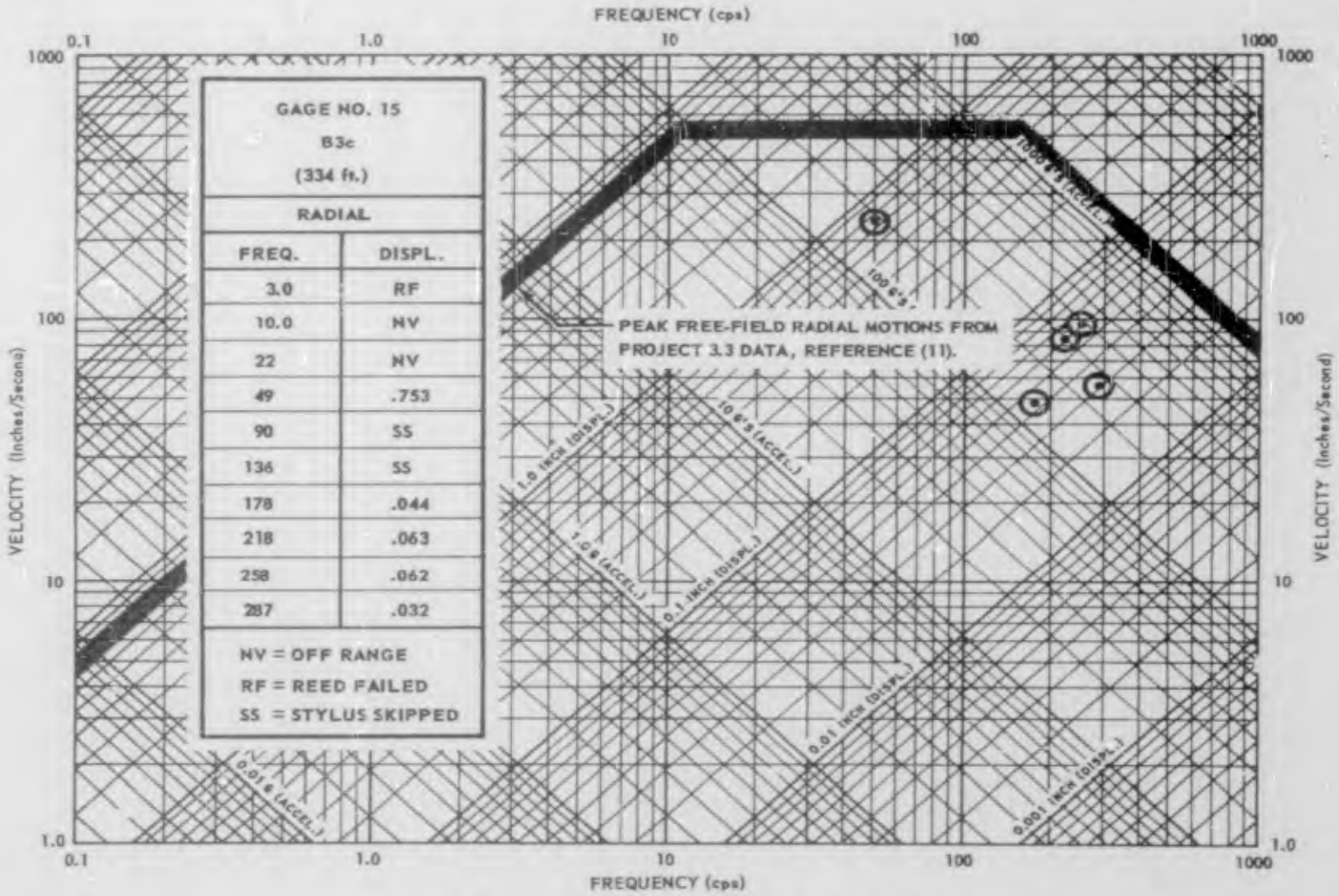

Figure 3.135 B3c, shock spectra (STL).

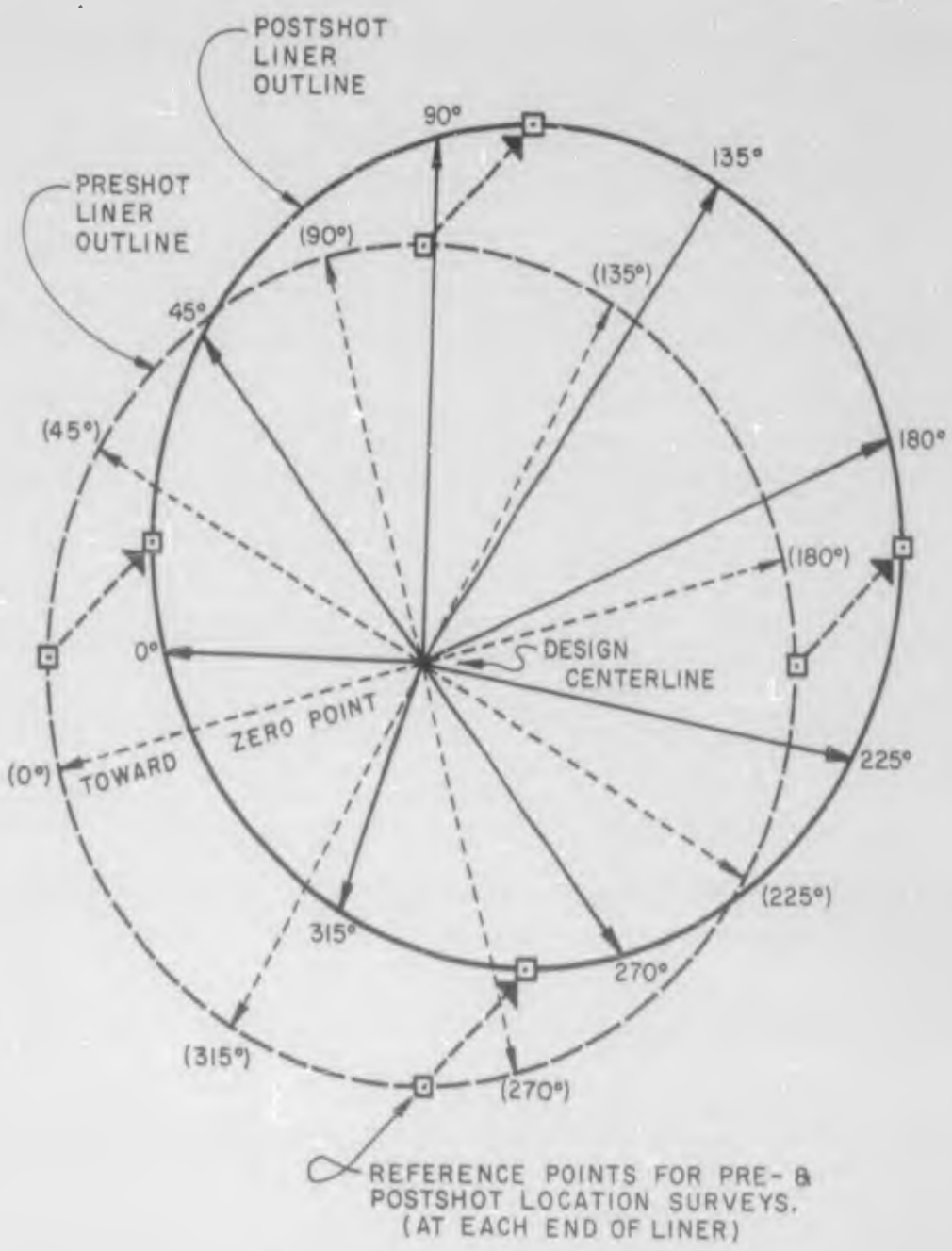

Figure 3.136 Survey methods for liner deformation and translation.

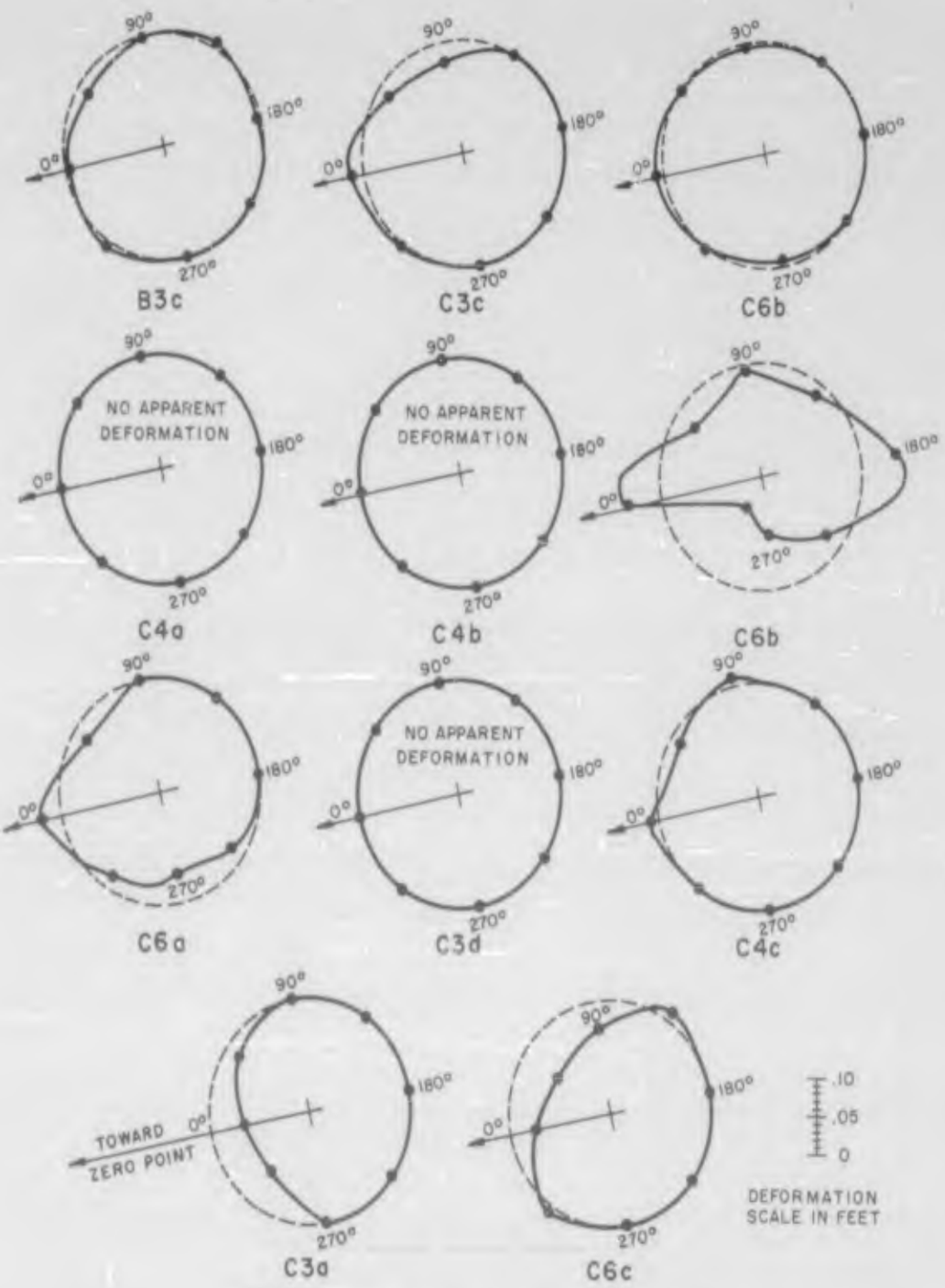

Figure 3.137 Exaggerated liner shapes.

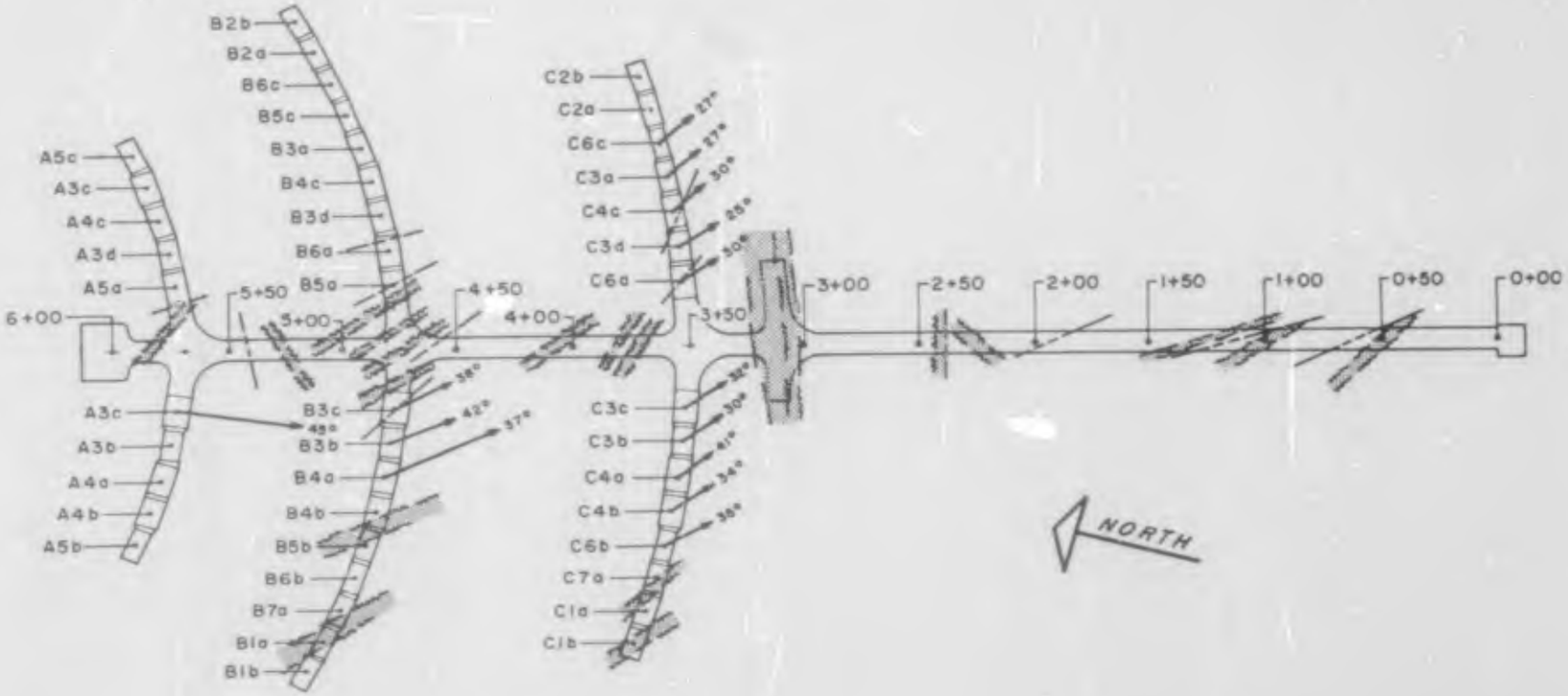

Figure 3.138 Translation of liners (plan view).

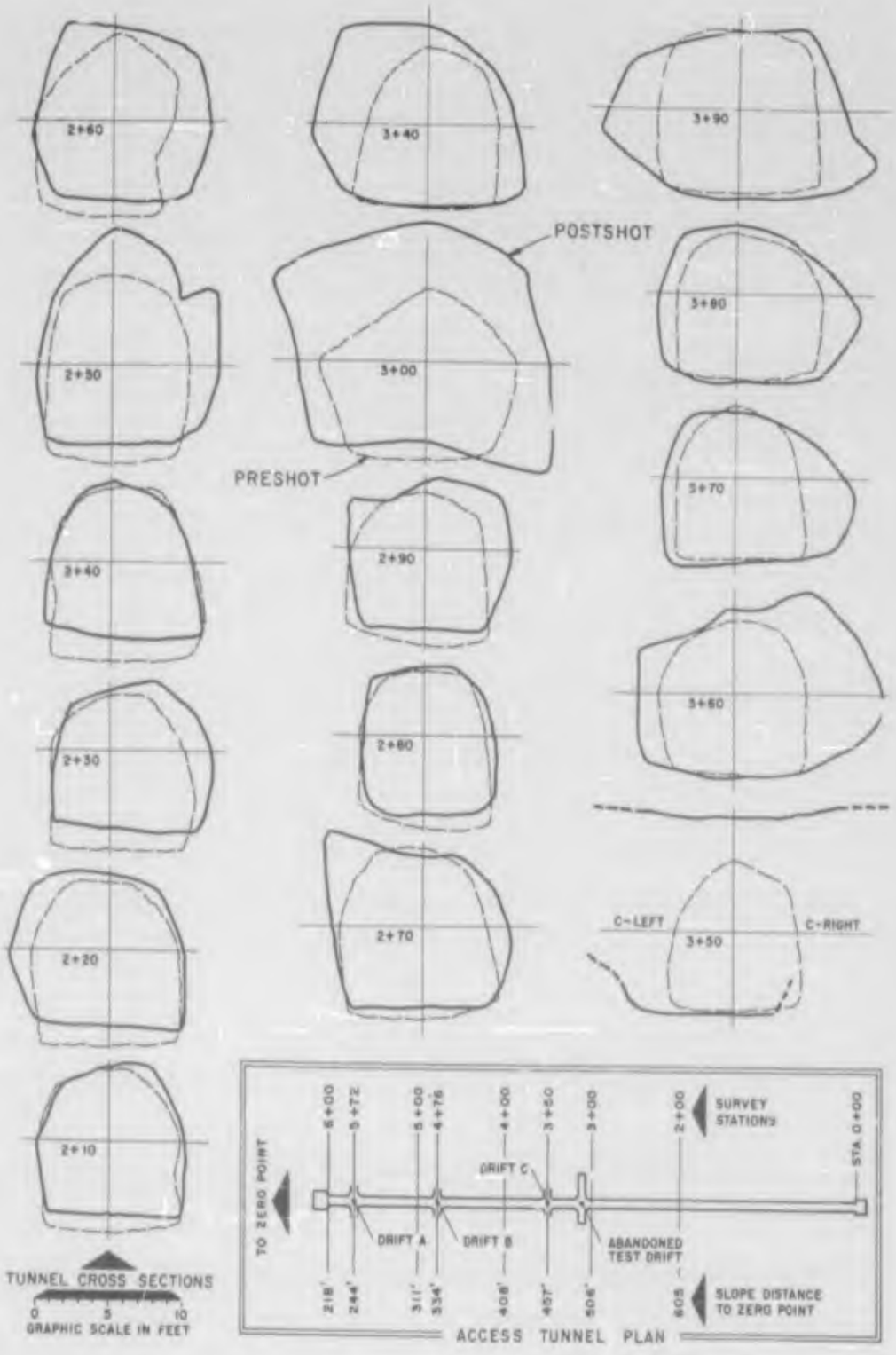

Figure 3.139 Access tunnel cross sections.

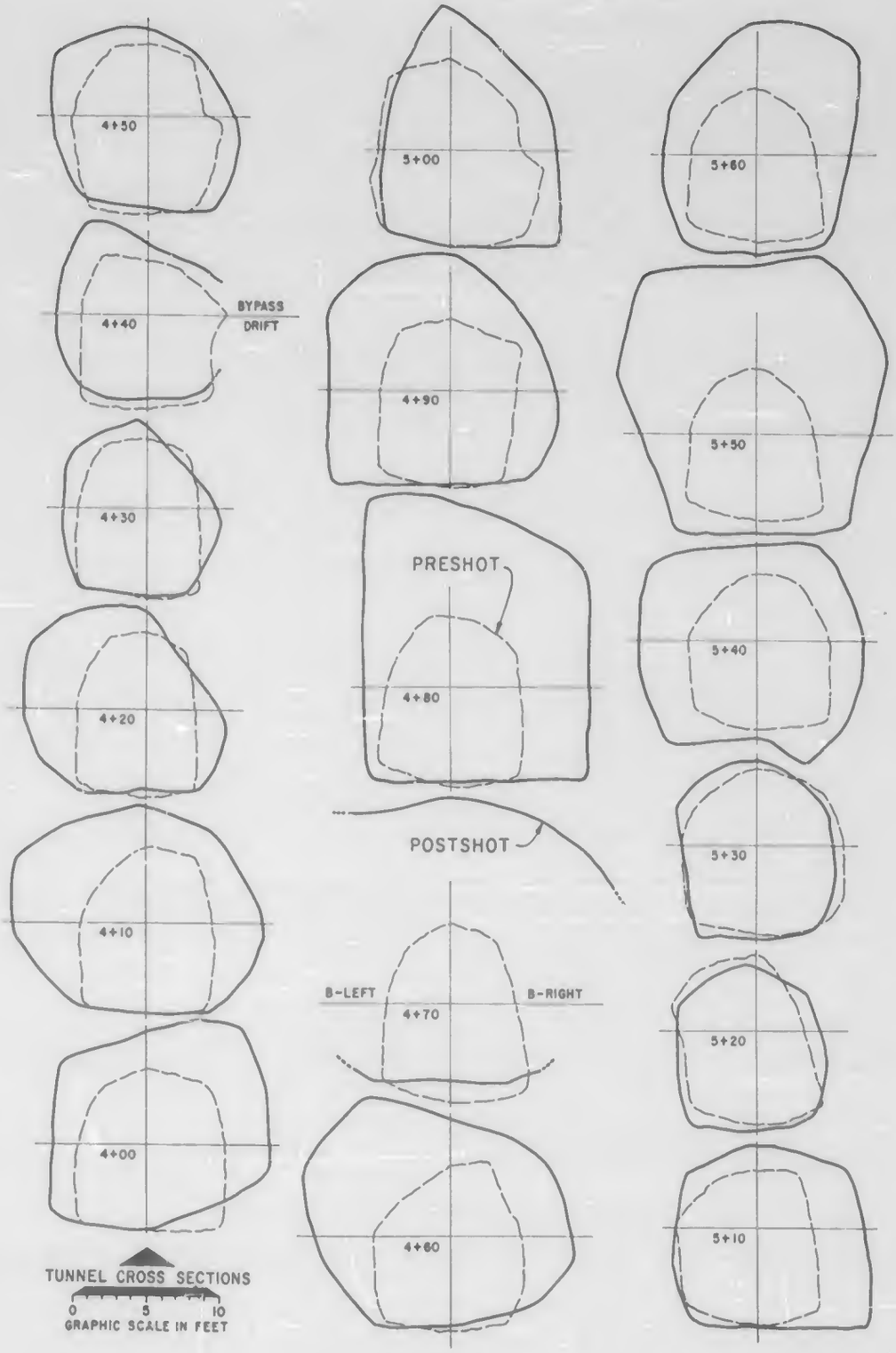

Figure 3.139 Continued.

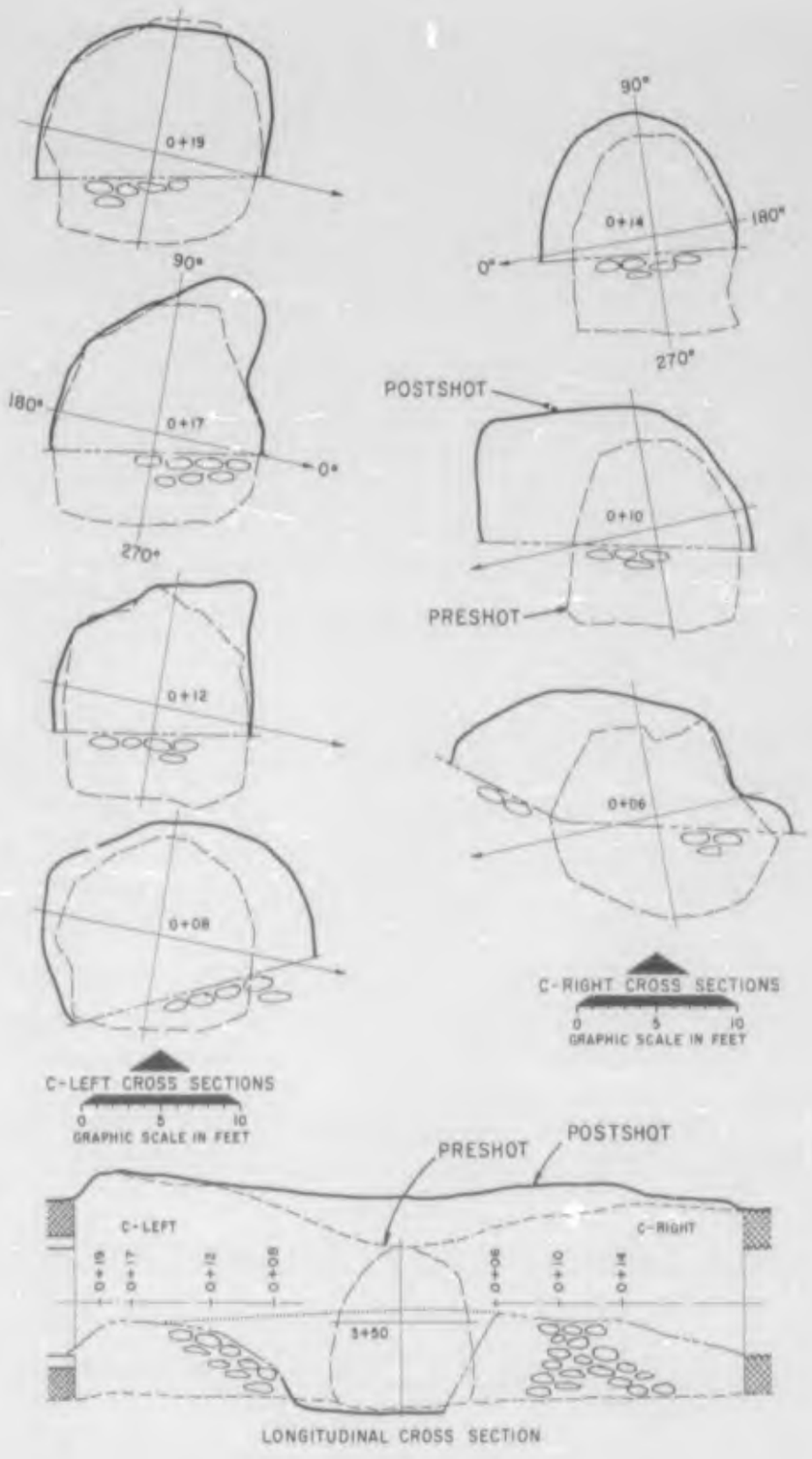

Figure 3.140 Cross sections, C Drift transition zones.

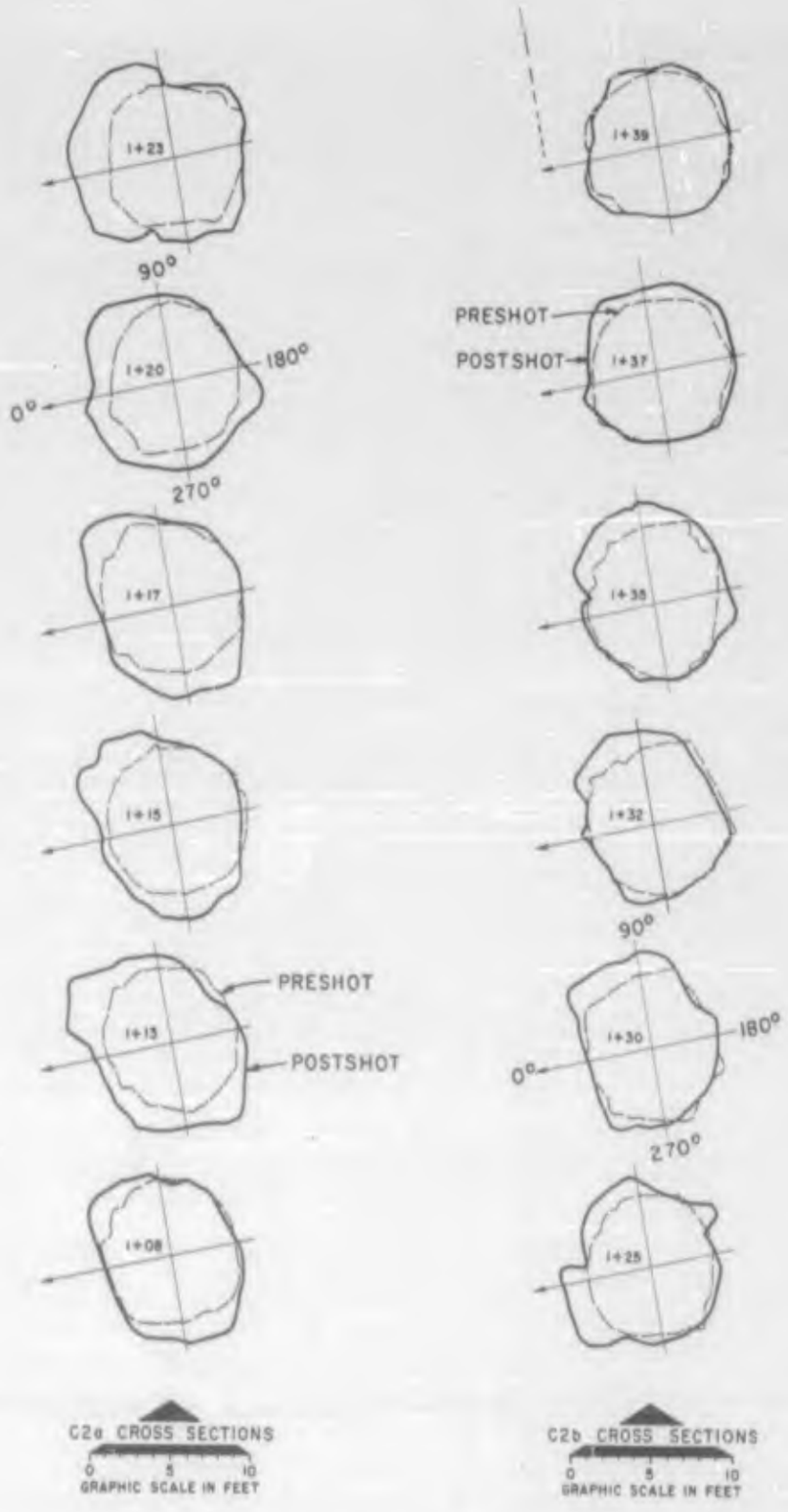

Figure 3.141 Cross sections, C2a and C2b.

SECRET

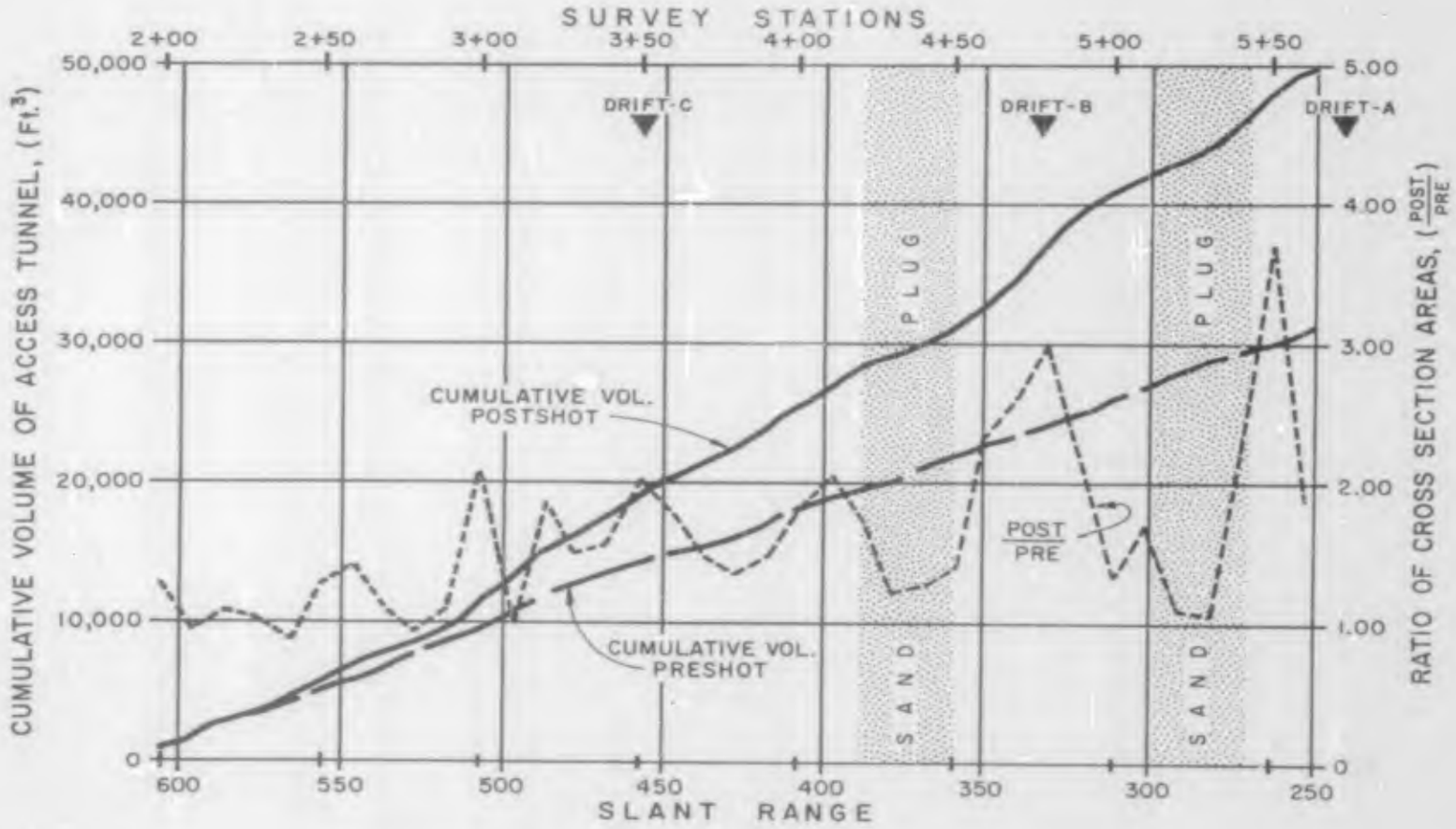

Figure 3.142 Access tunnel rock breakage.

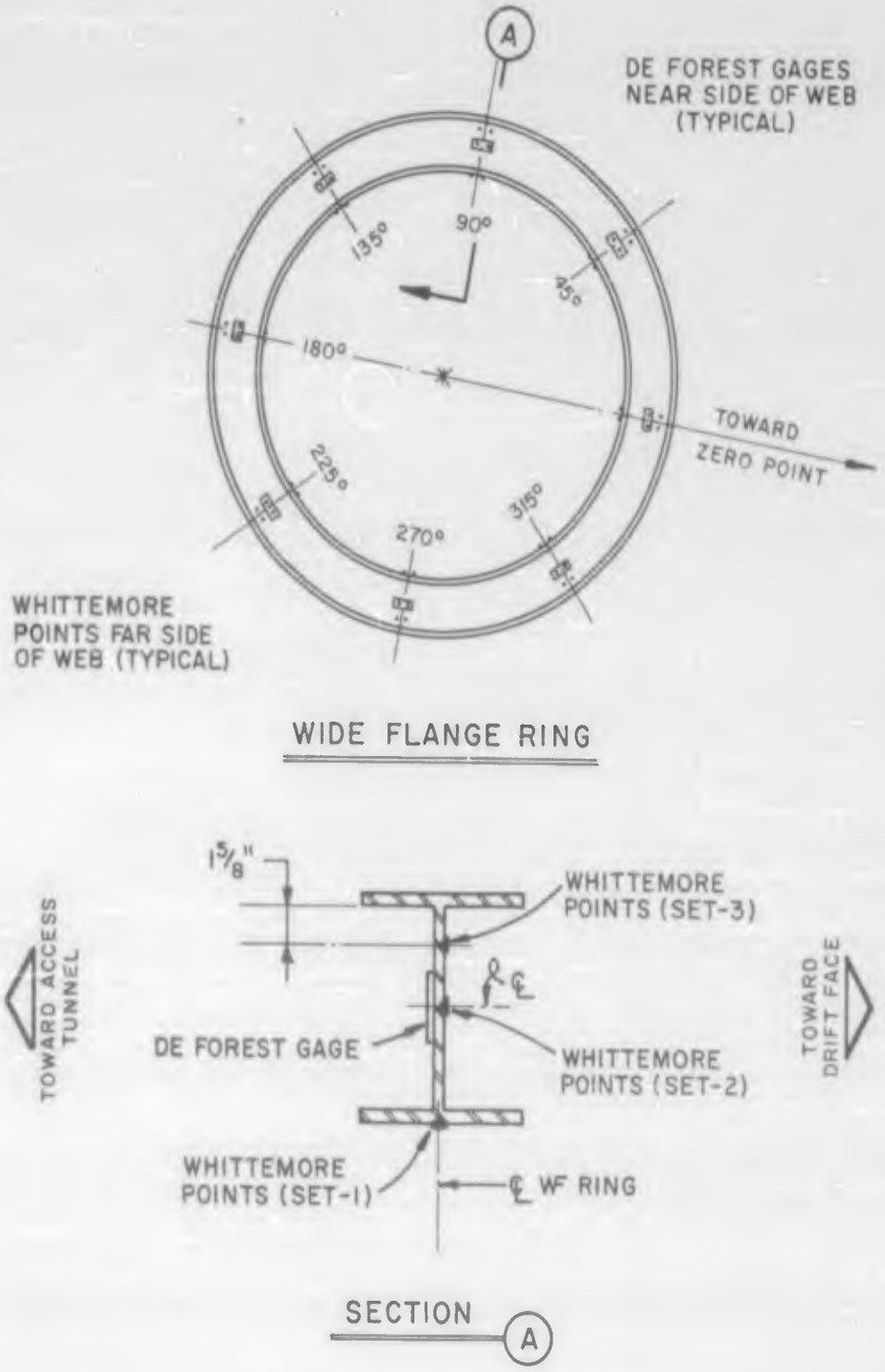

Figure 3.143 Locations of Whittemore measure points on wide-flange rings.

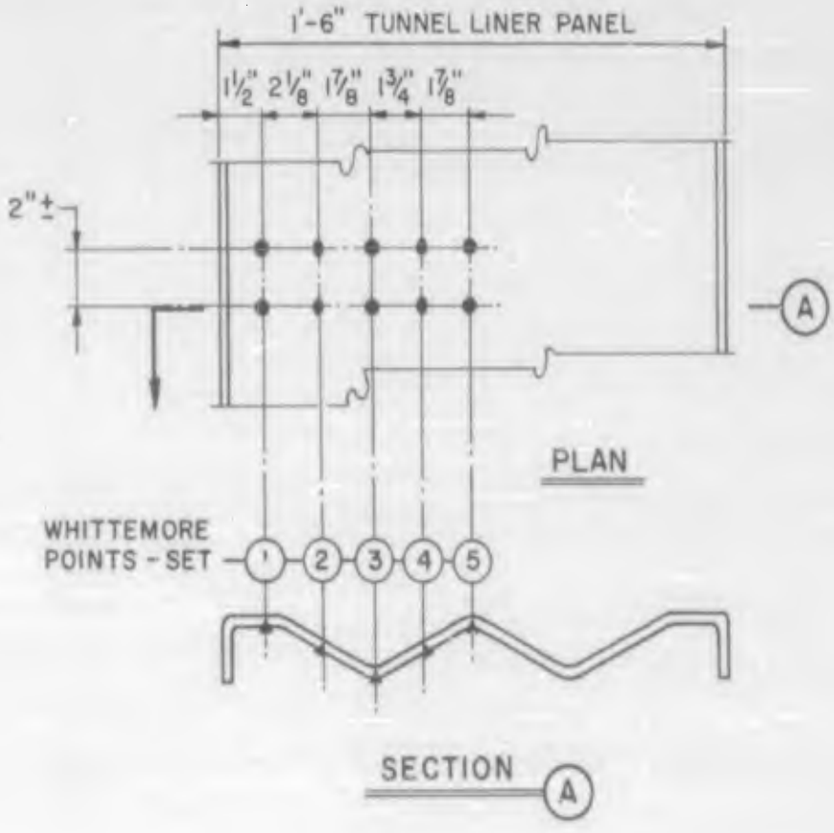

Figure 3.144 Locations of Whittemore measure points on tunnel liner panels.

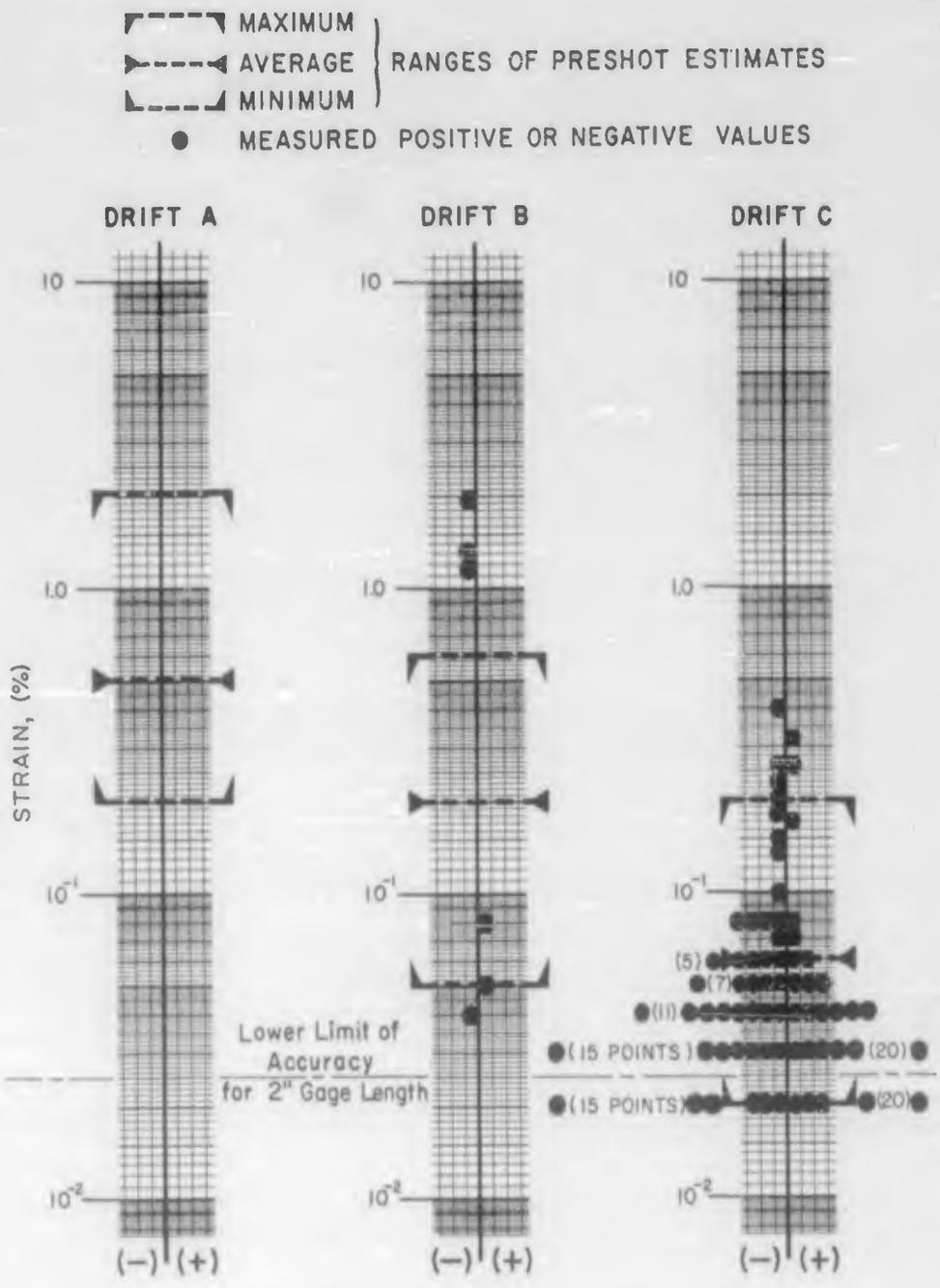

TEST DRIFTS	A	B	C
GAGES INSTALLED	199	477	204
RECORDS RECOVERED	0	7	196

Figure 3.145 Circumferential strain in lining (static).

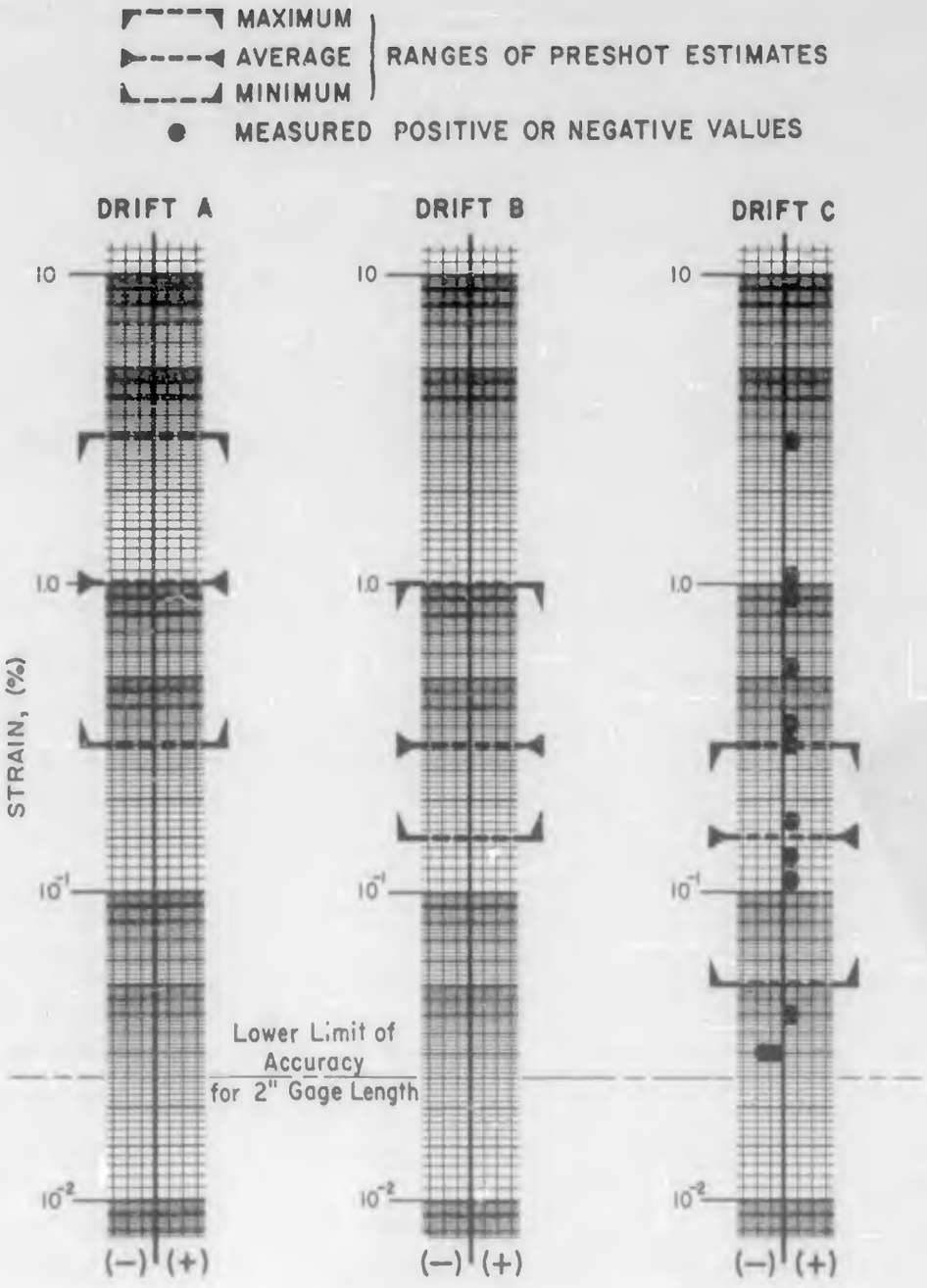

TEST DRIFTS	A	B	C
GAGES INSTALLED	16	16	16
RECORDS RECOVERED	0	0	16

Figure 3.146 Longitudinal strain in lining (static).

CHAPTER 4

DISCUSSION

4.1 INTERPRETATION AND SIGNIFICANCE OF DATA

Chapter 3 presented the preliminary data from several projects in Program 3. These data consisted of both physical damage observations and instrumentation results. Generally speaking, the effects of the explosion were approximately consistent with pre-shot estimates, although the quantity of data fell below expectation. The principal factor which reduced the quantity of usable data was the excessive damage in B Drift.

Several conditions contributed to the increased damage in all the test drifts. First, the yield of the Hard Hat detonation exceeded that planned by about twenty percent, i.e., 5.9-kt vs. 5-kt anticipated yield. Second, the slant ranges to the test drifts from the shot point were less than originally planned, as follows:

	Planned	Actual
A Drift	250 feet	244 feet
B Drift	350 feet	334 feet
C Drift	500 feet	457 feet

Third, the rock encountered at the project site was not as competent as assumed in the experimental design.

All of these conditions contributed to the increase in the anticipated damage at the test drifts. This resulted in greater difficulty in re-entry for damage observations. It also damaged gages, which limited the recordings to early time responses in many cases.

As pointed out in Section 2.2, the instrumentation plan was designed to obtain as much information on liner response as possible with a rather limited number of electronic gages. The success of the plan was contingent upon a high recovery of data from the available gages.

A review of the preliminary response data revealed that sufficient data were not recovered in any one test section to adequately define the transient response of the test section opening or liner. Several factors precluded the possibility of making even limited quantitative analyses of response. These were: (1) heavy damage to electronic gages and cables resulting in serious loss of data from even the most fully instrumented test sections, (2) the significantly different modes of response of the various liner types precluded the possibility of extrapolation of data between liner types, and (3) the

unexpected modes of liner response produced an orientation mismatch between the axes of instrument location and the areas of maximum liner response.

There was, however, a sufficient quantity of qualitative data which, supplemented by the quantitative data, permits the transient response of the test sections and of the access tunnel to be reasonably well inferred. Accordingly, the following subsections present interpretations of response based upon recorded data and observations of damage.

4.1.1 Mode of Response.

Access Tunnel. The damage profile of the main access tunnel, shown in Figure 3.7, was distorted by the presence of the two sand plugs, two drilling alcoves, drift intersections, and several fault zones along the access tunnel. If one were to discount the influence of these discontinuities, the damage-distance relationships for the access tunnel would be approximately as shown in Table 4.1.

A comparison of the observed limits of the damage zones (reduced by cube root scaling to a yield of 5.0 kt) with the estimated ranges of damage,

shows that there was close agreement for Zones 3 and 4. The somewhat greater observed limits for Zone 2 and the Point of Closure might have been influenced by the jointed nature of the granite.

The Lawrence Radiation Laboratory (LRL), University of California, is currently conducting a program of cavity exploration which includes extension of the original access tunnel from Station 6+16 to the boundary of the collapse chimney encountered at Station 7+31. The preliminary results of this work are given in Reference 18. An examination of the access tunnel extension revealed that the rock, although disturbed, was sufficiently competent that no support sets were required. It was also noted that the crushed zone in the free-field had not been encountered even though the exploration tunnel at Station 7+31 was approximately 115 feet from the zero point. Therefore, it is evident that no part of the original tunnel complex was within Zone 1.

The percentage of access tunnel rock breakage, in terms of the original cross sectional area,

versus the slant range to the zero point is shown in Figure 4. 1. The data points representing the drill alcoves, the drift intersections, the fault at abandoned C Drift, and the sand plugs are identified so that the influence of these discontinuities on tunnel damage can be readily compared. The breakage data points from the unlined circular test section, C2a and the inferred breakage for B2a are also plotted for comparison.

It can be seen that the fault zone at the abandoned C Drift and the test drift intersections have enhanced the amount of damage along the access tunnel. The effect of the alcoves on breakage, however, is not known because of insufficient data points. The two sand plugs were effective in reducing the tunnel damage where they were located in the access tunnel.

Comparison of the data from the access tunnel with those obtained from the test drifts indicates that the rock breakage appears to be of the same order. It might be concluded that the orientation of the opening did not have a material effect on rock

breakage quantities although the modes of failure may have differed for the two orientations. Therefore, it is believed that the data in Figure 4.1 can be used for purposes of estimating rock breakage quantities for circular tunnels oriented either parallel or perpendicular to the direction of stress wave travel.

Generally speaking, the breakage appears to vary as the inverse cube of the slant range at close-in ranges but drops off rapidly beyond Zone 3. This attenuation rate of three for breakage is somewhat larger than the attenuation rates for free-field particle velocity (2.4) and stress (2.5) but smaller than the rate of attenuation for acceleration (5.1), shown in Figure 3.115.

The peak values of strain measured around the access tunnel at Stations S and T were tabulated in Table 3.3 and shown in Figures 3.116 and 3.117. The stations were located within the two sand plugs. The amounts of tunnel breakage at these two stations are given in Figure 4.1. It can be seen that breakage at the closer-in Station S was approximately 5

percent while that at Station T was approximately 22 percent. This inconsistency in breakage quantities at the two stations may be a significant factor in the observed differences in the sign and magnitude of recorded strains at these two stations. The variations in geology and degree of sand plug compaction may have contributed to the differences in strain distribution and tunnel response.

The readings around Station S are characterized in the strain records by instantaneous peak values, whereas the peak readings around Station T are extensive plateaus. Although the records at Station S were less than 30 msec and at Station T generally less than 200 msec in duration because of cable breaks, it is believed that the transient strain records reflect the postshot condition and extent of breakage around an opening filled with sand.

Test Sections. The observed deformations of the drift opening, the backpacking, and the liner were not generally symmetrical about the

0^{o} to 180^{o} diameter. In all test drifts, the major axis of the damaged postshot drift opening was generally oriented in the 70^{o} to 250^{o} direction. Also, the measured directions of test section translation were at steeper vertical angles than would have resulted from truly radial translations. Table 3.7 shows that the liners in all drifts were translated at vertical angles from sixteen to thirty degrees steeper than the theoretical angles. These asymmetrical effects may have been influenced by the geological environment of the project site.

The extent of the crushing of the backpacking was a function of the drift location and the type of liner supporting the backpacking. In A Drift the long axis of the ovalled backpacking was oriented approximately parallel to the 70^{o} to 250^{o} diameter. In B Drift the long axis was approximately 120^{o} to 300^{o}, while in C Drift the long axis was approximately 160^{o} to 340^{o}. The ovalling and distortion of the liner were found to be a function of the liner's strength relative to that of backpacking material.

For a rigid liner (reinforced concrete), the distorted shape was usually similar to the crushed shape of the backpacking. For a flexible liner, such as the tunnel liner plates, the liner collapsed by telescoping or buckling of the plates, depending on the relative strength of the bolts to the liner plate. For these cases, the backpacking could not develop its full crushing strength.

The performance of the unlined test sections, the concrete liner cast against rock, and the horseshoe-shaped sections was poor in comparison with the sections with backpacking. In many cases, severe floor heave was observed in these test sections. For this reason no direct comparisons of response could be made between the horseshoe-shaped test sections included in this project and those tested in Hardtack - Phase II projects. Several test sections with backpacking in B Drift also exhibited some upheaval of the floor, but not quite as severe. Generally speaking, the quadrant between 90° and 180° remained the least damaged at all ranges.

The rock breakage and resulting floor upheaval in the test drifts might be due to a combination of crushed material from stress concentrations at approximately 250° and broken rock from the vicinity of 340° as depicted in Figure 4.2.

Based on the observed damage of the test sections, the response of a liner is a function of the relative effects and magnitudes of the following parameters:

(1) the rock breakage from the zero point side (fly-rock);

(2) the rock breakage from stress concentrations at approximately 90° and 270° (crushing);

(3) the motion of the drift opening as a whole (translational);

(4) the presence of asymmetrical phenomena, such as non-ideal translation (anomalous);

(5) the dynamic characteristics of the backpacking material (decoupling); and

(6) the dynamic strength characteristic of the liner (response).

The influence of the first four parameters with respect to loading on the backpacking is generalized in Figure 4.2. An infinitely stiff liner with backpacking was chosen to illustrate the effects of the fly-rock, the crushed rock, and the translation, on the backpacking. In A and B Drifts, the effects of fly-rock and crushed rock are assumed to be the dominant parameters. In C Drift, the effect of crushed rock is assumed to be the dominant loading parameter. Qualitatively, the observed distortion of the backpacking is approximately consistent with the concept of loading shown in Figure 4.2. Removal of liners to determine rock breakage patterns around the various openings would be necessary to define the loading quantitatively.

The observed effects for each test section were given in Section 3.2 in terms of backpacking and liner response. To summarize the damage description given therein, Table 4.2 shows the

damage-distance relationship for each of the liner types tested. It can be seen that the response of the test liners changes rapidly as a function of range, varying from heavy damage to light damage with a relatively slight change in range.

The test section design, based on a strength compatibility of the backpacking and liner (see Subsection 1.4.5) was shown to be a valid concept. The rigid liners with backpacking clearly demonstrated the value of this type of structural system in maintaining the integrity of an opening in rock under severe loading conditions. Correlations between loading and response were not possible because of the limited recovery of transient response data and the need for additional information on rock breakage around lined test sections. As an interim design procedure, however, it appears that providing an ample thickness of a relatively weak backpacking material, together with a rigid tunnel liner (as outlined in Subsection 1.4.5), gives nearly the required strength. Some extra liner strength should be

provided to account indirectly for the transient effects not fully evaluated at this time. Also, the thickness of the backpacking should be sufficient to prevent locking of this material from tunnel opening translation and deformation and from rock breakage. The rock quantities and velocities involved may be estimated by consideration of the data given in Figures 3.115, 4.1, and 4.2.

4.1.2 Influence of Range on Shock Parameters, Response, and Shock Spectra.

Shock Parameters. A comparison of the free-field measurements with the preshot estimates was shown in Figure 3.115. It can be seen that the measurements were approximately equal to the postshot estimates. Since it appears that the increase in detonation yield and the lower granite competency did not have any great influence on the recorded shock parameters, it would seem that these factors were compensating. However, this cannot be considered conclusive because of the uncertainties in estimating shock parameters. The recorded

shock parameters do approximately verify the rate of attenuation assumed for acceleration, velocity, stress, strain, and displacement as a function of range.

Response. The observed damage in the test sections shows that their response changed rapidly with range. The response was characteristic of that of ductile structures under dynamic loadings of long duration,(i.e., after general yielding the response tended to be relatively sudden). This behavior was particularly evident in the unlined test sections and the reinforced concrete liners cast against the rock. The liners with backpacking fared better because of the ability of the filler material to absorb some shock and to accommodate distortions. However, once a liner reached a certain level of response, the damage to the liner was significant. In terms of protection, this means that the damage to a given liner type with backpacking changes abruptly from heavy to light damage with a relatively small increase in range. The zones of extremely heavy damages and

of light damage would be broad, and the zone in which intermediate (moderate) damage takes place would be relatively narrow. Hence, care should be taken in extrapolating directly the observed and empirical results, particularly in the zone of moderate damage.

The results from the STL displacement shock spectra measurements were shown in Figures 3.124 through 3.135. Generally, only the higher frequency reeds were effective in obtaining readings. The data for the lower frequency range were generally not obtained for reasons noted in these figures. Trapezoids representing peak values of measured free-field radial displacement, velocity, and acceleration were shown for comparison of the peak radial inputs with the recorded gage response in the vertical and radial directions. The radial input motions were used throughout, because no vertical input data were taken at the ranges of the test drifts.

It can be seen that the trapezoids (free-field inputs) had formed an upper bound for all the shock spectra measurements taken in the tunnel liners with foam backpacking in B and C Drifts. However, the trapezoid for C3a (concrete liner cast directly against the rock) fell below the recorded data points. It should be noted that the shock spectra recorded in C3a had the highest readings recovered in this project. They are approximately a factor of two greater than those recorded in B3b where the liner damage was much greater than at C3a. This would indicate that the backpacking material was of significant value in attenuating the higher frequency shock transmitted to the concrete liner; however, these spectra did not reflect the extent of damage to the liner.

The shock spectra data points from liners with backpacking in C Drift (Figures 3.129, 3.130, and 3.132) fell only slightly below the trapezoid, whereas the data points obtained in B Drift (Figures 3.133, 3.134, and 3.135) fell significantly below

the trapezoid for B Drift. A possible reason for this difference in attenuation is the yielding or plastic deformation of the foam backpacking in B Drift. The foam backpacking in C Drift (sections C3b, C3c, and C4b) apparently behaved elastically; whereas the foam in B Drift (sections B3b and B3c) deformed plastically, thereby providing greater attenuation. The plastic yielding of the foam is effective in limiting the shock loads transmitted to the liners because this yielding takes place under an essentially constant stress. Hence, the shock transmitted through a foam which is deforming plastically below locking is only slightly stronger than shock transmitted through the same foam which is deforming elastically just below the yield point. Thus, the degree of shock attenuation for a given backpacking material is a function of the amount of deformation of the backpacking which takes place during the loading. The greater deformations result in a greater attenuation of shock transmitted through the backpacking.

From the data obtained in the liners backpacked with foam in B and C Drifts, the radial shock spectra (high frequencies) varied approximately as the inverse square of the range, whereas the free-field acceleration attenuated approximately as the inverse fifth power of the range. This difference in attenuation rates may be accounted for by the greater reduction in shock transmitted through the backpacking behaving plastically as mentioned in the previous paragraph.

With regard to the attenuation of shock spectra in the access tunnel, it was found from the three vertical component reed gages installed at ranges of 457 feet, 723 feet, and 1,340 feet that the shock spectra was attenuated as the inverse fourth power (or slightly less) of the range. Comparison of the vertical component reed gage results with the trapezoid (peak radial motion input) shows that the shock spectra data fell approximately in line with the trapezoid. It appears, therefore, that the vertical shock spectra is of the same order and

has approximately the same attenuation rate as the radial input parameters. The correlation of the radial component reed gages at 457 feet and 723 feet with the radial input trapezoid was not as well defined. The data points at the 457-foot range were somewhat below the trapezoid and the data points at the 723-foot range were somewhat above. This indicates that the access tunnel radial shock spectra attenuated at a lower rate than the corresponding vertical shock spectra. In an absolute sense, the vertical spectra are greater than the radial spectra at the 457-foot range, whereas the vertical spectra are slightly lower than the radial spectra at the 723-foot range. The attenuation of the radial shock spectra between 457 feet and 723 feet appears to be approximately proportional to the inverse square of the range. This attenuation rate is approximately the same as the attenuation rate for the radial shock spectra measured in the tunnel liners.

4.1.3 Influence of Backpacking on Response.

Types. There was little difference in the amount of damage between liners backpacked

with comparable thicknesses of foam or cinders. Comparison of liners with backpacking against those without backpacking (concrete liner cast against rock) shows that the former suffered significantly less damage. The shock spectra (radial component) appeared to be reduced by a factor of about four when foam backpacking was used. Because no shock spectra records were recovered from liners with cinder backpacking, no inferences can be drawn on the relative effectiveness of cinder and foam for shock spectra attenuation.

Thickness. There was a considerable difference in the observed damage to the test liners for different thicknesses of foam backpacking. The thicker foam appeared to reduce liner damage considerably. However, the measured shock spectra (radial component) in these test sections were about the same regardless of thickness. This could be explained as follows. The recovered shock spectra are mostly in the high-frequency range, above 100 cps. The damage, however, is probably more

sensitive to the lower frequencies where no data were obtained because of reed damage. It is considered possible for the higher frequency measurements to be approximately equal and, at the same time, for the observed damage to be significantly different.

Construction. Two methods for placement of the foam backpacking were used in the construction of the test sections, i.e., a cast-in-place method and a precast method. Several differences in the backpacking properties resulted. The precast foam units were thinner than the corresponding cast-in-place foam. Also, laboratory test samples indicated that the precast foam was somewhat stronger than the cast-in-place foam as shown in Tables 1.7 and 1.8. Another notable difference was continuity; the precast foam had gaps between units, whereas the cast-in-place foam was monolithic. The test results have not indicated any strong evidence of differences in the response, although it is believed that the cast-in-place foam might have had some

advantages in its greater thickness, lower strength, and continuity.

4.1.4 Influence of Liner Type on Response.

Liners with Backpacking. Three basic liner types were tested with foam or cinder backpacking. These types were designated as (1) rigid, (2) flexible, and (3) rigid-flexible. The mode of loading on all liners in a given drift was about the same. However, the extent of damage varied considerably for the different liner types because of their different response characteristics. In terms of survival, the best type was the rigid liner (reinforced concrete). The degree of damage to both the flexible liners (tunnel liner plate) and rigid-flexible liners (wide flange rings with lagging) was about the same.

Unlined Sections. Two types of unlined test sections were tested: (1) bare rock and (2) openings reinforced with rock bolts and mesh. The rock breakage patterns around these two types of test sections were about the same, although there

was less apparent damage in the test section with rock bolts and mesh. The principal weakness in the test section lined with mesh was the failure of the mesh at the rock bolt bearing plate. No failures of the rock bolts were observed. Since the expanded metal mesh that was used had only nominal strength, the full value of the bolts was not developed. A mesh of greater strength, flexible enough to conform to surface irregularities, would probably have been materially more effective in containing the broken rock.

Reinforced Concrete Liners Cast Against Rock. A comparison of the reinforced concrete liners cast against rock with the concrete liners with backpacking shows that the former sustained more damage than the latter. In C Drift, the recorded shock spectra in the liner cast against rock, C3a, exceeded the recorded effects in the similar liners with backpacking by a factor of about four. As mentioned earlier, the recorded shock spectra in C3a were of greater magnitude than any of the spectra data recovered for this

project. Hence, it is believed that the effectiveness of a backpacking material in reducing the high-frequency components of shock spectra has been demonstrated.

Horseshoe-Shaped Sets. This type of tunnel liner is more vulnerable to such effects as local faulting and floor heave than the basic liner types. It has limited application to protective construction because of its directional strength properties.

4.1.5 Influence of Site Geology on Response.

The damage to tunnels without liners was markedly affected by local variances in rock competency. Within areas of local faulting, rock breakage and tunnel collapse were substantially more severe than in adjoining areas of more competent rock.

The influence of geologic defects on response was more evident in the unlined than in lined test sections, because the effects of such discontinuities and weaknesses were readily observed from the rock breakage. In the lined test sections, rock breakage had to be inferred.

Another indication of the influence of geology on response is the parallelism of the horizontal components of liner translation with the northwesterly trending fault system as shown in Figure 3.138. The contribution of the geologic environment to the vertical components of liner translation was not as obvious. Other factors, such as stress relief in an upward direction (to the surface), might also have influenced the vertical angle of translation.

4.1.6 Influence of Opening Configuration on Response.

Orientation. Comparison of the measured rock breakage around the access tunnel (oriented approximately parallel to the direction of shock) with that of the test drifts (oriented perpendicular to shock direction) revealed no obvious difference in degree of damage with opening orientation. Hence, it was suggested previously in Subsection 4.1.1 that the breakage data obtained from the access tunnel are applicable to either tunnel orientation.

Shape. The primary purpose of including square, unlined test sections in B and C Drifts was to permit the comparison of response of square and

circular openings. Unfortunately, the extensive damage to all test sections in B Drift and the anomalous failure of the square test sections in C Drift, due to incompetent rock, resulted in a complete loss of data for comparison. In addition, the electronic strain data recovered from the unlined test sections in B Drift were incomplete. Therefore, no conclusion can be made as to the influence of shape of opening on damage.

Size. The two transition zones of C Drift and Test Sections C2a and C2b afforded the most direct comparison of tunnel diameter with response. These four openings were at the same range from zero point, circular in shape, and in equally competent rock. The transition zones at C Drift left and right were nominally 11-1/3 and 10 feet in diameter respectively, while C2a and C2b were 8 feet.

The type of damage of all four openings appeared to be the same; i.e., the maximum rock breakage apparently occurred at 70° and at 250°.

Also, the percentage of area increase due to rock breakage was about the same as can be seen by comparing Figures 3.140 and 3.141. It is therefore apparent that within the range of tunnel sizes compared, there were no appreciable differences in response.

4.1.7 Influence of Construction on Response.

Materials. Construction materials of uniform and known strength properties were specified for the test sections in this project. This was done to minimize the number of variables affecting the response, thereby simplifying analyses. The properties of the materials used in the test section construction were tabulated in Tables 1.7 through 1.12. From the experimental standpoint, it appears that the desired properties and uniformity were obtained.

Construction. The quality of construction plays an important part in the integrity of any structure. It is particularly important in test projects

where laboratory standards are desired under field conditions. Pre- and postshot examinations of all test sections indicated that a high quality of construction was exhibited throughout the project. There was no evidence of premature or anomalous failures attributable to poor fabrication or assembly of liners and liner components.

4.2 EVALUATION OF TEST RESULTS

4.2.1 Reliability of Test Data.

Transient Measurements. Test Section Response Measurements, Project 3.2 (SRI).

This project obtained 68 records from the 108 channels installed (Table 4.3). The peak values were presented in Table 3.1. Figures 3.105 through 3.113 are graphs showing the data points, type of measurement, and test drift locations. The preshot estimates given in Table 1.4 are indexed on these figures for reference purposes. It can be seen that the majority of measurements fell within the preshot estimates. Most of the remainder

fell below these estimates with only a few data points higher than the estimated maxima.

As mentioned in Chapter 3, many of the gages and gage mounts were found to be loose or damaged. This damage might have caused some spurious responses. Whether this had any material effect on the reliability of the recovered data has not been evaluated.

Particle Motion Measurements, Project 3.3 (SC). The peak values of the free-field measurements made by Project 3.3 were presented in Table 3.2. A comparison of this data with the preshot estimates (Figures 1.6 and 1.7) was shown in Figure 3.115. In general the free-field data and the preshot estimates made for this project agree. It is considered that these data are reliable.

The peak values of strain measured around the access tunnel at two stations were presented in Table 3.3 and in Figures 3.116 and 3.117. These data were interpreted in Subsection 4.1.1. Although

the records from the two stations are not consistent with each other in that the strains measured in comparable holes were often not of the same sense, these variances might have reflected the differences in tunnel response resulting from differences between geologic and sand plug structure of the two stations. However, it is noted that the data points from Stations S and T are generally consistent in that the recorded peak compressive strains are numerically of the same order as the free-field strains, while the peak tensile strains are approximately an order of magnitude greater than the free-field strains. Therefore, the data from this instrumentation are considered reliable.

Fly-Rock Photography, Project 3.11 (EG&G). No data were obtained from this project because of the damage to cameras and the radiation exposure of the film.

Mechanical Measurements.

DeForest Gage Data. The records of circumferential strain from the gage targets were

reproduced in Figure 3.119.

The peak values of strain from these records were plotted in Figure 3.118. It can be seen that most of the peak values of strain for liners in C Drift were within the upper values of the pre- shot estimates. The residual circumferential strains in C Drift as determined by Whittemore gage measurements, Figure 3.145, were concentrated within the lower values of the preshot estimates. Because the Whittemore gage measurements are residual strains, while the deForest gage data represents peak strains, the data from these two types of measurements appear to be consistent and the deForest gage records recovered are considered reliable.

Diameter-Change Scratch Gage Data.

The results from the diameter-change scratch gages were given in Tables 3.4 and 3.5. Most of the vertical (90° to 270°) gages were bent toward the zero point, and the horizontal (0° to 180°) gages were bent downward. The amount of residual bending was given previously in Subsections 3.2.1 and 3.2.2,

where the postshot description of each test section was presented. The values shown in Tables 3.4 and 3.5 are the measured scratch lengths and do not reflect corrections required to compensate for bending of the scratch gages.

The peak values of liner deformation as recorded by the diameter-change scratch gages were given in Figure 3.120. The preshot estimates are also indexed in this figure. Because it is not possible to account for the magnitude of errors induced in the records of first motion and peak displacement by gage vibration (bending), the reliability of these values is not determinable. On the other hand, the values of permanent liner deformation are considered reliable, because the corrections for residual gage bending are negligible.

Compression-of-Filler Scratch Gage Data.

The results obtained by these scratch gages were presented in Table 3.4 and 3.5. These data points were shown in Figures 3.121 through 3.123, together

with the preshot estimates. Although there was inherent difficulty in anchoring these gages in the rock, and it was impossible to inspect the anchorage, the gages that were recovered were in good condition. Therefore, it is believed that the results are reliable.

Reed Gage Data, Project 3.12 (STL).

The shock spectra data obtained by the reed gages were shown in Figures 3.124 through 3.135. These generally provided data points at the higher frequencies. Only a few data points were recorded at the lower frequency ranges. It can be seen that the data points are generally consistent between reeds and also between gages. It is, therefore, considered that the reed gage data are reliable.

Static Measurements.

Survey Data. Conventional surveying techniques were employed to determine liner deformation, liner translation and rock breakage around unlined portions of the access tunnel and test drifts.

In Subsection 3.3.5, it was pointed out that the deformations within many of the liners were of the same order as the order of accuracy of the survey. As a result, the liner deformation data obtained by the survey were not reliable.

The magnitudes of rock breakage and of liner translation were well within the limits of accuracy of the surveys. Therefore, the data from these surveys is considered reliable.

Whittemore Gage Data. The Whittemore gage data were given in Table 3.7 and plotted by test drift locations in Figures 3.145 and 3.146. The measurements were taken to three-significant-figure accuracy, and the strains were computed from these values. It is believed that the strain data are accurate, particularly those values indicating larger strains. It is considered that the computed strain data from the Whittemore measurements are reliable.

4.2.2 Effectiveness of Instrumentation.

Transient Measurements.

Test Section Response Measurements, Project 3.2 (SRI). A summary of the number of records recovered

versus the number of gages installed is given in Table 4.3. Data recovery exceeded 60 percent.

As discussed in Subsection 4.2.1, there was considerable damage to gages and gage mounts which may have affected the reliability of the records obtained from these gages. Other factors which reduced the effectiveness of this instrumentation were: (1) the anomalous mode of failure of the liners composed of tunnel liner plates, (2) the loss of critical data from the most completely instrumented liners which precluded extrapolation of data to less completely instrumented liners of the same type, and (3) the orientation mismatch between the instrumentation locations and the areas of maximum liner response.

Particle Motion Measurements, Project 3.3 (SC). The free-field measurements and access tunnel strain measurements obtained by this project were presented in Subsection 3.3.1. As stated previously, the free-field results compared favorably with the preshot estimates.

The free-field instrumentation was considered effective in providing basic input data for correlation with the observed response of the test sections and the access tunnel.

The strain measurements taken at the two stations with sand plugs along the access tunnel provided useful information on the magnitude and distribution of transient strains. This instrumentation was effective in providing a basis for correlation of the measured free-field effects with tunnel response.

Fly-Rock Photography, Project 3.11 (EG&G). The use of stereo cameras to record fly-rock phenomena was ineffective in this experiment. No data were obtained, primarily due to radioactive fogging of film and damage to cameras.

Mechanical Gage Data.

DeForest Gages. Of the 137 deForest gages installed to measure circumferential strain, 43 were installed in C Drift. Of these, 31 were recovered in place and intact. The balance were

either loose or were not found. Only four gages were recovered in B Drift. This low percentage of recovery was due to heavy damage of the test sections and failure of the bonding agent used to mount the gages. Although the records from the gages recovered are considered reliable, this instrumentation as a whole was ineffective because of the great loss of data caused by failure of the method of fastening the gages.

Diameter-Change Scratch Gages. Because of the question as to the reliability of the recorded first motions and peak displacements discussed in Subsection 4.2.1, these gages are not considered effective in measuring transient changes of diameter.

Compression-of-Filler Scratch Gages. As in the case of the diameter-change gages, the scratch marks on the compression-of-filler scratch gages often gave an indication of the first motion. Since it was not possible to inspect the portion of

the gage behind the liner, the overall condition of the gages was not determinable.

In several test sections, some evidence of rotation of the liner was noted; this rotation may affect the interpretation of the scratch readings. However, the compression-of-filler measurements are subject to fewer uncertainties than the diameter-change gage results. Therefore, the gages installed are considered effective in measuring compression of the filler.

Reed Gage Data, Project 3.12 (STL).

It can be seen from the reed gage shock spectra shown in Figures 3.124 through 3.135 that the reed gages were effective in obtaining results in the higher frequency ranges. However, they were ineffective in securing data at the lower frequencies.

Static Measurements.

Surveying. As pointed out in Subsection 3.3.5, the deformations of Liner B3c and of many of the liners in C Drift were of the same

order as the order of accuracy of the deformation survey. Also, because of the limited access through most of the liners in B Drift where sufficient deformation could otherwise be reliably detected, postshot cross sections could not be taken. As a result, the liner deformation surveys were not effective.

The liner translation and the rock breakage surveys, however, produced considerable quantities of useful data and are therefore considered to have been very effective.

Whittemore Gage Data. These measurements were a highly effective means of determining the residual strains in the accessible liners.

4.3 FULFILLMENT OF PROJECT OBJECTIVES

The experimental plan of using three test drifts placed within zones of anticipated heavy, intermediate, and light damage, together with placement of several types of liners at each drift, has achieved the desired range of damage on the structures. The results of the test permit a direct comparison of the basic types of

liners and depict experimentally the performance of each. The concept of using a compressible backpacking material between the rock wall and the liner for attenuation of damage and shock effects was verified, although the instrumentation data did not precisely define, in a quantitative sense, the manner of loading and response of the test sections.

From the observed test section responses, the loadings were inferred; however, the assumed rock breakage patterns (Figure 4.2) and quantities (Figure 4.1) behind the test liners have not been verified by actual inspection. A program for future removal of selected liners for such an inspection is planned but not accomplished at this time. Because the determination of the mechanics of tunnel damage has not yet been fully documented, the formulation of loading (in terms of scaled range, rock properties, physical dimensions, and other factors) has been deferred. For this reason, the correlation between the loading and the response must also be deferred. When all of the data become available, the general objectives of obtaining information on the mechanics of the tunnel damage and on the loading and structural response of tunnel liners will have been satisfied.

The information obtained relative to the stated secondary project objectives is summarized as follows:

(1) Damage-distance relationships (access tunnel). The amount of access tunnel damage as a function of range was shown graphically in Figure 3.7 and numerically in Figure 4.1. The measured free-field shock parameters were given in Figure 3.115. It can be seen that the attenuation rate for rock breakage is approximately the same as for free-field stress and particle velocity. This is approximately valid at ranges from heavy breakage (about 100 to 300 percent of the original cross section) to light breakage (about 20 to 30 percent of the original cross section). The breakage falls off rapidly beyond the vicinity of the elastic range (reported in Reference 11 to be at 735 feet). The correlation of the observed breakage percentage with the measured shock parameters provides the necessary test data for improving design and analysis procedure for re-entry facilities involving underground nuclear tests.

(2) Damage-distance relationships (test drifts).

The amount of rock breakage in Section C2a (unlined) was shown in Figure 4. 1. These data points are based on pre- and postshot cross sections shown in Figure 3. 141. No data were available from the unlined test sections in B Drift because of inaccessibility due to damage. However, the unlined test sections can reasonably be assumed to be closed, i. e., the breakage is in excess of 100 percent. Based on the data points from C Drift and the inferred breakage in B Drift, it can be seen that the breakage percentages of the unlined sections are approximately the same as those observed in the main access tunnel. Accordingly, it can be assumed that the degree of damage is not markedly a function of orientation of the drift or tunnel with respect to the point of detonation. Therefore, as a first order approximation, the relationships for breakage versus range shown in Figure 4. 1 are considered applicable to both the access tunnel and the test drifts.

(3) Range at which liner is required. A summary of the damage-distance relationship for all test sections was given in Table 4.2. The damage-distance relationship for the access tunnel was given in Table 4.1. It was noted in the previous paragraph that the damage-distance relationships for the unlined test sections and the access tunnel were approximately the same. Because of the lack of test data on tunnel liners beyond C Drift, the performances of the first three liner types listed in Table 4.2 at ranges greater than 457 feet must be extrapolated. The damage zones for the access tunnel as given in Table 4.1 may be used as a basis for this extrapolation because of the similarity in the degree of damage to unlined openings of the two orientations. From this, the liner types to be considered for protection are given as follows: (a) Damage Zone 2: liners with backpacking, (b) Damage Zone 3: liners cast against rock, (c) Damage Zone 4: conventional tunnel liners, and (d) beyond Damage Zone 4: unlined.

(4) Shock Isolation. The shock spectra (higher frequencies) and trapezoids representing the peak radial free-field motions were shown in Figures 3.124 through 3.135. By direct comparison of the data (radial component) taken in C Drift, the shock spectra in liners with backpacking are a factor of about four lower than the shock spectra obtained in the liner cast against rock. At B Drift, it is believed that this shock attenuation (liner with backpacking versus liner against rock) is even larger, say a factor of 10 or more due to the plastic deformation of the foam backpacking. Thus, the foam backpacking was highly effective in reducing the levels of shock transmitted to the floors of the liners where all the shock spectra measurements were taken.

Comparisons of the reed gage data points in various liners with the free-field trapezoids lead to the following observations. In the liners with no backpacking, the acceleration spectra bounds are about four times the peak free-field acceleration. In liners at C Drift where the foam backpacking

behaved elastically, the acceleration spectra bounds are about equal to the peak free-field acceleration. In liners at B Drift, where the foam backpacking deformed plastically, the acceleration spectra bounds are about one-third the peak free-field acceleration. No correlation was made for the velocity or displacement bounds because of the insufficient reed gage data points at the intermediate and lower frequency ranges.

TABLE 4.1 DAMAGE–DISTANCE RELATIONSHIP FOR ACCESS TUNNEL

PRESHOT ESTIMATES (5.0 KT)		LIMIT OF DAMAGE ZONE	POSTSHOT OBSERVATIONS (5.9 KT)		
STATION	SLANT RANGE		STATION	SLANT RANGE	
				FROM 5.9 KT	SCALED TO 5.0 KT
6 + 40	190'	ZONE 1 (CRUSHED)	N.A.	N.A.	N.A.
5 + 20	300'	POINT OF CLOSURE	4 + 30	375'	350'
4 + 75	340'	ZONE 2 (SEVERE)	3 + 80	425'	400'
2 + 90	520'	ZONE 3 (MODERATE)	2 + 60	550'	520'
0 + 60	750'	ZONE 4 (LIGHT)	BLAST DOOR (0 + 37)	775'	730'

TABLE 4.2 DAMAGE–DISTANCE RELATIONSHIP FOR TEST LINERS

TYPES		A DRIFT 244 FT. TO ZERO	B DRIFT 334 FT, TO ZERO	C DRIFT 457 FT. TO ZERO
UNLINED		X	C	S–M
HORSESHOE-SHAPED TUNNEL LINER		X	C	S–M
REINFORCED CONCRETE LINER CAST AGAINST ROCK		C	C	M–L
FLEXIBLE LINER WITH BACKPACKING	THICK FILLER	C	C–S	N
	THIN FILLER	C	C–S	N
RIGID-FLEXIBLE LINER WITH BACKPACKING	THICK FILLER	X	X	X
	THIN FILLER	C	C–S	N
RIGID LINER WITH BACKPACKING	THICK FILLER	S	N	N
	THIN FILLER	C	S	N

C - COMPLETE COLLAPSE
S - SEVERE DAMAGE
M - MODERATE DAMAGE
L - LIGHT DAMAGE
N - NEGLIGIBLE DAMAGE
X - NOT TESTED

THICK FILLER - 20" OR 24" FOAM ONLY
THIN FILLER - 5" OR 9" FOAM OR CINDER

TABLE 4.3 SUMMARY OF RECORDS RECOVERED VERSUS GAGES INSTALLED (PROJ 3.2)

	REFER TO FIGURE NO.	GAGES INSTALLED			RECORDS RECOVERED		
		A	B	C	A	B	C
DIAMETER CHANGE IN LINING	3.105	9	12	1	8	11	0
VELOCITY OF LINER (FOAM)	3.106	4	8	1	2	7	1
VELOCITY OF LINER (CINDER)	3.107	2	4	0	2	4	—
VELOCITY OF LINER (CAST AGAINST ROCK)	3.108	1	1	0	0	1	—
PRESSURE ON LINING	3.109	4	11	2	3	9	2
CIRCUMFERENTIAL STRAIN IN LINING	3.110	3	13	0	2	7	—
LONGITUDINAL STRAIN IN LAGGING	NO DATA	0	2	0	—	0	—
CIRCUMFERENTIAL STRAIN IN ROCK	3.111	2	18	0	0	3	—
RADIAL STRAIN IN ROCK	3.112	1	7	0	0	4	—
COMPRESSION OF FILLER	3.113	0	2	0	—	2	—
TOTALS		26	78	4	17	48	3
		108			68		

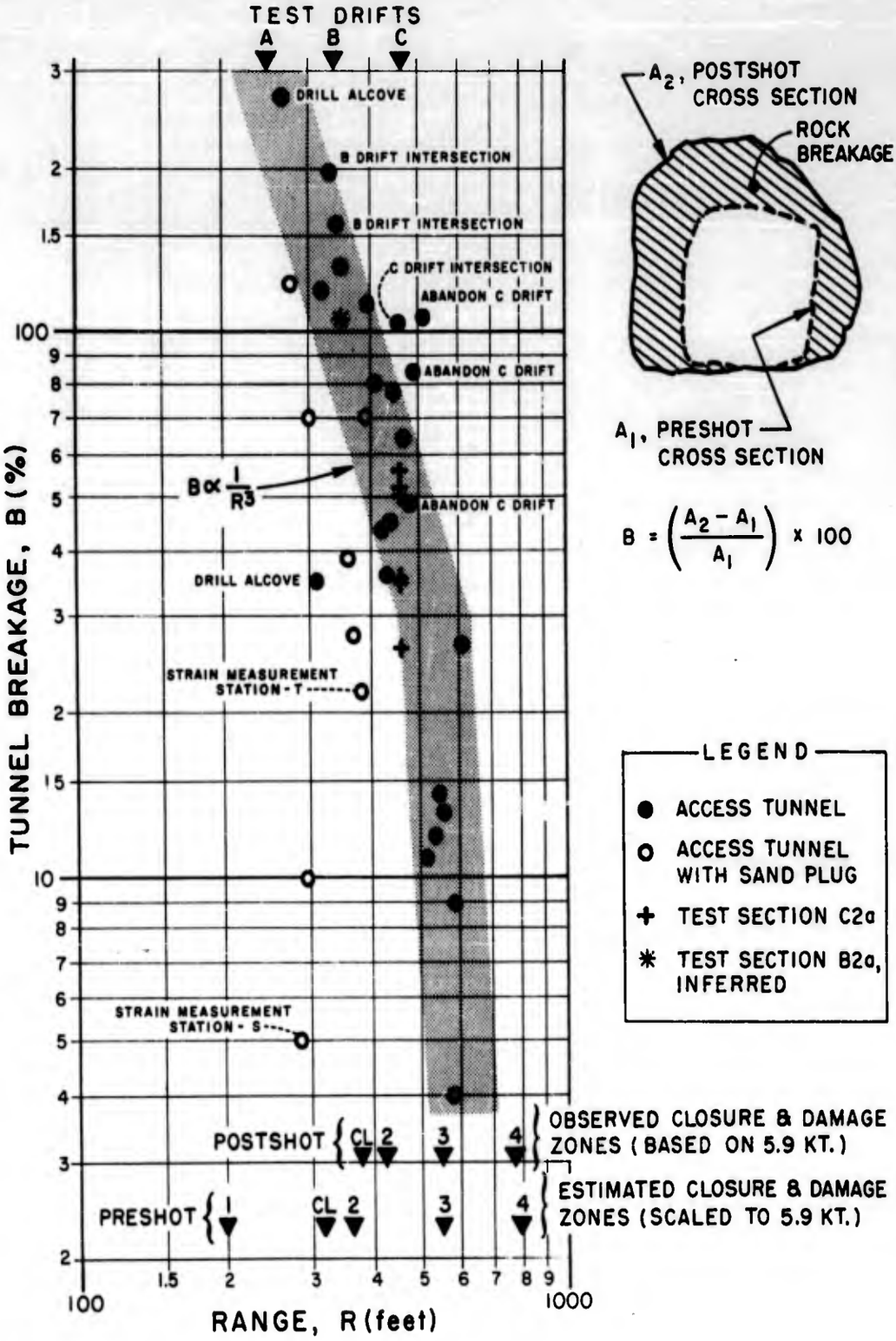

Figure 4.1 Rock breakage versus range, access tunnel and test drifts.

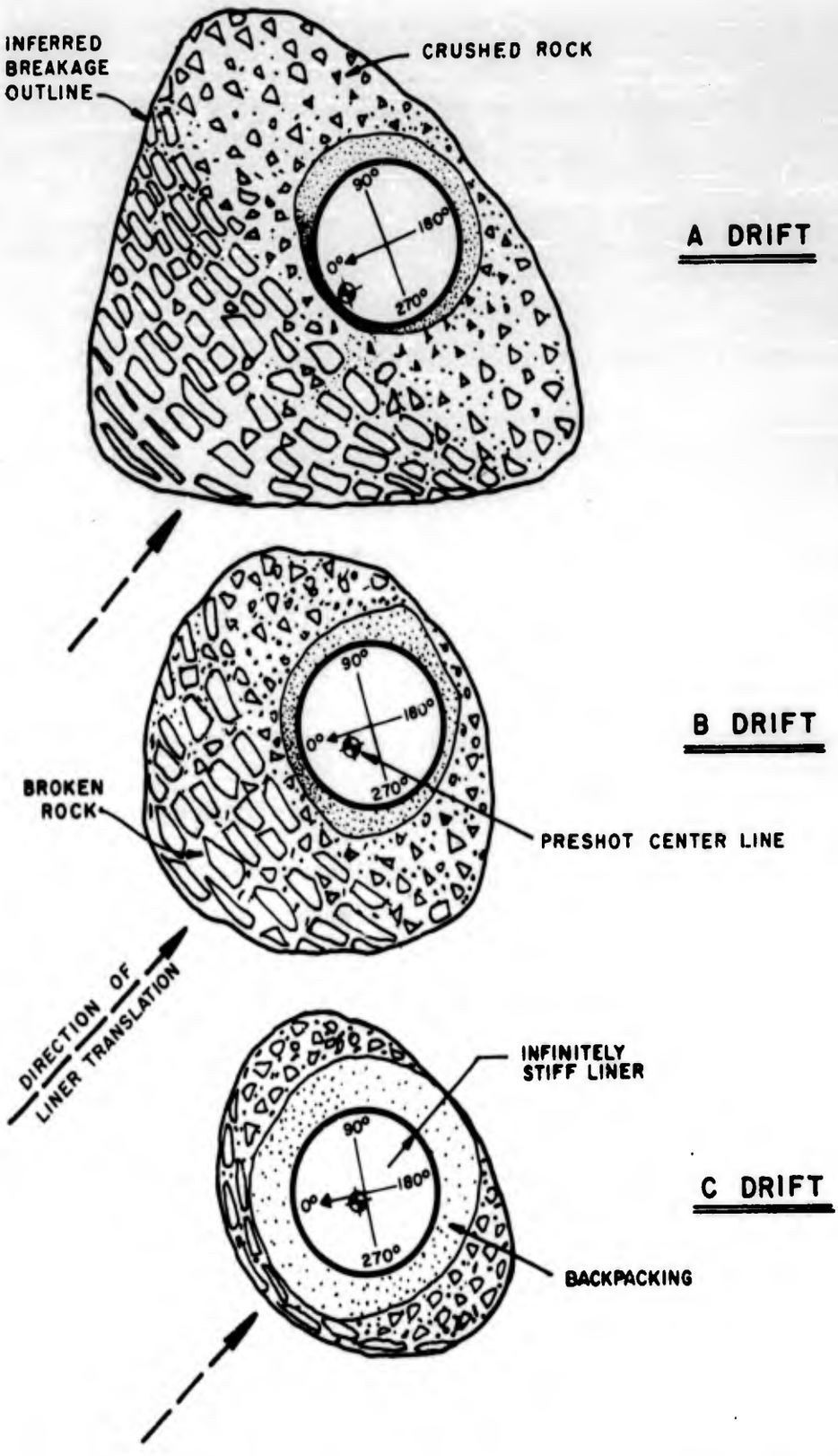

Figure 4.2 Generalized loading conditions on backpacking.

CHAPTER 5

CONCLUSIONS

The Hard Hat event provided a considerable amount of qualitative and quantitative test information on the free-field effects and on the response of tunnels and tunnel liners to the effects of a contained nuclear detonation. The data recovered from the instrumentation as well as visual observations of damage were presented in Chapter 3, and interpreted in Chapter 4. In addition, the significance of the results was discussed in terms of fulfillment of the project objectives and verification of the experimental concepts presented in Chapter 1. From these discussions, the following conclusions are drawn:

(1) The analytical approach given in Chapter 1 was effective in estimating the free-field effects (see Figure 3.115). It was also an effective basis for determining the locations of the three test drifts at ranges of desired damage. The experimental results were inconclusive, however, in verifying the limit of spalling, compressive failure, and tensile splitting.

(2) The empirical approach given in Chapter 1 was effective in estimating the point of tunnel closure and the limits of Zones 2, 3, and 4. However, the estimated limit of Zone 1 from this approach was too high. In fact, it was observed that none of the preshot openings were within Zone 1.

(3) The experimental concept of testing identical test sections in the three test drifts, subjected to widely different levels of damage, provided useful comparative response data.

(4) The effectiveness of the instrumentation plan was reduced by the heavy damage in B Drift where over seventy percent of the electronic response gages were installed. Another factor which reduced its usefulness was the orientation mismatch between the axes of instrument location and the areas of maximum liner response. However, sufficient quantitative data were recovered to permit description of the test liner response in a general manner.

(5) The concept of using a backpacking material between the tunnel liner and the rock wall to absorb the loading was validated by the test results. The least damaged test section at each test drift was found to be the rigid-type line (reinforced concrete) with thick foam backpacking.

(6) The intensity of damage to the unlined access tunnel and the unlined test sections was markedly affected by the competency of the rock. Rock breakage was substantially greater within local areas of weakness, such as fault zones, than in areas of more competent rock. The two sand plugs within the access tunnel materially reduced the amount of rock breakage at their locations.

(7) The damage-distance relationships for the access tunnel are as follows:

Limit of Damage	Observed Range (5.9 kt)	Range Scaled to 1.0 kt
Zone 1	Not observed	-
Point of closure	375 feet	210 feet
Zone 2	425 feet	235 feet
Zone 3	550 feet	300 feet
Zone 4	775 feet	430 feet

These damage-distance relationships appear to be applicable to the unlined test sections as well.

(8) The rock breakage around tunnels or drifts, in terms of percentage increase in the original cross sectional area, varied from approximately 300 percent at A Drift (244-foot range) to approximately 30 percent at a range of 550 feet. Rock breakage

decreased approximately as the inverse cube of the range over this distance, which corresponds to a scaled range from 135 $W^{1/3}$ to 300 $W^{1/3}$, where W is yield expressed in kilotons.

This attenuation rate for rock breakage is slightly greater than that of the free-field stress and particle velocity between the same scaled ranges.

(9) The damage to a given test section changes rapidly from heavy to light with a relatively small increase in range. The region within which the intermediate damage to tunnel liners occurs is relatively narrow.

(10) From the experimental results, the following liner types should be considered for protection:

Hard Hat Liner Types	Damage Zone	Range (ft) (5.9kt)	Scaled Range (ft) (1.0kt)
Composite (liner w/ backpacking)	2	425 or less	235 or less
Simple (cast against rock)	3	550 or less	300 or less
Conventional Tunnel Supports	4	775 or less	430 or less
Unlined	-	775 or more	430 or more

(11) The polyurethane foam backpacking was highly effective in reducing the high-frequency components of the liner response spectra. This reduction was found to be a factor of about four at

C Drift where the foam backpacking behaved elastically. The reduction was even greater (a factor of ten or more) at B Drift where the foam responded plastically. Hence, the foam was effective in reducing both shock and damage to the liners.

No response spectra data were obtained from liners with cinder backpacking. However, there were no significant differences in damage between liners backpacked with either foam or cinders of comparable thicknesses.

APPENDIX A

PHYSICAL PROPERTIES AND METHODS OF APPLICATION OF POLYURETHANE FOAM

INTRODUCTION

A.1 OBJECTIVE

The objective of this appendix is to review the physical characteristics of polyurethane foam and to discuss briefly the various methods of application of this material. Since the use of polyurethane foam as a shock isolation material has been quite limited, particular emphasis is given to those properties that can be used to evaluate the suitability of this material for various shock isolation applications.

A.2 BACKGROUND

A.2.1 Historic Review. The chemistry of the polyurethanes is based on a class of organic compounds known as isocyanates. These compounds, though known for over a century, had elicited little interest until 1937, when Dr. Otto Bayer of Germany began experimenting with diisocyanates as a means of producing a synthetic fiber competitive with nylon (Reference

14). The significance of his work was not recognized until after World War II. In 1945, the Office of the Quartermaster General sent a group of technical observers to investigate this phase of the German plastics industry.

The initial report of this investigation stimulated further interest in isocyanate-based plastics. The United States Air Force became interested in the possible special application of these materials for aircraft radomes. Subsequently, in September, 1946, the Goodyear Aircraft Corporation began an Air Force-sponsored research project for a system of rigid alkyd-isocyanate foams, from which a polyester resin which could be foamed with tolylene diisocyanate was developed.

During the latter part of 1947, Lockheed Aircraft Corporation began an independent study of the application of rigid polyurethane foams for radomes and for filling aircraft components by poured-in-place methods. The most important result of the Lockheed work was the development of the first two-component system of foaming, based on a polyester resin and a diisocyanate prepolymer. These components could be blended at room temperature, and poured-in-place to fill voids.

From this early work and through widespread patent and license agreements, the production of polyurethane raw materials and finished products has developed into a large (more than 100,000,000 pounds in 1961) commercial industry.

A.2.2 Previous Shock Isolation Tests. In 1959, an experimental program was conducted by the Armour Research Foundation. Models, composed of rigid aluminum cylinders, two inches in diameter and eight inches long, were mounted vertically in dry Ottawa sand with one end exposed. A wrapping of 1/4- or 1/2-inch-thick, two-pcf, flexible polyurethane foam was placed around each cylinder. Shock input was from the detonations of 0.02-pound surface HE (Tetryl) charges placed three feet from the model. Acceleration measurements were made at three points on the models. Results of these tests with flexible polyurethane foam indicated that this material was effective for shock isolation (Reference 15).

In addition to the Armour Research Foundation experimental program described above, a considerable amount of work has been done on the use of polyurethane foams as shock isolation materials for packaging and air drop applications. The

results of such investigation can be found in a series of reports by the Structural Mechanics Research Laboratory of the University of Texas under contract with the Quartermaster Research and Development Command, U.S. Army.

A.2.3 Project Hard Hat. It is believed that this project was the first large-scale test program in the use of rigid polyurethane foam as a tunnel liner shock isolation material. A nominal six-pcf-density foam having an average yield strength of 150 psi was used.

THEORY

A.3 CHEMISTRY

Polyurethanes comprise a relatively new class of polymer in which the repeating unit is the urethane linkage. Briefly, this linkage is formed by the reaction of an isocyanate group from one of the reacting components and a hydroxyl group of a polyester (or a polyether) which is present in the other reacting component. These urethane linkages connect the long polyester molecules in a manner analogous to the formation of chain link fence, where the double-ended isocyanate groups (the diisocyanates) represent the cross-ties or cross-links. However, the

process of this polymerization departs from the fence analogy in that it results in a three dimensional structure.

In the absence of other reactions, the above-mentioned polymerization would result in a solid plastic mass. However, when small amounts of water are blended in the polyester before combining with the diisocyanate, the latter reacts with water to liberate carbon dixoide, bubbles of which are entrapped by the viscous polyester resin as it is being cross-linked by the remaining diisocyanate. The end result of these steps is a plastic foam in which the bubbles are permanent part of the finished, fully reacted plastic material.

By varying the amount of water added, hence the amount of carbon dioxide liberated, the foam density may be varied. Similarly, by varying the make-up of the polyester resin, which governs the spacing of the cross-link points, a flexible or a rigid foam may be formulated. Through further changes in the polyester resin, a wide range of foam strengths may also be obtai: d. To this basic system, traces of agents such as foam stabilizers and catalysts may be added. The former helps to achieve a fine and uniform cell structure in the foam, while the latter serves to control both the speed of

the total reaction and the extent to which heat is liberated during its course.

In one major variation from the basic system described above, a volatile liquid, such as one of the Freon refrigerants, is substituted for water as the blowing agent. These liquids, unlike water, do not react chemically to liberate gas but volatilize, due to the heat generated by the exothermal reaction.

The prepolymer technique developed by Lockheed Aircraft Corporation is now in almost universal use. Basically, all of the diisocyanate portion of a system is pre-reacted at the chemical plant with about half of the hydroxyl-containing material, in the absence of water or other blowing agent. This preliminary step generates about one-half of the total heat which otherwise would have been liberated by a single step or the one-shot process. Because of less heat generation in the final reaction and other desirable physical and chemical characteristics, the prepolymer technique is more amenable to field installation where process control is more difficult. To complete the reaction in the final step, the prepolymer component is reacted with the remainder of the hydroxyl-containing material to which water or a volatile liquid has been added.

For Project Hard Hat, the prepolymer technique was used. The prepolymer component consisted of a polyether and tolylene diisocyanate. The hydroxyl-containing material was composed of a high molecular weight polyether, a tertiary amine as catalyst, an emulsifier, and a combination of Freon and water as the blowing agent.

A.4 PHYSICAL PROPERTIES

By virtue of its cellular structure in which the long polyester (or polyether) molecules are connected and cross-braced in a three-dimensional frame work, polyurethane foam exhibits a high strength-to-weight ratio. For the same reason, it also possesses good resistance against oxidation and other chemical attacks. Since foam is made of closed and non-connecting cells, adsorption of water and other non-reacting liquids occurs mainly on the exposed surfaces, where the cellular structure has been disturbed.

Properties, such as static yield strength and modulus of elasticity in compression, tension, and shear, vary directly with foam density but inversely with temperature (Reference 16). Figure A.1 illustrates these foam characteristics.

The static yield strain under unconfined compression tests generally occurs between five and ten percent, depending on foam formulations and densities. Under such tests, a stress-strain diagram usually indicates a linear relationship up to about seventy percent of the yield strain. From there on, the stress-strain diagram is slightly curved until the yield point is reached. When loaded beyond its yield point, the foam enters into the so-called plastic region, where it undergoes extensive deformation with little or no increase in stress. The extent of this plastic region, which depends on foam formulations and density, ranges from 40 to 70 percent strain. Further application of the load results in locking of the material due to the complete collapse of its cellular structure. This is characterized by a sharp increase in compressive stress. Stress-strain diagrams of some polyurethane foam systems are shown in Figures A.1 and 1.28.

In a free-rise condition, where the foam is not subjected to confining pressure, compressive yield strength and modulus of elasticity measured parallel to the direction of foam-rise are higher, by up to fifteen percent, than those measured normal to the direction of foam-rise. This anisotropic property may be

attributed to the fact that the foam cells roughly assume the shape of a prolate spheroid, in which the long axis is oriented parallel to the direction of foam-rise where the strength is the greatest. This characteristic is most pronounced in low density foam. Foam having density greater than fifteen pcf generally exhibits isotropic strength properties.

There is little information on the strength properties of foam subject to rapid rate of loading. Preliminary findings, based on limited scale of dynamic testing with rates of loading up to 2,000 inches per minute, indicate that, for polyurethane foam with density less than ten pcf, there were no significant differences between static and dynamic properties, such as strength in compression, tension and flexure, and respective modulus of elasticity. For higher density foam, test results show that these properties were numerically less than the static values (see Reference 17). Similarly, the lack of stress-rate effect of foam was also observed during the course of investigation conducted by the Structural Mechanics Research Laboratory of the University of Texas, under contract with the Quartermaster Research and Development Command, U. S. Army. However, preliminary results from recent laboratory experiments

performed by the Sandia Corporation indicate that polyurethane foam of the type identical to the precast foam used in Project Hard Hat exhibits significant increase in yield strength when subjected to drop tests with height of drop varying from 6 inches to about 11 feet. Since the results of this experiment have not been fully evaluated at this writing, it is believed that more work is required before the dynamic properties of foam can be ascertained. Of particular importance in the use of foam as a backpacking material is the knowledge of the shape of its dynamic stress-strain diagram, from which the strain energy that can be absorbed may be determined.

Other physical properties of foam which are not mechanical in nature can be mentioned briefly. Polyurethane has low dielectric constants, low power loss, and is practically transparent to electromagnetic waves; hence, it has found wide applications in radomes. The thermal conductivity of 2-pcf foam is in the range of 0.2 Btu/hr/sq ft/^{o}F/in, which places it among the better heat insulators. In general, higher density foam exhibits higher thermal conductivity.

A.5 FOAMING PROCEDURES

A.5.1 General Statement. The process of making foam plastics requires combining two or more components in the proper chemical ratio, blending them until homogeneous, and pouring the liquid into a mold (or container) to be filled. In a matter of minutes, depending on the catalyst employed, the liquid becomes a creamy color as the first gas is evolved. The whole mass will subsequently rise and eventually gel, having assumed the contours of the mold.

The density of the blended liquid is approximately seventy pcf. Therefore, knowing the amount of the liquid poured, the geometry of the mold, and the density of the final product for which a particular foam system has been formulated, the height of the foam-rise can be estimated with fair accuracy. The height to which most foam systems are designed to rise is about two or three feet. Excess rise is usually accompanied by thermal fissures in the interior of the foam mass, due to the exothermal reaction.

In general, the slower the rise time which is governed by the catalyst used, the higher the foam mass can rise without incurring thermal fissures. If the desired foam thickness is such that multiple pours are required, the succeeding pour is made when the foam from the previous pour is no longer tacky. This takes place in about ten to thirty minutes.

In a free rise situation, the foam mass rises under the influence of the evolved gas until the pressure in the cells is at an equilibrium with that of the surroundings. The density is determined by the amount of water or other blowing agent added to the mixture. However, in a closed blow condition, the foam mass is restrained by the mold surfaces from rising to as low a density as in a free rise. This closed blow results in an internal pressure in the mold which may reach as much as 35 psi.

The density gradient across a section of the foam is primarily a function of the temperature gradient. Cool mold surfaces and heat sinks cause a higher density foam skin because of the lack of complete bubble expansion. On the other hand, excessive mold temperature also results in a high density skin, due to the

reduction of material viscosity which allows the bubble to effervesce. In practice, the high density skin is only a fraction of an inch in thickness.

A.5.2 Methods of Foaming. The methods of producing foam may be divided into two general classes. The first is a method utilizing batch mixing technique, and the second is one where the continuous mixing technique is used.

Batch mixing represents the simplest method of foaming. All the foam components are first measured into one container and then mixed. Mixing may be accomplished by hand, or by use of power stirrer, depending on the quantity of the liquid to be handled. After thorough mixing, the mixture is poured into the mold to be foamed. Batches up to 150 pounds have been poured with little difficulty, and equipment designed to handle larger batches is under development. The advantages of batch mixing are: (1) simplicity and low cost of equipment, and (2) the entire liquid mixture risesat the same time. Its disadvantages are: (1) unwieldy in large batches, (2) limited

mixing time available in large quantity, and (3) difficulty of duplicating uniformity in mixing. This method was used to produce the precast foam units during the final phase of construction for Project Hard Hat.

In a continuous mixing process, the foam components are proportionately metered to a common chamber, where the components are mixed and discharged. The mixing chamber (or mixing head) can be of various designs; generally, it is compact and light enough to be handled by the operator. Inside the mixing head, there is a power-driven or air-driven agitator which serves to mix the various foam components. The advantages of the continuous mixing method are: (1) better control of metering and mixing, achieving a higher degree of uniformity of the foam mixture, and (2) ability to handle large quantities of foam materials. Its disadvantages are: (1) high fixed cost of the equipment and (2) usually not feasible for application to small quantity, limited-use items.

Within the continuous mixing family, there is a further division of operations according to the manner by which the liquid is discharged from the mixing chamber. They are: (1) continuous machine pouring, (2) spraying, and (3) frothing.

In continuous machine pouring, the mixed components are simply discharged from the mixing chamber in a steady stream. Delivery rate of liquid up to 100 pounds per minute has been achieved successfully. In the initial phase of construction for Project Hard Hat, this technique was used to cast the foam in place behind the liners.

Spraying involves forcing the mixed liquid through a nozzle under high pressure. The atomized particles impinge on the surface to be sprayed and subsequently rise. Currently, low density (about two pcf) sprayed foams are within the existing state of art. Foam thickness up to about two inches has been sprayed in one pass. Investigation has shown there is weakness in strength at the boundary of successive sprays. The apparent advantage of this method is that spraying is little affected by gravity, because the atomized particles adhere to the surface and do not flow.

In frothing, a highly pressurized solvent having a low boiling point is included in the mixing head of the foam equipment along with other foam components. The mixture is discharged through a valve and, upon expansion, assumes a froth-like

appearance. This initial expansion amounts to between 70 and 90 percent of its final volume. By the use of this technique, the problems associated with anisotropic properties due to direction of foam-rise, as well as to density gradient, can largely be eliminated. As in the case of spraying, frothed foam is limited in application to low density foam systems. At present, there is a lack of adequate machinery and process information.

A.6 CURING CONDITIONS

The requirements for curing differ for different foam systems and vary in accordance with the thickness of the foam. Curing time varies proportionally with the thickness. Some foams attain maximum strength properties after curing for two or three days at room temperature. This curing time may be reduced to eight to ten hours by heating the foam to between 120° and 150°F. Other foam systems may require a cure of one-half hour at 250°F or one hour at 220°F per inch of foam thickness to reach optimum properties. Generally, the required curing time is inversely proportional to the surface-to-volume ratio of the foam.

A.7 SAFETY PRECAUTIONS

One of the raw materials from which polyurethane foam is made is tolylene diisocyanate. This material cannot be considered toxic but rather as an irritant to the mucous membranes, particularly of the respiratory system and the eyes. When the concentration of tolylene diisocyanate in the air approaches 0.5 ppm, irritation to the nose and throat generally occurs. This may be followed, upon prolonged exposure especially at higher concentration, by shortness of breath and a general asthmatic condition. Therefore, the first precautionary measure is to equip the operators and those persons that may be working in the contaminated area with fresh-air masks and goggles. If work is performed in a confined area, such as tunnels, adequate ventilation must be provided. For those who handle the chemicals, protective clothing is necessary. Should spillage of the chemicals occur, rubbing alcohol can be used with great effectiveness to counteract the diisocyanates. Water should not be used, however, since it is not miscible with the diisocyanates and tends to spread the latter, causing more harm.

SUMMARY

The production of polyurethane foams has become, in recent years, a rapidly growing industry. Wide application of this product can be found in thermal insulation, structural reinforcement, packaging, and various other fields. Chemically, polyurethane is formed by the reaction of the organic isocyanates and polyester or polyether resin. Physical properties of foam cover a wide range of values, depending on a number of variables. Lacking at this time is information on the dynamic properties of foam which otherwise would permit, with greater assurance, quantitative evaluation of the foam as a shock isolation material.

Several methods of application are available, with advantages or limitations inherent in each.

Since the volatile vapor of certain isocyanates is a respiratory irritant rather than a toxic chemical, proper handling of the raw materials in a comparatively simple manner is all that is required during a foaming operation.

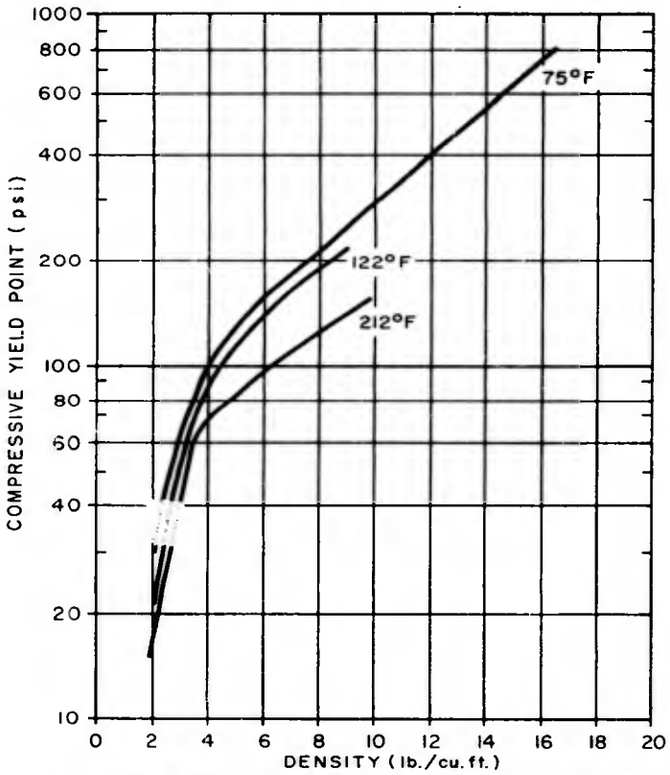

DENSITY VS. YIELD STRENGTH FOR POLYESTER BASED FOAM

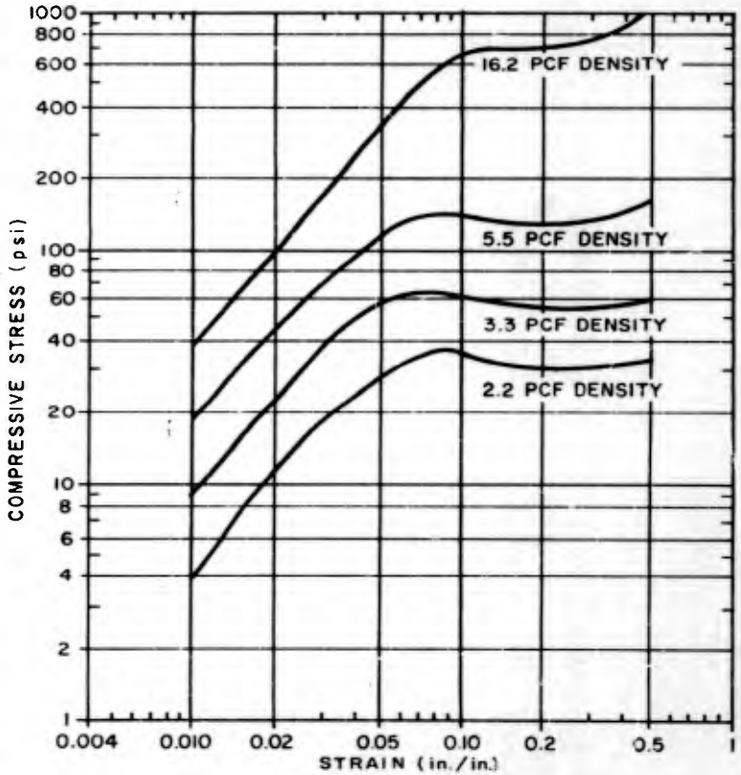

STRESS-STRAIN DIAGRAMS FOR POLYESTER BASED FOAM AT 75° F.

Figure A. 1 Physical properties of polyurethane foam.

APPENDIX B

INVESTIGATION OF PERLITE CONCRETE, AERATED CEMENT, AND EMULSIFIED ASPHALT AERATED CONCRETE AS ALTERNATE BACKPACKING MATERIALS

INTRODUCTION

B.1 OBJECTIVES

The purpose of the work described in this appendix was to investigate light-weight concrete mixtures that could be substituted for the polyurethane foam as a shock isolation material for tunnel liners.

Specifically, it was desired to obtain a mixture that would ideally meet the following requirements: (1) possess static stress-strain characteristics, under compressive load, similar to those of polyurethane foam; (2) made of materials which are readily available; (3) capable of being installed under restricted underground conditions; (4) require no special equipment or techniques for placement; (5) have uniform strength when poured; (6)be amenable to simple field tests to provide adequate quality control, and (7) be nearly impervious to water.

B.2 BACKGROUND

In view of the difficulties experienced by the lump-sum contractor in his efforts to cast polyurethane foam of specified quality behind the liners, it appeared prudent to investigate the use of substitute materials. Accordingly, the Nevada Testing Laboratories, Ltd. (NTL), Las Vegas, Nevada, was retained in August 1960, to perform experimental work on various light-weight concrete mixtures suitable for this application. At the end of this investigation in October 1960, two light-weight concrete mixtures were selected as the most promising. These were air-entrained concrete, utilizing exfoliated perlite as an aggregate, and an air-entrained neat cement mixture without aggregate.

In June 1961, NTL was again engaged to investigate means of waterproofing the two mixtures, with emphasis on the air-entrained cement mixtures. This phase of the work was terminated in August 1961.

B.3 MATERIALS

Insofar as practical, all materials used in this experimental work were in accordance with applicable standards of the American Society of Testing Materials (ASTM). The materials used were as follows: (1) Portland cement, ASTM C150-59; (2) hydrated lime, ASTM C207-49; and (3) perlite aggregate, ASTM C35-59.

During the early phases of the investigation, it was found that the latter specifications permitted sufficient variation between bags of the perlite aggregate to affect seriously the reproducibility of physical properties between successive pours. Consequently, the aggregate used during the remainder of the test program was produced in accordance with ASTM C35-59, modified as follows:

B.3.1 Gradation Requirements. This gradation is compared with the ASTM standard in Figure B.1.

Sieve Size	Percent Retained by Volume
No. 8	0
No. 10	0-5
No. 16	5-30
No. 20	25-55
No. 30	55-80
No. 50	80-95
No. 100	88-100

B.3.2 Density. The maximum density variation allowed was between 7-1/2 and 8 pcf, loose and dry weight.

B.3.3 Volume. The volume of each bag was specified to be four cubic feet, plus or minus one-twentieth cubic foot.

B.3.4 Impurities. Not more than two pounds of unexpanded impurities were allowed for each four-cubic-foot bag of perlite aggregates. Unexpanded impurities were defined as materials with a specific gravity greater than one. It was specified that during the bag-filling operations in the plant, water would be added uniformly for dust control at the rate of one-half gallon per four-cubic-foot bag.

B.3.5 Air-Entraining Agent. Two commercially available air-entraining agents, Daralite and Elastizell, were tested.

Daralite, which resembles a liquid soap solution, can be used as received. Elastizell was received in the form of a concentrated solution which was diluted with water in a pre-mix tank. The tank was connected by rubber tubing to a nozzle which could be preset to deliver a desired amount of air-entraining agent. Compressed air was then connected to the pre-mix tank and forced the solution through the nozzle, which upon leaving the nozzle expanded into a stiff lather. The nozzle was preset to deliver sixty gpm of froth-like lather.

B.3.6 Emulsified Asphalt. Two kinds of emulsified asphalt were used as waterproofing additives in the course of this investigation. They were Bitumuls DM-1h (SS-2), normally used as a roadway seal coat, and Hydropel, an emulsified asphalt specifically produced as a waterproofing admix for concrete.

B.4 MIXING AND PUMPING

During the experimental program, a number of small, trial laboratory batches of perlite concrete were produced and tested. The more promising mixtures were reproduced in four-cubic-foot batches, using full-scale equipment, to determine the

feasibility of the proposed placement method. Additional refinements were made in the mixtures during these full-scale tests.

The full-scale batches of perlite concrete were mixed in an eight-cubic-foot capacity plaster mixer and then pumped through 100 feet of two-inch-inside-diameter flexible hose to simulate field emplacement. Sample cylinders were taken at the mixer and at the hose discharge to determine the effect of pumping the materials. However, none of the air-entrained neat cement mixtures were pumped.

Experimentation with piston-type pumping equipment and screw-type pumping equipment demonstrated that the screw-type pump was more desirable. It was found that the screw-type pump would not cause the air-entrained froth to break down or be removed from the concrete mix. A Moyno screw-feed pump was finally chosen. It was also determined that Elastizell was a more stable air-entraining agent than Daralite for this application.

B.5 CURING

Generally, the test cylinders from a given batch were cured and tested as follows: (1) some of the cylinders were tested

after air drying for 24 hours, and (2) the remaining cylinders were air dried for 24 hours and then oven dried for another 24 hours before testing.

B.6 TESTING

The testing machine used was a Baldwin-Lima-Hamilton Universal testing machine, Model No. L-120, having ranges of 0-6,000 pounds or 0-120,000 pounds. The strain was determined with a 2-3/4-inch-diameter visual-reading dial indicator having a range of 1.000-inch with 0.001-inch graduations.

In order to simulate closely the actual loading conditions, two test procedures were developed. A confined compression test was used to approximate the gross motion of the rock wall against the backpacking material and liner. A penetration test was devised to simulate the effects of fly-rock penetration.

B.6.1 Confined Compression Test. The test specimens as removed from the pouring mold were approximately seven inches in diameter and seven inches in height. They were tested while confined within a thick-walled metal cylinder having

an average inside diameter of 6.968 inches. A flat steel disc, 6-7/8 inches in diameter and 3/4 inch thick, served as the confining piston. The rate of strain was maintained at two percent per minute.

B.6.2 Penetration Test. Preliminary penetration tests were conducted to determine the optimum size of the penetrating piston. Results of these trials indicated that the smaller diameter pistons produced smoother stress-strain curves and more reproducible results.

It was noted that the smaller pistons also gave consistently higher stress values at given strains. This was believed to be caused by the fact that, as the piston was forced into the specimens, the material ahead of the piston was crushed and compacted, causing lateral expansion which produced a cone-shaped hole instead of a cylindrical one. The effective bearing area was, therefore, somewhat greater than the area of the piston face.

When the recorded load was divided by the piston area, an apparent unit stress greater than the actual stress was obtained. This phenomenon was apparently more pronounced when using a smaller piston than a larger one. Based upon the

foregoing observations, a 1-13/16-inch-diameter piston was selected for all subsequent testing.

Test specimens of either six by six or seven by seven inches in diameter and height, respectively, were placed in a sheet metal jacket and banded with three Sure-Tite clamps. The penetrating piston was then forced into the test sample at a strain rate of two percent per minute.

B.6.3 Water Absorption Test. Water absorption tests on specimens of the light-weight concrete produced during the initial laboratory effort revealed that both materials were extremely pervious. This was considered detrimental to their possible underground application as shock isolation materials for two reasons: (1) water is frequently encountered underground, and (2) a saturated material would transmit a hydrostatic load with little attenuation to the liners in case of shock loading.

To determine the amount of water absorbed, the specimens were air cured for 24 hours. This was followed by oven curing at 150°F for a period varying from one to three days, at the end of which time the weight of the specimens was determined. The specimens were then immersed in a water bath kept at

approximately 80°F for one to three days. The weight was again determined and percent absorption by weight was calculated.

RESULTS AND DISCUSSION

B.7 RESULTS

At the conclusion of the initial laboratory program, two air-entrained, light-weight concrete mixtures were recommended by NTL as most nearly satisfying the requirements for alternate backpacking materials. These were: (1) mixtures using expanded perlite as an aggregate and (2) a simple aerated cement mixture. Techniques for full-scale field placement were developed. In addition, technical specifications were written for field installation of the perlite concrete.

B.7.1 Perlite Concrete. The recommended perlite concrete mix consisted of the following:

	lb
Cement, Type III	40.0
Perlite, four ft^3 including water for dust control	33.0
Hydrated lime	10.0
Water	62.7
Air-entraining agent (Elastizell) froth, 1.33 ft^3	4.3
Average unit batch weight, wet	150.0

Wet densities at mixer discharge:

Theoretical (computed at 100 percent yield)	37.5 pcf
Actual (average of four batches)	39.2 pcf

Typical test curves for perlite concrete are shown in Figure B.2.

B.7.2 Aerated Cement. This test mix consisted of a large amount of air-entraining agent in the following proportion:

Cement, Type III	64.0 lbs
Water	32.6 lbs
Air-entraining agent (Elastizell) froth, 1.85 ft^3	6.0 lbs
Average unit batch weight, wet	102.6 lbs
Approximate wet density	30.0 pcf
Approximate dry density	24.0 pcf

Typical test curves for aerated cement are shown in Figure B.3

B.7.3 Emulsified Asphalt Mix. Lower yields of concrete were noted when Hydropel was added in place of Bitumuls. No appreciable difference in waterproofing was noted between the two additives. In view of the foregoing observations and considering that Hydropel was more expensive, Bitumuls was selected for the final experimental work.

The addition of small quantities of Bitumuls appeared to impair the set of perlite concrete but did not impair the set of foamed cement. The addition of Bitumuls also appeared to stabilize the entrained air bubbles with longer mixing times. However, this held true up to a critical cement-water ratio of about 2-1/2 to 1 and for foamed concrete containing 1-1/2 to 2 gallons per cubic foot of Bitumuls. Larger amounts of Bitumuls actually altered the concrete properties to such an extent that the desirable stress-strain criteria could not be maintained.

Excessive shrinkage in the Bitumuls mix presented problems, but the addition of aluminum powder tended to counteract the shrinkage effect. About four grams of No. 101 aluminum powder were added per cubic foot of foamed cement.

Absorption tests performed on specimens of Bitumuls indicated a reduction in the maximum water absorption by weight to about thirty percent, which was equivalent to one-half-inch surface penetration for six-inch diameter cylinders.

A typical laboratory emulsified asphalt mix consisted of the following:

Cement, Type III	8.90 lbs
Water	4.56 lbs
Air-entraining agent, (Elastizell) froth	2.38 gals
Bitumuls	0.78 gal
Typical yields	0.511 to 0.571 $ft.^3$
Typical density	31 to 37 pcf
Typical water absorption, by weight (soaked from 24 to 72 hours)	10 to 30 percent

B.8 DISCUSSION

In general, the physical properties of the experimental mixtures tested appeared to be extremely sensitive to slight variations in proportions of the ingredients. This could have been the result of difficulty in accurately measuring small quantities of certain ingredients such as the air-entraining froth. On the other hand, the relatively high volumes of froth required to limit the strength of the mix to that of the polyurethane foam may have resulted in unstable mixtures.

Observations during water absorption tests indicated that water only permeated about one-half inch around the

The addition of small quantities of Bitumuls appeared to impair the set of perlite concrete but did not impair the set of foamed cement. The addition of Bitumuls also appeared to stabilize the entrained air bubbles with longer mixing times. However, this held true up to a critical cement-water ratio of about 2-1/2 to 1 and for foamed concrete containing 1-1/2 to 2 gallons per cubic foot of Bitumuls. Larger amounts of Bitumuls actually altered the concrete properties to such an extent that the desirable stress-strain criteria could not be maintained.

Excessive shrinkage in the Bitumuls mix presented problems, but the addition of aluminum powder tended to counteract the shrinkage effect. About four grams of No. 101 aluminum powder were added per cubic foot of foamed cement.

Absorption tests performed on specimens of Bitumuls indicated a reduction in the maximum water absorption by weight to about thirty percent, which was equivalent to one-half-inch surface penetration for six-inch diameter cylinders.

A typical laboratory emulsified asphalt mix consisted of the following:

periphery of the test specimens, and this occurred only at those places where an otherwise smooth surface of the specimens was damaged during stripping of the forms. Therefore, it appeared that water absorption may not be a serious problem for a light-weight concrete mixed with emulsified asphalt, especially when the overall thickness is much greater than one-half inch.

CONCLUSIONS

During this investigation, experimental light-weight concrete mixtures exhibiting favorable stress-strain characteristics for shock isolation applications were produced.

The limited scope of the investigation precluded the development of a refined, proved material. However, the test results suggest that the light-weight concrete has good potential, and that additional development work may result in suitable shock-isolation materials from this source.

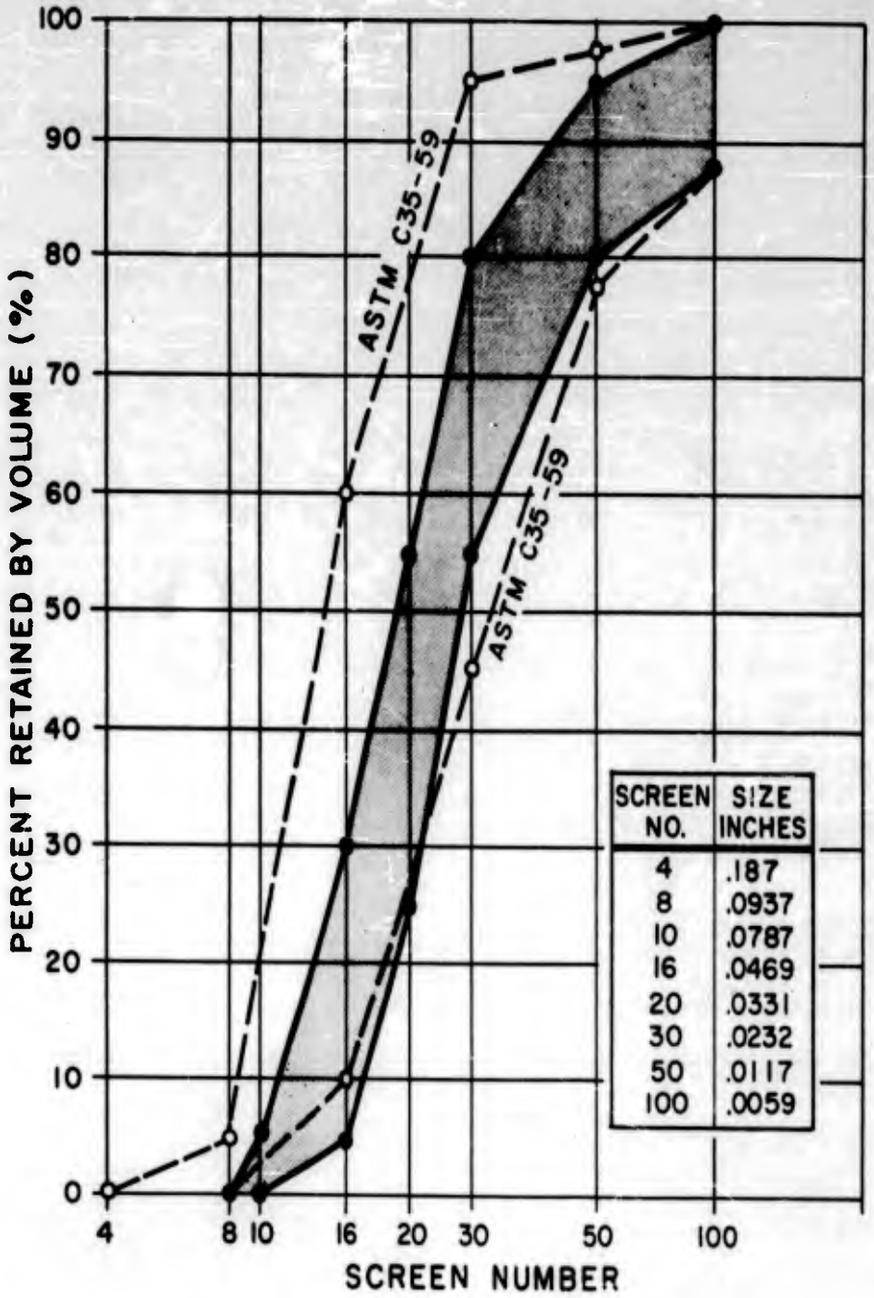

Figure B.1 Comparison of recommended grading requirements with ASTM specifications for perlite aggregate.

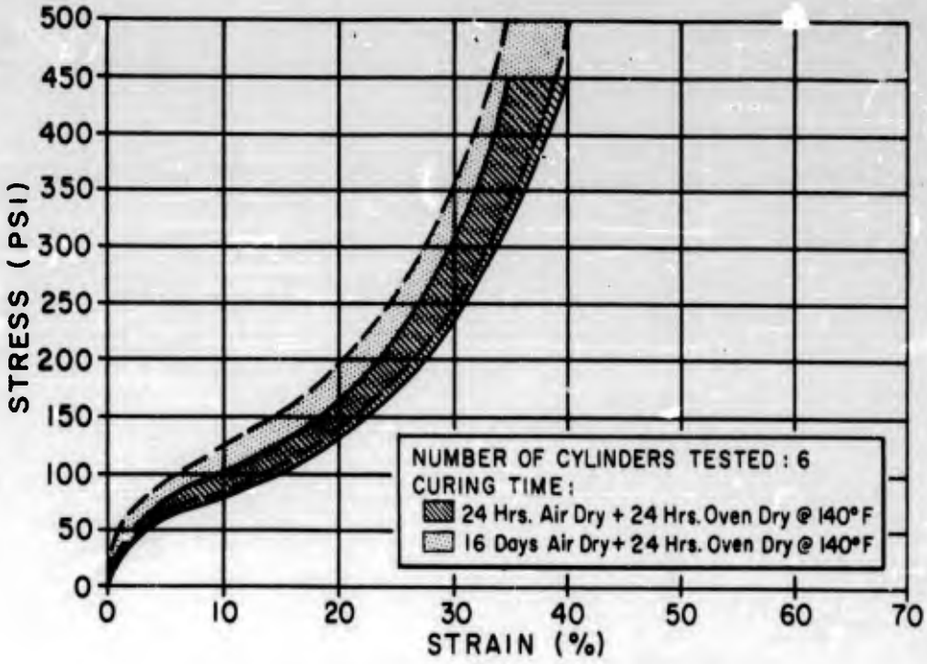

(a) CONFINED COMPRESSION TESTS

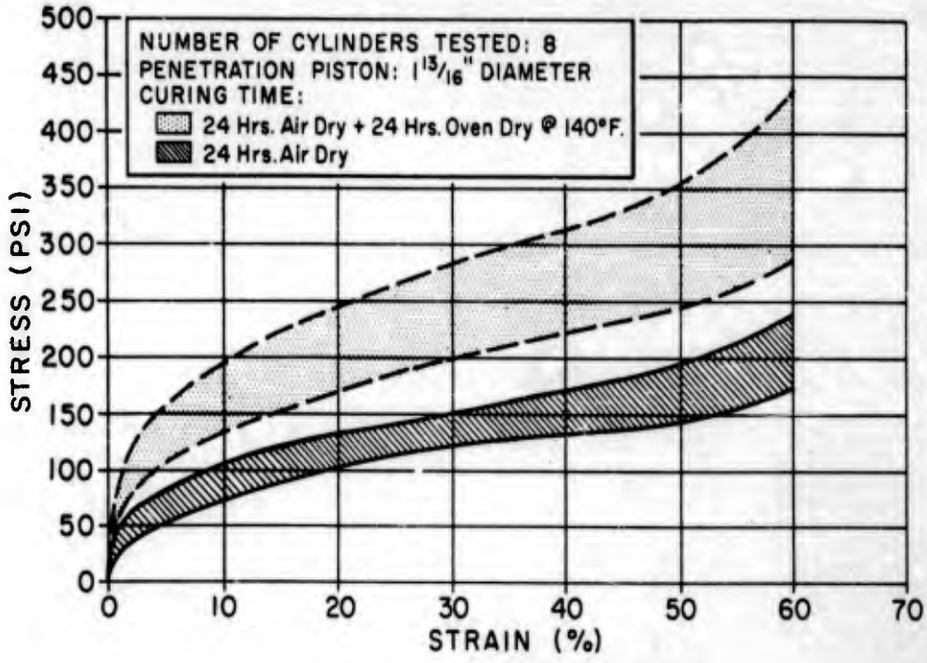

(b) PENETRATION TESTS

Figure B.2 Range of stress-strain curves of final perlite concrete test mix.

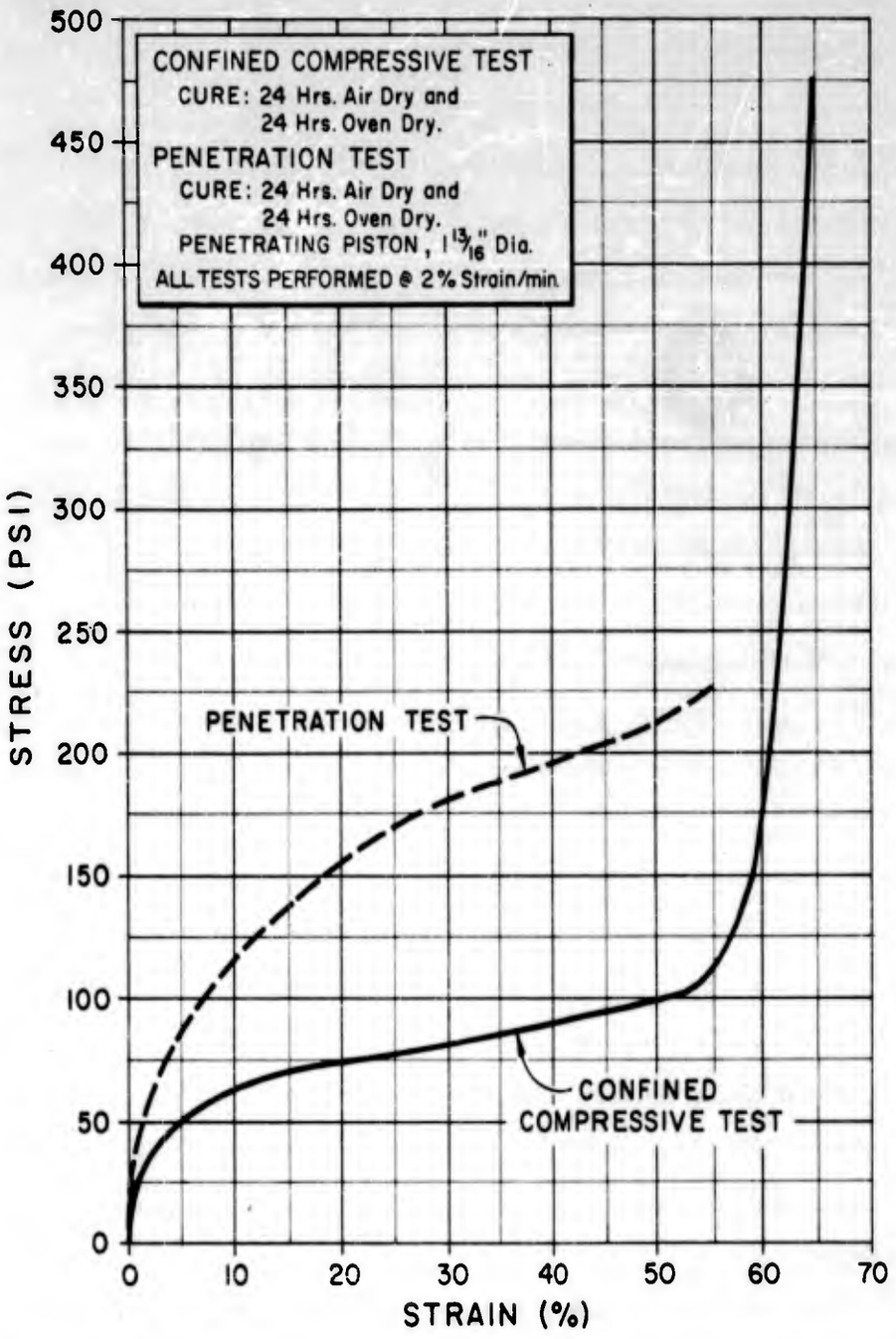

Figure B.3 Typical stress-strain curves from penetration and confined compressive tests on foam-cement.

REFERENCES

1. Engineering Research Associates, Division of Remington Rand, Inc.; "Underground Explosion Test Program, Final Report, Volume II, Rock"; April 1953; for the Department of the Army, Corps of Engineers; Contract No. DA-04-167-ENG-298; Confidential.

2. A.A. Lee and E.Y. Wong; "Evaluation of Blast and Shock Effects on Tunnel Support Structures"; Project 26.13, Operation Hardtack, Phase II; ITR-1714; Holmes and Narver, Inc., November 1959; Unclassified.

3. Mike S. Johnson and Donald E. Hibbard; "Geology of the Atomic Energy Commission Nevada Proving Grounds Area, Nevada"; Bulletin 1021-K, U.S. Department of the Interior, Geologic Survey, 1957.

4. F.N. Houser and F.G. Poole; "Preliminary Geologic Map of the Climax Stock and Vicinity, Nye County, Nevada, Miscellaneous Geologic Investigations, Map 1-328"; U.S. Department of the Interior, Geologic Survey, 1960.

5. F.N. Houser and F.G. Poole; "Granite"; Exploration Hole, Area 15, Nevada Test Site, Nye County, Nevada—Interim Report, Part A, Structural Petrographic and Chemical Data, Trace Elements Memorandum Report 836, U.S. Department of the Interior, Geological Survey, July 1959.

6. R.D. McArthur and J.W. Skrove; "Underground Geology of the Lollipop Site"; Station 1500, Nevada Test Site—Interim Report, University of California, Lawrence Radiation Laboratory, Livermore, California; September 1960; Unpublished.

7. N.M. Newmark; "Notes on Tests of Tunnel Linings in Granite"; August 1959; Unpublished; Confidential.

8. J.L. Merritt; "Basis for Selection of Drift Locations"; Contract AF29(601)-2151; Department of Civil Engineering, University of Illinois, Urbana, Illinois; October 1959; Confidential.

9. L.H. Klotz and J.L. Merritt; "Static Stress-Strain Curves and Energy Absorbing Characteristics of Materials Investigated For Use As Shock-Isolation Media"; Phase II of Final Report (Draft), Contract AF29(601)-2151, Department of Civil Engineering, University of Illinois, Urbana, Illinois; November 1961.

10. L.M. Swift; "Electronic Measurements in Rock and Tunnel Liner Structures"; Project 3.2, Operation Nougat, Shot Hard Hat, POIR-1802; Stanford Research Institute, Menlo Park, California; Secret.

11. W.R. Perret; "Free-Field Ground Motion Studies in Granite"; Project 3.3, Operation Nougat, Shot Hard Hat, POR-1803, April 1963; Sandia Corporation, Albuquerque, New Mexico; Official Use Only.

12. Bruce M. Carder and Leslie P. Donovan; "Fly-Rock Photography"; Project 3.11, Operation Nougat, Shot Hard Hat, POIR-1805, June 1962; Confidential Formerly Restricted Data.

13. M.V. Barton and J.M. Lindahl, "Displacement Spectrum Measurements"; Project 3.12, Operation Nougat, Shot Hard Hat, POR-1806; Confidential.

14. B.A. Dombrow; "Polyurethanes"; Reinhold Publishing Corporation, New York, 1957.

15. E. Sevin; "Ground Shock Isolation of Buried Structures"; Armour Research Foundation, Chicago 16, Illinois; August 1959, TR-59-47.

16. E. Tufts; "Properties of Rigid and Semi-Rigid Urethane Foams"; Published by Elastomer Chemicals Department, E.I. du Pont De Nemours & Co., Wilmington, Delaware; August 1957.

17. R.H. Supnik and M. Silberberg; "Properties of Foams and Laminates Under Shock Loading"; The Society of Plastic Engineers Journal, Vol. 15, No. 1, January 1959.

18. R.D. McArthur, "Geologic and Engineering Effects, The Hard Hat Event"; University of California Lawrence Radiation Laboratory, Livermore, California; February 1963; Preliminary.

DISTRIBUTION

Military Distribution Categories 14 and [illegible]

ARMY ACTIVITIES

1 CHIEF OF R & D DA
2 AC OF S INTELLIGENCE DA
3 CHIEF OF ENGINEERS DA
4- 5 ARMY MATERIAL COMMAND
6 CHIEF OF TRANSPORTATION DA
7- 8 U S ARMY COMBAT DEVELOPMENTS COMMAND
9 DIRECTOR OF SPECIAL WEAPONS DEVELOPMENT OFFICE
10 U S ARMY ARTILLERY BOARD
11 U S ARMY AIR DEFENSE BOARD
12 U S ARMY COMMAND AND GENERAL STAFF COLLEGE
13 U S ARMY AIR DEFENSE SCHOOL
14 U S ARMY ARMORED SCHOOL
15 U S ARMY ARTILLERY & MISSILE SCHOOL
16 U S ARMY AVIATION SCHOOL
17 U S ARMY INFANTRY SCHOOL
18 U S ARMY ORDNANCE & GUIDED MISSILE SCHOOL
19 CHEMICAL CORPS TRAINING COMD
20 ENGINEER SCHOOL
21 ARMED FORCES INSTITUTE OF PATH
22 ARMY MEDICAL RESEARCH LAB
23 WALTER REED ARMY INST OF RES
24 ENGINEER RESEARCH & DEV LAB
25 WATERWAYS EXPERIMENT STATION
26 PICATINNY ARSENAL
27 DIAMOND ORDNANCE FUZE LABORATORY
28- 29 BALLISTIC RESEARCH LABORATORY
30 WHITE SANDS MISSILE RANGE
31 U S ARMY MUNITIONS COMMAND
32 U S ARMY ELECTRONIC PROVING GROUND
33 U S ARMY COMBAT SURVEILLANCE AGENCY
34 THE RESEARCH & ANALYSIS CORP

NAVY ACTIVITIES

35- 36 CHIEF OF NAVAL OPERATIONS OP03EG
37 CHIEF OF NAVAL OPERATIONS OP-75
38- 39 CHIEF OF NAVAL RESEARCH
40- 42 BUREAU OF NAVAL WEAPONS DLI-3
43 BUREAU OF SHIPS CODE 423
44 BUREAU OF YARDS & DOCKS
45 U S NAVAL RESEARCH LABORATORY
46- 47 U S NAVAL ORDNANCE LABORATORY
48 NAVY ELECTRONICS LABORATORY
49 U S NAVAL MINE DEFENSE LAB
50- 51 U S NAVAL RADIOLOGICAL DEFENSE LAB
52- 53 U S NAVAL CIVIL ENGINEERING LAB
54 U S NAVAL SCHOOLS COMMAND TREASURE ISLAND
55 U S NAVAL POSTGRADUATE SCHOOL
56 U S NAVAL SCHOOL PORT HUENEME
57 NUCLEAR WEAPONS TRAINING CENTER ATLANTIC
58 NUCLEAR WEAPONS TRAINING CENTER PACIFIC
59 U S NAVAL DAMAGE CONTROL TNG CENTER
60 NAVAL AIR MATERIAL CENTER
61 U S NAVAL AIR DEVELOPMENT CENTER
62 US NAVAL AIR SP WPNS FACILITY
63 U S NAVAL MEDICAL RESEARCH INSTITUTE
64 DAVID W TAYLOR MODEL BASIN
65 U S NAVAL ENGINEERING EXPERIMENT STATION
66 U S NAVAL SUPPLY R&D FACILITY
67 NORFOLK NAVAL SHIPYARD
68- 71 U S MARINE CORPS CODE AO3H

AIR FORCE ACTIVITIES

72 HQ USAF AFTAC-TD
73 HQ USAF AFRDC-AE
74 HQ USAF AFRDR-NU
75 HQ USAF AFOCE [illegible] FICE
76 HQ USAF OPERATIONS ANALYST
77- 81 HQ USAF AFCIN [illegible] VCE
82 AC OF S INTELLIGENCE [illegible] TECHNOLOGY
83 DC OF S RESEARCH [illegible]
84 THE SURGEON GENERAL
85 TACTICAL AIR COMMAND
86 AIR DEFENSE COMMAND [illegible] D
87 AIR FORCE SYSTEMS COMMAND [illegible] DIVISION
88 AIR FORCE BALLISTIC SYSTEMS
89 RADC-RAALD,GRIFFISS AFB
90 PACIFIC AIR FORCES
91 SECOND AIR FORCE
92- 93 AF CAMBRIDGE RESEARCH CENTER
94- 98 AFSWC KIRTLAND AFB NMEX
99-100 AIR UNIVERSITY LIBRARY
101 LOWRY AFB
102 SCHOOL OF AVIATION MEDICINE
103-105 AERONAUTICAL SYSTEMS DIVISION
106-107 USAF PROJECT RAND
108 AIR TECHNICAL INTELLIGENCE CENTER
109 OFFICE OF AEROSPACE RESEARCH
110 HQ USAF AFORD

OTHER DEPARTMENT OF DEFENSE ACTIVITIES

111 DIRECTOR OF DEFENSE RESEARCH AND ENGINEERING
112 ASST TO THE SECRETARY OF DEFENSE ATOMIC ENERGY
113 ADVANCE RESEARCH PROJECT AGENCY
114 WEAPONS SYSTEM EVALUATION GROUP [illegible] ON & LOGISTICS
115 ASST SECRETARY OF DEFENSE INSTALL
116-119 DEFENSE ATOMIC SUPPORT AGENCY
120 FIELD COMMAND DASA
121 FIELD COMMAND DASA FCTG
122-123 FIELD COMMAND DASA FCWT [illegible] E ADMINISTRATION
124 NATIONAL AERONAUTICS & SPACE AGENCY
125-126 DEFENSE INTELLIGENCE AGENCY SAFETY BOARD
127 ARMED SERVICES EXPLOSIVES
128 JOINT TASK FORCE-[illegible] OM
129 COMMANDER-IN-CHIEF PACIFIC
130 COMMANDER-IN-CHIEF ATLANTIC FLEET
131 COMMANDER-IN-CHIEF [illegible] AND
132 STRATEGIC AIR [illegible]
133 CINCONAD [illegible] OF DEFENSE CIVIL DEFENSE
134-136 ASST SECRETARY

CAT. A 2

POP CIVILIAN DIS [illegible]
[illegible] ELECTRODYNAMICS INC PASADENA
137 UNITED TECH LAB LOS ANGELES ATTN SUSSHOLZ
138 SPA CAMBRIDGE MASS ATTN HANSEN
139 M COAST &GEODETIC SURVEY WASHINGTON ATTN MURPHY
140 STANFORD RESEARCH INST MENLO PARK ATTN VAILE
141 SANDIA CORP SANDIA BASE ALBUQUERQUE ATTN CLASS DOC
142 US GEO SURVEY DENVER COL ATTN ROACH
143 US GEO SURVEY DENVER COL ATTN PAKISER
144 HOLMES AND NARVER FOUNDATION LOS ANGELES
145 ARMOUR RESEARCH FOUNDATION CHICAGO
146 GEOPHYSICS CORP OF AMERICA BEDFORD MASS
147 GEOTECHNICAL CORP GARLAND TEXAS
148 GEN AMERICAN TRANS CORP NILES ILL
149 DEPT OF CIVIL ENGR UNIV OF ILL URBANA ILL ATTN NEWM
150 UNITED SERVICES BURLINGAME CALIF
151

ATOMIC ENERGY COMMISSION ACTIVITIES

152-154 AEC WASHINGTON TECH LIBRARY
155-156 LOS ALAMOS SCIENTIFIC LAB
157-161 SANDIA CORPORATION
162-171 LAWRENCE RADIATION LAB LIVERMORE
172-175 NEVADA OPERATIONS OFFICE,LAS VEGAS
176 DTIE OAK RIDGE,MASTER
177-206 DTIE OAK RIDGE SURPLUS

CONFIDENTIAL